THE UNIVERSITY
of EDINBURGH

VIBRATION-BASED DAMAGE IDENTIFICATION WITH ENHANCED FREQUENCY DATASET AND A CRACKED BEAM ELEMENT MODEL

Thesis submitted for the degree of
Doctor of Philosophy

Chuanchuan Hou

Institute for Infrastructure and Environment

School of Engineering

The University of Edinburgh

May, 2016

Table of Contents

Declaration i

Lay Summary i

Acknowledgements iii

Abstract iv

1 Introduction 1

1.1 Background 1

1.1.1 Limitation of the conventional modal data 2

1.1.2 Modelling errors in the conventional damage model 3

1.2 Objectives and Scope 8

1.3 Organization of the thesis 9

2 Literature review 11

2.1 Recent progress in modal testing practices 11

2.2 Model updating with enhanced frequency dataset 16

2.2.1 Antiresonances (zeros) of driving FRF curves 16

2.2.2 Artificial boundary condition (ABC) frequencies 21

2.3 Crack modelling in beams 23

2.3.1 Models based on stress fields 23

2.3.2 Methods based on the discrete spring model 26

2.3.3 Cracked beam element based on local flexibility and fracture mechanics 27

2.4 Crack modelling for box section beams 30

2.4.1 One-dimensional beam element for box section beams 30

2.4.2 Stress intensity factors for cracked box section beams 31

3 Experimental study of generating ABC frequencies and application in model updating 33
3.1 Introduction 33
3.2 Overview of ABC concept and basic formulation 33
3.3 Experimental investigation of modal testing for ABC frequencies 36
3.3.1 Test structure and modal testing programme 37
3.3.2 Modal testing results 44
3.4 Discussion on the measurement accuracy of ABC frequencies 47
3.4.1 Errors pertaining to imprecise excitation location 48
3.4.2 Errors pertaining to the sensor mass 54
3.4.3 Errors pertaining to additive noise 54
3.4.4 Verification of accuracy of extracted ABC frequencies from test data 55
3.5 Extracting ABC frequencies from damaged beams and damage identification 57
3.5.1 Test specimens and modal testing results 58
3.5.2 Damage identification through FE model updating 59
3.5.3 Model updating considerations 62
3.5.4 FE model updating (damage identification) results 64
3.6 Extraction of ABC frequencies from some more sophisticated structure conditions 67
3.6.1 Aluminum beams with high stiffness 67
3.6.2 RC beams with realistic boundary conditions 72
3.7 Summary and conclusions 76
4 A cracked beam element model and its implementation for Identification of cracks in thick beams 79
4.1 Introduction 79

4.2 Cracked beam element model 79
4.2.1 Model formulation 80
4.2.2 Discussion on the cracked beam stiffness matrix 83
4.3 Forward verification of the cracked beam element model 87
4.3.1 Forward verification for the dynamic properties 87
4.3.2 Discussion of the thick beam effects 93
4.4 Cracked damage identification using the cracked beam element model 97
4.4.1 General considerations 97
4.4.2 Adaptive discretization 98
4.4.3 Parameter updating algorithm 100
4.4.4 Application examples 100
4.5 Summary and conclusions 113
5 Experimental investigation of crack identification in thick beams 115
5.1 Introduction 115
5.2 Experimental programme 117
5.2.1 Test specimens 117
5.2.2 Modal testing setup 118
5.2.3 Modal testing results 120
5.3 Verification of the prediction of modal properties by the cracked beam element model 122
5.4 Crack damage identification using the cracked beam element model 126
5.4.1 General consideration 126
5.4.2 Model updating results with a standard mesh setting 127
5.4.3 Crack damage identification with less modal information and coarser mesh setting 129

5.5 Crack damage identification with ABC frequencies 131
5.5.1 Obtaining ABC frequencies from the tested beams 131
5.5.2 FE model updating with ABC frequencies 133
5.6 Summary and conclusions 136
6 Crack modelling and identification in box section beams 138
6.1 Introduction 138
6.2 Cracked beam element model for box section beams 139
6.2.1 One-dimensional beam element for intact box section beams 140
6.2.2 Crack model formulation 140
6.2.3 Stress intensity factors (SIFs) for cracked square box beams 145
6.3 Application of the cracked beam element in vibration analysis and crack damage identification 148
6.3.1 Vibration analysis with the cracked beam element 149
6.3.2 Crack damage identification using the cracked beam element model 151
6.3.3 Performance of the cracked beam element model on thin-walled box section beams 153
6.4 Experimental verification with the cracked beam element model 156
6.4.1 Test specimens 156
6.4.2 Modal testing setup 157
6.4.3 Modal testing results 158
6.4.4 Verification of the prediction of modal properties by the cracked beam element 162
6.4.5 Model updating and crack damage identification 163
6.5 Summary and conclusions 165
7 Conclusions and recommendations for further research 167
7.1 Conclusions 167

7.1.1 ABC frequencies and their applications in model updating 167
7.1.2 Crack identification in thick beams with a cracked beam element 168
7.2 Recommendations for further research 170
References 172
Appendix A: Stress intensity factors (SIFs) for box section beams 180
Appendix B: List of publications 182

Figures and Tables

Figure 1.1 Example beams with a length to sectional depth ratio of 10 (Unit: mm) ... 5

Figure 1.2 Numerically simulated and predicted frequency shifts 7

Figure 2.1 Stiffness reduction of cracked element 24

Figure 2.2 Discrete spring model 26

Figure 3.1 Illustration of artificial boundary condition frequency measurement settings 36

Figure 3.2 Test setup (Unit: mm) 37

Figure 3.3 Data acquisition system in modal testing 39

Figure 3.4 Representative recorded impact force and acceleration signals 40

Figure 3.5 RFP technique for noisy antiresonances and two-pin ABC frequencies .. 42

Figure 3.6 Representative driving FRF and two-pin ABC frequency function curves 43

Figure 3.7 Mass-normalized mode shapes 46

Figure 3.8 Modal testing operation when obtaining one-pin ABC frequencies 48

Figure 3.9 Numerical model for investigation of errors in one-pin ABC frequency . 51

Figure 3.10 One-pin ABC frequencies versus Δd relationships 52

Figure 3.11 Two-pin ABC frequencies versus Δd relationships 53

Figure 3.12 Damages in steel beams 58

Figure 3.13 Updating results with J_1 64

Figure 3.14 Updating results with J_2 65

Figure 3.15 Updating results with J_3 65

Figure 3.16 Updating results with J_4 65

Figure 3.17 Updating results with J_5 66

Figure 3.18 Examples of intact and cracked aluminium beams 68

Figure 3.19 Modal testing setup for aluminium beams 69
Figure 3.20 Modal testing setup of the RC beam 72
Figure 3.21 Driving FRF curves 73
Figure 3.22 Measured and predicted displacement-normalized mode shapes 74
Figure 3.23 Measured and predicted ABC frequency function curves 75
Figure 3.24 Beam element model for the RC beam 76
Figure 4.1 Loading state of a cracked beam element 80
Figure 4.2 Influence of crack depth ratio on the elements of stiffness matrix 85
Figure 4.3 Influence of crack location on the elements of stiffness matrix 86
Figure 4.4 Boundary conditions of the beams 88
Figure 4.5 Mesh of the FE model with solid elements 88
Figure 4.6 Comparisons between numerically simulated and predicted frequency shifts ($\alpha = 0.3$) 90
Figure 4.7 Comparisons between numerically simulated and predicted frequency shifts ($\alpha = 0.5$) 91
Figure 4.8 Comparison between MAC results from two different models ($\alpha = 0.3$) 92
Figure 4.9 Comparison between MAC results from two different models ($\alpha = 0.5$) 93
Figure 4.10 The influence of shear deformation and rotational inertia ($\alpha = 0.5$) 94
Figure 4.11 Influence of coupling effect between longitudinal and transverse vibrations 96
Figure 4.12 Mode shapes of the 3rd mode of the intact and cracked beams 97
Figure 4.13 Relationship between the crack influence range and the beam element 99
Figure 4.14 Updating results of beams with $\alpha = 0.3$ 103
Figure 4.15 Updating results of cantilever beam with $\alpha = 0.5$ 105
Figure 4.16 Updating results of cantilever beam with $\alpha = 0.3$ 106

Figure 4.17 Updating results of cantilever beam with $\alpha = 0.5$ 107

Figure 4.18 Updating results of cantilever beam with $\alpha = 0.3$ 108

Figure 4.19 Updating results of cantilever beam with $\alpha = 0.5$ 108

Figure 4.20 Examples with adaptive updating strategy (Unit: mm) 109

Figure 4.21 Updating results of beams with non-centred crack..... 110

Figure 4.22 Updating results with adapted mesh 112

Figure 4.23 Beam with multiple cracks 112

Figure 4.24 Updating results of beam with multiple cracks 113

Figure 5.1 Beam specimens and configurations of cracks 118

Figure 5.2 Modal testing setup..... 119

Figure 5.3 Measured FRF curves 120

Figure 5.4 Measured mass-normalized mode shapes from all 5 beam specimens... 121

Figure 5.5 Comparison between frequency shifts..... 124

Figure 5.6 Comparison between MAC results..... 125

Figure 5.7 Updated crack depth ratios (α) with standard mesh setting 128

Figure 5.8 Updated crack depth ratios (α) with coarser mesh setting 130

Figure 5.9 RFP technique for noisy antiresonances and two-pin ABC frequnecies 132

Figure 5.10 Updated crack depth ratios (α) with J_3 134

Figure 5.11 Updated crack depth ratios (α) with J_4 135

Figure 6.1 Crack development of box beam section..... 141

Figure 6.2 Loading state of a cracked beam element..... 142

Figure 6.3 FE model of the cracked box beam 146

Figure 6.4 Parametric study results for F^{V}_{I2}..... 147

Figure 6.5 Comparison of K^{V}_{I2} from FE modelling and Eq. (6.14) 148

Figure 6.6 Numerically simulated beam (Unit: mm)..... 149

Figure 6.7 Comparisons between numerically simulated and predicted frequency shifts 150

Figure 6.8 Updated crack depth ratios (α) of box beams (t_s/B = 0.1) 153

Figure 6.9 Comparisons between numerically simulated and predicted frequency shifts 155

Figure 6.10 Updated crack depth ratios (α) of box beams (t_s/B = 0.02) 156

Figure 6.11 Box beam specimens 156

Figure 6.12 Modal testing setup 158

Figure 6.13 Driving FRF curve at point P4 of beam H0 159

Figure 6.14 Comparisons of measured mode shapes from top and bottom accelerometers 160

Figure 6.15 Measured mode shapes for the first three bending mode from all 5 beam specimens 161

Figure 6.16 Comparisons between measured and predicted frequency shifts 162

Figure 6.17 Model updating results of crack depth ratios α 164

Table 1.1 Identified D_e values from different modes 6

Table 3.1 Measured and predicted natural and one-pin ABC frequencies (Unit: Hz) 44

Table 3.2 Measured and predicted two-pin ABC frequencies (Unit: Hz) 45

Table 3.3 Measured natural and ABC frequencies of damaged beams (Unit: Hz) 59

Table 3.4 Parametric setting for GA 63

Table 3.5 Measured and predicted natural and one-pin ABC frequencies (Beam B0; Unit: Hz) 69

Table 3.6 Measured and predicted natural and one-pin ABC frequencies (Beam B2; Unit: Hz) 70

Table 3.7 Measured and predicted natural and one-pin ABC frequencies (Beam B4; Unit: Hz)..... 70

Table 3.8 Measured and predicted two-pin ABC frequencies (Beam B0; Unit: Hz) 71

Table 3.9 Measured and predicted two-pin ABC frequencies (Beam B2; Unit: Hz) 71

Table 3.10 Measured and predicted two-pin ABC frequencies (Beam B4; Unit: Hz) 71

Table 3.11 Measured and predicted natural and ABC frequencies (Unit: Hz) 73

Table 4.1 Parametric settings for GA..... 101

Table 4.2 Updating results of free-free beam with $\alpha = 0.3$..... 102

Table 4.3 Updating results of simply supported beam with $\alpha = 0.3$ 102

Table 4.4 Updating results of cantilever beam with $\alpha = 0.3$..... 102

Table 4.5 Updating results of free-free beam with $\alpha = 0.5$..... 104

Table 4.6 Updating results of simply supported beam with $\alpha = 0.5$ 104

Table 4.7 Updating results of cantilever beam with $\alpha = 0.5$..... 104

Table 4.8 Updating results of cantilever beam with 5 elements 108

Table 4.9 Updating results of cantilever beams with non-centred crack 110

Table 4.10 Updating results with adapted mesh (Beam1) 111

Table 4.11 Updating results with adapted mesh (Beam2) 111

Table 4.12 Updating results of beam with multiple cracks..... 113

Table 5.1 Crack information of the aluminium beam specimens 118

Table 5.2 Measured natural frequencies f_N (±% denotes relative change from B0) 120

Table 5.3 Parametric settings of GA 127

Table 5.4 Updated crack locations (l_c) with standard mesh setting 127

Table 5.5 Updated crack locations (l_c) with coarser mesh setting 130

Table 5.6 One-pin ABC frequencies with ‘pin’ at P4 (f_A) 132

Table 5.7 Two-pin ABC frequencies with 'pins' at P4 and P10 (f_A) 132

Table 5.8 Updated crack locations (l_c) with J_3 134

Table 5.9 Updated crack locations (l_c) with J_4 135

Table 6.1 Cantilever box beams with $t_s/B = 0.1$ (Unit: Hz) 150

Table 6.2 MAC results between numerically simulated and predicted mode shapes 151

Table 6.3 Parametric settings for GA 152

Table 6.4 Updated crack locations (l_c) of the beams (Unit: mm) 153

Table 6.5 Cantilever box beams with $t_s/B = 0.02$ (Unit: Hz) 154

Table 6.6 Crack depth and location information 157

Table 6.7 Measured and predicted natural frequencies of beams H0, H1 and H2 (Unit: Hz) 160

Table 6.8 Measured and predicted natural frequencies of beams H3 and H4 (Unit: Hz) 161

Table 6.9 MAC results between measured and predicted mode shapes 163

Table 6.10 Model updating results of crack locations l_c (Unit: mm) 164

Declaration

I hereby declare that,

This thesis was composed by me and the work contained therein was solely the work of the author except otherwise acknowledged in the text.

No part of this thesis has been submitted for any other degree or professional qualification.

Signed: 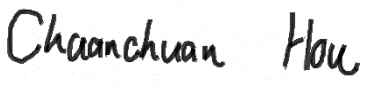

Chuanchuan Hou

The University of Edinburgh

Date submitted: 31/05/2016

Lay Summary

Like human beings, structures age and sometimes can get ill for various reasons. Damages can occur in the structures as a result of overloading, temperature effect, corrosion, impact, earthquake or fire. If not noticed and treated, small damages could lead to a catastrophic failure of the global structure. So it is important to keep monitoring the health condition of the structures during their service lives. In engineering, it is called 'structural health monitoring (SHM)'. There are several different approaches for SHM. One of the commonly used approaches is vibration-based. We have a structure and we use a hammer or other tools to excite it. The structure will vibrate due to the excitation. If we use suitable sensors such as accelerometers to record the vibration signals, it is possible to extract information that relates to the health condition of the structure. A simple explanation is that damage will change the way a structure vibrates.

In vibration-based SHM, one commonly applied method is the so-called model-based method. The basic idea here is that we do measurement on the real structure and extract inherent information from the vibration signals. At the same time, we establish a numerical model to represent the structural condition of the real structure. With the numerical model, we can calculate the same kind of information as obtained from the actual measurement for the structure. If the numerical model describes well the state of the real structure, the calculated information should match the measured counterpart. If it does not, as would usually be the case because of some unknown physical parameters, we then adjust the parameters in the numerical model to eventually get the calculated information to match the measured one. When this is achieved, the parameters adjusted or updated from this process should represent the physical state of the structure. By examining the updated parameters, we can check whether there is damage in the real structure.

The study presented in this thesis has been aimed at improving the robustness of the above approach from two important aspects. Firstly, it endeavours to enhance the information we can derive from the vibration of the structure. This part of the work has been devoted to expand the amount of frequency information that can be

extracted from the structure and investigate the practicality of obtaining such frequencies in a physical measurement environment. Secondly, it is about the description of the structural damage, particularly the cracks, in a more rigorous manner in the numerical model. In this way, the numerical model represents the crack damages more accurately and hence promotes more reliable identification of the crack damage from the model updating process.

Acknowledgements

I would like to express my gratitude and appreciation to my supervisor Professor Yong Lu for his unreserved support during my PhD study. He spent countless time discussing my topics with me and giving advice on research methodologies. His guidance means a lot to my academic career and I will always appreciate that.

The research reported in the thesis is partly funded by the Chinese Scholarship Council and the University of Edinburgh through a joint scholarship for my PhD study. I wish to thank the Chinese Scholarship Council and the University of Edinburgh for their support during all these years.

I thank the laboratory technicians in IIE for their support with my experimental work. Jim and Derek, thanks very much for the help.

I also want to thank my colleagues and friends in IIE - Chris, Colin, Harry, Hussain, JP and Utibe, with whom I had many enjoyable conversations about research and many other topics. I wish to thank Fengchen, Rongxin, Xiaobo and Jiaming for their company and help in my everyday life and research.

I am so grateful to have some local friends in Edinburgh during these years. I will always remember the joy I had with James, Donald, Avril, David, Serena, and Veronica. I will miss the days we went out to cinemas, trips and bars.

I would like to give special thanks to my girlfriend Shengfang. She sacrificed so much during these years and her support always means a lot to me.

Finally, I wish to thank my parents Tianhua and Xuehui, my sister Wanwan for always being there for me.

Abstract

Damage identification is an important topic in structural assessment and structural health monitoring (SHM). Vibration-based identification techniques use modal data to identify the existence, location and severity of possible damages in structures, often via a numerical model updating procedure. Among other factors influencing the practicality and reliability of a damage identification approach, two are of primary interest to this study. The first one concerns the amount and quality of modal data that can be used as 'response' data for the model updating. It is generally recognised that natural frequencies can be measured with relatively high accuracy; however, their number is limited. Mode shapes, on the other hand, are susceptible to larger measurement errors. Seeking additional modal frequency data is therefore of significant value. The second one concerns the errors at the numerical (finite element) model level, particularly in the representation of the effect of damage on the dynamic properties of the structure. An inadequate damage model can lead to inaccurate and even false damage identification.

The first part of the thesis is devoted to enhancing the modal dataset by extracting the so called 'artificial boundary condition' (ABC) frequencies in a real measurement environment. The ABC frequencies correspond to the natural frequencies of the structure with a perturbed boundary condition, but can be generated without the need of actually altering the physical support condition. A comprehensive experimental study on the extraction of such frequencies has been conducted. The test specimens included steel beams of relatively flexible nature, as well as thick and stiffer beams made from metal material and reinforced concrete, to cover the typical variation of the dynamic characteristics of real-life structures in a laboratory condition. The extracted ABC frequencies are subsequently applied in the damage identification in beams. Results demonstrate that it is possible to extract the first few ABC frequencies from the modal testing in different beam settings for a variety of ABC incorporating one or two virtual pin supports. The inclusion of ABC frequencies enables the identification of structural damages satisfactorily without the necessity to involve the mode shape information.

The second part of the thesis is devoted to developing a robust model updating and damage identification approach for beam cracks, with a special focus on thick beams which present a more challenging problem in terms of the effect of a crack than slender beams. The priority task has been to establish a crack model which comprehensively describes the effect of a crack to reduce the modelling errors. A cracked Timoshenko beam element model is introduced for explicit beam crack identification. The cracked beam element model is formulated by incorporating an additional flexibility due to a crack using the fracture mechanics principles. Complex effects in cracked thick beams, including shear deformation and coupling between transverse and longitudinal vibrations, are represented in the model.

The accuracy of the cracked beam element model for predicting modal data of cracked thick beams is first verified against numerically simulated examples. The consistency of predictions across different modes is examined in comparison with the conventional stiffness reduction approach. Upon satisfactory verification, a tailored model updating procedure incorporating an adaptive discretisation approach is developed for the implementation of the cracked beam element model for crack identification. The updating procedure is robust in that it has no restriction on the location, severity and number of cracks to be identified. Example updating results demonstrate that satisfactory identification can be achieved for practically any configurations of cracks in a beam. Experimental study with five solid beam specimens is then carried out to further verify the developed cracked beam element model. Both forward verification and crack damage identification with the tested beams show similar level of accuracy to that with the numerically simulated examples.

The cracked beam element model can be extended to crack identification of beams with complex cross sections. To do so the additional flexibility matrix for a specific cross-section type needs to be re-formulated. In the present study this is done for box sections. The stress intensity factors (SIF) for a box section as required for the establishment of the additional flexibility matrix are formulated with an empirical approach combining FE simulation, parametric analysis and regression analysis. The extended cracked beam element model is verified against both FE simulated and

experimentally measured modal data. The model is subsequently incorporated in the crack identification for box beams. The successful extension of the cracked beam element model to the box beams paves the way for similar extension to the crack identification of other types of sections in real-life engineering applications.

1 Introduction

1.1 Background

Vibration based structural damage identification is an important topic in the area of structural health monitoring (SHM). It employs modal data, including natural frequencies and mode shapes, to identify the possible damages in the structures. It is generally recognized that there are four levels of damage identification: 1) determining whether there is damage in the structure; 2) determining the location of the damage; 3) determining the severity of the damage; 4) predicting the remaining service life of the damaged structure (Rytter, 1993). There has been a large amount of research published in SHM literature. Doebling, et al. (1996) and Sohn, et al. (2004) have presented two extensive reviews on the related topics.

Generally, the various types of damage identification methods can be subdivided into model-based and non-model-based methods (Farrar and Doebling, 1997). Non-model-based methods directly employ the changes of modal parameters to identify the possible damages in the structures. Damage identification methods based on the direct comparison of changes to modal data, such as mode shape curvature or modal strain energy, belong to this category (Pandey, et al., 1991; Shi and Law, 1998). Model-based damage identification methods, on the other hand, require a sound model for the structure, which can be a detailed finite element (FE) model or a simplified structural model, to predict the dynamic properties of the real-life structure. The model can then be updated by matching the measured modal data from the structure to indicate the possible damages.

FE model updating is to adjust the parameters of the numerical model to fit the measured response of the structure (Friswell and Mottershead, 1995; Mottershead, et al., 2011). To get an accurate and meaningful updating, two essential factors must be dealt with carefully, namely 1) there must be sufficient amount of modal data with high accuracy as input data for the updating; 2) the numerical model should be able to represent the real-life structures as close as possible to avoid any significant model errors. The two aspects will be separately discussed as follows.

1.1.1 Limitation of the conventional modal data

The first requirement is quite a natural one as it is not possible to get correct output from an erroneous input. Also, to avoid under-determination for the updating solution, the number of accurate modal data must be larger than that of updating parameters. In vibration based model updatings, natural frequencies and mode shapes are the most often used modal data.

It is generally recognized that the measured modal frequencies have quite high accuracy but the errors in the measured mode shape displacement can be much larger (Jones and Turcotte, 2002; Mottershead and Friswell, 1993). Moreover, in practice generally only the translation mode shapes of a system at some discrete points can be measured and this necessitates the mode shape expansion or FE model reduction and such process introduces additional errors.

Many mode shape-based techniques have been developed for fault identification (Pandey, et al., 1991). These techniques utilize changes in the mode shapes or in the mode shape derivatives. Although many such techniques have proven as effective using clean data generated from numerical simulations, their application in practice has been rather limited since the mode shapes of higher orders can hardly be measured with the required accuracy. The difficulties in utilizing the measured mode shapes in actual damage detection have been demonstrated in a number of laboratory experimental studies, whereby in most cases only the first and second mode shapes were proven as useable in the mode shape based approaches (Qiao, et al., 2007; Ratcliffe, 1997; Shi and Law, 1998; Shi, et al., 2000).

When it comes to using the natural frequency information for the damage detection, an obvious limitation is that only the first few modes of natural frequencies can be measured from a structure and thus the total number of useable frequencies is very limited. This renders the use of natural frequencies alone to be insufficient for solving relatively complex problems involving many variable parameters. Therefore, an enhanced ability to acquire additional modal frequency data is highly desirable in the general damage detection and structural identification field.

1.1.2 Modelling errors in the conventional damage model

Modelling errors come from the assumptions made to characterise the mechanical behaviour of the physical structure. Mottershead et al. (2011) has listed several possible modelling error sources, such as inappropriate simplifications of the structure or erroneous modelling of boundary conditions. When there are modelling errors, it is still possible to update the model and reproduce the measured data of the structure. But the updated model might lose its physical meaning and may not be able to predict the structure response under a different type of loading or beyond the frequency range used in the updating.

In model-based damage identification, there is another possible source of modelling errors, which is the modelling of damages or in general terms the choice of the damage parameters. Damage in a structure is generally localised, thus its effect on the structural response can vary with different loading and deformation conditions. From the structural modelling point of view, the effect of the localised damage can be more comprehensively represented if a detailed continuum FE model is employed. However, a detailed continuum model can hardly be adopted for general damage identification purpose due to the inherent restrictions relating to the damage sensitivity and the limited amount of measurement information. For this reason, simplified models are generally required.

Herein we use beam type structures as example. Beam elements are commonly used for FE model of beam structures. In a beam component, damage often takes the form of cracks. Several different damage models have been used in previous studies to represent the effect of cracks. Friswell and Penny (2002) reviewed the subject of crack modelling for structural health monitoring. Generally there are four representative crack models for beams. The first one, which is arguably most widely used, is the local stiffness reduction method. It models the effect of crack by a reduction of the bending stiffness of the cracked beam segment. The second one is the discrete spring model. It divides the cracked beam into different segments at the possible damage locations. The segments are pinned together and rotational springs are added at the damage locations to simulate the remaining bending stiffness. By adjusting the stiffness of the rotational spring, different levels of damage can be

simulated. The third approach stems from establishing the local flexibility of the cracked beam in relation to the strain energy release rate. The strain energy can be evaluated with the fracture mechanics. The last approach derives a continuous vibration equation for the cracked beam based on assumed stress and strain fields around the crack area.

Among the four crack models, the reduced stiffness method is the simplest method and is still the predominant approach widely used in model updating and damage identification of beams, especially in civil engineering structures (Cerri and Vestroni, 2003; Dilena and Morassi, 2009; Unger, et al., 2006). As a result, the reduced stiffness model is chosen to demonstrate the modelling error.

The reduced stiffness method is most often implemented by a reduction of the modulus of elasticity, or the flexural rigidity, for a cracked beam element. In terms of the element stiffness, this means the relationship between the stiffness matrix of a cracked element and the intact element is as follows:

$$\mathbf{K}_{\mathrm{e}}^{\mathrm{d}} = (1 - D_{\mathrm{e}})\mathbf{K}_{\mathrm{e}}^{0} \tag{1.1}$$

where, $\mathbf{K}_{\mathrm{e}}{}^{0}$ and $\mathbf{K}_{\mathrm{e}}{}^{\mathrm{d}}$ are the element stiffness matrices of the intact and cracked elements, respectively. D_{e} is the parameter which indicates the severity of the crack. D_{e} ranges between 0 and 1; larger D_{e} value means deeper crack in the element.

The implication of the reduced stiffness method is that the stiffness matrix of the cracked element is proportional to that of the intact one. It treats the stiffness reduction as uniform to all degrees of freedom in the cracked element. This can only happen if the actual reduction of the rigidity along the length of the cracked element is uniform. Obviously this is not true in a real cracked beam. The stress will exhibits a concentration at the crack tip and decay rapidly as the location moves away from the crack. As a result, the plane section assumption used in the Euler and Timoshenko beam theories will not be met in the immediate neighbouring region of the crack location. The materials in the vicinity of both sides of the crack will not be stressed and thus contribute little to the stiffness of the section (Sinha, et al., 2002).

As a result, using the element stiffness matrix of Eq. (1.1) will introduce modelling error into the global stiffness matrix of the FE model, which will in turn result in

errors in the predicted modal data. The modelling error can sometimes be so large that the element damage severity predicted by this method, which is presented with the parameter D_e, could become inconsistent and even contradictory when different sets of modal data are employed. Numerical examples are used to demonstrate this effect in what follows.

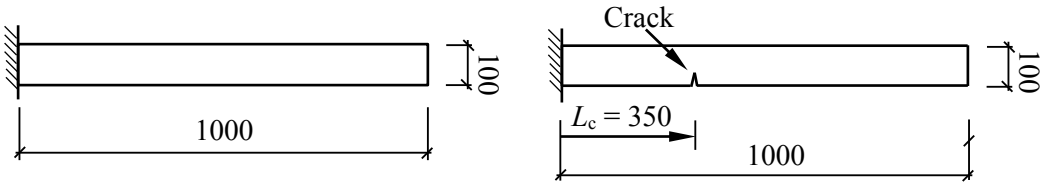

(a) Intact (b) Cracked

Figure 1.1 Example beams with a length to sectional depth ratio of 10 (Unit: mm)

A beam with a length to sectional depth ratio (L/B) of 10 is used to demonstrate the problem with the reduced stiffness method, as shown in Figure 1.1. Beams of such slenderness are typical in civil engineering structures. The crack is located at L_c = 0.35L from the left end and the crack depth is assumed to be 0.4B.

To generate the required numerically simulated modal data for the beam, a refined FE model using continuum solid elements (CPS8R in ABAQUS) is employed to simulate the beam and natural frequencies and mode shapes of the first 6 modes are obtained. The beam is then modelled with Timoshenko beam elements with a high accuracy 3rd order shape function. The Timoshenko beam is discretised into 10 elements of equal length, and the crack is thus incorporated in the 4th element.

There is no simple physical relationship to determine the stiffness reduction factor D_e for the assumed crack. Following the idea of parameter identification, D_e may be determined from an FE model updating process to fit the measured modal data. In the present demonstrative case, there is only one unknown parameter, being the stiffness reduction ratio D_e of the 4th element, to be determined. Therefore one modal frequency is enough for the updating. The first 6 numerically simulated natural frequencies are used to identify D_e separately. The results are presented in Table 1.1.

Table 1.1 Identified D_e values from different modes

Mode	D_e
1	0.653
2	0.636
3	0.119
4	0.111
5	0.668
6	0.491
Mean	0.446
Standard deviation/mean	0.592

It can be seen that the D_e results based on the first two modes are quite close, around 0.6. It means 60% of the element stiffness is lost due to the crack. However, modes 3 and 4 yield very low D_e values, indicating very light damage. The ratio of the standard deviation to the mean value is as large as 0.592. It means that for the beam with a slenderness ratio of order of 10, which is common in structural engineering applications, no consistent D_e value can be obtained from different modes with the reduced stiffness model.

Upon further check of the mode shapes and the mode shape curvature, which are not shown here, it can be found that for mode 4, the cracked element is at a relatively small curvature location, and this would cause the respective modal properties to be less sensitive to the changes (of stiffness) at the cracked location. However, this is not the case for mode 3, for which the mode shape curvature at the cracked location is relatively high. Therefore, the discrepancy in the equivalent stiffness reductions shown in Table 1.1 can only be concluded as a result of different stiffness effect of the same physical crack in different modes. That is to say, the usual stiffness reduction approach, whereby a single stiffness reduction factor over a certain element length is employed to represent the effect of a physical crack, is inherently flawed, especially when applied on thick beams under consideration.

A further perspective of the issue with the reduced stiffness approach is demonstrated by performing an updating for an optimized D_e value by the best fit to all of the 6 modes. The D_e value so obtained in this case is 0.635. The modal frequencies with this stiffness factor for the cracked element stiffness are then calculated, and these are compared with the numerically simulated data in Figure 1.2. It can be seen that only mode 1, mode 2 and mode 5 match reasonably well in the results, the 3rd and 4th modes have quite large errors of order of 4-6% in absolute terms with respect to the baseline frequencies.

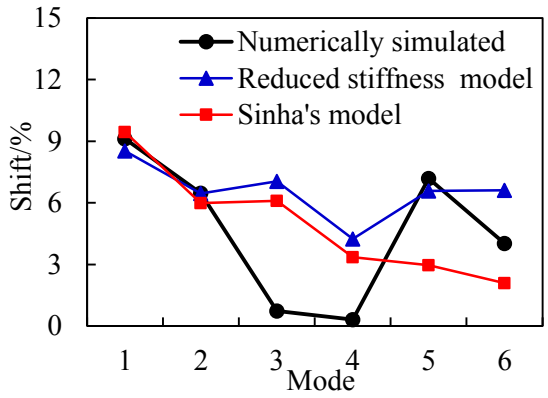

Figure 1.2 Numerically simulated and predicted frequency shifts

A seemingly straightforward consideration in improving the situation, still using the stiffness reduction approach, would be to refine the element discretization such that the variation of the stiffness change surrounding a crack could be better represented. However, in a real updating problem where the crack location is not known, this approach would imply an increase by many times the number of unknown parameters, and hence is unlikely to be implementable. Moreover, even with a refined discretization, the result may not turn out to be satisfactory. Herein the same cracked beam example is used to demonstrate this. We employ Sinha, et al. (2002)'s method, which will be discussed in more detail in Chapter 2. This method describes the stiffness distribution surrounding a crack by a shape function, and so is essentially of similar effect to refining the discretization. The estimated frequency shifts with Sinha's model are shown in Figure 1.2. It can be seen that the result has not improved significantly from those using the simple stiffness reduction approach.

The above numerical examples demonstrate that with the reduced stiffness model, inconsistent or conflicting indications of the severity of the crack damage are unavoidable from using data from different modes. Using an optimized procedure could reduce the overall error in matching the modal frequencies collectively, but this procedure does not address the inherent problem that a cracked region in a thick beam cannot be fully represented by a single stiffness reduction factor; consequently the result can still yield large errors in some of the modal frequencies. The implication is that in the inverse damage identification process, in which the crack location is also unknown, and there may be multiple cracks involved, marked errors can result from the use of the stiffness reduction method. To overcome this problem, a more accurate model needs to be considered to represent the crack in a damage identification or model updating application.

1.2 Objectives and Scope

In correspondence with the two challenges discussed above in the vibration-based damage identification practice, the key objectives of this research are two folds. The first one is to enhance the frequency dataset from modal tests by employing the so called 'artificial boundary condition' (ABC) frequencies. The concept of ABC frequencies is first explained and experimental modal tests are carried out to extract ABC frequencies from some laboratory-scale structures, including 3 relatively flexible steel beams, 5 relatively rigid aluminium beams and an RC beam. The accuracy of ABC frequencies is comprehensively evaluated. Finally, the performance of ABC frequencies in model updating and damage identification is verified with the experimental beams.

The second topic concentrates on the modelling and damage identification of cracks in relatively thick beams. As discussed in Section 1.1.2, modelling errors in the conventional damage model are quite large for thick beams and some more sophisticated model is required. The first task in this part of study is to establish a suitable crack model for thick beams. After a comprehensive review of several crack modelling approaches as available from the literature, a cracked beam element model

for crack identification is formulated based on the local flexibility and fracture mechanics principles. The adequacy of the model is verified in a forward manner by comparing the predicted natural frequencies of the cracked beam with the 'actual' results generated from a refined finite element analysis. Subsequently, the cracked beam element model is implemented in a general finite element model updating procedure. An adaptive model updating strategy is developed to tackle the randomness of crack locations so the method can be applied on beams having arbitrary number of cracks at arbitrary locations. The developed cracked beam element model and model updating strategy are lastly verified against modal testing results of 5 laboratory-scale aluminium beams.

The developed crack modelling and identification framework is then extended to be applied on specific beam types, herein beams with box section. An extended cracked beam element model is developed to suit the fracture mechanical properties of box section beams. The extended model is verified against numerically simulated and experimental modal data for both forward modal estimation and inverse crack identification performance.

1.3 Organization of the thesis

The thesis is subdivided into 7 chapters. The first chapter is the introduction. In Chapter 2, a survey of relevant topics in the area of vibration-based damage identification is presented, including the recent progresses in modal testing practices, the application of antiresonances in model updating, the advantages and short backs of the existing crack models and the relative topics on modelling of box section beams.

In Chapter 3, the possibility of extraction good quality one-pin and two-pin ABC frequencies is tested with experimental beams. A relative simple modal testing setup with a flexible steel beam is first employed in the modal tests. Several possible error sources in the measured frequencies are discussed and the accuracy of the measured ABC frequencies is evaluated. Subsequently, the effectiveness of incorporating the measured ABC frequencies in model updating and damage identification application

is illustrated. Finally, ABC frequencies are extracted from modal tests of a group of thick and stiff aluminium beams and an RC beam to evaluate their measurement accuracy from more sophisticated structural conditions.

In Chapter 4, a robust crack damage identification approach via model updating is developed for thick beams. A cracked beam element model is first formulated based on local flexibility and fracture mechanics. Its accuracy in estimating of modal parameters is subsequently verified with numerical examples. To identify cracks in beams with arbitrary number of cracks at arbitrary locations, an adaptive model updating strategy is developed. The crack damage identification procedure is verified with various types of practical crack scenarios to show its robustness. The conventionally used crack model, i.e., the reduced stiffness model, is also employed throughout the verification to serve as a comparison to the current model.

In Chapter 5, the crack damage identification procedure with the cracked beam element model is further verified with experimental modal testing results. Five aluminium thick beams with different configurations of cracks are prepared and modal tested. The first few modes of natural frequencies and mode shapes are obtained from the tests. The measured results are then used to verify the accuracy of the cracked beam element as well as the effectiveness of the crack damage identification procedure. The effectiveness of incorporation ABC frequencies in the crack identification of the aluminium beams is also checked.

In Chapter 6, the crack identification problem of box section beams is investigated. The crack identification procedure developed in Chapter 4 is employed for the box section beams. First the cracked beam element model presented in Chapter 4 is extended to model cracks in box section beams. To formulate the local flexibility matrix, the stress intensity factors of the box section beams are established with an empirical approach. The crack beam element model is then verified with numerically simulated and experimentally measured modal data for both modal data prediction and crack damage identification.

Chapter 7 presents the conclusions of the current study and recommendations on further research directions.

2 Literature review

There is a large amount of literature in the area of vibration based damage identification. In this chapter, some of the most related topics are reviewed. The content is organized as follows. First the recent practices in modal testing and model updating are reviewed to provide a general picture of the current research scope. The second part concentrates on the past efforts to enhance the conventional modal dataset and the most prominent one is by using the antiresonances of driving frequency response function (FRF) curves. The third topic is about the crack modelling in beam-type structures. Some of the most notable models developed in the past decades are summarized and commented to determine the most suitable option for further development and implementation in the modelling of thick cracked beams. As part of the development to extend the crack model to box section beams, some issues relating to the modelling of box section beams are summarized in the last section.

2.1 Recent progress in modal testing practices

Modal testing is to 'test the components or structures with the objective of obtaining a mathematic description of their dynamic or vibration behaviour' (Ewins, 1984). With modal testing the modal data, including but not limited to natural frequencies and mode shapes, of the structures can be obtained and used for purposes such as model updating of the numerical models for the structures and identification of the possible damages.

Modal testing for method development is usually carried out in laboratory as the environment is relatively easy to control. The environmental noise level can be minimized while the structures are made easier to excite and measure.

Casas and Aparicio (1994) applied modal testing and damage identification on several groups of simply-supported reinforced concrete beams. A total of 8 intact and damaged RC beams with dimensions as $L \times b \times h = 1500 \times 100 \times 70$ mm (where L, b, h are the span length, sectional width and height, separately) were tested with impact

hammer. Damages in the beams were presented as concrete cracks induced with formwork dispositions during concrete pouring, which was represented with parameters as damage location, extension as well as second moment area of the damaged area in this study. Natural frequencies of the first two modes and mode shape amplitude of the first mode were obtained from the tests and were then used to do damage identification on the beams. Finite element modal updating was used to do damage identification. Generally good results were obtained with the identification procedure.

Peeters, et al. (1996) conducted static and dynamic tests on undamaged and damaged reinforced concrete beams. The beam had a total length of 6 m and rectangular cross section as 200 × 250 mm. Static load was first applied on the simply supported beam to induce damages along the beam span. Subsequently dynamic tests were applied on the beam with free-free boundary conditions. Both impact hammer and electromagnetic exciter were used to excite the structure. Although the excitation force can be measured in the tests, only the output signals were used to do modal analysis in the time domain. Eigenvalues and mode shapes of the first several bending and torsion modes were obtained. The study showed that eigenvalues generally decreased due to damage while damping tended to increase. Mode shapes were also be influenced.

Ndambi, et al. (2002) compared the workability of several criteria in damage identification, including natural frequencies, Modal Assurance Criterion (MAC), Coordinate Modal Assurance Criterion (COMAC), strain energy, and flexibility matrices. RC beams (6000 × 200 × 250 mm) were used in laboratory modal testing. The RC beam was first statically loaded in induce damages and six degrees of loading were applied. After each static loading, dynamic modal testing was carried out. The beams were suspended with elastic springs to simulate free-free boundaries in modal testing and electromagnetic shaker was used to apply the excitation. With the 12 accelerometers attached on the beam, response of the beam both in bending modes and torsion modes can be recorded. The obtained natural frequencies and mode shape derivatives were used to do damage identification and the results were

compared. It showed that each criterion has its advantages and disadvantages, and strain energy method seemed to have the highest accuracy.

Morassi and Rocchetto (2003) experimentally studied the influence of damage on the modal parameters of steel-concrete composite beams. Four steel-concrete beams, two with partial connection and two with total connections were tested under impact excitation. Damage was induced in the beams by removing the concrete near the connections in the slab. The boundary conditions of the beams were free-free and both longitudinal and transverse excitations were carried out. Natural frequencies, mode shapes as well as damping ratios of the first 7 flexural modes, and natural frequencies and damping ratios of the first 5 longitudinal modes were obtained from the modal testing. The obtained parameters were then used to evaluate the sensitivities of the natural frequencies and mode shapes of to the damages.

Cerri and Vestroni (2003) presented modal testing results on reinforced concrete beams with dimensions as $L \times b \times h = 2250 \times 100 \times 150$ mm. The damage states of the beams were created by applying static loading in the mid-span of the beam. Seven load steps were applied on the beam and in corresponding seven degrees of damage can be recorded. In modal testing, the beams with free-free boundary conditions were excited by pseudo-random force transmitted by a shaker. The first five modes of natural frequencies were derived from the dynamic test results. Subsequently the obtained natural frequencies were used to do damage identification. Similar to Casas and Aparicio (1994), three parameters, i.e., damage location, extension and degree of stiffness reduction were chosen to represent the damages. The objected function established in the damage identification procedure is based on the theoretical frequencies of Euler's beam with consideration of damage parameters. Results show that good agreements on damage extension and degree of stiffness reduction can be achieved provided that the location of the damage is known. However, if the location is not known, the problem will be ill-conditioned.

Unger, et al. (2006) studied the damage identification of a post-tensioned RC beam. One challenge for damage identification of such structures is that the cracks in the beam might close due to the prestressing. The beam was gradually damaged under bending and after each static loading it was modal tested. In the modal testing

program, the beam was supported on air cushions to simulate free-free boundary conditions. The beam was excited by a falling weight at the end of the beam end. As the impact force was not measured, modal testing was carried out through time domain stochastic subspace identification method. Natural frequencies and mode shapes of the first four modes of bending and torsion modes were obtained. FE updating was then applied to do damage identification and it was found that damage pattern was difficult to be identified in the early damage state but can be detected at the final failure stage.

Zonta and Bernal (2006) employed a 200×300×5600 mm RC beam to compare the performances of several mode shape-based damage identification methods. It was stated that directly comparing the mode shapes measured before and after the damage of the structure could not always provide correct damage location for the structure. So the mode shape information needs to be rearranged to form some mode-shape based derivatives to increase the sensitivity to damages. Two of the common approaches were employed in for comparison in the paper, the first one being the strain-flexibility method and the second one being the Damage Locating Vectors (DLV) method. Damages in the beam were created by gradually loading the structure under a three-point loading system. Damage identification results on the same beam showed that the strain-flexibility method was able to give information on the severity of the damage while the DLV method could only provide the position of the damage. But in real-life measurements, the DLV method tends to be more robust when measurement noise, modal truncation and modelling errors are presented.

Moaveni, et al. (2008) did modal testing on a large-scale carbon/epoxy shell composite beam. The beam was damaged under four-point bending. In modal testing, the beam was simply supported and two different types of excitation methods were applied, namely, excitation with a electrodynamic shaker and impact with a hammer. It was found that the signal to noise ratio (SNR) of the impact response data is much higher than that of shaker and as a result, the impact data were used in the followed analysis. Natural frequencies, damping ratios and mode shapes of the first five modes were obtained and used in the updating of the composite beam.

Baghiee, et al. (2009) did a comparative study on the effectiveness of several damage identification methods, namely the natural frequency change based method, Modal Assurance Criterion (MAC) based method, Coordinate Modal Assurance Criterion (COMAC) based method and Modal curvature change based method. Modal tests were carried out on 9 RC beams with different concrete strength and steel ratios. The beams were damaged under four-point load bending and CFRP were used to strength the beams after damage. Boundary conditions of the beams were set to be free-free and impact hammer was used to excite the structure. The first four modes of natural frequencies and mode shapes were obtained for the beams. The sensitivities of listed damage indicators were compared and the authors stated that natural frequencies are strongly influenced by environmental factors, such as concrete shrinkage and temperature, and as a result is not a good indicator for damage identification. While the COMAC values calculated based on curvature are more reliable for damage identification.

Tsang and Chu (2011) performed modal testing on three RC cantilevered balcony structures. Damages in the structures were induced by gradually cutting the steel bar sectional area in the tensile area of the slab. During modal testing, the slab was fixed on a thick RC with a massive pedestal base. Impact hammer was used to excite the structure and the FRF curves were obtained. From the FRF curves, the first three natural frequencies were obtained.

Razak and Fayyadh (2013) experimentally studied the relationship between the natural frequencies and the composite effects in reinforced concrete. Two simply-supported RC beams (2200 × 150 × 250 mm) with different steel ratios were gradually damaged by three-point bending load. After each static loading, modal testing was applied on the beam. Electromagnetic shaker was used to apply white noise excitation on the beam and acceleration data were measured at the same time. Frequency response functions were calculated and natural frequencies were obtained through curve-fitting. Test results show that the composite effects in the beams have different effects on different modes of natural frequencies.

The above mentioned modal testing practices mainly focus on RC or composite structures. Literature about modal tests on steel structures, including steel beams and

space structures, can be found in Section 2.2.1. From this review it can be seen that in many of the modal testing practices for method development, the tested structures have often be set in a free-free support condition to avoid brining in the complexities from the boundaries. Some tests put the structures on simply supported or cantilever boundaries, such as Moaveni, et al. (2008) and Tsang and Chu (2011). For this kind of tests, it is important to evaluate the influence of boundary supports. If necessary, the supports should be treated as unknown parameters in the model updating process. Impact hammer was the most often used excitation method in laboratory while shaker was also employed in some studies. Signal processing techniques, such as windowing and averaging, were generally employed for extracting modal parameters. It can be seen that generally the first 3-7 modes of natural frequencies and mode shapes were obtained from the tests, whereas damping ratios were not frequently extracted and used for damage identification purpose.

2.2 Model updating with enhanced frequency dataset

As stated in Chapter 1, the two conventional modal data have inevitable short backs. To enhance the modal dataset, the antiresonances of driving FRF curves and the so-called artificial boundary condition (ABC) frequencies have been studied in the past two decades.

2.2.1 Antiresonances (zeros) of driving FRF curves

In the late 90s, several researchers noticed the potential value of antiresonances in driving FRF curves. Rade and Lallement (1998), Wahl, et al. (1999) pointed out that the zeros of driving FRF can be related to the resonances of the structure with extra boundary constrains, which offers an alternative for physical mass/stiffness modification to enlarge the modal database. As the measurement of the zeros can be more accurate than mode shapes and theoretically their number could be infinite, it seemed to provide an effective way to enlarge reliable experimental modal data.

Mottershead (1998) investigated the sensitivity of zeros to damage. It shows that the sensitivities of zeros can be expressed as a linear combination of the sensitivities of

eigenvalues and eigenvectors. What's more, their sensitivities are mainly contributed from the nearest eigenvalues and eigenvectors. Hanson, et al. (2007) verified the sensitivities of zeros based on numerical and experimental tests. The aim is to check the contribution ratio of sensitivity from eigenvectors in the zeros. If the ratio is relatively large, it means that the contribution of sensitivity from mode shapes is large. They used a 2-DOF model of a rigid beam supported on two springs to do theoretical modelling. Results show that the ratio highly depends on the geometry of the model and the choice of updated variables. The zeros contain little information from the eigenvectors at some calculation scenarios. The subsequent experimental verification on a 2-DOF rigid beam and a petrol generator showed that the participation of antiresonances does not improve the updating results noticeably. The works by Mottershead (1998) and Hanson, et al. (2007) showed that although the number of 'zeros' sets is infinite in theory, not all of them are effective for structural identification.

The use of antiresonances in model updating and damage identification has been a subject of much attention in the research community over the last 15 years or so. A comprehensive review of the exist studies is presented below.

D'Ambrogio and Fregolent (2000) employed a combination of 6 resonances and 72 antiresonances from 12 driving FRF curves to update a frame structure in laboratory. The total number of unknown parameter is 16. The updated results are quite satisfactory, with an average error or 0.2% for resonances and 0.5% for antiresonances. Considering that the number of resonances is much smaller than the updated parameters, it strongly proves the effectiveness of antiresonances in the updating process. D'Ambrogio and Fregolent (2003) then applied the updating on the GARTEUR benchmark structure using both resonances and antiresonances. Results again show that better updating could be obtained compared with using resonances alone.

Jones and Turcotte (2002) updated a 6-m flexible truss structure with two different set of modal data: one with 11 resonances, the other with 11 resonances and 21 antiresonances. The number of updating parameter is 7. It shows that the updating

results with both resonances and antiresonances produce a 48% better correlation to measured FRF curves than those with only resonances.

Dilena and Morassi (2004) investigated the use of antiresonances for detection of symmetric crack in beams. Identification of symmetric cracks is always a challenge if only natural frequencies are used as natural frequencies are global properties. Test results on a rod and a beam show that the non-uniqueness of the problem could be avoided when antiresonances are used. However, it was found that the identification results with antiresonances could be worse that those with resonances in some data set. The reason is that the measurement errors in antiresonance might be larger than the frequency shifts brought by damage.

Bamnios, et al. (2002), Douka, et al. (2004) and Dharmaraju and Sinha (2005) discussed the possibility of using antiresonances for crack identification in beams. Bamnios, et al. (2002) stated that crack in beam will bring substantially changes in antiresonances of FRF curves and the changes depend on the location and size of the crack. As a result the first antiresonance can be used as an indicator of crack in the beam. However, the experimental results of a beam offered by Dharmaraju and Sinha (2005) showed that it is quite difficult to achieve this goal. For in-field test, it might be more difficult due to the high noise level.

Lu and Tu (2004) employed resonances and antiresonances in the updating of a numerical multi-building frame. There are 6 updating parameters and only less than 4 natural frequencies are used, along with a selected group (2-5) antiresonance frequencies in the updating. The updating results showed high accuracy, which proves that the antiresonances provided new information to the modal data.

D'Ambrogio and Fregolent (2004) tried to use ‘virtual antiresonances’, which can be obtained from a truncated modal expansion, as an alternative to driving point antiresonances. Three groups of modal data, namely, resonances with antiresonances, resonances with virtual antiresonances, resonances with mode shapes, were used to update the ‘GARTEUR’ structure. It showed that good results can be achieved for all of the three groups and the best result came from the use of mode shapes. In the following verification of results on modified structure, updated parameters from

antiresonances and virtual antiresonances shower higher accuracy than those from mode shapes.

Nam, et al. (2005) established a 3-DOF mechanical system (with 6 updated parameters) and updated it with resonances and/or antiresonances. It showed that the maximum error in the results would be 1.81% if only 3 resonances were used. However, 100% accuracy can be achieved when 4 antiresonances from driving point FRFs were added in the modal data.

Kyprianou, et al. (2005) presented an inverse problem of structural modification with resonances and antiresonances. A portal frame with the leg on the right-hand side missing was used as an example. A beam was added to the original structure and modal parameters were used to identify the cross-section dimensions of it. Resonances and antiresonances were used in the identification. It showed that both resonances and antiresonances gave acceptable results.

Giannoccaro, et al. (2006) investigated the sensitivities of resonances and antiresonances to fatigue damage of steel bar. Test results demonstrated that both resonances and antiresonances showed clear shifts when fatigue damage was induced. However, there is larger uncertainty in the determination of antiresonances, which means that there might be larger errors in the measurement of antiresonances.

Dilena and Morassi (2009) did damage identification on rods with resonances and antiresonances. Acceptable results, both on the location of damage and stiffness deterioration, can be achieved, as long as the frequency shifts brought by damages are larger than noise and experimental errors. However, it also noticed that antiresonances are less easy to be measured than resonances, and they are more affected by noise and experimental errors. Dilena and Morassi (2010) then applied the approach to numerical and experimental beams, and similar conclusions were obtained for the beams.

Meruane and Heylen (2011) tried to use antiresonances from transfer FRFs in modal updating. They used parallel genetic algorithms to solve the matching problem for zeros in transfer FRFs. To demonstrate the effectiveness of antiresonances, two different groups of modal data were used, one with resonances and antiresonances, and the other with resonances and mode shapes. Damage identification with the two

groups of modal data was done on a gas exhaust system and a steel truss. Results showed that the antiresonance from transfer FRFs could be used in the updating. However, it also showed that the updating accuracy from mode shapes was higher than that from antiresonance, although the measurement accuracy of the former one was believed to be higher than the latter one.

Meruane (2013) used antiresonances with artificial neural networks to do modal updating. Only antiresonances from driving point FRFs were used as modal data. A damaged 8-DOF mass-spring system and a free ends steel beam were used in the investigation. Results showed that good updating results could be obtained for both of the structures. It proved that the antiresonances have large potential for the updating of real structures.

Meruane (2013) developed a method for antiresonances measurement from transmissibility functions, which can be used in output-only measurement tests. The antiresonances obtained were then used to do damage identification on a 8-DOF mass-spring system and a gas exhaust system. Two different sets of modal data, one with antiresonances, the other with resonances and model shapes, were used in the updating. Good results were obtained for both sets. However, higher accuracy was achieved with antiresonances for the mass-spring system, while better results were obtained with model shape data for the gas exhaust system.

Wroblewski, et al. (2014) did damage identification on a rotor system with resonances and antiresonances. Test results showed that with resonances and antiresonances, the location of the damage could be accurately obtained, however, the magnitude of damage was under predicted, the authors believed that the reason lies in the fact that some part of the rotor is difficult to model in the FE model.

The above summarized studies generally show that antiresonances can be employed to enhance the model updating of experimental structures. Comparisons of updating results with antiresonances and with mode shapes indicate that similar accuracy could be achieved. This suggests that antiresonances can serve as an alternative to mode shapes in the finite element model updating.

2.2.2 Artificial boundary condition (ABC) frequencies

Theoretically speaking, antiresonances in a particular FRF may be determined from the eigenmode analysis by eliminating a row and a column from both the stiffness and mass matrices of the original system, with the row and column corresponding to the force and response positions of the FRF, respectively (Mottershead, 1998). When the row and the column being eliminated are of the same number, i.e., a driving-point FRF case, then the antiresonances are exactly the natural frequencies of the modified system by adding a pin (restraint) to the corresponding DOF. It should be noted that no simple physical translation may be made of the situation where the eliminated row and column are of different numbers.

The above perspective of the driving-point antiresonances is in line with the more general concept of perturbed natural frequencies of a structure, in which case the boundary condition of the structure is to be physically altered (perturbed) so as to generate additional frequency information (Li, et al., 1995). The idea of the perturbed boundary condition frequencies, albeit novel, has found little scope of application because of the obvious impracticality of physically changing the boundary condition of a real structure. The driving-point antiresonances can be seen as a special case of the perturbed natural frequencies via adding one single pin support at a time; but by identifying the antiresonances on the driving point FRF of the "as-is" structure the need of physically adding the pin support is avoided.

The possibility of obtaining a diverse range of "perturbed" natural frequencies without the need of physically imposing additional supports has been theoretically established by Gordis (1996) and (1999) through the introduction of the concept of artificial boundary condition (ABC) frequencies. Using this approach, the natural frequencies of a structure with 'artificially' added (i.e. virtual) pin supports at certain locations may be derived from the incomplete frequency response function (FRF) matrix measured from the original structure. The term of 'artificial boundary condition' reflects the fact that, although the frequencies thus derived are equivalent to the natural frequencies of the perturbed system, the perturbed boundary conditions need not be actually imposed. In the case of one-pin ABC frequencies, the situation degenerates to the driving-point antiresonances (zeros) of the original structure with

a virtual pin added at the driving point. For this reason, and to be consistent with the general ABC frequencies discussed in the current study, hereinafter the driving-point antiresonances will be referred to as 'one-pin ABC frequencies'.

With the incorporation of the ABC frequencies, the modal frequency dataset can potentially be expanded drastically.

A series of studies has been conducted in this research group to evaluate the effectiveness of incorporating ABC frequencies in a comprehensive structural identification process (Lu and Tu, 2008), and look into the potential issues in extracting ABC frequencies from physical tests (Lu, et al., 2008; Mao and Lu, 2011). Lu and Tu (2008) did modal testing on a steel beam and obtained two-pin ABC frequencies from the tests. It was found that ABC frequencies can be obtained from the tests generally. However, there might be fault peaks in the ABC frequency function curves which are not real ABC frequencies. It was believed that high noise level and misalignment of sensors and impact positions might be the reasons for that. Mao and Lu (2011) tried to get one-pin and two-pins ABC frequencies from a steel beam and a slab in the lab. After a properly designed signal processing strategy, including applying RFP and SVD techniques, ABC frequencies can be obtained from the tests with acceptable accuracy. Continued effort is being made to evaluate different experimental aspects of extracting the ABC frequencies and improve the measurement accuracy, especially for ABC frequencies with more than one pin and in different structural and measurement configurations, and the use of such frequencies in structural damage identification.

As noticed by Mottershead (1998) and Hanson, et al. (2007), antiresonances from different locations have different sensitivities to the structural parameters. Selection of 'best' ABC configurations with high sensitivity thus becomes an important task. Tu and Lu (2008) employed binary genetic algorithm in combination with sensitivity analysis to select the ABC configurations with large sensitivity to damage. Their application of the method on numerical examples of frame structures showed that more accurate results can be obtained when the selected ABC frequencies were used in the modal updating process, compared with situations when only natural

frequencies were used. Gordis and Papagiannakis (2011) developed a selection strategy for ABC configurations based on QR decomposition with column pivoting.

2.3 Crack modelling in beams

The general influence of cracks on the vibration of beams has been extensively studied in the past, and comprehensive reviews have been published previously (Dimarogonas, 1996; Friswell and Penny, 2002). Most of these studies have been concerned about the vibration formulation for a cracked beam with known crack parameters, namely location and crack depth, and limited use has been made of these models for inverse crack identification or finite element model updating purposes. In this section, the key considerations and basic modelling outcome of a few representative methods are summarised.

2.3.1 Models based on stress fields

The presence of a crack in the beam will change the stress and strain fields in the vicinity of the crack. By assuming the stress and strain distributions in this area, the vibration equation of a cracked beam may be established.

Christides and Barr (1984) studied the vibration of Bernoulli-Euler beams with one or more pairs of symmetric cracks on both top and bottom sides of the beam. The bending stress in the vicinity of the crack is assumed to decay exponentially from its maximum value at the cracked section to the uncracked value in a certain distance away from the crack. With the assumed stress variation, a vibration function can be obtained for cracked Bernoulli-Euler beams. For a beam with rectangular section, the following function can be obtained:

$$EIQw^{iv} + 2EIQ'w''' + EIQ''w'' + \rho A\ddot{w} = 0 \tag{2.1}$$

where EI is the bending stiffness of the intact section, ρA is the mass of a unit length, and w is the transverse displacement. Q is an integrated crack function, $Q(x) = \left[1 + C\exp\left(-2\alpha|x - x_0|/d\right)\right]^{-1}$, where $C = I_0/I_d\text{-}1$, x_0 is the location of the crack,

d is the depth of the section and α is a coefficient obtained from experimental data, which is 0.667 according to Christides and Barr (1984).

It can be seen that the above equation is similar to that of the intact Euler beam. The only difference is that an 'equivalent' bending stiffness distribution $EIQ(x)$ is used in the function, instead of a constant value EI, as illustrated in Figure 2.1.

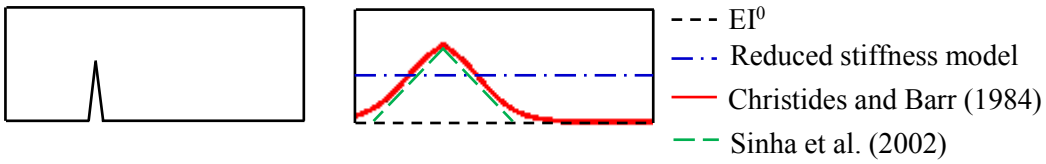

(a) Cracked beam segment (b) Stiffness distribution

Figure 2.1 Stiffness reduction of cracked element

In Christides and Barr (1984), the solution of coefficient α is only against the fundamental natural frequency. Shen and Pierre (1990) applied the same theory to evaluate both the natural frequencies and mode shapes of the cracked beam up to the lowest 3 modes. They used a Galerkin-type solution to calibrate the vibration function with finite element modelling results and got a new value for the coefficient α, as 1.936. The same authors then extended the theory to Euler beam with a single-edge crack (Shen and Pierre, 1994).

Chondros, et al. (1998) avoided assuming a stress field and established the displacement field in the vicinity of the crack based on Castigliano's theorem and the crack strain energy derived from the fracture mechanics. Once the displacement field is obtained, the strain and stress fields can be calculated, and subsequently a continuous beam vibration equation is established. The method is able to consider both single-edge and double-edge open cracks.

The above theories only considered bending deformation in the beams. Carneiro and Inman (2002) considered shear deformation in the continuous vibration function of cracked beams, extending the crack model to Timoshenko beams. They used a similar bending stress field assumption as in Shen and Pierre (1994). As the shear deformation is involved, they suggested a shear stress disturbance function. The function is based on a quadratic distribution of shear stress along the section depth.

Similar to normal stress, the shear stress is assumed to decay exponentially from the crack location with the same decay rate as normal stress.

The developed continuous beam vibration equations can be employed to calculate the natural frequencies and mode shapes of cracked beams, provided that the crack depth and location are known. However, it is not easy to directly employ the continuous vibration equations in damage identification practice, especially when more than one crack is presented in the beams. For damage identification purpose especially when the finite element updating approach is employed, a discretised cracked beam element model need to be developed.

Sinha, et al. (2002) proposed a cracked Euler-Bernoulli beam element based on Christides and Barr's theory. They simplified the bending stiffness distribution about the crack $EIQ(x)$ to a linear form, as shown in Figure 2.1. A cracked beam element can then be formed with the simplified stiffness distribution and cubic shape functions for standard Euler-Bernoulli beam element. In the developed stiffness matrix, the effect of the crack can be modelled with two parameters: the crack depth and the crack location. With the cracked beam element, both forward calculation and damage identification can be carried out. The first advantage of this model is that a 'realistic' distribution of bending stiffness surrounding the crack is used and expressed with crack parameters in the model. Therefore in principle both the crack depth and location can be obtained in damage identification. Also, as the crack is described locally with an individual beam element, there is no specific limit on the number of cracks in the beam. Examples of beams with two cracks were given and it was shown that reasonably good damage identification results could be achieved.

It should be noted that in the above model the distribution of the bending stiffness within a cracked beam element is based on an assumed exponential-type stress decay near the crack tip, and the stress decay rate α is obtained by fitting the first natural frequency of experimental cracked beam. Different α values may be obtained if another mode is used in the fitting, as has been shown in Shen and Pierre (1990). Consequently, inconsistent predictions may result for higher modes if the same α value is used, and this is evident from the example shown in Chapter 1. Moreover, the shear deformation is not included in the model. The example beams used in

Sinha, et al. (2002) had slenderness ratios in the range of 40-70, so the accuracies observed there could not be extended to thicker beams with a smaller slenderness ratio in terms of the effect of the shear deformation in a cracked beam. Finally, the model does not consider the coupling effect between the longitudinal and transverse modes, which, as will be discussed in Chapter 4, will have important influences in thick beams.

2.3.2 Methods based on the discrete spring model

This type of methods treats the cracked beam as two segments pinned together at the crack location. A rotational spring is added to the pin to model the effective bending stiffness in the cracked region.

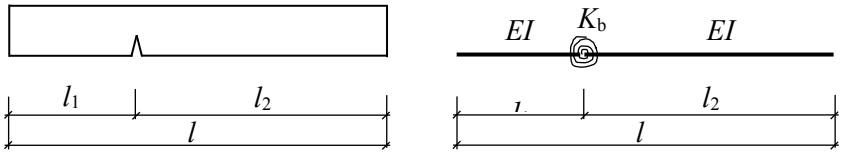

(a) Cracked beam segment (b) Cracked beam model

Figure 2.2 Discrete spring model

A typical discrete spring model is shown in Figure 2.2. The stiffness of the spring is related with the depth of the crack and can be obtained with fractural mechanics (Liebowitz, et al., 1967; Okamura, et al., 1973; Ostachowicz and Krawczuk, 1991).

The discrete spring model can be used to develop a continuous vibration function for a cracked beam. One representative example is Lele and Maiti (2002). It assumes that the two segments both follow Timoshenko's vibration equations. The rotational stiffness of the spring obtained by Ostachowicz and Krawczuk (1991) is used. The boundary conditions at the crack location can be established with the continuity of displacement, moment and shear force, and a jump in the slope which can be calculated with the rotational stiffness of the spring. The global vibration function can then be solved with the boundary conditions at the beam ends and crack location.

By covering the rotational spring element in one element, the model can also be used to develop cracked beam elements, such as the ones developed by Viola, et al. (2002)

and Mehrjoo, et al. (2014). In Viola, et al. (2002), the pinned segments were assumed to follow Timoshenko's theory and described with cubic shape functions. The shape functions were solved with the boundary conditions at the element nodes and crack location. With the shape functions and the unit displacement method, the stiffness matrix for the cracked beam element can be derived. Mehrjoo, et al. (2014) obtained a Timoshenko-theory based macro element for the cracked beam. They used the superposition principle and unit displacement method to obtain the stiffness matrix for the element without a need to use the shape functions.

Modelling the effect of the crack with a dimensionless spring should be a reasonable assumption if the influence range of the crack is relatively small with respect to the length of the beam (in the continuous vibration theory) or the length of the cracked element (in the macro beam element). Otherwise, using a dimensionless spring to represent the crack effect could introduce larger errors, especially for higher modes. Another problem is that the coupling of longitudinal and transverse vibration in a cracked beam cannot be reflected in the model.

2.3.3 Cracked beam element based on local flexibility and fracture mechanics

The third approach directly employs the local flexibility brought by the crack to calculate the stiffness of the cracked beam element. A brief review of this approach, hereinafter referred to as the "cracked beam element" model, is summarized below.

The local flexibility matrix of the cracked beam was initially introduced in the 1980's by Dimarogonas and Papadopoulos (1983), Papadopoulos and Dimarogonas (1987) and Papadopoulos and Dimarogonas (1987). According to fracture mechanics, for a cracked structure under a constant load F, the energy release rate G for the crack growth is equivalent to the rate of increase of the total strain energy U_T (Tada, et al., 2000). As a result, the total strain energy of the structure with a crack area A_c will be:

$$U_T = U_0 + U_c \tag{2.2a}$$

$$U_c = \int_{A_c} G \mathrm{d}A \tag{2.2b}$$

where U_0 is the strain energy of the intact structure under the constant load, U_c is the additional strain energy brought by the crack, and A_c is the effective crack area.

The energy release rate G can be expressed with the Stress Intensity Factors (SIFs) of the crack as (Tada, et al., 2000):

$$G = \frac{1}{E'}\left(K_{\mathrm{I}}^2 + K_{\mathrm{II}}^2 + \frac{1}{1-\nu} K_{\mathrm{III}}^2 \right) \tag{2.3}$$

where, K_{I}, K_{II}, and K_{III} are the stress intensity factors for three different types of cracks, namely opening, sliding and tearing; For plane stress, $E'=E$, and for plane strain, $E'=E/(1-\nu)$, where ν is the Poisson's ratio of the material.

With the total strain energy of the cracked beam, the flexibility can then be obtained by invoking Castigliano's theorem as:

$$c_{ij} = \frac{\partial U_{\mathrm{T}}}{\partial F_i \partial F_j} = \frac{\partial U_0}{\partial F_i \partial F_j} + \frac{\partial U_{\mathrm{c}}}{\partial F_i \partial F_j} \tag{2.4a}$$

$$\text{or} \qquad c_{ij} = c_{ij,0} + c_{ij,\mathrm{c}} \tag{2.4b}$$

where, c_{ij} is the total local flexibility and F_i is the force applied on the i^{th} DOF of the beam node. $c_{ij,0}$ is the flexibility of the intact beam element, and $c_{ij,\mathrm{c}}$ is the additional flexibility due to the presence of the crack.

The details of the flexibility matrix have been well documented (Dimarogonas and Papadopoulos, 1983). The flexibility matrix can be easily converted to a stiffness matrix for the cracked beam element through matrix inversion and a transformation matrix $\boldsymbol{T}$. This approach was used by the original authors in the analysis of the vibration of cracked beams and the investigation of the effect of coupling between transverse and torsional or longitudinal vibrations (Papadopoulos and Dimarogonas, 1987; Papadopoulos and Dimarogonas, 1987).

The same general approach via the additional flexibility due to a crack has been employed by several other authors to derive the cracked beam element for the beam vibration analysis or detection of a crack. Qian, et al. (1990) developed FE model with the cracked beam element to study the dynamic behaviour of a beam with crack closure. Lee and Chung (2000) incorporated the cracked beam element in a

procedure involving the rank-ordering technique to detect a crack with just the first four natural frequencies. However, the proposed procedure was limited to a single crack in a beam. Moreover, the effect of axial force was not considered. Zheng and Kessissoglou (2004) looked upon the cracked beam element with an arbitrary crack location, and examined the effect of the relative location of the crack on the additional flexibility of the beam element and hence the free vibration properties of the beam. Darpe, et al. (2004) studied the effect of coupling between bending, longitudinal and torsional vibrations of a circular shaft using the cracked beam element approach. The cracked segment was modelled using the cracked beam element while the remaining beam was modelled using the intact beam element model. Modelling of the 'breathing' behaviour of a crack during the rotor operation was also investigated. Nahvi and Jabbari (2005) employed the cracked beam element model in a flexural condition, without considering the axial DOFs, in a finite element analysis to generate the natural frequencies and mode shapes for a beam with a single crack. The FE results are used in a match-up procedure to identify the location and depth of the crack in an experimental beam.

In summary, it seems fair to state that the cracked beam element model formulated on the basis of the additional flexibility has overall superiority comparing to the other approaches. Using this model, the effects of a crack on the various aspects of the beam vibration, including coupling among the transverse, torsional and longitudinal vibrations, have been studied. The utilisation of the model for the detection of cracks in a beam has also been explored but this has largely been limited at a very basic level, and mostly with consideration of just a single crack. There is still a considerable scope to develop a more comprehensive approach to extend the use of this basic model to more complete identification of crack damages in a beam. Factors such as the randomness of the crack location, crack depth and the possible presence of multiple cracks should ideally all be taken into account.

2.4 Crack modelling for box section beams

2.4.1 One-dimensional beam element for box section beams

The static and dynamic characteristics of box beams can be solved with three-dimensional elasticity or three-dimensional finite element modelling (Liew, et al., 1995). However, these approaches generally involves complicated formulations or a large number of degree of freedom, which are not convenient for engineering applications, especially for model updating and damage identification purposes. On the other hand, one-dimensional beam element provides a simple but powerful model for the beam-like structures. In the area of model updating and damage detection of beam structures, Euler-Bernoulli or Timoshenko beam elements have been generally employed to form the numerical models (Cerri and Vestroni, 2003; Moaveni, et al., 2008; Unger, et al., 2006).

The classical Euler-Bernoulli or Timoshenko beam elements should also be able to model the box beams. However, it is well known that for thin-walled box beams under loading, some in-plane deformation cannot be neglected, such as warping, distortion and shear lag-effect. The result of warping and in-plane deformation is that the basic assumption for the classical beam elements, which is the plane section assumption, can no longer be held (Kim and Kim, 1999). When the classical beam elements are used in the static or dynamic analysis of thin-walled box beams, modelling errors will exist in the results. To overcome this issue, some more advanced one-dimensional beam models have been developed in the past to account the warping, distortion or shear-lag effect in thin-walled box beams. Carrera, et al. (2011), Carrera and Varello (2012) developed a refined beam theory for thin-walled structure with in-plane stretching considered. The obtained beam element has 9 degrees of freedom at each node, resulting in an 18×18 stiffness matrix. It shows that the developed model is able to model the in-plane deformation of thin-walled structures and predict the dynamic response very well. Kim and Kim (1999) developed a two-noded C^0 continuous thin-walled box beam element with the coupled deformation of torsion, warping and distortion considered. At each node, the axial rotation, warping, and distortion are used as degrees of freedom, and the resulted stiffness and mass matrices are of size 6×6. Another group of one-

dimensional beam elements tries to induce the shear-lag effect in the bending analysis of box girders (Luo, et al., 2002; Zhang and Lyons, 1984; Zhang and Lin, 2014; Zhou, 2010). These models used Reissner (1946)'s assumption of displacement function for shear lag warping to obtain the shear-lag induced axial stress distribution. The relationship between the vertical deflection and shear-lag induced angular rotation of the beam section can then be established. The beam stiffness matrix can be obtained from the strain energy of the beam element, in which the shear-lag induced rotation is generally used as an independent degree of freedom. As a result, the size of the stiffness matrix will be larger than the classical Euler-Bernoulli or Timoshenko stiffness matrix and the bending stiffness of the beam model is reduced due to the existence of shear-lag effect. Numerical results show that the prediction of deflections of transversely loaded beams with the new beam models will be larger than those with the classical models.

2.4.2 Stress intensity factors for cracked box section beams

The stress intensity factors (SIFs) are defined to represent the strength of the stress fields surrounding the crack-tip (Tada, et al., 2000). They are determined by the boundaries of the cracked body and loads imposed. SIFs for plane problems have been well established in the past, such as the handbook by Tada, et al. (2000). For 3D structures however, it is difficult to use some universal formation to calculate the SIFs as the shape of the 3D structures can be quite complicated. In the past several decades, many studied have tried to obtain the SIFs for various 3D structures. Tada, et al. (2000) summarized some of the methods, such as the boundary collocation method and the finite element methods. Toribio, et al. (2009), and Brighenti and Carpinteri (2013) provided some comparative reviews on the SIF calculations.

On dealing with the SIFs of thin-walled structures, such as T section, I section and box section structures, there have also been some studies in the past (Zerbst, et al., 2009). Two theoretically approaches are summarized here. The first one is the method developed by Kienzler and Herrmann (1986), Bažant (1990), and Gao and Herrmann (1992). The basic idea is that the strain energy release rate for the crack extension can be linked to the energy release rate for the crack widening. As the

crack widening energy is quite easy to obtain based on the bending theory, the strain energy release rate can then be calculated. In Kienzler and Herrmann (1986)'s theory, there is a coefficient β in the relationship between the energy of crack extension and widening. Bažant (1990) argued that this coefficient can only be obtained based on optimum fitting of the exact solution. Gao and Herrmann (1992) later showed that the coefficient can also be obtained based on simple asymptotic matching with standard limiting crack solutions. Dunn, et al. (1997) used Herrmann's method to obtain SIFs for I-section beams. To obtain the coefficient β in Herrmann's equation, FE modelling was used to get empirical data and then a simplified equation was obtained based on best-fit of the data. The obtained results were used to predict the fracture toughness of the I-section beams and quite accurate results were obtained. Ricci and Viola (2006) applied the method on T-section beams. They extended Herrmann's theory to all of the three modes of cracks. In their calculation, the value of β was taken as 1. The obtained SIFs were then used to develop a line-spring model for the cracked T-beams.

Another method is developed by Xie, et al. (1998), Xie and Wang (2004). They defined an integral G^* which is referred to as the crack mouth widening energy release rate. The integral G^* can be expressed with the SIFs. On the other hand, it can be obtained from the bending theory of beam. In the end, the SIFs can be calculated. Xie's method is actually quite close to Herrmann's method, both of which convert the crack extending problem to the crack widening one. The method has been used by several studied on different types of structures. Xie and Wang (2004) used it in T-section and I-section beams. Xie, et al. (2004) applied it on rectangular hollow tubes. Dotti, et al. (2013) calculated the mode I SIF of thin-walled beams made of laminated composites with the G^* conception and Dotti, et al. (2013) applied it on thin-walled open beams. Ghafoori and Motavalli (2011) used several different approaches to calculate the SIFs for I-section beam, Xie's method, Herrmann's method and FE approximation. It seems that Herrmann's method provided better results.

3 Experimental study of generating ABC frequencies and application in model updating

3.1 Introduction

As reviewed in Section 2.2.1, one-pin ABC frequencies (antiresonances or zeros) have shown good performance in model updating of experimental structures. But ABC frequencies with more than one pin have not been extensively studied from experimental prospects. Also, there is a lack of investigation on the measurement accuracy of ABC frequencies, although it is generally believed that antiresonances can be measured with similar accuracy as resonances (2003; D'Ambrogio and Fregolent, 2000).

This chapter presents a comprehensive experimental study into the extraction of the ABC frequencies in laboratory experiments, and the utilisation of such frequencies in the damage identification through a finite element model updating process. It will be shown that, with a carefully conducted modal testing procedure and the use of appropriate data processing techniques, reliable ABC frequencies can be obtained for damage identification purposes. Possible error sources in the measured ABC frequencies will be discussed and the accuracy of the obtained ABC frequencies will be evaluated. Furthermore, the experimental ABC frequencies before and after damage have been extracted to demonstrate the sensitivity of the measured ABC frequencies to damage. Subsequently, FE model updating is presented in which different sets of the modal data, including different combinations of natural modes and/or ABC frequencies, to illustrate the effectiveness of incorporating the ABC frequencies in a practical damage identification application. Finally, the possibility of extracting ABC frequencies from some more sophisticated structure conditions are evaluated with a group of stiff aluminium thick beams and an RC beam.

3.2 Overview of ABC concept and basic formulation

As mentioned in the review, modal frequency data for a given structure with added (perturbed) supports provide extended response information which can be used in the

structural parameter identification. However, the practicality of such a seemingly attractive idea has been hindered by the fact that imposing added support(s) on a real structure is not normally feasible.

The theoretical work by Gordis (1996) and (1999) paved a way for the potential application of the idea of the perturbed boundary frequencies in real structures. In the above publications, it was shown that the natural frequencies of a structure with additional pin supports may be determined by manipulating the frequency response functions measured on the 'as-is' structure, without the need to actually impose the additional supports. The perturbed natural frequencies obtained in this way are thus called "artificial boundary condition" frequencies, or in short ABC frequencies herein, to reflect the fact that the required additional supports are virtual. The theoretical basis of the method is outlined below.

By partitioning between the measured and unmeasured coordinate sets (degrees of freedom, or DOFs), the steady state response of a linear system at a forcing frequency ω (rad/s) may be written as:

$$\left(\begin{bmatrix} \mathbf{k}_{mm} & \mathbf{k}_{mo} \\ \mathbf{k}_{om} & \mathbf{k}_{oo} \end{bmatrix} - \omega^2 \begin{bmatrix} \mathbf{m}_{mm} & \mathbf{m}_{mo} \\ \mathbf{m}_{om} & \mathbf{m}_{oo} \end{bmatrix} \right) \begin{Bmatrix} \mathbf{x}_m \\ \mathbf{x}_o \end{Bmatrix} = \begin{Bmatrix} \mathbf{f}_m \\ \mathbf{f}_o \end{Bmatrix} \tag{3.1}$$

where, **k** and **m** are stiffness and mass matrices, **x** and **f** are vectors of generalized response and excitation amplitudes, respectively. Subscript 'm' represents measured DOFs and subscript 'o' refers to the unmeasured DOFs ('omitted coordinate set' or OCS). The OCS is effectively a reduced system, in which all the measured DOFs are restrained or pinned to the ground.

Introducing the impedance matrix, $\mathbf{Z}=\mathbf{k}-\omega^2\mathbf{m}$, Eq. (3.1) can be re-written as:

$$\begin{bmatrix} \mathbf{Z}_{mm} & \mathbf{Z}_{mo} \\ \mathbf{Z}_{om} & \mathbf{Z}_{oo} \end{bmatrix} \begin{Bmatrix} \mathbf{x}_m \\ \mathbf{x}_o \end{Bmatrix} = \begin{Bmatrix} \mathbf{f}_m \\ \mathbf{f}_o \end{Bmatrix} \tag{3.2}$$

Assuming no excitations are imposed on the omitted DOFs, i.e., $\mathbf{f}_o=\mathbf{0}$, from Eq. (3.2) we can get:

$$(\mathbf{f}_m) = \left(\mathbf{Z}_{mm} - \mathbf{Z}_{mo}\mathbf{Z}_{oo}^{-1}\mathbf{Z}_{om}\right)(\mathbf{x}_m) \tag{3.3}$$

or

$$\frac{\mathbf{f}_m}{\mathbf{x}_m} = \mathbf{H}_{mm}^{-1} = \left(\mathbf{Z}_{mm} - \mathbf{Z}_{mo}\mathbf{Z}_{oo}^{-1}\mathbf{Z}_{om}\right) \tag{3.4}$$

where, $\mathbf{H}_{mm} = \mathbf{x}_m/\mathbf{f}_m$ is the measured frequency response function (FRF) matrix containing m×m FRF entries (hence incomplete) from the "as-is" structure..

Eq. (3.4) establishes the inherent relationship between the inverse of $\mathbf{H}_{mm}$ and the dynamic characteristics of the OCS as represented by $\mathbf{Z}_{oo}$, such that at the natural frequencies of the OCS, $\mathbf{Z}_{oo}^{-1}$ is singular, hence $\mathbf{H}_{mm}^{-1}$ is also singular, and vice versa. Therefore, by identifying the singularities from the elements of $\mathbf{H}_{mm}^{-1}$, one can determine the natural frequencies of the OCS, i.e., the frequencies of the structure as if it was physically pinned at the measured DOFs.

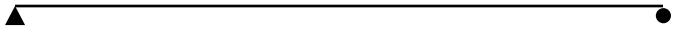

(a) Simply-supported beam being measured

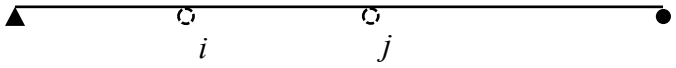

(b) Beam with a 'perturbed' boundary condition with added pins at '*i*' and '*j*' (imaginary)

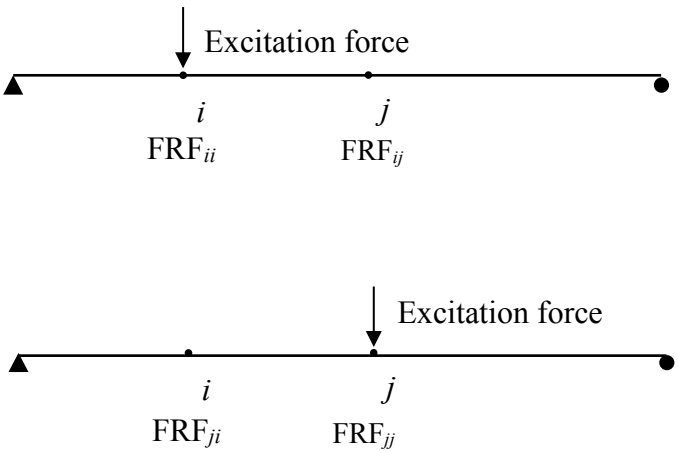

(c) Artificial boundary condition frequency measurements

Figure 3.1 Illustration of artificial boundary condition frequency measurement settings

The above statement can be more conveniently illustrated using an example shown in Figure 3.1, where (a) shows a simply-supported beam, (b) depicts a 'perturbed' boundary condition with two additional pin supports at '*i*' and '*j*', for which the modal frequencies are to be evaluated, and (c) shows the actual measurement settings. Instead of physically imposing the two additional pins as indicated in Figure 3.1(b), the modal frequencies under such a boundary condition can be determined by measuring the (2×2) FRF matrix on the original beam at points '*i*' and '*j*' shown in Figure 3.1(c) and subsequently identifying the singularities from the inverted FRF matrix.

3.3 Experimental investigation of modal testing for ABC frequencies

Previous studies using numerically simulated structures (Tu and Lu, 2008) have demonstrated the effectiveness of incorporating ABC frequencies with one to two pins in the identification of structural parameters and detection of structural damage. The key to bringing the approach of involving ABC frequencies in practical applications rests upon the reliability and accuracy in the acquisition of the ABC frequencies from measured responses. In this section, an experimental exploration on extracting ABC frequencies from physical measurements is presented with a laboratory experiment. Issues and possible improvements with regard to the quality of FRF measurements from an experimental modal testing point of view are highlighted and discussed.

The driving-point antiresonances, i.e. one-pin ABC frequencies as we shall call herein in the context of the present study, have been actually obtained in modal testing and applied in model updating in the past, as reviewed in Chapter 2. But experimental information on obtaining two-pin ABC frequencies from physical experiments has been scarce. This section aims to discuss the extraction of both one-pin and two-pin ABC frequencies from the experiments.

3.3.1 Test structure and modal testing programme

To avoid unnecessary complications from possible structural uncertainties in the experimental study concerned within this section, the test setup has been kept as simple as possible. The test specimen included steel beams in intact and damaged states. The beams had an identical length of 1020 mm, and a cross-section of width 50 mm and depth 6 mm. The beams were tested under a fixed-end condition, with both ends clamped onto steel supports through bolts and clamping plates, as shown in Figure 3.2. The steel supports were considerably stiffer than that of the beam to satisfy the requirement of a fixed support.

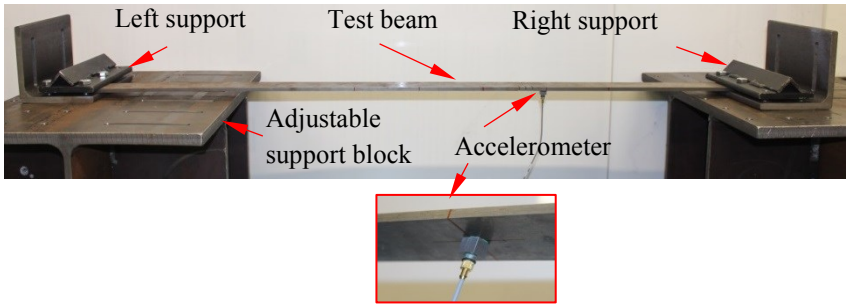

(a) Test specimen setup

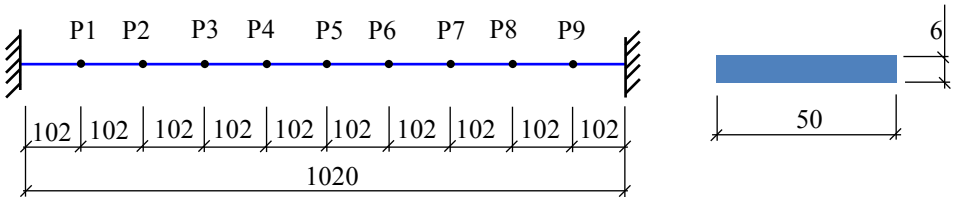

(b) Dimensions and test points

Figure 3.2 Test setup (Unit: mm)

In the experiment, an instrumented impact hammer (B&K type 8206-002) was used to excite the test beam. A built-in loading cell in the hammer allows the impact force be measured in detail during the excitation. The impact pulse was controlled via using a hammer tip; in the present experiment a plastic tip was found to be suitable to excite the relatively flexible beam. Preliminary tests showed that the hammer with the plastic tip was able to generate a flat force spectrum in the range of 0-1000 Hz, which covered comfortably the frequency range of interest for the test beam.

Response of the beam was measured with modal testing accelerometers (B&K Delta Tron® 4508 B 003 type). The accelerometers have a measuring range of ±700 m/s2 and a frequency range of 0.3-8000 Hz, sufficient to cover the vibration of the steel beam. The accelerometers are light weighted (4.9 g) as compared to the unit segment weight of the test steel beam; therefore the influence of transducer mass on modal testing results was negligible. Because the driving point FRF curves are required as part of the FRF matrix in order to determine the ABC frequencies, all accelerometers were attached to the bottom side of the steel beam (Figure 3.2(a)). The accelerometers were located along the centreline of the beam width, and the impact force was applied on the top side of the beam, also along the beam centreline.

During the experiment, a measurement array was arranged by dividing the beam into a number of segments along its length, herein 10 segments were considered, giving rise to 9 measurement points (the two end supports are excluded from the measurements), as shown in Figure 3.2(b).

For simplicity and without losing generality, the experimental study was focused on two-pin ABC frequencies, with two virtual pin supports, in addition to the simpler one-pin ABC frequencies. As a matter of fact, with just one and two-pin supports a large number of variations in the support locations can already be configured, providing a large variety of ABC frequency combinations. It is also worth noting that the extraction of ABC frequencies involves inversion of the incomplete FRF matrix whose dimension increases with the number of the artificial pins, therefore using more than 2-pins would introduce increased complexity in the influence of the measurement errors. To facilitate the measurements for all one- and two-pin configurations, two accelerometers are required and these were attached to two measurement points (i and j) on the test structure at any one time, as illustrated earlier in Figure 3.1.

The impact force and acceleration response signals were acquired with a data acquisition module (National Instruments 9234), as shown in Figure 3.3(a). From the trial tests it was found that the vibration amplitude was sufficient with respect to the noise level; the peak signal to noise ratio was maintained at around 70dB. Hence, good quality signals were acquired consistently by the integrated testing,

instrumentation and data acquisition system. A control interface was designed with Labview to monitor, acquire and store measurement data on a PC, as shown in Figure 3.3(b). Several characteristics of the measured data need to be monitored during the test, including the maximum level of impact force and acceleration, and the spectrum of the impact force.

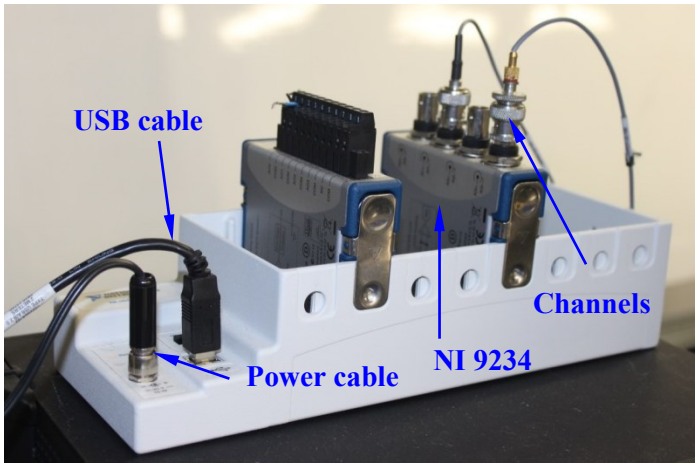

(a) NI 9234 data acquisition system

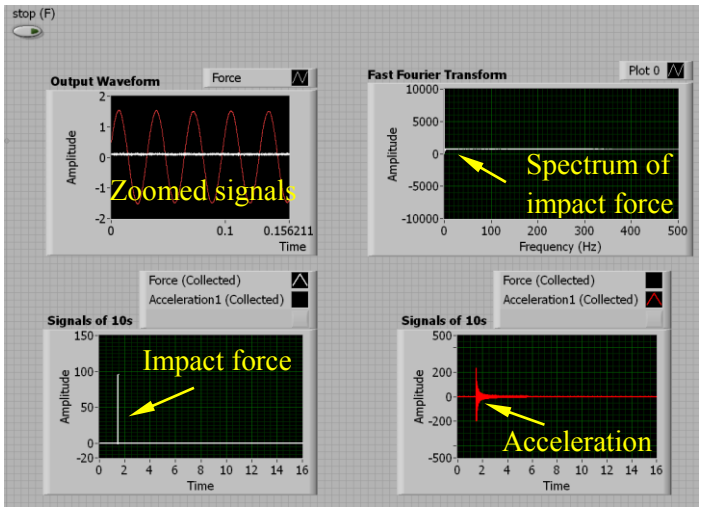

(b) Labview interface

Figure 3.3 Data acquisition system in modal testing

The impact force lasts for a very short duration, on the order of 0.5~1 millisecond. Because FRFs are needed to generate the ABC frequency function curves, it was

essential that the details of the impact force time history be captured with high accuracy; otherwise spurious peaks could occur on the FRFs. Therefore a sufficiently high sampling rate was required. After some trial testing with different sampling rates and comparing the obtained FRF curves, a sampling rate of 25600 Hz was found to be adequate for capturing the accurate shape of the impact force and obtaining good FRF curves, and this sampling rate was employed for both input and output signals during the tests. One further requirement for transient modal testing is that the response signals of the structure should be fully recorded to avoid leakage in modal analysis (Ewins, 1984). To this end, a record duration was set at 16 s, which proved to be adequate to both cover the useful signal and maintain a manageable data size. Representative input force and output acceleration signals obtained from the tests are shown in Figure 3.4.

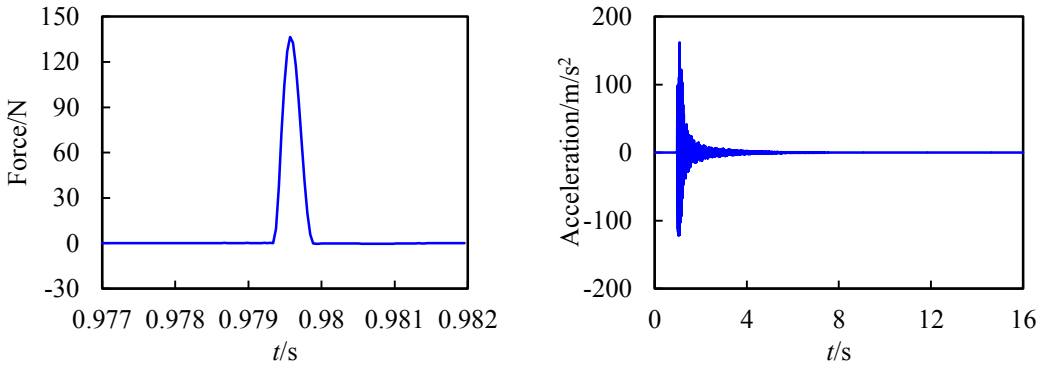

(a) Impact force (Zoomed) (b) Acceleration

Figure 3.4 Representative recorded impact force and acceleration signals

Three different groups of tests were carried out to obtain the natural modes, one-pin ABC frequencies and two-pin ABC frequencies, respectively. More details follow.

(1) The first test was to obtain natural frequencies as well as mode shapes of the beam. As mentioned earlier the beam was evenly divided into 10 segments, resulting in 9 measurement points along the beam length. To obtain the mode shapes, a complete row or column of the FRF matrix needs to be measured. In the present test the response measurement location was fixed while the impact location moved from one point to the next along the beam length. To avoid nodal point in any of the first few mode shapes an accelerometer was fixed at location P7 (Figure 3.2), and 9

different measurements with excitation at each of the 9 measurement points, respectively, were carried out.

(2) One-pin ABC frequencies can be obtained from the driving point FRF curves. As representation, three driving points (or ABC pin locations) at P4, P7 and P8, respectively, were tested. For each case, the accelerometer and impact were arranged at the same location (one at the bottom one at the top).

(3) Two-pin ABC frequencies are from the beam with two virtual pin locations. Again as representation, three two-pin configurations were chosen in the tests, with pins at (P2, P5), (P4, P7) and (P4, P8), respectively. For each configuration, two accelerometers were attached at the virtual pin locations and the excitation was imposed at the two locations separately. Referring to Figure 3.1 again, to measure the FRFs for the two-pin ABC frequencies with the two virtual pins at locations (i, j), the excitation (impact) is firstly applied at location i while the responses are measured at both i and j, yielding FRF_{ii} and FRF_{ij}. Subsequently the excitation is applied at j while the responses are measured again at i and j, yielding FRF_{ji} and FRF_{jj}. Thus, four FRF curves are obtained, including two driving-point FRFs and two transfer FRFs. This completes the measurement for the two-pin ABC configuration of (i, j). The same procedure was repeated for all selected two-pin ABC configurations.

The FRF curves are calculated by the following equation:

$$H(\omega) = \frac{X(\omega)}{F(\omega)} \tag{3.5}$$

where, $X(\omega)$ is the Fourier transform of the output signal and $F(\omega)$ is the Fourier transform of the input signal, $H(\omega)$ is the measured FRF curve.

From the definition in Section 3.2, the two-pin ABC frequency function curves can be calculated as:

$$\begin{bmatrix} A_{ii} & A_{ij} \\ A_{ji} & A_{jj} \end{bmatrix} = \begin{bmatrix} H_{ii} & H_{ij} \\ H_{ji} & H_{jj} \end{bmatrix}^{-1} \tag{3.6}$$

where, A_{ij} (i, j=1, 2) are the elements of the inverse of the incomplete FRF matrix, which effectively form the two-pin ABC frequency functions with the resonance in

each of these functions being the ABC frequencies. Hereinafter A_{ij} will be referred to simply as ABC frequency function.

In obtaining the measured FRF curves, standard force windowing is applied on the impact force curve and a rectangular window with the same duration as the impact force is used. With the force window, the noises in the blank area of the impact force curve will be eliminated while the force shape is not distorted. To reduce the effect of noises in acceleration data, 5 repetitive tests were performed to allow for an average on the resulting FRF curves.

After the above process the FRF curves are generally of good quality in the resonance regions, and it should be straightforward to identify natural mode parameters such as natural frequencies and mode shapes based on peak-picking methods. However, the FRF curves in some antiresonance regions are still 'noisy' which makes it difficult to pick out the exact antiresonance (one-pin ABC) frequencies. On such example is shown in Figure 3.5(a). The same problem can also affect two-pin ABC frequency curves, as shown in Figure 3.5(b).

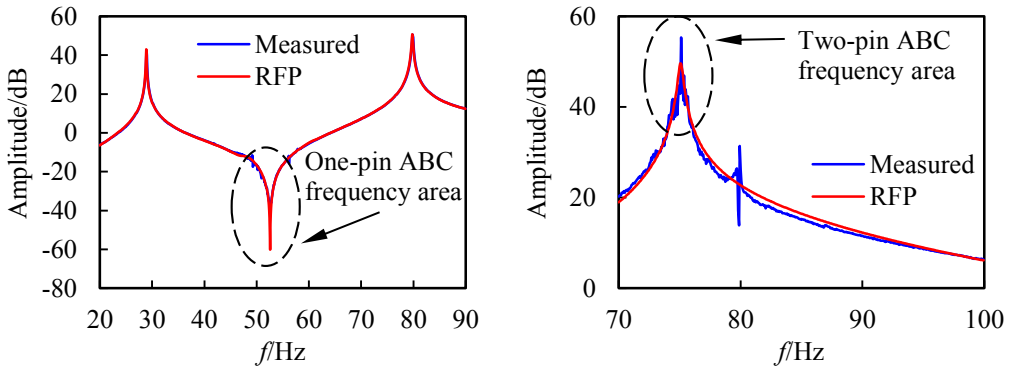

(a) FRF curve (close-in) (b) Two-pin ABC frequency function curve (close-in)

Figure 3.5 RFP technique for noisy antiresonances and two-pin ABC frequencies

To tackle this problem, a multi-DOF modal analysis method, namely the Rational Fraction Polynomial (RFP) method, is employed in the process to extract the ABC frequencies. The basic idea of the RFP method is that theoretically an FRF can be expressed in terms of rational fraction polynomials. With numerical manipulations on a measured FRF curve, the coefficients of the polynomials can be obtained. The actual modal parameters can then be extracted from the polynomial form of the FRF

curve. Richardson and Formenti (1982) employed orthogonal polynomials in the RFP method and made it suitable for computer-based calculation. It was found that the out-of-range modes of the FRF curves can be considered with the RFP method. Richardson and Formenti (1982) also showed that by adding additional terms in the polynomial of the numerator, the FRF curve can still be well interpreted with the RFP method after additional noise is added to the original curve. As a result, it is quite suitable for extraction of ABC frequencies from noise-contaminated FRF and ABC frequency function curves.

The RFP method with orthogonal polynomials developed by Richardson and Formenti (1982) is employed here to obtain ABC frequencies which would otherwise be difficult to determine with the peak-picking method due to noise in the curves. To obtain one-pin ABC frequencies, RFP is applied on the FRF curves directly. But when obtaining the two-pin ABC frequencies, RFP is applied on the ABC frequency function curves instead of the original FRF curves.

The effect of RFP on FRF curves and ABC frequency function curves is shown in Figure 3.5. It can be seen that the processed FRF and ABC frequency function curves from using RFP match quite well the measured curves overall, and at the same time the valleys, as well as peaks, are cleared up, paving the way for the extraction of the ABC frequencies from the RFP curves.

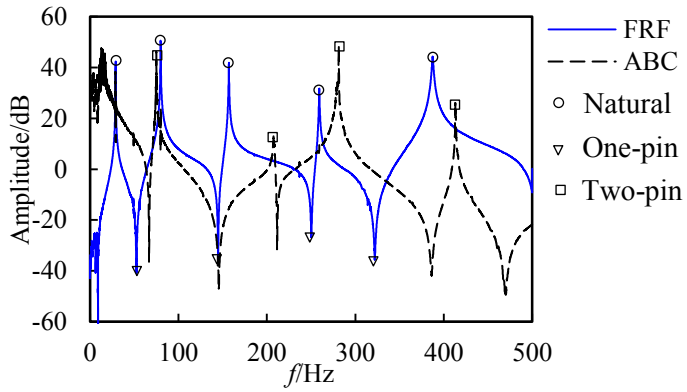

Figure 3.6 Representative driving FRF and two-pin ABC frequency function curves

Figure 3.6 presents representative driving FRF and ABC frequency function curves for a two-pin scenario in a combined plot. The natural (resonance) frequencies, one-pin ABC (antiresonance) frequencies, as well as two-pin ABC frequencies are also

marked in the plot. While one-pin ABC frequencies are simply driving-point antiresoannce and are subject to the same measruement constraints as antiresoannces, it can be observed clearly from the plot that the two-pin ABC frequencies are not necessarily connected to antiresonances. This fact is self-explanatory from the theoretical formulation outlined in Section 3.2; the results shown in Figure 3.6 provides direct insight into the relative relationships among the resonance, antiresonance and multi-pin ABC frequencies.

3.3.2 Modal testing results

The implementation of the above mentioned data processing procedure proved to work well in this experiment towards generating the ABC frequencies. From Figure 3.6 it can be seen that both the FRF curve and ABC frequency function curve exhibit satisfactory quality; the noise level in the curves is relatively low, and resonances and antiresonances can be clearly identified from the FRF curve as well as the two-pin ABC frequency function curve. With the basic peak-picking, deep-picking methods and RFP technique, the natural frequencies, mode shapes and one-pin and two-pin ABC frequencies can now be obtained conveniently.

Table 3.1 Measured and predicted natural and one-pin ABC frequencies (Unit: Hz)

Mode	Natural frequency			One-pin at P4			One-pin at P7			One-pin at P8		
	f_{0Nm}	f_{0Nc}	ε/%	f_{0Am}	f_{0Ac}	ε/%	f_{0Am}	f_{0Ac}	ε/%	f_{0Am}	f_{0Ac}	ε/%
1	28.9	29.0	**0.3**	66.8	66.2	**-0.8**	52.6	51.4	**-2.2**	41.4	41.2	**-0.5**
2	79.9	79.9	**0.0**	145.8	145.8	**0.0**	146.0	143.6	**-1.7**	117.3	115.0	**-1.9**
3	157.0	156.6	**-0.3**	211.9	210.1	**-0.8**	247.3	251.8	**1.8**	231.0	227.1	**-1.7**
4	259.2	259.2	**0.0**	385.1	386.2	**0.3**	322.6	321.0	**-0.5**	380.6	375.8	**-1.3**
5	387.3	388.3	**0.3**	-	-	-	-	-	-	-	-	-
Mean			**0.1**			**0.5**			**1.5**			**1.3**

Table 3.2 Measured and predicted two-pin ABC frequencies (Unit: Hz)

Mode	Pins at P2 and P5			Pins at P4 and P7			Pins at P4 and P8		
	f_{0Am}	f_{0Ac}	ε/%	f_{0Am}	f_{0Ac}	ε/%	f_{0Am}	f_{0Ac}	ε/%
1	95.6	95.4	**-0.2**	139.8	138.6	**-0.9**	116.5	113.5	**-2.6**
2	218.6	212.2	**-2.9**	211.4	209.2	**-1.1**	172.5	169.7	**-1.6**
3	305.9	303.9	**-0.7**	298.2	299.5	**0.5**	376.1	369.1	**-1.8**
4	533.9	542.0	**1.5**	452.4	452.3	**0.0**	471.6	471.8	**0.0**
Mean			**1.3**			**0.6**			**1.5**

Table 3.1 and 3.2 summarize the measured natural frequencies and one-pin and two-pin ABC frequencies of the intact steel beam. In the tables, 'f_N' represents natural frequencies and 'f_A' represents ABC frequencies. Subscript '0' indicates the beam is intact, subscript 'm' denotes measured data while subscript 'c' denotes predicted data. The predicted data are from calibrated finite element model of the beam, which will be discussed slightly later.

Figure 3.7 illustrates the first five mass-normalized mode shapes of the intact beam (Named as B0). Mode shape results of two damaged beams, Beam B1 and B2, which will be studied in Section 3.5, are also presented in the figures. In all, the first 5 natural modes, including natural frequencies and mode shape displacements at the measured locations could be obtained from the tests. On the other hand, the first 4 ABC mode frequencies for each of the two-pin configuration can be determined from the tests without ambiguity.

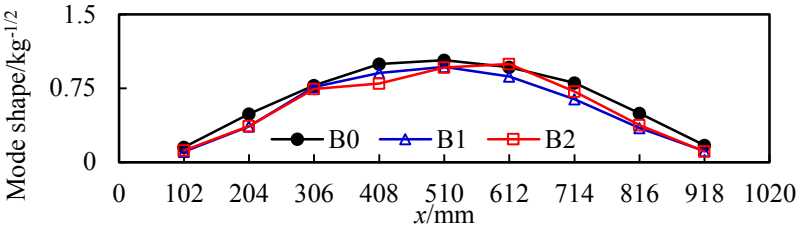

(a) 1st mode

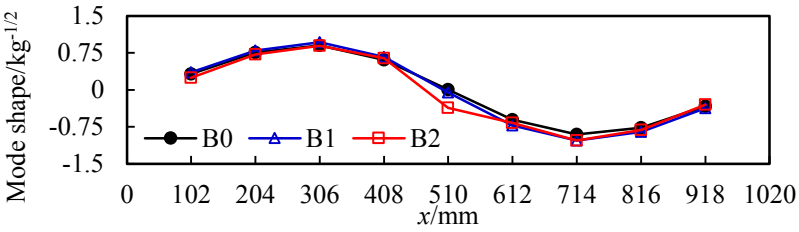

(b) 2nd mode

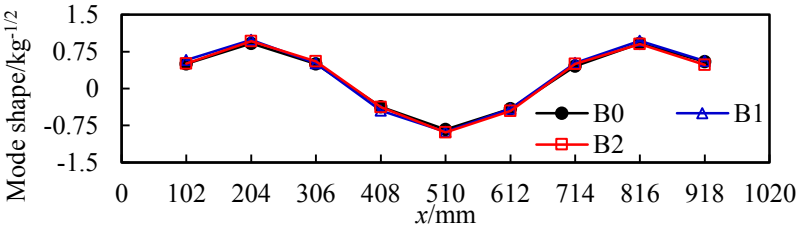

(c) 3rd mode

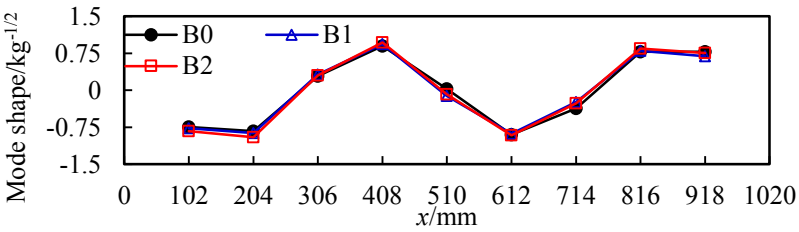

(d) 4th mode

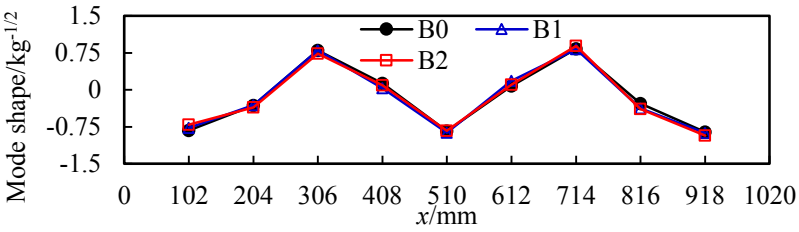

(e) 5th mode

Figure 3.7 Mass-normalized mode shapes

3.4 Discussion on the measurement accuracy of ABC frequencies

From the previous section, it has been established that the first few (4 herein) ABC mode frequencies are obtainable from a standard modal testing and data processing procedure. This section examines the accuracy in the measured ABC frequencies in terms of the susceptibility of these frequencies to some common variability in conducting the physical tests, such as the actual position of the impact strike.

It is generally believed that antiresonances will have similar measurement accuracy as resonances (2004; D'Ambrogio and Fregolent, 2000), and as such when these data are employed in a parameter identification (model updating) process, uniform weighting is generally used regardless resonances or antiresonances (D'Ambrogio and Fregolent, 2003; Meruane and Heylen, 2011). Non-uniform weighting for resonances and antiresonances has also been considered; for example Jones and Turcotte (2002) assigned different weighting factors for resonances and antiresonances based on the assumption that the coefficient of variance of antiresonances is 2 times of that of resonances. However, in the context of the general ABC frequencies with more than one pin, there is a lack of analysis on the accuracy of the measured ABC frequencies from a modal testing procedure.

Natural frequencies and ABC frequencies share the same character in that they both are associated with the peaks on the FRF curve or ABC frequency function curve, respectively. However there exist fundamental differences between the two types of frequencies. While the natural frequencies are independent of the excitation and response measurement locations, the ABC frequencies depend closely upon the locations of excitation and response. This characteristic is similar to the well-known location-dependent characteristic of the antiresonances, which in the driving-point case are simply a special case of the ABC. As a consequence, any imprecision in the excitation and measurement locations could bring errors into the ABC frequencies.

Errors in the modal data come from different sources in the modal testing and analysis procedure, including the experimental data acquisition procedure, the signal processing procedure and the modal extraction procedure (Ashory, 1999). Herein the following error sources are examined here; (1) errors due to misalignment of the

excitation location and the sensor location, (2) errors due to sensor mass, and (3) additive noise.

3.4.1 Errors pertaining to imprecise excitation location

Input location error could arise from the limitation of modal testing setup or manual operation. For example, one-pin ABC frequencies are obtained from driving antiresonances. To get driving FRF curves, we need the input excitation and the output response measurement locations in the structure to be identical. However this is hard to achieve in practice. Usually there are three alternative options to deal with driving point measurements (Ewins, 1984). The first one is to use an impedance head which can measure both the impact force and excitation response at a single point. The second one is to place the sensor alongside but as close as possible to the excitation point, as shown in Figure 3.8. As the excitation location is actually shifted from the theoretical target point, the ABC frequencies will be affected. The third option may be suitable for thin structure such as the steel beam tested herein, and in this approach the impact and the output sensor are placed in line but on opposite sides of the structure. However there is still no 100% guarantee of achieving the exact alignment, especially when the excitation (e.g. an impact hammer) is handled manually. For these reasons, a detailed examination of the sensitivity of the one-pin and two-pin ABC frequencies to the misalignment of the impact and output response locations is deemed to be instructive.

The scenario is illustrated in Figure 3.8. The target driving FRF is at point i, H_{ii}, and the sensor is placed at i. Assuming the impact point is offset by a distance of Δd, at point i'. We shall examine the sensitivity of ABC frequencies to Δd.

Figure 3.8 Modal testing operation when obtaining one-pin ABC frequencies

(1) Sensitivity analysis

The sensitivity of antiresonances from an FRF curve H_{kj} to parameter p has been given in Mottershead (1998), which is a linear combination of sensitivities of eigenvalues and eigenvectors. It is convenient to get an explicit sensitivity relationship for driving function H_{ii}, i.e. one-pin ABC frequencies f_A. If we take Δd as a structural parameter, and consider that eigenvalues will not change with Δd, we can get the sensitivity of f_A^2 to Δd, as:

$$\frac{\partial f_A^2}{\partial \Delta d} = \frac{\sum_{k=1}^{N} \frac{\partial \varphi_{ik}}{\partial \Delta d} \det\left(\mathbf{\Lambda} - f_A^2 \mathbf{I}\right)_k \varphi_{ik}}{\sum_{k=1}^{N} \varphi_{ik} \left(\sum_{\substack{p=1 \\ p \neq k}}^{N} \det\left(\mathbf{\Lambda} - f_A^2 \mathbf{I}\right)_{k,p} \right) \varphi_{ik}} \tag{3.7}$$

where, $\mathbf{\Lambda}$= diag(λ_n), n=1, 2, …, N, and λ_k is the n^{th} eigenvalue; the subscripts k, p on the matrix ($\mathbf{\Lambda}$-$f_A^2\mathbf{I}$) mean that the k^{th} and p^{th} rows and columns have been deleted. $\partial\varphi_{ik}$ is the change of mode shape element φ_{ik} due to the change of excitation location; in the example considered here,

$$\partial\varphi_{ik} = \varphi_{i'k} - \varphi_{ik} \tag{3.8}$$

It is actually the difference of the mode shape elements at point i' and i.

It is clear from Eq. (3.7) that the sensitivity of f_A^2 is a linear combination of the sensitivities of the mode shape element at point i from different modes. In other words, the error brought by the location misalignment in the one-pin ABC frequency is a linear combination of shifts in the mode shape element at the driving point due to the misalignment.

The same procedure can be applied on two-pin ABC frequencies. From Eq. (3.6), the two pin ABC frequencies are actually frequency points which satisfy:

$$H_{ii}(\omega) \cdot H_{jj}(\omega) - H_{ij}(\omega) \cdot H_{ji}(\omega) = 0 \tag{3.9}$$

In the two-pin situation, the excitation location errors involve two contributions, one from the actual point i', which is Δd_1 away from point i, and one from the actual point j', which is Δd_2 away from point j. So the measured two-pin ABC frequencies manifest as satisfying:

$$H_{i'i}(\omega)\cdot H_{j'j}(\omega)-H_{i'j}(\omega)\cdot H_{j'i}(\omega)=0 \tag{3.10}$$

The FRF curves can be expressed in terms of the eigenmode data (Mottershead, 1998), as:

$$H_{ij}(\omega)=\sum_{k=1}^{N}\frac{\varphi_{ik}\varphi_{jk}}{\left(\lambda_k-\omega^2\right)} \tag{3.11}$$

With Eq. (3.10) and (3.11), the two-pin ABC frequencies f_A can be determined from:

$$\sum_{p=1}^{N}\sum_{\substack{q=1\\q\neq p}}^{N}\varphi_{i'p}\varphi_{j'p}\left(\varphi_{ip}\varphi_{jq}-\varphi_{jp}\varphi_{iq}\right)\det\left(\mathbf{\Lambda}-f_A^2\mathbf{I}\right)_{p,q}=0 \tag{3.12}$$

The sensitivity of f_A^2 to Δd_1 and Δd_2 can be calculated following a similar approach as the ansiresonance sensitivity:

$$\frac{\partial f_A^2}{\partial \Delta d_1}=\sum_{p=1}^{N}\frac{\sum_{\substack{q=1\\q\neq p}}^{N}\varphi_{jq}\left(\varphi_{ip}\varphi_{jq}-\varphi_{iq}\varphi_{jp}\right)\det\left(\mathbf{\Lambda}-f_A^2\mathbf{I}\right)_{p,q}}{\sum_{p=1}^{N}\sum_{\substack{q=1\\q\neq p}}^{N}\varphi_{ip}\varphi_{jq}\left(\varphi_{ip}\varphi_{jq}-\varphi_{iq}\varphi_{jp}\right)\left(\sum_{\substack{m=1\\m\neq p,q}}^{N}\det\left(\mathbf{\Lambda}-f_A^2\mathbf{I}\right)_{p,q,m}\right)}\cdot\frac{\partial\varphi_{ip}}{\partial\Delta d_1} \tag{3.13a}$$

$$\frac{\partial f_A^2}{\partial \Delta d_2}=\sum_{q=1}^{N}\frac{\sum_{\substack{p=1\\p\neq q}}^{N}\varphi_{ip}\left(\varphi_{ip}\varphi_{jq}-\varphi_{iq}\varphi_{jp}\right)\det\left(\mathbf{\Lambda}-f_A^2\mathbf{I}\right)_{q,p}}{\sum_{p=1}^{N}\sum_{\substack{q=1\\q\neq p}}^{N}\varphi_{ip}\varphi_{jq}\left(\varphi_{ip}\varphi_{jq}-\varphi_{iq}\varphi_{jp}\right)\left(\sum_{\substack{m=1\\m\neq p,q}}^{N}\det\left(\mathbf{\Lambda}-f_A^2\mathbf{I}\right)_{p,q,m}\right)}\cdot\frac{\partial\varphi_{jq}}{\partial\Delta d_2} \tag{3.13b}$$

Thus the shift of a two-pin ABC frequency f_A due to the location errors can be calculated as:

$$df_A^2=\frac{\partial f_A^2}{\partial\Delta d_1}\cdot d\Delta d_1+\frac{\partial f_A^2}{\partial\Delta d_2}\cdot d\Delta d_2 \tag{3.13c}$$

Eq. (13) showed that, similar to one-pin ABC frequencies, the error brought by the location misalignment in two-pin ABC frequencies is also a linear combination of shifts of the mode shape displacements at the two virtual pin locations.

Considering that the offset distance Δd can be controlled within a reasonably small range, with an upper limit of the order of the size of the sensor (when placed on the same side of the impact strike), it can be assumed that the mode shape variation within this range is linear. On this basis, and using the expressions in Eq. (3.7) and (3.13), it can be demonstrated that the relationship between the error in ABC frequencies and Δd, Δd_1 or Δd_2 are approximately linear. Numerical examples are used to demonstrate these relationships.

(2) Numerical demonstration

A fixed-end beam is used to analyse the errors in the one-pin ABC frequencies brought by location misaligning. Figure 3.9 shows that FE model setup.

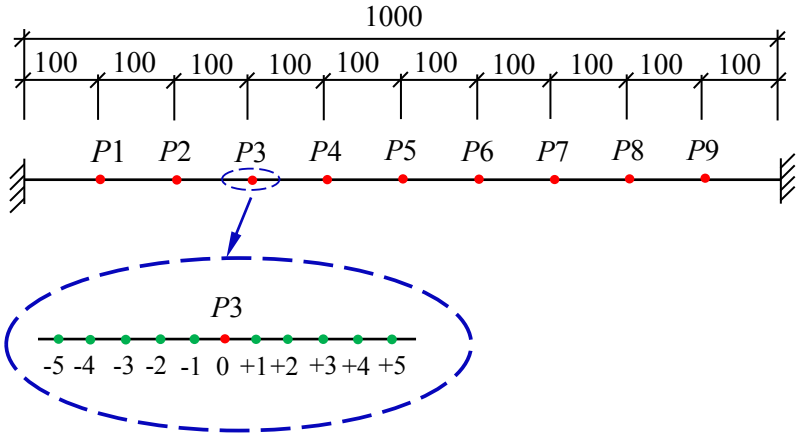

Figure 3.9 Numerical model for investigation of errors in one-pin ABC frequency

Basic parameters of the beam are: $L \times b \times h$=1000 × 50 × 6 mm. Elastic modulus and Poisson's ratio of the material are 210 GPa and 0.3, respectively. The target driving point was put at five different locations, respectively, along the beam to cover all areas. The offset distance Δd was assumed to be 5mm at maximum based on the laboratory experience for the current test specimen dimension, and in the FE simulation 11 samples of Δd varying between -5 mm and +5 mm at an equal interval of 1mm were used, as shown in Figure 3.10. As a result 11 FRF curves are obtained for each target driving location. In total 55 FRF curves are obtained.

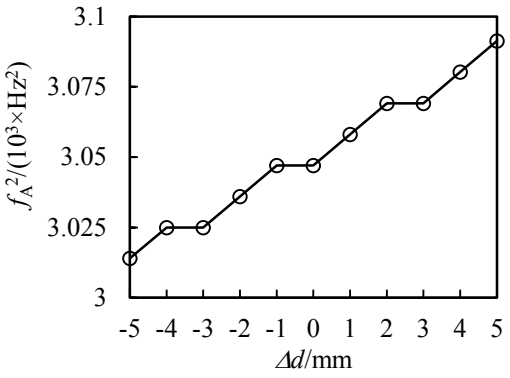

(a) 1st mode

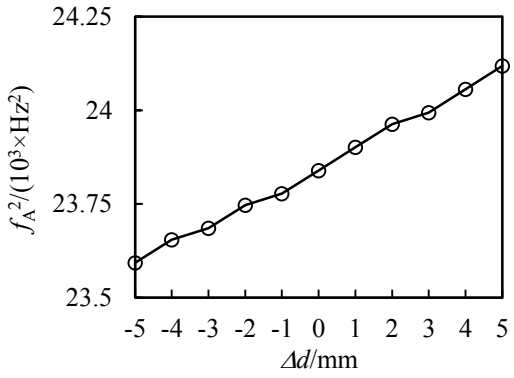

(b) 2nd mode

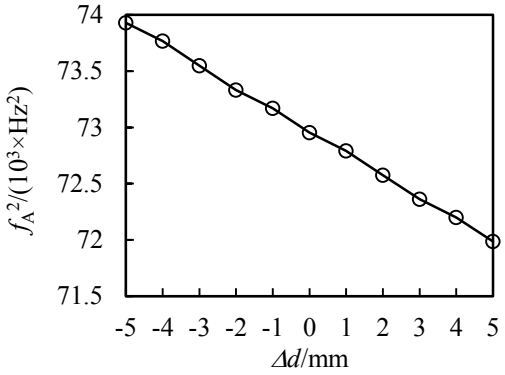

(c) 3rd mode

Figure 3.10 One-pin ABC frequencies versus Δd relationships

The antiresonance frequencies at driving point 3 are used as an example. Figure 3.10 shows the antiresonance eigenvalues versus Δd relationships. It can be seen that the curves of the first three modes are generally linear. Results from the other points show similar results.

The same numerical beam can be used to study the errors in two-pin ABC frequencies. Take the two-pin ABC frequencies at pin locations (P3, P4) for example. The relationships between f_A^2 and location errors Δd_1 and Δd_2 are shown in Figure 3.11, which are all approximate planes. It shows that the relationships are approximately linear.

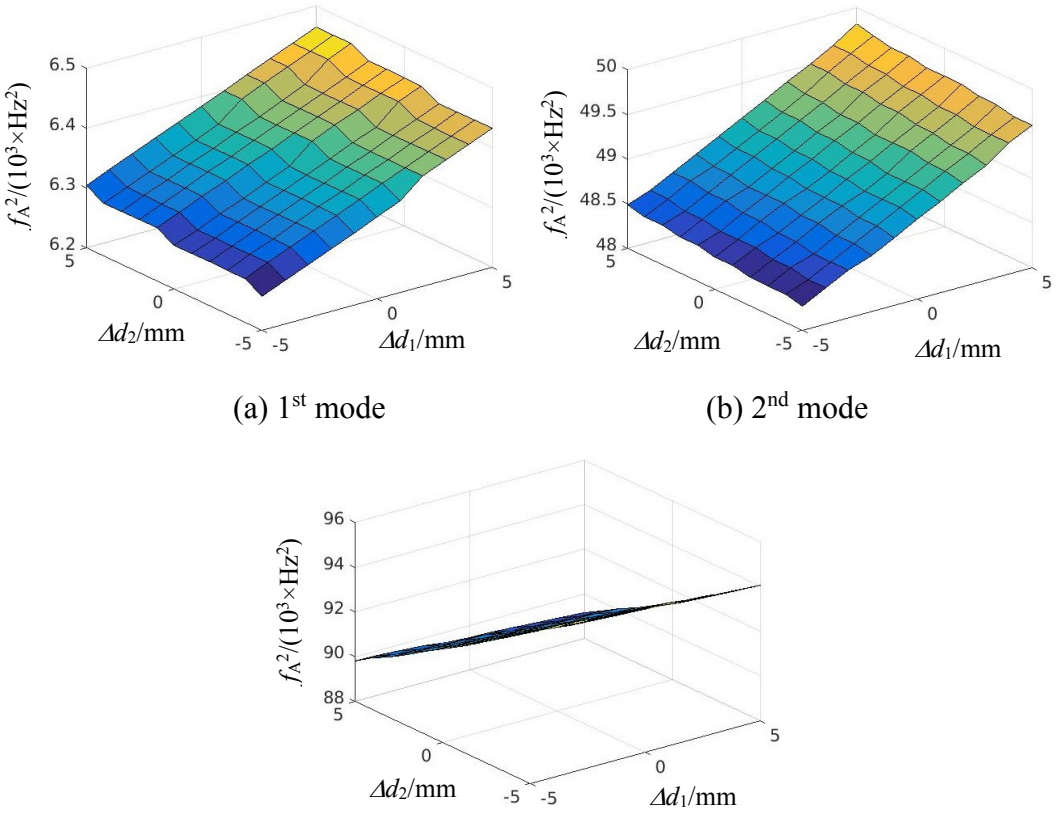

(a) 1st mode (b) 2nd mode

(c) 3rd mode

Figure 3.11 Two-pin ABC frequencies versus *Δd* relationships

(3) Modal testing strategy for ABC frequencies

The approximately linear relationship between the ABC frequency squared and the location error leads to a proposed testing operation for the measurement of ABC frequencies in terms of mitigating the location errors, which can be stated as follows. a) Generally speaking, a sufficient number of repeated tests should be performed with the impact being imposed around the target location in a random manner, and the obtained ABC frequencies (squared) should be averaged in order to cancel out the errors due to the location misalignment. b) When the sensor and impact need to be applied on the same side of the structure (as would be the case for civil engineering structures), such that the precise location is occupied by the sensor, repetitive tests should be performed with the impact being applied on both sides of the sensor, and average of the resulting ABC frequencies (squared) should be taken.

3.4.2 Errors pertaining to the sensor mass

It is well known that the testing devices attached to the structure, such as a sensor or a shaker stinger, will alter the dynamic properties of the tested structure itself to a certain extent due to the presence of an additional mass. Several studies have been conducted to find ways to cancel out the mass effect of sensors (Ashory, 1999). As far as antiresonances and ABC frequencies are concerned, however, these frequencies can be deemed as immune to the effect of a sensor mass so long as sensors are only attached at the 'pin' positions. This is because ABC frequencies are by virtue the natural frequencies of the structure with the measured nodes being 'pinned'. Consequently there should be no vibration in the ABC system at the locations of the sensors.

3.4.3 Errors pertaining to additive noise

It is generally known that the commonly used FRF curve estimators H_1 and H_2 are biased to the uncorrelated additive noise, as shown below (He and Fu, 2001).

$$\hat{H}_1(\omega)=\frac{\hat{S}_{XF}(\omega)}{\hat{S}_{FF}(\omega)}=H(\omega)\left(1+\frac{S_{MM}(\omega)}{S_{FF}(\omega)}\right)^{-1}=\alpha_1(\omega)H(\omega) \tag{3.14a}$$

$$\hat{H}_2(\omega)=\frac{\hat{S}_{XX}(\omega)}{\hat{S}_{XF}(\omega)}=H(\omega)\left(1+\frac{S_{NN}(\omega)}{S_{XX}(\omega)}\right)=\alpha_2(\omega)H(\omega) \tag{3.14b}$$

where, 'F' stands for the excitation force; 'M' stands for the additive noise in the excitation force; 'X' stands for the output response; 'N' stands for the additive noise in the output response. $S(\omega)$ is the auto- or cross- spectrum of the signals. $H(\omega)$ is the real value of FRF curves. The symbol '^' indicates the term is an estimator.

It is clear from Eq. (3.14) that the amplitude of the FRF curves will be biased when additive noise is present. For the extraction of one-pin ABC frequencies, as the quality of FRF curve around the antiresonant area is of main concern, H_1 should be a better estimator over H_2 due to the fact that the response of the structure is quite insignificant at antiresonances and α_2 is relatively large. If the spectrum of the force is generally smooth and α_1 does not have a large variation around the antiresonances, the extracted one-pin ABC frequencies can be seen as unbiased.

When H_1 or H_2 are used as the estimator of FRF, the two-pin ABC frequencies calculated with Eq. (3.9) can be written as:

$$\hat{H}_{ii}(\omega)\cdot\hat{H}_{jj}(\omega)-\hat{H}_{ij}(\omega)\cdot\hat{H}_{ji}(\omega)=a_{ii}(\omega)a_{jj}(\omega)H_{ii}H_{jj}-a_{ij}(\omega)a_{ji}(\omega)H_{ij}H_{ji}=0 \quad (3.15)$$

In modal testing, we use the same excitation force to obtain FRF_{ii} and FRF_{ij} (Excitation at point i), and the same excitation force to obtain FRF_{ji} and FRF_{jj} (Excitation at point j). As a result, when H_1 is used as the estimator, we will have $\alpha_{ii}=\alpha_{ij}$, $\alpha_{ji}=\alpha_{jj}$. We can see from Eq. (15) that the two-pin ABC frequencies from the FRF estimators will be unbiased to the values from real FRF curves. When H_2 is used as the estimator, from Eq. (14b) we can see that the coefficient α_2 will depend on the SNR (signal-to-noise ratio) of the response. As the SNR could be different for the four responses, the obtained two-pin ABC frequencies could be biased, especially when the driving and transfer FRF curves have distinctive SNRs. From this point of view, H_1 should also be a better choice under such conditions.

From the above analysis on the effects of a few common error sources, it can be argued that the measured ABC frequencies are generally unbiased to such errors, and through properly designed modal testing and signal processing strategies the influence of these errors can be minimised. We can therefore postulate that the measurement of ABC frequencies can achieve similar accuracy as that of the natural frequencies. In the next section, we shall examine the accuracy in the measured ABC frequencies from the experiment against the predicted results from a calibrated (updated) finite element model.

3.4.4 Verification of accuracy of extracted ABC frequencies from test data

The ABC frequencies generated from the experimental data are verified against numerically simulated ABC frequencies from a carefully calibrated FE model to evaluate their accuracy. Once a finite element model is calibrated to a satisfactory degree, the computation of the ABC frequencies is straightforward as these frequencies are simply the natural frequencies of the structure when the artificial pin constraints are physically imposed, and this can be done easily with the FE model. However, the FE model should be accurate enough to represent the test beam, and to

this end a calibration updating of the basic properties of the FE model needs to be carried out beforehand.

To be consistent with the measurement arrangement in the experiment, in the FE model the beam is discretised into 10 elements, corresponding to the 10 segments in the test. To compensate the coarse discretisation and to take into account the shear deformation and rotational inertia, high order (cubic) Timoshenko beam elements are used to establish the FE model and this ensures a minimal modelling error. The boundary conditions of the beam model follow the experiment and are fixed. The density and Poisson's ratio of the material are known constants for the steel material and are 7850 kg/m^3 and 0.3, respectively. The bending stiffness as represented by the beam flexural rigidity EI is unknown and needs to be identified (updated). Since the intact beam is highly uniform, a single flexural rigidity value is updated from the FE model updating.

For the updating of a single variable, we choose to employ only the natural frequencies as these data are deemed to have the highest measurement accuracy. The first five natural frequencies as available from the experiment are employed and accordingly the objective function, which is to be minimised in the updating process, is formed as follows:

$$J = \sum_{i=1}^{5} \mathrm{abs}\left(\frac{f_{0\mathrm{Nc}i}^2 - f_{0\mathrm{Nm}i}^2}{f_{0\mathrm{Nm}i}^2} \right) \tag{3.16}$$

where, $f_{0\mathrm{Nm}i}$ and $f_{0\mathrm{Nc}i}$ stand for the measured and calculated i^{th} natural frequencies of the intact beam.

It should be noted that in the above objective function, unit weights are applied to different modes of modal data. It is generally known that the extracted modal data from physical measurements are in nature not determined values due to the presence of various types of errors. The error in a specific modal parameter such as a specific order of resonance frequency or mode shape may be evaluated with respect to the source errors using statistical analysis approaches. On this basis, it would be possible to design an objective function with a maximum likelihood approach and determine the weights accordingly (Mthembu, et al., 2009; Marwala, 2010). However, the main

interest of this study is focused on the soundness of the representing (FE) model, whereas the objective functions are employed only for relative comparison purpose. For this reason, the probabilistic aspect of the objective functions is not involved.

The parameter *EI* in the beam model is iteratively adjusted to achieve minimum of the objective function *J*. The result for *EI* is 168.9 $N \cdot m^2$. A comparison between the measured natural frequencies and the computed ones using the above property is given in Table 3.1. It can be seen that the results match very well.

The updated FE model is then employed to compute the one-pin and two-pin ABC frequencies in a forward manner (adding actual pin(s)). The results are presented in Tables 3.1 and 3.2, in which the relative differences between the measured and predicted frequencies are also included (the term ε in percent). In the tables, the mean values of the errors are calculated based on their absolute values.

It can be seen that the measured and predicted ABC frequencies match quite well with each other. The average error is less than 1.5%, which is about the order that is generally known to the measurement of the natural frequencies. It is worth noting that the error in the natural frequencies shown in Table 3.1 is considerably small (average about 0.1%) in the present case, and this is attributable to the fact that the FE model has been calibrated against these measured natural frequencies, therefore a near zero difference between the measured and predicted values is expected and this may not be directly comparable with the differences in the subsequently calculated ABC frequencies.

From the above verification against the predicted results, it can be concluded that both one-pin and two-pin ABC frequencies can be measured with good accuracy from actual experiment.

3.5 Extracting ABC frequencies from damaged beams and damage identification

Sections 3.3 and 3.4 have demonstrated that good quality one-pin and two-pin ABC frequencies can be obtained from modal testing in a physical measurement

environment and the accuracy of the measured ABC frequencies is similar to the generally recognised measurement accuracy of the natural frequencies. In this section the effectiveness of employing ABC frequencies in the damage identification is evaluated with comparison to the use of conventional modal data.

3.5.1 Test specimens and modal testing results

Two steel beams with the same properties as the one reported in Section 3.3, but with the introduction of damages, were tested under the same procedure as described in Section 3.3. The damages were intended to represent a realistic scenario where identification using a global method with modal data could be possible. To this end, the damages were created in the beam by making several cuts within a limited length to simulate a sensible reduction of the flexural rigidity over the area, as shown in Figure 3.12. In the first beam, denoted as B1, the cuts were spread slightly less than a segment length, in the area between 300 mm to 400 mm from the left support. The saw cuts were made with a width of 1 mm and depth of 12.5 mm, and the interval between the cuts was 10 mm. The damage area was located between the points P3 and P4 shown in Figure 3.2. The resulting stiffness reduction as equivalent over a whole segment was about 40%. The second beam, denoted as B2, had exactly the same pattern of cuts located between points P3 and P4, but it had a second damage area between points P7 and P8 with cuts spreading over half of the segment length. Therefore, the first beam effectively represented a scenario with a single damage zone, whereas the second beam represented a scenario with multiple damaged zones.

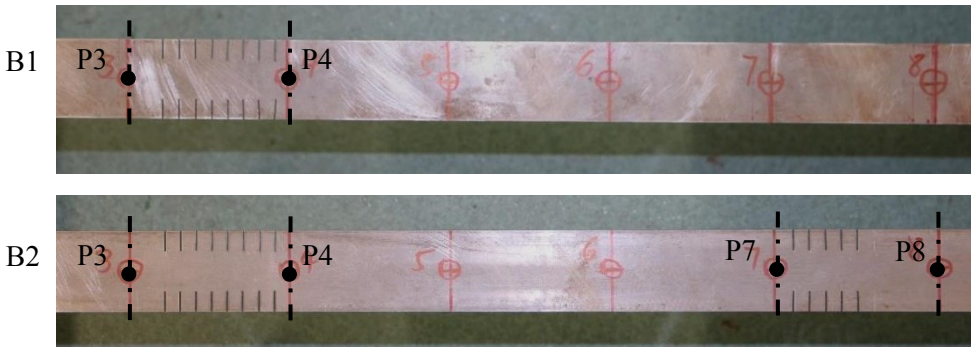

Figure 3.12 Damages in steel beams

The modal testing procedure described in Section 3.3 was applied on the two damaged beams and the same types of modal data, including the first 5 modes of natural frequencies and mode shapes and the first 4 modes of one-pin and two-pin ABC frequencies from selected configurations, were obtained. The measured natural frequencies and selected ABC frequencies are listed in Table 3.3. The measured mode shapes have been presented in Figure 3.7. In the table, the subscript 'd' denotes damaged beams. Comparing with Table 3.1 and 3.2, it shows that the damages will bring a decrease of 0.3-5% to natural and ABC frequencies of beam B1 and a decrease of 2-11% to those of beam B2.

Table 3.3 Measured natural and ABC frequencies of damaged beams (Unit: Hz)

Mode	Natural frequency		One-pin at P4		One-pin at P7		Two-pin at P4 and P7	
	B1	B2	B1	B2	B1	B2	B1	B2
1	28.4	28.3	65.2	62.6	49.7	46.5	137.8	137.1
2	77.1	74.3	142.9	142.9	144.4	142.1	203.4	200.5
3	156.6	153.3	205.3	201.3	243.3	242.3	295.9	286.4
4	248.6	248.5	385.1	368.6	49.7	301.9	433.7	433.9
5	377.9	370.0	-	-	-	-	-	-

3.5.2 Damage identification through FE model updating

The measured modal data are employed to do damage identification through FE model updating for the two damaged beams. To evaluate the effectiveness of different types of the modal data in the FE model updating, a comparative study is carried out with different combinations of the dataset to include natural frequencies, one-pin or two-pin ABC frequencies, and mode shapes, separately or in a mixed fashion.

Different objective functions are formed in accordance with different types of modal data employed, and parallel updating procedures are performed with different objective functions to compare the outcome. The objective functions are established with the residuals of the modal data. In what follows, different types of residuals are

described first, and the objective functions combining different residuals and hence different combinations of the modal data are presented next.

(1) Residual from natural frequencies

The residual from natural frequencies is defined as R_f in Eq. (3.17a). It gauges the difference between theoretical (from FE model) and measured frequencies for the damaged beam. To minimise the influence of the model error, the measured and theoretical natural frequencies for the damaged beam are normalised with respect to their undamaged counterparts, and the residual is formulated from the normalised values:

$$R_{\mathrm{f}} = \frac{1}{N_{\mathrm{f}}} \sum_{i=1}^{N_{\mathrm{f}}} \mathrm{abs}\left(\frac{f_{\mathrm{dNm}i}^2}{f_{0\mathrm{Nm}i}^2} - \frac{f_{\mathrm{dNc}i}^2}{f_{0\mathrm{Nc}i}^2} \right) \tag{3.17a}$$

where, $f_{\mathrm{N}i}$ represents the i^{th} natural frequency; subscripts 'c' and 'm' stand for the FE calculated and the measured data, respectively; and subscripts 'd' and '0' stand for the damaged and intact states of the beam, respectively. N_{f} is the number of modes used.

(2) Residual from ABC frequencies (one-pin or two-pin)

A similar form of residual, defined as R_{A}, is formed for one-pin and/or two-pin ABC frequencies:

$$R_{\mathrm{A}} = \frac{1}{N_{\mathrm{A}}} \sum_{i=1}^{N_{\mathrm{A}}} \mathrm{abs}\left(\frac{f_{\mathrm{dAm}i}^2}{f_{0\mathrm{Am}i}^2} - \frac{f_{\mathrm{dAc}i}^2}{f_{0\mathrm{Ac}i}^2} \right) \tag{3.17b}$$

where, $f_{\mathrm{A}i}$ represents the i^{th} mode of ABC frequency (one-pin or two-pin). N_{A} is the number of ABC modes used.

(3) Residual from Modal Assurance Criterion (MAC)

Mode shapes may be applied to form the residual by directly using the mode shape changes or mode shape derivative changes. Residuals from these two different types of data might provide different results for model updating, so both methods are employed in the updating analysis here.

Firstly the widely used mode shape derivative, Modal Assurance Criterion (MAC), is used here to gauge the effect of damage from the perspective of the mode shapes, and this is defined as:

$$\mathrm{MAC}_i = \frac{\left(\phi_{0i}^{\mathrm{T}}\phi_{\mathrm{d}i}\right)^2}{\left(\phi_{0i}^{\mathrm{T}}\phi_{0i}\right)\left(\phi_{\mathrm{d}i}^{\mathrm{T}}\phi_{\mathrm{d}i}\right)} \tag{3.17c}$$

where, ϕ_i stands for the i^{th} mode shape vector of the beam; subscripts '0' and 'd' stand for mode shapes of the intact and damaged beam, respectively.

The residual is then formed by taking into account the difference between the measured and predicted MAC values of the first N_{MAC} modes, as:

$$R_{\mathrm{MAC}} = \frac{1}{N_{\mathrm{MAC}}}\sum_{i=1}^{N_{\mathrm{MAC}}}\left(\mathrm{MAC}_{\mathrm{m}i} - \mathrm{MAC}_{\mathrm{c}i}\right)^2 \tag{3.17d}$$

where, subscripts 'c' and 'm' stand for the FE calculated and measured MAC values, respectively.

(4) Residual from mode shape changes

As mentioned, the residual can also be directly formed from mode shape changes, as shown in Eq. (3.17e). The first N_{MS} modes of mode shapes are used in the formula. To make the mode shape displacements comparable, both the measured and predicted mode shapes are displacement-normalized.

$$R_{\mathrm{MS}} = \frac{1}{N_{\mathrm{MS}}N_{\mathrm{N}}}\sum_{i=1}^{N_{\mathrm{MS}}}\sum_{j=1}^{N_{\mathrm{N}}}\mathrm{abs}\left(\varphi_{\mathrm{m}ji}^{\mathrm{d}} - \varphi_{\mathrm{c}ji}^{\mathrm{d}}\right) \tag{3.17e}$$

where, ϕ_{ji} is the j^{th} element in the i^{th} displacement-normalized mode shape vector. The superscript 'd' stands for damaged beam and N_{N} is the total number of elements in each mode shape vector, which is 9 in the current measurements.

The objective functions can then be formed with different combinations of the above residuals. Five different types of objective functions are used in the comparative study, as listed below. In all of the objective functions, unit weights were applied to different types of modal data in the study here.

The first objective function is formed only with natural frequencies to serve as a reference for the other ones, as shown in Eq. (3.18a). The first five modes of natural frequencies are used in J_1.

$$J_1 = R_{\mathrm{f}} \tag{3.18a}$$

One-pin ABC frequencies are added in J_1 to form the second objective function J_2, as shown in Eq. (3.18b). The numbers in the subscript denote the 'pin' locations. In each configuration, the first three modes of one-pin ABC frequencies are used, making the total number of one-pin ABC frequencies involved in the objective function to be 9.

$$J_2 = R_{\mathrm{f}} + R_{\mathrm{A4}} + R_{\mathrm{A7}} + R_{\mathrm{A8}} \tag{3.18b}$$

Two-pin ABC frequencies are added to J_1 to form the third objective function J_3, as shown in Eq. (3.18c). Similar to Eq. (3.18b), the numbers in the subscript denote the 'pin' locations and the first three modes of two-pin ABC frequencies are used for each configuration. Similar to J_2, the total number of two-pin ABC frequencies involved in J_3 is also 9.

$$J_3 = R_{\mathrm{f}} + R_{\mathrm{A25}} + R_{\mathrm{A47}} + R_{\mathrm{A48}} \tag{3.18c}$$

The fourth objective function J_4 is formed by adding the MAC residual to J_1, as shown in Eq. (3.18d). Considering that in modal testing practice generally only the first couple of mode shapes may be measured with reliable accuracy, the first two mode shapes are used in this objective function.

$$J_4 = R_{\mathrm{f}} + R_{\mathrm{MAC}} \tag{3.18d}$$

The fifth objective function J_5 is formed by adding the mode shape change residual to J_1, as shown in Eq. (3.18e). Similar to J_4, the first two modes are used in J_5.

$$J_5 = R_{\mathrm{f}} + R_{\mathrm{MS}} \tag{3.18e}$$

3.5.3 Model updating considerations

The same FE model with 10 Timoshenko beam elements as established in Section 3.4 is used to model the damaged beams. The only difference is that damages are

now considered in the beam model. Here the damage is modelled as a reduction of the element stiffness for a beam element. A stiffness reduction ratio D_i is defined for the i^{th} element in the model by the following expression:

$$\mathbf{K}_{di} = (1 - D_i)\mathbf{K}_0 \tag{3.19}$$

where, $\mathbf{K}_0$ and $\mathbf{K}_d$ are the stiffness matrix of the intact and damaged beam element, respectively.

In the model updating, for generality each element in the beam model is assumed to have an unknown damage state which need to be updated. So totally there are 10 parameters to be updated, i.e., D_i, i=1, 2, …, 10.

For the search of the damage parameters the Genetic algorithm (GA) is employed. GA has been used widely as an optimization tool in engineering applications (Perera and Torres, 2006). Compared with using traditional methods, GA-based model updating has several advantages. For example, the GA searching results do not depend on the initial setting of the updating parameters, thus a global optimal result rather than a local one is generally guaranteed. Furthermore, there is no need to calculate the sensitivity matrix of the structure during the updating process, and this makes the updating more robust. There have been many successful applications of using GA in model updating problem, some of which are summarized in Perera and Torres (2006). In the present study, the standard GA function in Matlab has been used to update the FE model.

Table 3.4 Parametric setting for GA

Parameter	Setting
Population size	3000
Fitness limit	-Infinite
Max generation	1500
Crossover fraction	0.7
Mutation rate	0.02

The basic settings of the GA parameters are shown in Table 3.4. The convergence process of the GA calculation is monitored and it is found that a limit of maximum generation of 1500 is adequate to achieve satisfactory converging result in the present application.

3.5.4 FE model updating (damage identification) results

Five parallel updating procedures with five different objective functions listed in Eq. (3.18a-e) are carried out for the two damaged beams separately. The updating results are presented in Figure 3.13-3.17. In beam B1, the damaged element should be the 4th element, while in beam B2 the damaged elements should be the 4th and 8th elements. The equivalent element stiffness changes in the damage segments of the test beams were approximately 40% and 25% respectively, according to the cuts. This means the expected damage index D_i would be about 0.4 in element 4 for beam B1, and 0.4 in element 4 and 0.25 in element 8 for beam B2. The rest of the elements should have a D value being virtually zero (undamaged).

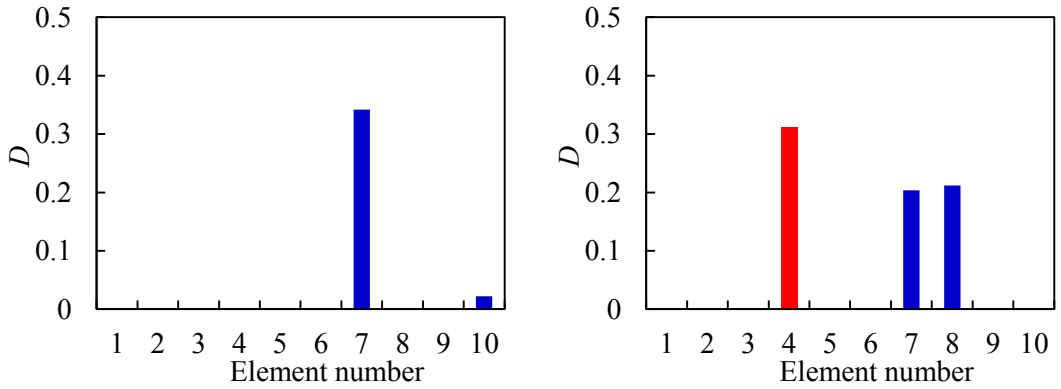

(a) B1 (b) B2

Figure 3.13 Updating results with J_1

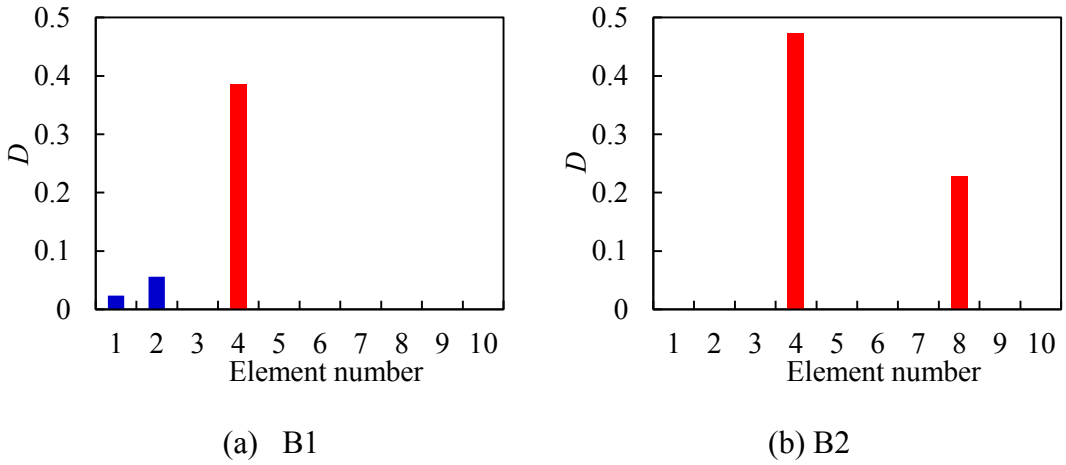

Figure 3.14 Updating results with J_2

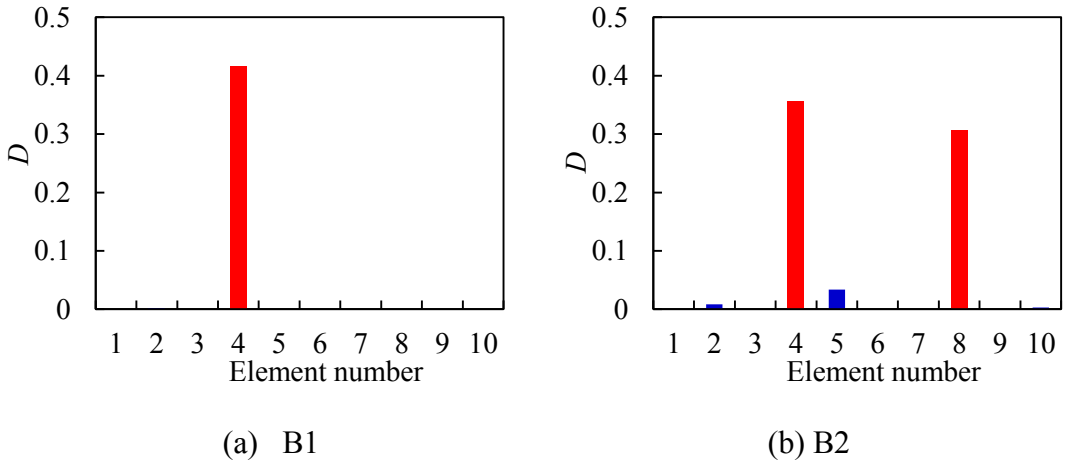

Figure 3.15 Updating results with J_3

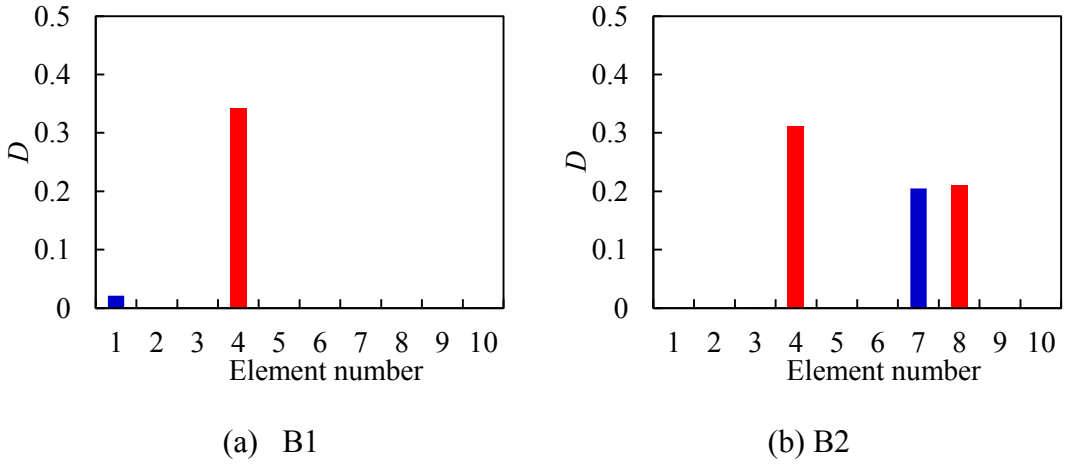

Figure 3.16 Updating results with J_4

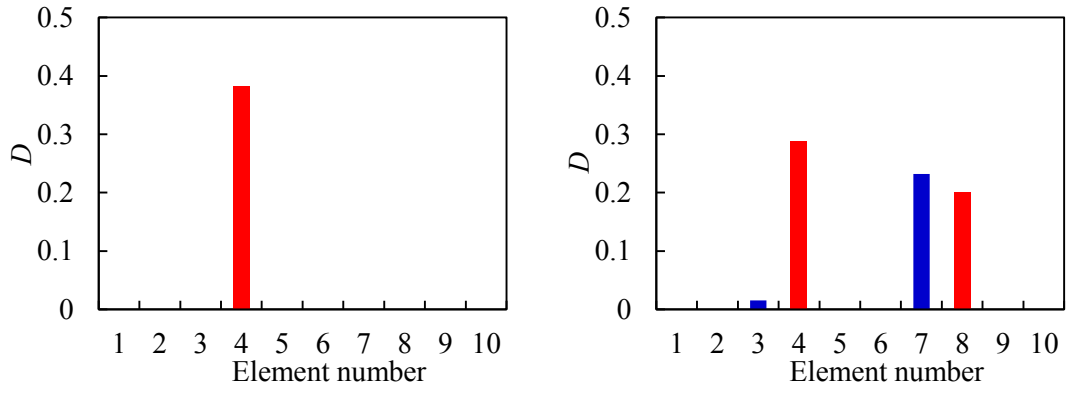

(a) B1 (b) B2

Figure 3.17 Updating results with J_5

It can be seen that when only the lowest five modes of natural frequencies are used in the updating (J_1, Figure 3.13), the correct damage element cannot be identified for beam B1, whereas in beam B2, a false crack is identified in the 7th element. The first reason for the failed updating is that natural frequencies are global scalar properties and cannot resolve the symmetry problem in terms of the damage location. As seen from the result for beam B1, the real damage should be in the 4th element but the identified damage is in the symmetric element along the beam span. Another reason here is that the number of unknown parameters (being updated) is larger than that of the input data, therefore it is an under-determined problem and consequently false identification of damages, such as the situation in beam B2, is basically inevitable.

When one-pin ABC frequencies are added into the objective function (J_2, Figure 3.14), it is found that the above issues are readily avoided and correct damage elements can be identified in both beam B1 and B2. Even better results are obtained when two-pin ABC frequencies are joined with the natural frequencies (J_3, Figure 3.15). These outcomes demonstrate that both one-pin and two-pin ABC frequencies can provide enhanced information with local features, thus enable a reliable and more robust updating process.

On the other hand, when mode shape information is added to the objective functions (J_4 and J_5, Figure 3.16, 3.17), good updating results can also be achieved for beam B1. However, a false damage element is identified in Beam B2 in both combinations. This is believed to be attributable to the measurement errors in the mode shapes.

The above comparisons between the updating results show that the incorporation of ABC frequencies performs very well in the damage identification of both single- and multiple-damaged beams, whereas use of the measured mode shapes show inconsistent performance in the damaged cases. Considering that ABC frequencies and mode shapes provide similar sort of information to the updating process, and the fact that the measurement accuracy of ABC frequencies can be more reliable than mode shapes, it may be concluded that ABC frequencies can be good alternatives to mode shapes in the model updating.

It should also be pointed out that in the present updating examples, only three sets of one-pin or two-pin ABC frequencies, corresponding to three pin location configurations, have been utilised. There exists an abundant choice of other possible configurations and as a result a lot more of such modal information can be available for the updating purposes. This special feature of ABC frequencies can be very useful when it comes to identification of a large number of unknown structural parameters, making the incorporation of the ABC frequencies potentially even more beneficial for general structural parameter identification.

3.6 Extraction of ABC frequencies from some more sophisticated structure conditions

The studies in Section 3.3-3.6 have shown that ABC frequencies can be extracted from relatively flexible structures with similar accuracy to natural frequencies. They also perform quite well in model updating processes. In this section, the possibility of extracting high quality ABC frequencies from some more sophisticated structures is evaluated. Two different types of structures, i.e., a group of stiff aluminium beams and a reinforced concrete (RC) beam with realistic boundary conditions, are used.

3.6.1 Aluminum beams with high stiffness

Five aluminium beams were tested in Chapter 5 to verify the cracked element model developed in Chapter 4. The dimension of the beams are with dimension as $L \times b \times h$ = 600 × 50.8 × 50.8 mm, where L, b and h are the span length, and width and height of

the section, respectively. It can be seen that the beams are relative thick with a length to sectional thickness ratio around 12. Material properties of beams are E = 71 GPa and ρ = 2700 kg/m^3. The specimens included an intact beam and four cracked ones with different numbers of cracks. Two beam specimens are shown in Figure 3.18 while detailed information of the cracked beams has been presented in Chapter 5 (Figure 5.1 and Table 5.1).

Figure 3.18 Examples of intact and cracked aluminium beams

Modal tests were carried out on the aluminium beams and results have been presented in Chapter 5. The boundary conditions of the beams were set to be free-free during the tests. The same modal testing equipment and signal processing strategy as presented in Section 3.3.1 were used for the aluminium beams. In the tests, several groups of measurements aiming at obtaining one-pin and two-pin ABC frequencies were included. Some of the test results have been shown in Table 5.2 and Figure 5.4.

The study here aims at evaluating the measurement accuracy of one-pin and two-pin ABC frequencies from the aluminium beams. Compared with the steel beams tested in Section 3.3, the aluminium beams have a much larger sectional thickness to length ratio. As a result, the natural frequencies of the aluminium beams are in a much higher frequency range. While the frequency range of the first five modes for the flexible steel beam is 30-400 Hz, the range for the aluminium beams is as high as 700 -8000 Hz. As it is always more challenging to obtain good measurement from higher frequency range due to the limitation of the test equipment, the aluminium beams are used to test whether it is possible to obtain good ABC frequencies from such extreme stiff structures.

Similar to the evaluation method presented in Section 3.4.4, the measured and predicted ABC frequencies should be both obtained and then the relative errors of the

ABC frequencies should be compared with those of natural frequencies. In Chapter 4 a cracked beam element model has been developed for the cracked beams and it has been proven to be accurate for estimating modal parameters in thick beams. Herein the cracked beam element model is used to predict the natural and ABC frequencies of the cracked beams. Results of three representative beams, one intact beam, one with a single crack and one with multiple cracks, are presented in Table 3.5-3.10, in which ε is the relative error between the measured and predicted values (in %). The pin numbers for ABC configurations for the beams are shown in Figure 3.19.

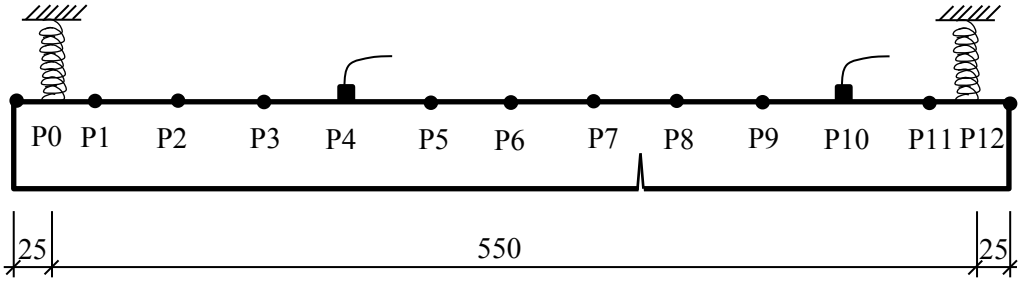

Figure 3.19 Modal testing setup for aluminium beams

Table 3.5-3.7 compare the measured and predicted natural and one-pin ABC frequencies. It can be seen that the errors in the natural frequencies are around 1% (in the range of 0.1%-2.5%). Errors in the one-pin ABC frequencies are in the similar range (in the range of 0.5%-2.7%). Only one result has a relatively high error as 3.6%.

Table 3.5 Measured and predicted natural and one-pin ABC frequencies (Beam B0; Unit: Hz)

Mode	Natural frequency			Pin at P4			Pin at 10		
	f_{0Am}	f_{0Ac}	ε/%	f_{0Am}	f_{0Ac}	ε/%	f_{0Am}	f_{0Ac}	ε/%
1	725.1	725.9	**0.1**	594.2	596.9	**0.5**	695.8	691.3	**0.6**
2	1912.6	1927.1	**0.8**	1387.4	1400.7	**1.0**	1806.1	1835.9	**1.6**
3	3547.3	3624.9	**2.2**	3466.7	3555.7	**2.6**	2835.8	2878.0	**1.5**
Mean			**1.0**			**1.3**			**1.3**

Table 3.6 Measured and predicted natural and one-pin ABC frequencies (Beam B2; Unit: Hz)

Mode	Natural frequency			Pin at P4			Pin at 10		
	f_{dAm}	f_{dAc}	ε/%	f_{dAm}	f_{dAc}	ε/%	f_{dAm}	f_{dAc}	ε/%
1	577.7	580.7	**0.5**	508.8	515.1	**1.2**	550.3	553.1	**0.5**
2	1702.3	1719.0	**1.0**	1140.1	1157.0	**1.5**	1651.1	1662.3	**0.7**
3	3493.4	3570.1	**2.2**	3440.4	3518.0	**2.3**	2703.4	2738.0	**1.3**
Mean			**1.2**			**1.7**			**0.8**

Table 3.7 Measured and predicted natural and one-pin ABC frequencies (Beam B4; Unit: Hz)

Mode	Natural frequency			Pin at P4			Pin at 10		
	f_{dAm}	f_{dAc}	ε/%	f_{dAm}	f_{dAc}	ε/%	f_{dAm}	f_{dAc}	ε/%
1	609.9	610.4	**0.1**	476.7	485.6	**1.9**	586.6	582.4	**0.7**
2	1481.7	1492.6	**0.7**	1079.6	1094.3	**1.4**	1425.5	1452.6	**1.9**
3	3228.7	3310.4	**2.5**	3125.4	3210.4	**2.7**	2629.3	2723.7	**3.6**
Mean			**1.1**			**2.0**			**2.1**

Table 3.8-3.10 show comparison results for two-pin ABC frequencies. Compared with natural frequencies and one-pin ABC frequencies, errors in two-pin ABC frequencies are higher. Quite a few results have errors around 2.5%-4.5%. The average errors of two-pin ABC frequencies are also higher than those of natural and one-pin ABC frequencies. Four groups of results have average errors larger than 2% while there is only one group for one-pin ABC frequencies.

One possible reason for higher measurement errors in two-pin ABC frequencies might be that it involves manipulation on multiple FRF curves to obtain the two-pin ABC frequencies. As the FRF measurement might be less promising in high frequency range, the obtained ABC frequencies would have higher error level.

Table 3.8 Measured and predicted two-pin ABC frequencies (Beam B0; Unit: Hz)

Mode	Pins at P0 and P12			Pins at P2 and P8			Pins at P4 and P10		
	f_{0Am}	f_{0Ac}	ε/%	f_{0Am}	f_{0Ac}	ε/%	f_{0Am}	f_{0Ac}	ε/%
1	331.9	324.2	**2.3**	545.7	555.8	**1.8**	562.3	555.8	**1.2**
2	1297.6	1257.7	**3.1**	1420.8	1390.4	**2.1**	1378.2	1390.4	**0.9**
3	2771.2	2723.5	**1.7**	2779.8	2684.8	**3.4**	2652.8	2684.8	**1.2**
Mean			**2.4**			**2.5**			**1.1**

Table 3.9 Measured and predicted two-pin ABC frequencies (Beam B2; Unit: Hz)

Mode	Pins at P0 and P12			Pins at P2 and P8			Pins at P4 and P10		
	f_{dAm}	f_{dAc}	ε/%	f_{dAm}	f_{dAc}	ε/%	f_{dAm}	f_{dAc}	ε/%
1	275.8	266.0	**3.5**	408.4	409.1	**0.2**	479.1	479.8	**0.1**
2	1174.6	1155.4	**1.6**	1313.1	1305.7	**0.6**	1137.4	1148.0	**0.9**
3	2699.1	2641.0	**2.2**	2714.4	2666.9	**1.7**	2596.3	2619.9	**0.9**
Mean			**2.4**			**0.8**			**0.7**

Table 3.10 Measured and predicted two-pin ABC frequencies (Beam B4; Unit: Hz)

Mode	Pins at P0 and P12			Pins at P2 and P8			Pins at P4 and P10		
	f_{dAm}	f_{dAc}	ε/%	f_{dAm}	f_{dAc}	ε/%	f_{dAm}	f_{dAc}	ε/%
1	283.8	270.9	**4.6**	452.5	459.0	**1.4**	452.4	453.3	**0.2**
2	1043.7	1016.6	**2.6**	1087.7	1076.9	**1.0**	1076.0	1091.1	**1.4**
3	2678.9	2643.7	**1.3**	2626.7	2551.2	**2.9**	2465.0	2566.5	**4.1**
Mean			**2.8**			**1.8**			**1.9**

Modal testing results on aluminium beams showed that very accurate one-pin ABC frequencies can still be obtained for stiff beams. Two-pin ABC frequencies can also

be obtained with relative high accuracy, although the accuracy is not as high as that of one-pin ABC frequencies. If comparing the frequency shifts of ABC frequencies due to the cracks to the measurement errors, it can be found that the errors are much smaller than the frequency shifts. The implication is that the extracted one-pin ABC frequencies should perform well in model updating and crack identification of the aluminium beams, which will be shown in Chapter 5.

3.6.2 RC beams with realistic boundary conditions

Modal testing is also carried out on an RC beam with realistic boundary conditions to extract one-pin and two-pin ABC frequencies. The tested beam is shown in Figure 3.20. The beam has a dimension of $L \times b \times h$ = 2000 × 100 × 200 mm. Two steel bars with diameter of 12 mm were placed as tensile reinforcement at the bottom side of the beam. During modal testing, the RC beam was placed at the top of two rollers to form simply supported boundary conditions, as shown in Figure 3.20(a).

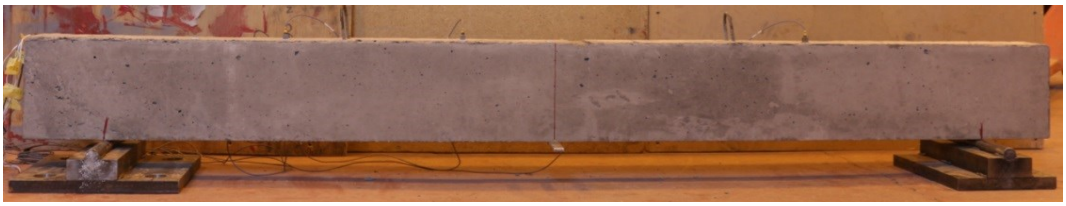

(a) Tested RC beam

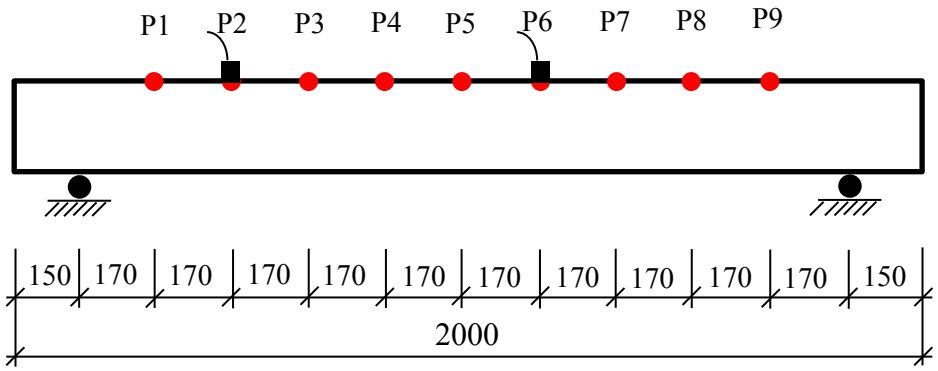

(b) Modal testing

Figure 3.20 Modal testing setup of the RC beam

The same modal testing equipment and signal process strategy as presented in Section 3.3.1 were used for the RC beam. 9 measurement points were marked on the top surface of the RC beam, as shown in Figure 3.20. Two accelerometers were attached at point P2 and P6. Excitation was applied successively from point P1 to P9 to measure the mode shapes of the beam. One-pin ABC frequencies with pin at P2 or P6, and two-pin ABC frequencies with pins at P2 and P6 can be also obtained from the tests. Measured driving FRF curves at point P2 and P6 are shown in Figure 3.21. It can be seen that the curves have clear resonances. With the pick peaking techniques, the mode shapes can be obtained and used to select the bending vibration modes from the resonant peaks.

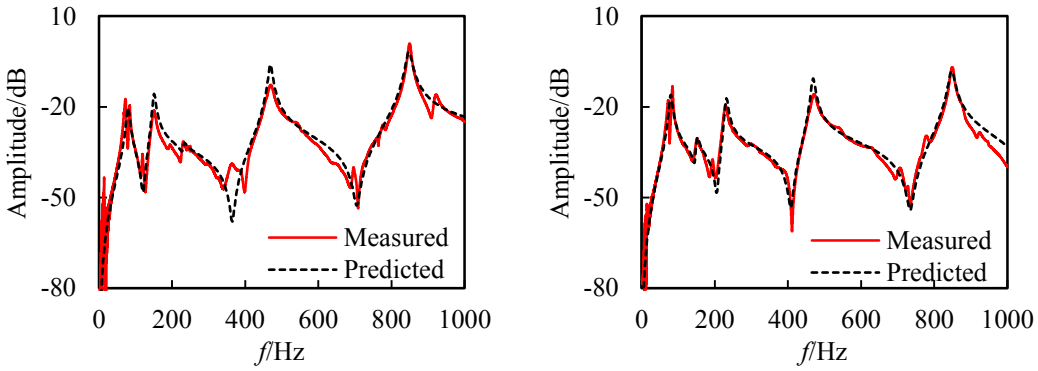

(a) at point P2 (b) at point P6

Figure 3.21 Driving FRF curves

Table 3.11 Measured and predicted natural and ABC frequencies (Unit: Hz)

Mode	Natural frequency			One-pin at P2			One-pin at P6			Two-pin at P2 and P6		
	f_{0Nm}	f_{0Nc}	ε/%	f_{0Am}	f_{0Ac}	ε/%	f_{0Am}	f_{0Ac}	ε/%	f_{0Am}	f_{0Ac}	ε/%
1	78.7	79.6	**1.1**	126.4	120.4	**4.8**	139.3	143.9	**3.3**	191.6	197.7	**3.2**
2	152.1	150.6	**1.0**	222.9	226.9	**1.8**	196.7	204.9	**4.2**	316.7	315.8	**0.3**
3	231.4	231.4	**0.0**	373.9	364.6	**2.5**	411.0	407.7	**0.8**	706.8	686.5	**2.9**
4	478.3	468.8	**2.0**	704.1	705.0	**0.1**	734.4	734.5	**0.0**	-	-	-
5	847.4	847.4	**0.0**	-	-	-	-	-	-	-	-	-
Mean			**0.8**			**2.3**			**2.1**			**2.1**

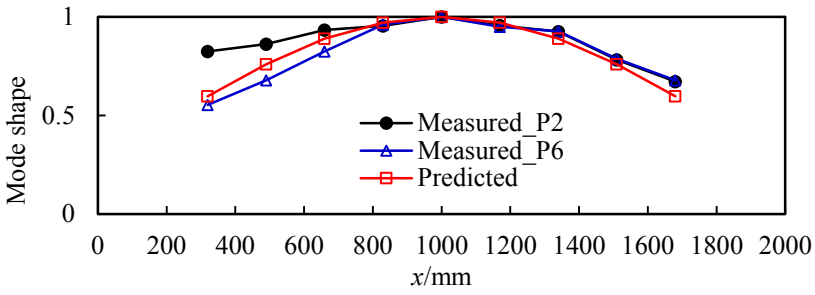

(a) 1st mode

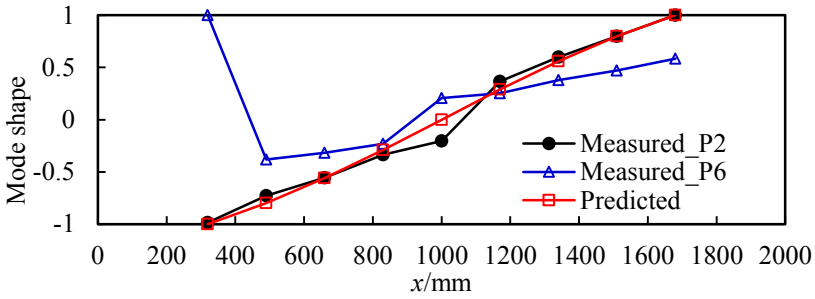

(b) 2nd mode

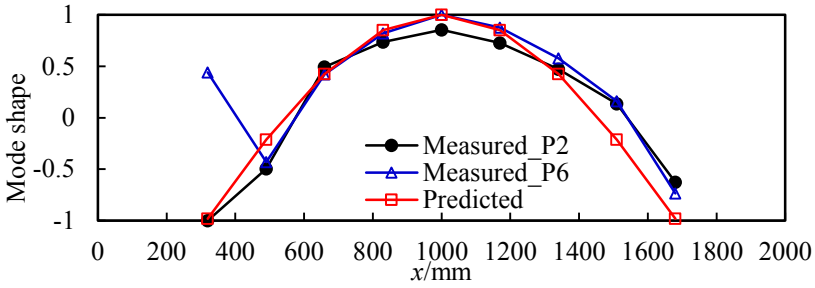

(c) 3rd mode

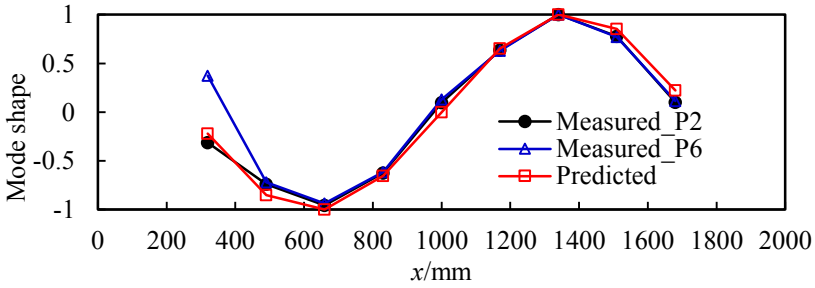

(d) 4th mode

Figure 3.22 Measured and predicted displacement-normalized mode shapes

First five modes of measured of natural frequencies and first four modes of displacement-normalized mode shapes are shown in Table 3.11 and Figure 3.22. As two accelerometers were attached on the RC beam, two sets of mode shapes were obtained. It can be seen that the two sets of mode shapes have notable discrepancies for the first three modes. The errors in the mode shape displacement at point P1 are extremely large for the measurement with accelerometer P6. The reason for this kind of error is not immediately clear.

To obtain the one-pin ABC frequencies, the antiresonances should be identified. It can be noticed that antiresonant areas of the curves have relatively poor quality compared with the resonant areas. The curves are noisy around these areas, and there are even no clear antiresonances at some modes. To extract the one-pin ABC frequencies, the RFP method is applied on the FRF curves and the first four modes of one-pin ABC frequencies are presented in Table 3.11.

Two-pin ABC frequency function curves can be calculated from the measured FRF curves, as shown in Figure 3.23. It is still easy to identify the first three resonances in the curves although it might be difficult to directly obtain the ABC frequencies. Similar to one-pin ABC frequencies, the RFP method is used to extract the two-pin ABC frequencies, as listed in Table 3.11.

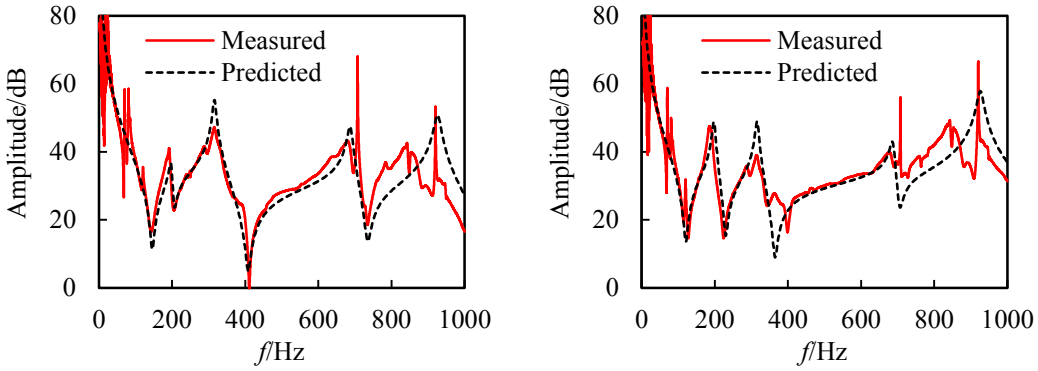

(a) at point P2 (b) at point P6

Figure 3.23 Measured and predicted ABC frequency function curves

A Timoshenko beam element model for the RC beam is then established and updated with the measured natural frequencies. The bending stiffness of the beam *EI* is set as one updating parameter. It is also noticed that the stiffness of the roller supports have

significant influence on the beam vibration, as a result, the vertical stiffness of the rollers, k_v, is set as the second updating parameter. The beam model is shown in Figure 3.24. The model is updated with the objective function as shown in Eq. (3.16), which is formed with the first five natural frequencies. The updated parameters are $EI = 2180$ kN·m^2 and $k_v = 22564$ kN/m.

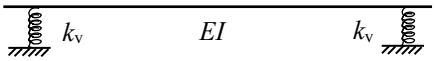

Figure 3.24 Beam element model for the RC beam

The updated beam model is then used to predict the natural frequencies, mode shapes and ABC frequencies of the beam. The predicted FRF and ABC frequency function curves are shown in Figure 3.21 and 3.23. The predicted curves generally agree well with the measured ones. Comparison of natural and ABC frequencies is shown in Table 3.11. It can be seen that the predicted natural frequencies match quite well with the measured results and the mean error is less than 1%. The accuracy of one-pin and two-pin ABC frequencies is lower, with mean errors around 2.1%. The first modes of one-pin and two-pin ABC frequencies have measurement errors as high as 3.2%-4.8%. Reasons for the lower measurement accuracy of ABC frequencies can be explained from the poor estimation of FRF curves away from the resonant areas. Many factors might have contributed to this, such as the additive and multiplicative noises from the roller supports, or nonlinear interaction between the beam and the supports.

3.7 Summary and conclusions

The ability to obtain good-quality additional modal frequency data is highly desirable in structural health monitoring and damage detection applications. Introducing ABC frequencies to the spectrum of modal data provides a promising opportunity to expand the modal frequency dataset and enhance its overall sensitivity for detecting and identifying structural changes, as has been demonstrated in the preceding studies using simulated ABC frequency data. However, to bring the approach closer to practical applications, acquisition of the ABC frequencies from real measured data is

a key. In the past, there has not been systematic investigation on the possibility of extracting high quality two-pin ABC frequencies from physical measurements. The accuracy of measured ABC frequencies, which is a key question to be answered before incorporating them into damage identification applications, is also not clearly answered.

In this chapter a comprehensive experimental investigation on the acquisition of ABC frequencies from laboratory experiments has been presented. The effects of general modal testing operation, data acquisition and signal processing have been examined systematically in the context of acquiring ABC frequencies, particularly with regard to producing smooth FRF curves in their entirety rather than focusing only on the modal peaks. Specific requirements, such as an accurate measurement of the excitation impact force history, as well as the use of RFP to enhance the identifiability of the ABC frequencies, have been highlighted. The possible error sources in the measurement of ABC frequencies have also been discussed.

Results from the representative beam experiments demonstrate that, with a careful implementation of modal testing and data analysis procedures, one-pin and two-pin ABC frequencies in the first few ABC modes for any pin location configurations can be obtained with good quality, and the accuracy can be comparable to that of the natural frequencies.

Through finite element model updating, it is shown that the incorporation of ABC frequencies in the data set significantly improves the parameter identification results, and both single- and multi-damage scenarios in the experimental beams can be identified correctly. In comparison, the results using combined natural frequencies and limited mode shapes exhibit less satisfactory results due to higher measurement errors in the mode shapes. Therefore, using ABC frequencies as alternatives to mode shapes is deemed promising in structural identification applications.

The possibility of extracting ABC frequencies from more sophisticated structure conditions is tested with a group of extremely stiff aluminium beams and an RC beam with realistic boundary conditions. Results showed that one-pin and two-pin ABC frequencies can still be extracted from the structures with reasonable accuracy, although the accuracy of ABC frequencies is no longer as high as that of natural

frequencies. The errors in some ABC frequencies can be as high as 3%-4%, which is due to the difficulty of obtaining high quality FRF curves not only around resonances but in the whole frequency range. For such situations, it is still possible to employ ABC frequencies for applications such as model updating and damage identification as long as the frequency shifts brought by the structural damages are much larger than the measurement errors, as proven in Chapter 5.

It should be noted that the investigation in this chapter is based on measurements in a laboratory environment. The same physical measurement and processing procedure can be applied to extract ABC frequencies in real-life applications. It can be anticipated, however, that some complexities in real life structures such as the real boundary conditions and ambient noise, could affect the accuracy in the extracted ABC frequencies. The influence of these real-life factors will require further investigation in the next stage of research in this direction.

4 A cracked beam element model and its implementation for Identification of cracks in thick beams

4.1 Introduction

The present chapter aims at developing a robust damage identification approach for cracks in beams, with a special focus on thick beams which present more complexity in terms of the effect of a crack than slender beams. The numerical example presented in Chapter 1 has clearly shown the importance of using a robust crack model for the modelling of cracked beams. The review in Chapter 2 shows that the cracked beam element model formulated on the basis of the additional flexibility has overall superiority comparing to the other approaches. As a result, this approach is employed to form the cracked beam element model for crack identification herein.

In this chapter, the basic formulation of the cracked beam element model is first described. The adequacy of the model is verified in a forward manner by comparing the predicted natural frequencies of the cracked beam with the numerically simulated results generated from a refined finite element analysis. Subsequently, the cracked beam model is implemented in a general finite element model updating procedure. To tackle the randomness of the crack location, an adaptive process is incorporated, so that the crack is always located around the middle of the beam element containing the crack in the final discretisation. For the updating of the model parameters, we employ the Genetic Algorithms (GA) to perform the searching process. All elements in the beam are subject to the updating for the crack parameters, thus the procedure can be applied in the identification of any location, severity or combination of cracks.

4.2 Cracked beam element model

The cracked beam element model based on local flexibility and fracture mechanics is adopted here for the development of a more reliable approach to the identification of cracks in thick beams. For the sake of completeness, the essential model formulation is described first. The model is then verified for the calculation of the natural frequencies and mode shapes of cracked thick beams in order to check the robustness

of the model for both lower and higher modes. The reduced stiffness model is used for the current model to compare with throughout the verification.

As a matter of clarity, herein we define 'thick' beams as those having a length to sectional thickness (depth) ratio in the range of 5 to 15. Such beams represent the majority of beams in civil engineering structures. As has been stated, the shear deformation and rotational inertia will have marked influence on the vibration of thick beams. Therefore the formulation of the cracked beam element is based on the Timoshenko beam theory. For the present study, a plane-stress beam with a rectangular section is considered. The same general approach and basic observations will apply for beams with other section geometry, but specific local flexibility (and hence stiffness) needs to be derived accordingly.

4.2.1 Model formulation

A cracked beam element with the full 6 DOFs in the two-dimensional space is shown in Figure 4.1. The crack is located at a distance of l_c from the left node and the crack depth is a. We define the ratio of crack depth a to the sectional depth h as the crack depth ratio α, $\alpha = a/h$. The width of the beam element is b.

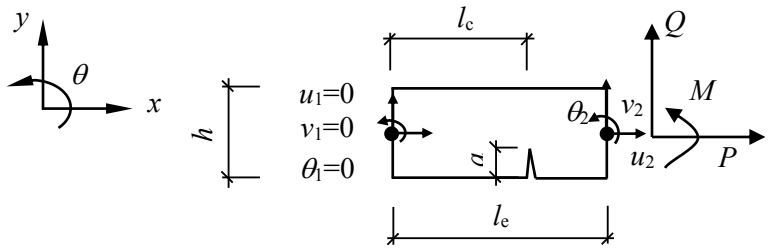

Figure 4.1 Loading state of a cracked beam element

It is well known that for relatively thick beams, the shear deformation and rotational inertia of the beams cannot be ignored. For cracked thick beams, the problem still exists. Several authors have observed the difference in the vibrational properties between Euler and Timoshenko models for cracked beams (Aydin, 2013; Kikidis and Papadopoulos, 1992; Lele and Maiti, 2002; Swamidas, et al., 2004). The general conclusion is that the relative difference between the modal data estimated from the

two models varies with the crack depth. To eliminate such modelling errors we have used Timoshenko beam model for the cracked element here.

Besides, the axial DOFs are considered in the cracked beam element formulation. It will be shown in the next section (4.2.2) that there will be coupling terms between the longitudinal and transverse or rotational DOFs in the stiffness matrix for the cracked element. The effect on the free vibration of the cracked beam is that coupling modes of longitudinal and transverse motions will appear, as has been extensively studied for shaft and rotor members (Darpe, et al., 2004; 1987; Papadopoulos and Dimarogonas, 1987). The coupling effect is stronger for thicker beams, as demonstrated by Kikidis and Papadopoulos (1992), and thus it is considered in the current model.

The flexibility of the cracked element can be established using the energy approach in conjunction with the fracture mechanics principle, as has been summarized in Section 2.3. As shown in Eq. (2.2), the strain energy in the cracked beam element under a generalised load is equal to the strain energy of the intact beam element plus the additional strain energy brought by the crack. The additional strain energy due to the presence of crack can be evaluated by the fracture energy. Let the 3 DOFs at the left node be fixed, and the generalised load be axial load P (u_2), shear force Q (v_2) and bending moment M (θ_2).

According to fracture mechanics, the additional strain energy brought by the crack U_c for the beam element in Figure 4.1 can be expressed as:

$$U_c = b\int_0^a G\mathrm{d}a \tag{4.1}$$

The relationships between the energy release rate G and the SIFs are given in Eq. (2.3). For the cracked element considered here, only the first two types of SIFs exist. The relationships between the SIFs and the applied loads from the standard fracture mechanics theory are expressed as:

$$K_{\mathrm{I1}} = \frac{P}{bh}\sqrt{\pi a}F_{\mathrm{I1}}(\alpha) \tag{4.2a}$$

$$K_{\mathrm{I2}} = \frac{6M}{bh^2}\sqrt{\pi a}F_{\mathrm{I2}}(\alpha) \tag{4.2b}$$

$$K_{\mathrm{II}} = \frac{Q}{bh}\sqrt{\pi a}F_{\mathrm{II}}(\alpha) \tag{4.2c}$$

where K_{I1} and K_{I2} takes into account the stress brought by axial force and moment, respectively, and K_{II} takes into account the stress brought by the shear force. $F_{\mathrm{I1}}(\alpha)$, F_{I2} (α) and $F_{\mathrm{II}}(\alpha)$ are dimensionless terms and they are expressed as (Tada, et al., 2000):

$$F_{\mathrm{I1}}(\alpha) = \sqrt{\frac{2}{\pi\alpha}\tan\frac{\pi\alpha}{2}} \cdot \frac{0.752 + 2.02\alpha + 0.37(1-\sin 0.5\pi\alpha)^3}{\cos 0.5\pi\alpha} \tag{4.3a}$$

$$F_{\mathrm{I2}}(\alpha) = \sqrt{\frac{2}{\pi\alpha}\tan\frac{\pi\alpha}{2}} \cdot \frac{0.923 + 0.199(1-\sin 0.5\pi\alpha)^4}{\cos 0.5\pi\alpha} \tag{4.3b}$$

$$F_{\mathrm{II}}(\alpha) = \frac{1.122 - 0.561\alpha + 0.085\alpha^2 + 0.180\alpha^3}{\sqrt{1-\alpha}} \tag{4.3c}$$

For current loading case with axial force P, shear force Q and bending moment M, the strain energy release rate G can be written as (Tada, et al., 2000):

$$G = \frac{1}{E'}\left[\left(\frac{P}{bh}\sqrt{\pi a}F_{\mathrm{I1}}(\alpha) + \frac{6(M+Ql_e-Ql_c)}{bh^2}\sqrt{\pi a}F_{\mathrm{I2}}(\alpha)\right)^2 + \left(\frac{Q}{bh}\sqrt{\pi a}F_{\mathrm{II}}(\alpha)\right)^2\right] \tag{4.4}$$

On the other hand, the strain energy of an intact Timoshenko beam element U_0 can be calculated as:

$$U_0 = \frac{1}{2}\int_0^{l_e}\left[\frac{(M+Ql_{\mathrm{e}}-Qx)^2}{EI} + \frac{Q^2}{GA_{\mathrm{e}}} + \frac{P^2}{EA}\right]\mathrm{d}x \tag{4.5}$$

where, A_{e} is the effective shear area of the beam section and for rectangular section, A_{e}=5/6A.

With Eq. (2.4), (4.4) and (4.5), the additional and intact flexibility for the cracked beam element can be calculated respectively as:

$$c_{ij,c} = \frac{\partial^2}{\partial F_i \partial F_j}\int_0^a \frac{b}{E'}\left[\left(\frac{P}{bh}\sqrt{\pi a}F_{\mathrm{I1}}(\alpha) + \frac{6(M+Ql_e-Ql_c)}{bh^2}\sqrt{\pi a}F_{\mathrm{I2}}(\alpha)\right)^2 + \left(\frac{Q}{bh}\sqrt{\pi a}F_{\mathrm{II}}(\alpha)\right)^2\right]\mathrm{d}a \tag{4.6a}$$

$$c_{ij,0} = \frac{\partial^2}{\partial F_i \partial F_j} \frac{1}{2} \int_0^{l_e} \left[\frac{(M + Ql_e - Qx)^2}{EI} + \frac{Q^2}{GA_e} + \frac{P^2}{EA} \right] dx \tag{4.6b}$$

where, i, j = 1, 2, 3, and F_1=P, F_2=Q, F_3=M.

It can be seen that there are 2 parameters representing the crack information in c_{ij}, as crack depth a and crack location l_c.

The complete 6×6 stiffness matrix for the element can be obtained by inverting the flexibility matrix and satisfying the force equilibrium in the elements, as follows:

$$K_c = T * C^{-1} * T^T \tag{4.7}$$

where $\boldsymbol{C}$ is the 3×3 flexibility matrix with c_{ij} as its elements. $\boldsymbol{T}$ is the transforming matrix,

$$T = \begin{bmatrix} -1 & 0 & 0 \\ 0 & -1 & 0 \\ 0 & -l_e & -1 \\ 1 & 0 & 0 \\ 0 & 1 & 0 \\ 0 & 0 & 1 \end{bmatrix} \tag{4.8}$$

4.2.2 Discussion on the cracked beam stiffness matrix

For any relative location and depth of the crack, the additional and intact flexibility terms can be evaluated from Eq. (4.6), and subsequently the stiffness matrix can be calculated according to Eq. (4.7). In a standard form, $\boldsymbol{K_c}$ can be written as:

$$K_c = \begin{bmatrix} k_{11} & k_{12} & k_{13} & k_{14} & k_{15} & k_{16} \\ & k_{22} & k_{23} & k_{24} & k_{25} & k_{26} \\ & & k_{33} & k_{34} & k_{35} & k_{36} \\ & & & k_{44} & k_{45} & k_{46} \\ & sym & & & k_{55} & k_{56} \\ & & & & & k_{66} \end{bmatrix} \tag{4.9}$$

The stiffness terms in the matrix can be subdivided into two groups; the diagonal elements k_{ii} (i=1, 2, …,6), which represent the driving stiffness of the 6 DOFs, and the off-diagonal elements k_{ij} (i, j=1, 2, …,6, and $i \neq j$), which represent the coupling

between two different DOFs. It should be noticed that the elements in the stiffness matrix are not all independent. Due to the force equilibrium relationship, some elements are the linear combination of others. For example, there are relationships as $k_{12} = -k_{24} = -k_{15} = k_{45}$, and $k_{26} = k_{22}*l_e - k_{23}$.

To illustrate the influence of the crack parameters on the elements of the matrix, it is convenient to use a numerical example. We use a beam element with l_e = 100 mm, h = 100 mm, b = 50 mm and the material properties are set as E = 2.01 GPa, ν = 0.3 and ρ = 7850 kg/m^3. A crack is set at a distance l_c from the left node, with a depth ratio $\alpha = a/h$. The ranges of the two crack parameters are set as: α = 0-0.5, and l_c = 0-50 mm.

Firstly the influence of the crack depth ratio is examined. Let the crack location be fixed at l_c = 25 mm and the crack depth ratio α varies in the above mentioned range to observe the trend of the matrix elements. For those stiffness elements which have the same absolute value, only the common absolute value is presented.

To demonstrate the crack effect we define a ratio β_{ij} in Eq. (4.10), where k_{ij} (α = 0) is the value of the stiffness element for the intact beam element. It should be noted that some off-diagonal elements such as k_{12}, k_{13} and k_{16} have zero values for the intact beam, and for these elements a reference value at α = 0.05 is used as the respective denominator in the calculation of β_{ij}.

$$\beta_{ij} = \frac{k_{ij}(\alpha)}{k_{ij}(\alpha = 0)} \tag{4.10}$$

The β_{ij} versus α relationships are presented in Figure 4.2. The diagonal elements of the stiffness matrix are shown in Figure 4.2(a), and it can be seen that in general these stiffness values reduce markedly with the increase of the crack depth ratio. The reduction of the diagonal elements is quite natural and it is in line with the stiffness reduction due to the crack. It is worth noting, however, that different DOFs show different rate of stiffness reduction. In the current example, element k_{33} (rotational stiffness) has the largest sensitivity to α; for α = 0.3, the ratio of k_{33} is about 0.6 as compared to k_{22} (translational stiffness) of about 0.85.

For the off-diagonal elements, it can be seen from Figure 4.2(b) that element k_{26}, which represents the transfer stiffness between the translational DOF of the left node and the rotational DOF of the right node, has a slight increase instead of decrease when α is in the range of 0-0.35. This is because from equilibrium k_{26} can be calculated as $k_{22}*l_e - k_{23}$. When the reduction rate of $k_{22}*l_e$ is smaller than that of k_{23}, k_{26} will increase as appears in Figure 4.2(b).

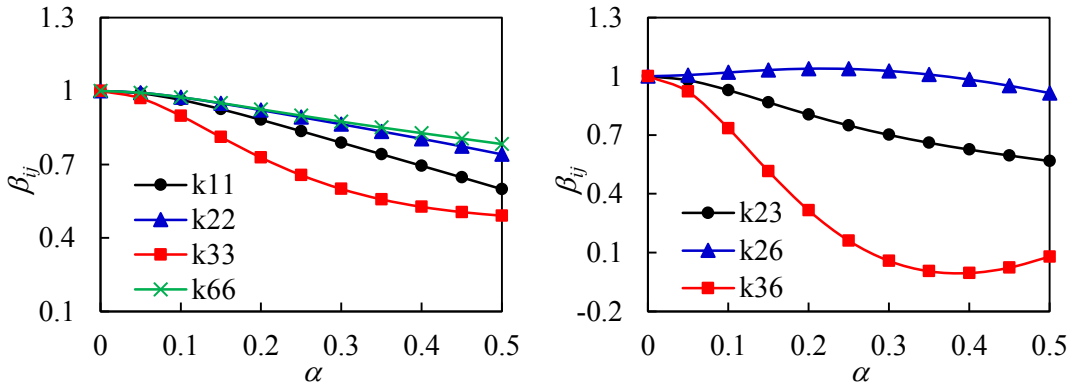

(a) Diagonal elements (b) Off-diagonal elements relating translational and rotational DOFs

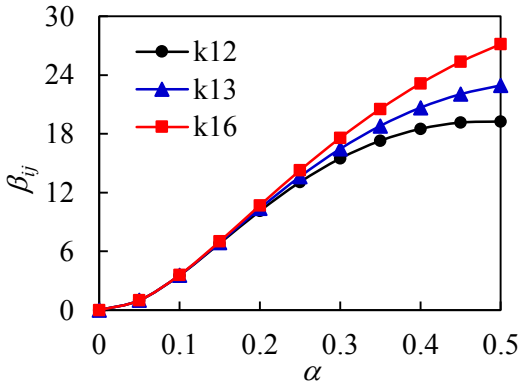

(c) Off-diagonal elements relating longitudinal and translational or rotational DOFs

Figure 4.2 Influence of crack depth ratio on the elements of stiffness matrix

The off-diagonal elements that represent the transfer stiffness between the longitudinal and translational or rotational DOFs, such as k_{12}, k_{13} and k_{16}, are shown in Figure 4.2(c). It should be noted that these elements are all zero in the matrix for the intact beam. But they are no longer zero when an asymmetric (single-edge) crack is present which brings eccentricity to the cracked section. The absolute values of

these elements increase persistently with increase of the crack depth. The result of these off-diagonal elements being non-zero is that coupling between the longitudinal and translational modes will appear in the structural vibration.

To observe the influence of crack location l_c on the stiffness matrix elements, the crack depth ratio α is fixed as 0.5 and the crack is gradually moved from the left node to the middle of the beam element. A location influence ratio γ_{ij} is defined with respect to the stiffness when the crack is located at the left end of the beam element as:

$$\gamma_{ij} = \frac{k_{ij}(l_c)}{k_{ij}(\alpha = 0.5, l_c = 0)} \tag{4.11}$$

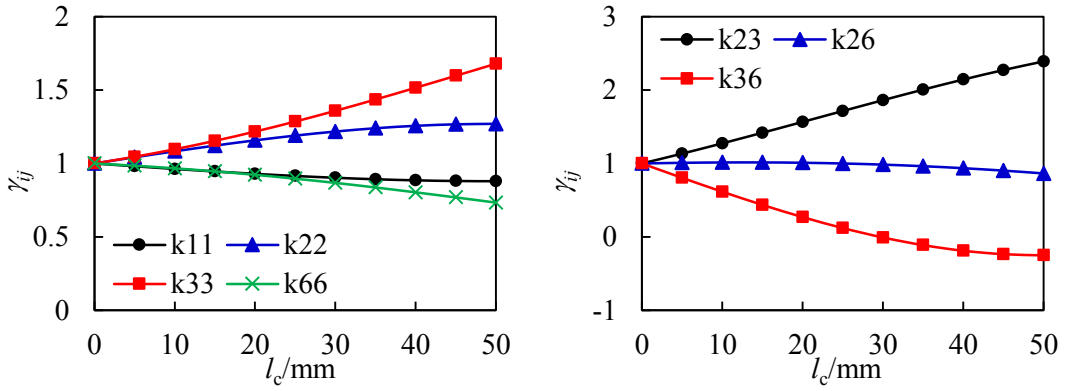

(a) Diagonal elements (b) Off-diagonal elements relating translational and rotational DOFs

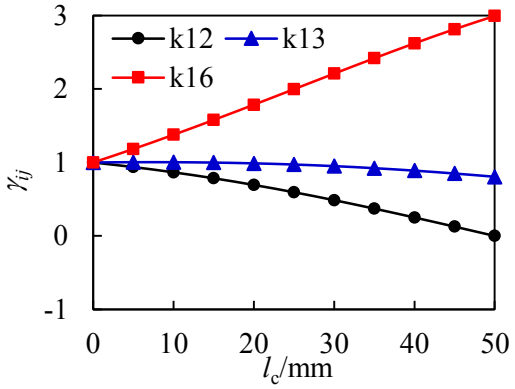

(c) Off-diagonal elements relating longitudinal and translational or rotational DOFs

Figure 4.3 Influence of crack location on the elements of stiffness matrix

Figure 4.3 illustrates the γ_{ij} versus l_c relationships. Different trends are observed for the different stiffness elements. Take the diagonal elements for example, k_{22} and k_{33} increase with l_c while k_{11} and k_{66} show the opposite trend.

The above analysis shows that the changes of the matrix elements in relation to the changes of the crack parameters differ significantly from what may be represented by assuming a uniform change of the element stiffness as adopted in the reduced stiffness model. Some stiffness elements will decrease to a varying extent with the increase of crack parameters, while some other elements will increase. The transfer stiffness elements relating the axial and translational or rotational DOFs, which are zero in the intact beam matrix, will no longer be zero in the cracked beam element. These actual effects of the crack parameters on the beam stiffness matrix illustrate from a mathematic point of view why the reduced stiffness model cannot accurately predict the modal parameters of the example cracked beam shown in Chapter 1.

4.3 Forward verification of the cracked beam element model

4.3.1 Forward verification for the dynamic properties

The performance of the cracked beam element described in Section 3.1 in the analysis of the beam vibration, herein concerning particularly the modal frequencies and mode shapes, is verified with numerical examples. A beam with the following properties is simulated: $L \times b \times h$ = 1000×50×100 mm. Material properties are set as: E = 201 GPa, ν = 0.3, ρ = 7850 kg/m^3.

The crack is set at L_c = 350 mm from the left support of the beam. Two crack depth ratios, α = 0.3 and 0.5, are used in the calculations.

Several representative boundary conditions, namely free-free, simply supported (with a span as 1000 mm), and fixed-free (cantilever), are considered in the verification, as shown in Figure 4.4.

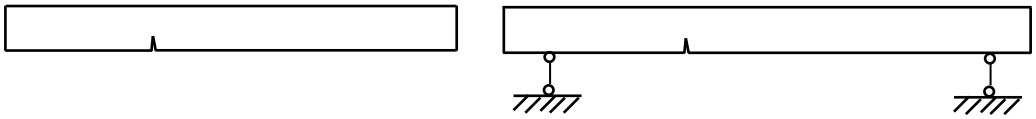

(a) Free-free (b) Simply supported

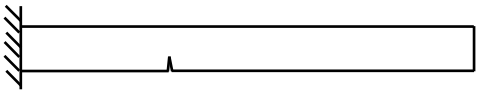

(c) Cantilever

Figure 4.4 Boundary conditions of the beams

For the verification within this chapter, we shall use refined continuum finite element model with solid elements to produce the benchmark data for the comparison of the results from the cracked beam element model. Using refined FE model with solid elements can represent sufficiently well the spatial effect of the cracks on the beam behaviour, and at the same time does not involve complications from sources such as measurement errors and other imperfection from physical tests, and therefore serves exactly the purpose of examining the soundness of the cracked beam element model. In the subsequent descriptions, the term 'numerically simulated data' will refer to the simulated data from the numerical experiments using the refined finite element model unless specified otherwise.

To accurately model the effect of the crack, the mesh density is increased towards the crack tip, as depicted in Figure 4.5.

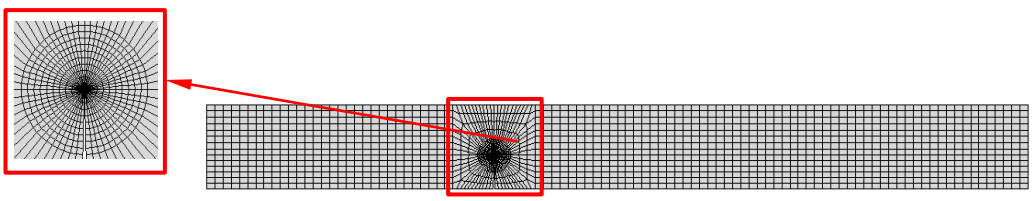

Figure 4.5 Mesh of the FE model with solid elements

In the parallel model using beam elements, 10 Timoshenko beam elements, including 9 intact and 1 cracked, are used. Timoshenko stiffness and mass matrices with high-accuracy cubic shape functions are used for the intact elements, while the cracked beam element model described in Section 4.2 is used for the cracked element. Both longitudinal and transverse modes are calculated with the FE model but only the transverse modes are discussed below. To verify the accuracy of the cracked beam element model, two indicators are used in the comparison. The first one is the shift of the natural frequency brought by the crack, S_i,

$$S_i = \frac{f_i^0 - f_i^{\mathrm{d}}}{f_i^0} \times 100\% \tag{4.12}$$

where f_i^0 and f_i^{d} are the i^{th} natural frequencies of the intact and cracked beams, respectively. The numerically simulated and predicted natural frequency shifts will be compared.

The second indicator is the Modal Assurance Criterion (MAC), which measures the consistency of two mode shapes,

$$\mathrm{MAC}_i = \frac{\left| \{\phi_i^{\mathrm{m}}\}^T \{\phi_i^{\mathrm{c}}\} \right|^2}{\left| \{\phi_i^{\mathrm{m}}\}^T \{\phi_i^{\mathrm{m}}\} \right| \cdot \left| \{\phi_i^{\mathrm{c}}\}^T \{\phi_i^{\mathrm{c}}\} \right|} \tag{4.13}$$

where, $\{\phi_i^{\mathrm{m}}\}$ and $\{\phi_i^{\mathrm{c}}\}$ are the numerically simulated and predicted i^{th} mode shapes of the cracked beam, respectively.

The reduced stiffness method, as defined in Eq. (1.1), is also used in a separate beam model to facilitate a cross-comparison with the cracked beam element model. An 'equivalent' reduced elemental stiffness ratio (D_{e}) for a given crack scenario is obtained through a model updating procedure to give a best fit to all the first five natural frequencies.

Frequency shifts of the first 6 modes are compared in Figure 4.6 and 4.7. It can be seen that the numerically simulated and predicted results using the cracked beam element model match quite well for all modes.

In contrast, the reduced stiffness model can only predict the frequency shifts consistently for the first two modes, and large errors occur in the higher modes, and for some modes the percentage error is even larger that the frequency shift itself. This echoes the discussions in Chapter 1 and Section 4.3.

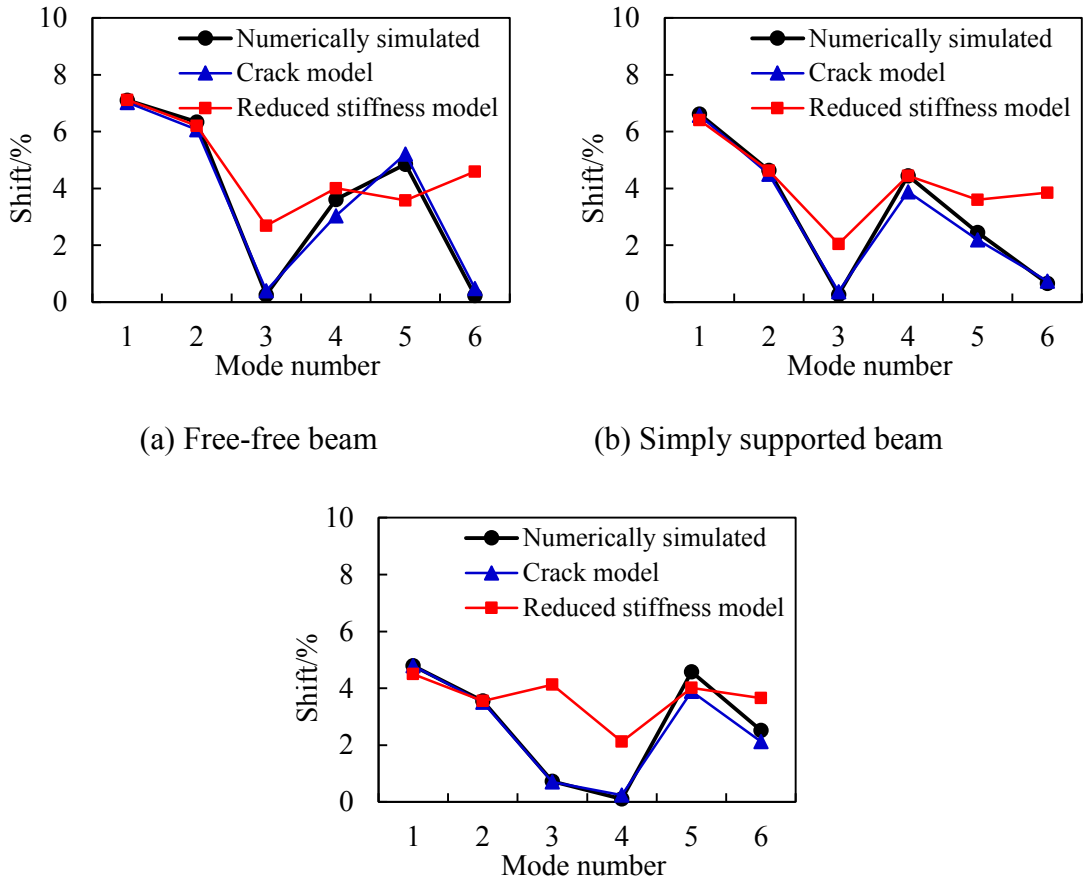

(a) Free-free beam

(b) Simply supported beam

(c) Cantilever beam

Figure 4.6 Comparisons between numerically simulated and predicted frequency shifts ($\alpha = 0.3$)

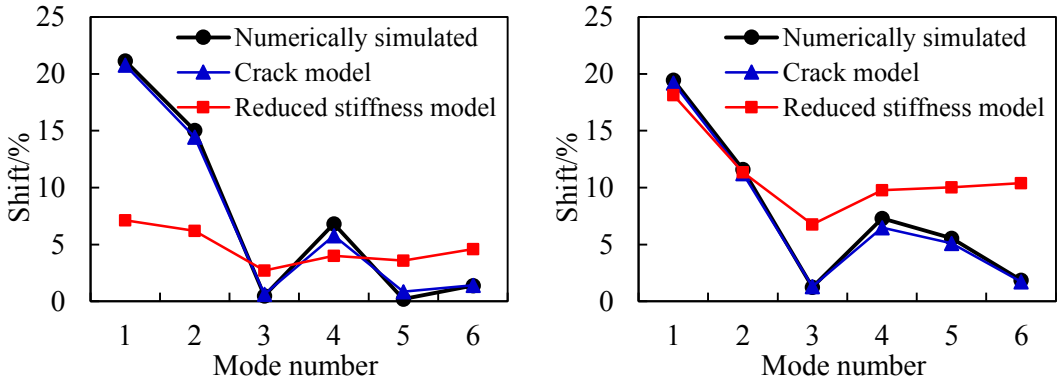

(a) Free-free beam (b) Simply supported beam

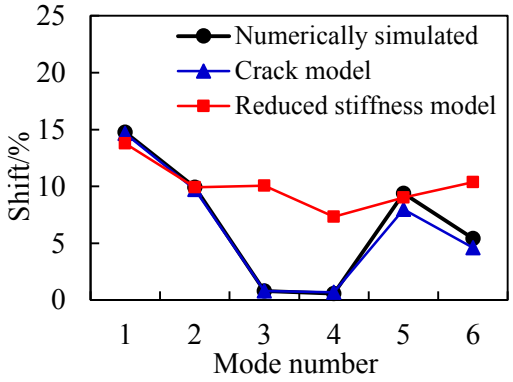

(c) Cantilever beam

Figure 4.7 Comparisons between numerically simulated and predicted frequency shifts ($\alpha = 0.5$)

The MAC results for the first 6 mode shapes are compared. The results for beams with $\alpha = 0.3$ and 0.5 are shown in Figure 4.8 and 4.9, respectively. It can be seen that the MAC values with the crack model are all greater than 0.99, indicating very good match between the numerically simulated and predicted mode shapes. The reduced stiffness model is also able to get quite satisfactory MAC values for lower modes; however, the results are not so good for higher modes, especially for beams with a larger crack depth ratio.

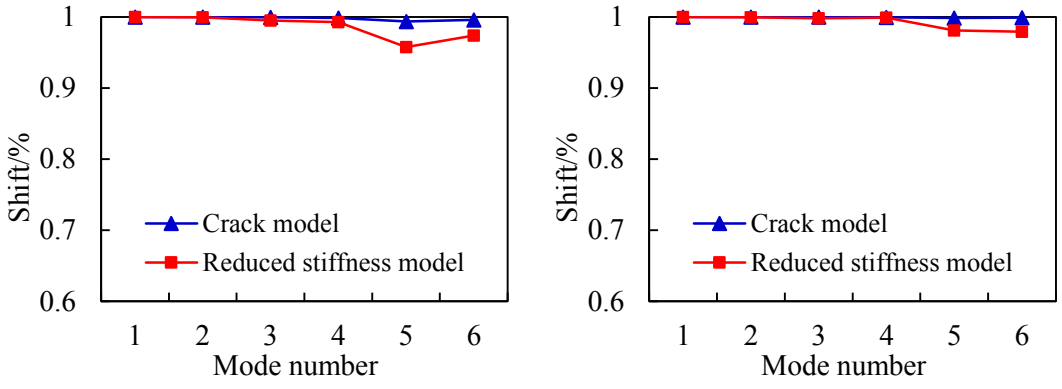

(a) Free-free beam (b) Simply supported beam

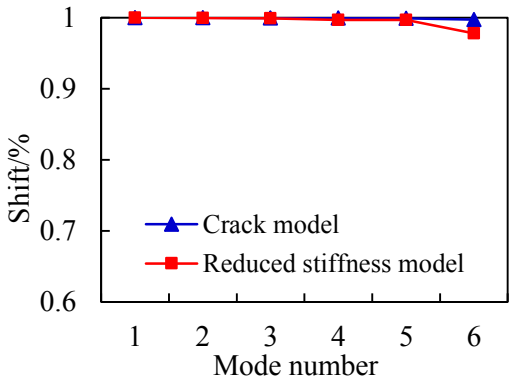

(c) Cantilever beam

Figure 4.8 Comparison between MAC results from two different models ($\alpha = 0.3$)

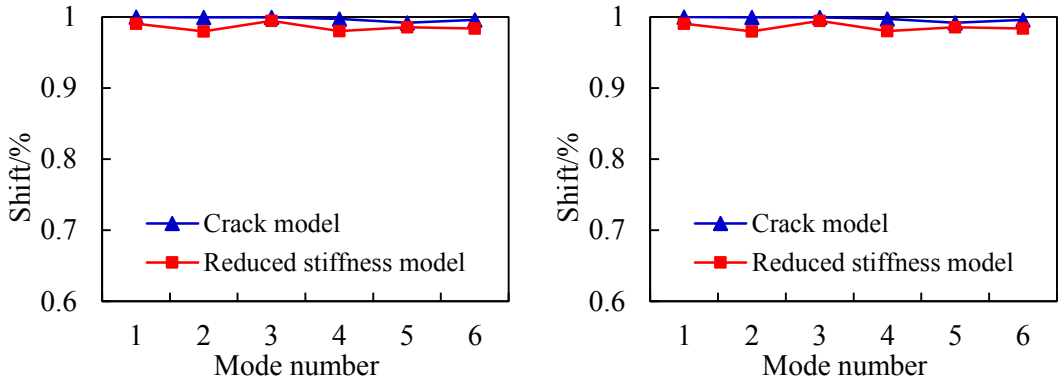

(a) Free-free beam (b) Simply supported beam

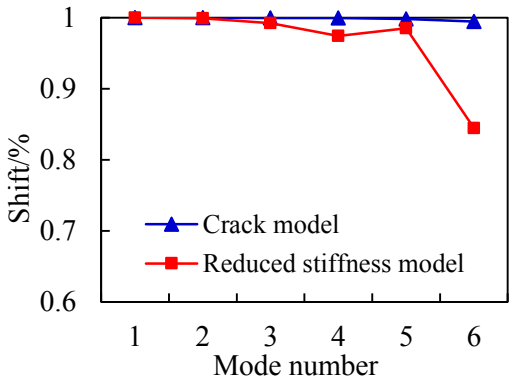

(c) Cantilever beam

Figure 4.9 Comparison between MAC results from two different models ($\alpha = 0.5$)

The comparisons show that the cracked beam element model is able to predict the natural frequencies as well as the mode shapes of the cracked beam for a sufficient number of 6 modes with very good accuracy. The reduced stiffness method, in contract, can only produce satisfactory results for the lowest 2-3 modes, and errors in the higher modes are significant.

4.3.2 Discussion of the thick beam effects

As highlighted in Section 4.2.1, two important effects are considered for the modelling of cracked thick beams, i.e., the shear deformation and rotational inertia, and the coupling between longitudinal and transverse vibrations. The effects are studied here with the cracked beam element model.

(1) Influence of shear deformation and rotational inertia

The classic Timoshenko beam theory is able to consider the shear deformation and rotational inertia effects while the Euler's beam theory cannot. Herein the cracked beam element model is degenerated to fit to the Euler's beam theory by setting the strain energy brought by the shear deformation to zero in Eq. (4.7). The Euler' beam theory- based cracked beam element model is then used to predict the vibration properties of the beams with $\alpha = 0.5$, as shown in Figure 4.10.

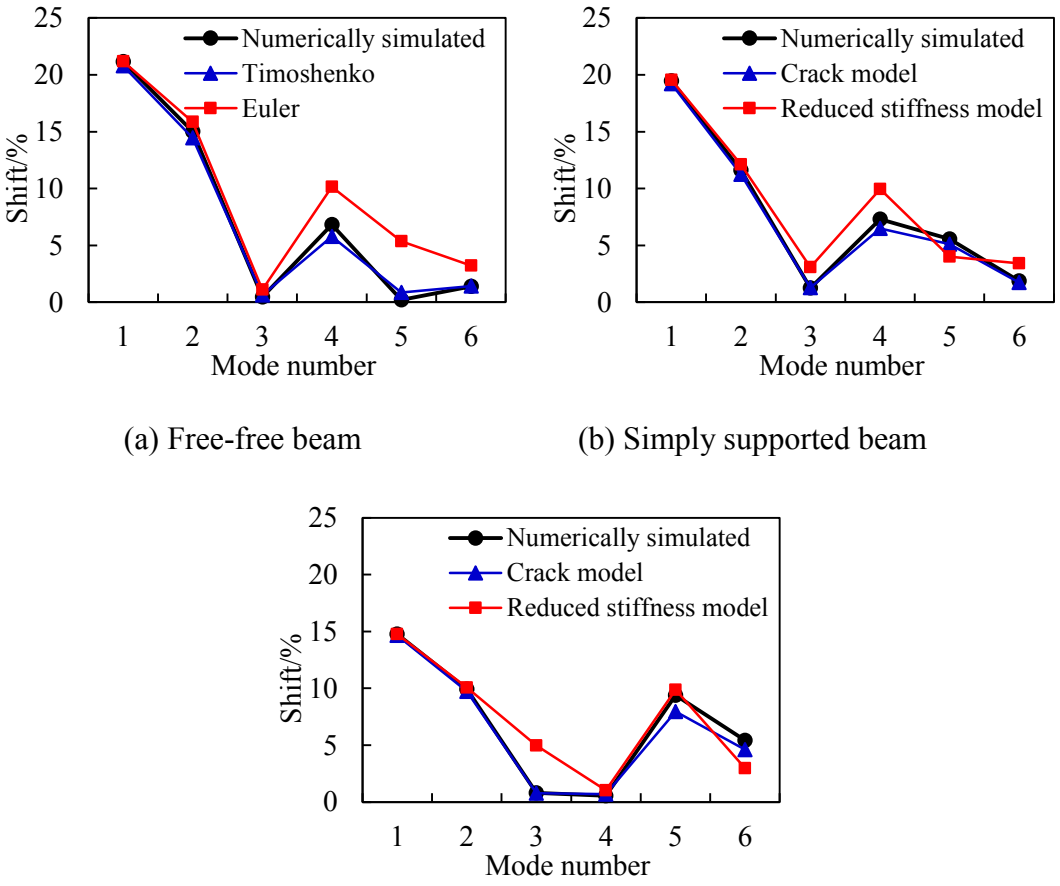

(a) Free-free beam

(b) Simply supported beam

(c) Cantilever beam

Figure 4.10 The influence of shear deformation and rotational inertia ($\alpha = 0.5$)

It can be seen that the crack model based on Euler's theory can predict the results with similar accuracy to the one based on Timoshenko's theory for lower modes. However, for higher modes, the errors in the results can be quite large in some of the modes. The reason is that for lower modes, the predicted results from Euler and Timoshenko beams are quite close for both the intact and cracked beams. As a result, the predicted frequency shifts are also quite close. For higher modes, as has been

stated by Kikidis and Papadopoulos (1992), the errors between the Euler and Timoshenko predictions for the cracked beams will be generally lower from those for the intact beams. The reason is that the presence of crack reduces the sectional area of the beam and consequently less shear deformation is involved near the cracked section, reducing the difference between using Timoshenko and Euler beam models. As a result, the frequency shifts will be different for the two models. For model updating involving high modes of information, Timoshenko beam is a better choice for cracked thick beams.

(2) Influence of coupling between longitudinal and transverse vibrations

The influence of the coupling effect is demonstrated with the same beam scenarios used before. A modified cracked beam element model without considering the coupling effect is created from the full cracked beam element matrix presented in Section 4.2, by omitting the axial DOFs. So in the modified beam model there are only two DOFs at each node. The results of the beams with $\alpha = 0.5$ are presented in Figure 4.11. It can be seen that most of the modes still match quite well with the numerically simulated data. However, some of the modes, such as the 5th and 8th modes in the free-free beam, and the 3rd mode in the cantilever beam, have quite large errors in the predicted results. The reason is apparently attributable to the fact that in a cracked beam these modes are significantly affected by the coupling effect between the longitudinal and transverse motions.

It is noted that both the 3rd and 4th modes have very insignificant frequency changes due to the crack. This is due to a) the crack location is close to a nodal point, in this case the 4th mode, and b) there exists coupling between the transverse and longitudinal modes, which results in the 4th mode being insensitive to the particular crack as well. Indeed, if the coupling effect does not exist in the beam, such a situation is not possible for both adjacent modes as only one of them would have a nodal point close to the crack. It can be seen from the predictions in Fig. 4.11(c) that when the coupling effect is not considered, the frequency shift of the 3rd mode is actually quite large. However, due to the existence of longitudinal vibration brought by the coupling effect, the actual nodal point of the 3rd mode is shifted towards the crack and thus the actual frequency change of the 3rd mode becomes insignificant as

well. It is worth noting that the cracked beam element model incorporating the coupling effect can accurately predict such minor frequency change of the 3rd mode, as shown in Fig. 4.6(c) and 4.7(c).

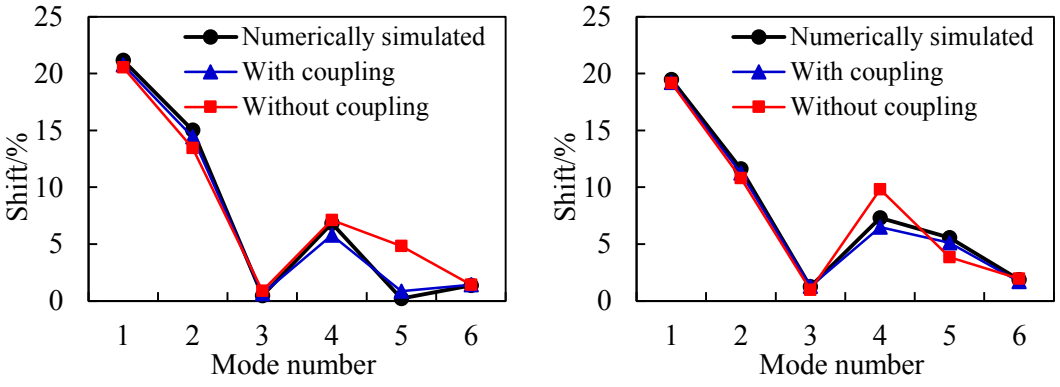

(a) Free-free beam (b) Simply supported beam

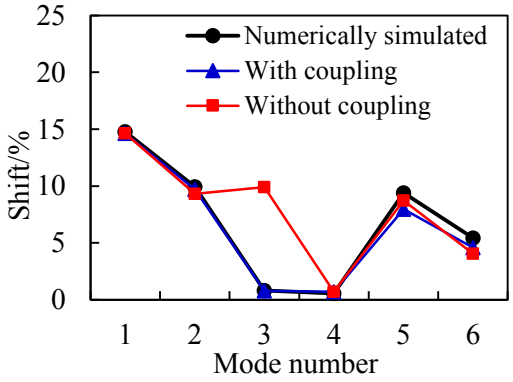

(c) Cantilever beam

Figure 4.11 Influence of coupling effect between longitudinal and transverse vibrations

Take the 3rd mode in the cantilever beam for example (f_0 = 1283 Hz)**.** The transverse as well as longitudinal mode shapes of the current mode are shown in Figure 4.12. For the intact beam, as no coupling happens between the vibrations of the two directions, there is no vibration in the longitudinal direction due to bending. However, for the cracked beam, the transverse vibration of the beam will bring vibration to the axial direction due to the eccentricity of the crack section. So it can be seen that there is also quite strong longitudinal vibration in the structure and the associated longitudinal mode shape is quite close to the 1st mode of the longitudinal vibration. This is because that that the natural frequency of the 1st longitudinal mode

(f_0 = 1266.5 Hz) is very close to that of the 3rd transverse mode. So a noticeable vibration of this mode will appear. As a result, the natural frequency of the coupled mode is greatly altered compared with the uncoupled ones. If the axial part is omitted in the calculation, there will be quite large modelling errors. The errors could bring marked errors in the model updating and damage identification results. So for thick beams, it is deemed to be necessary to consider the coupling effect, i.e. to include the axial degrees of freedom in the beam model and beam formulation.

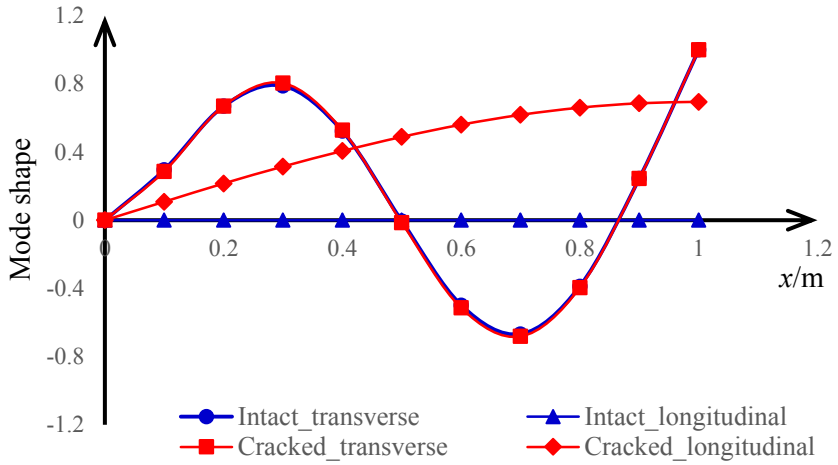

Figure 4.12 Mode shapes of the 3rd mode of the intact and cracked beams

4.4 *Cracked damage identification using the cracked beam element model*

In this section the cracked beam element model will be implemented in a finite element model updating framework for the identification of crack damage in structural beams.

4.4.1 General considerations

In this approach, the beam in question is discretized into a suitable number of beam elements. The following rules should be taken into consideration when deciding the mesh size: a) the model should be sufficiently accurate in representing the vibration properties of the beam while at the same time keep the updating parameters as few as

possible, b) it should facilitate representation of single crack or multiple cracks across the length of the beam; in this respect it should be consistent with the cracked beam element formulation with consideration of the influence range of a crack.

Considering that the influence range of a major crack would be the order of the beam depth, it is reasonable to adopt a discretization with individual element length l_e equal or around the sectional depth. As demonstrated in previous sections, a Timoshenko beam model with this level of discretization while using the cubic-shape function will be sufficiently accurate for at least the first 6 modes, which should well cover the actual measurable number of modes in structural beams in practice.

For model updating purpose, each beam element is assumed to be a possible cracked element and hence is modelled with the pair of variable crack parameters (α_i , l_{ci}), namely the crack depth ratio and the relative location within element i.

It can be seen that the total number of variable parameters to be updated when using the cracked beam element model is twice the number of beam elements in the model, or twice the number of variable parameters when using the reduced stiffness model. But as both the location and depth of the crack can be updated from the cracked beam model, and to achieve a similar updating effect many times more refined discretisation would have to be employed in a reduced stiffness approach, the updating demand with the cracked beam model is in effect considerably reduced.

4.4.2 Adaptive discretization

Another important aspect that needs to be handled appropriately is the possible conflict between the beam discretisation and the physical influence range of a crack, in a situation where a crack is too close to one end of an individual element, making the effect of such a crack to "spill over" to the adjacent element. To illustrate the situation, we only need to use a conceptual analysis. Assume that the influence range of the crack is symmetric to the crack (which is not necessarily true in real structures) and that the crack influence range is contained within an individual element length. If the mesh of the beam model is made in such a way that the crack is around the centre of a cracked element, we can be generally satisfied that the influence of an individual crack is covered within a single element, as shown in Figure 4.13(a). Thus, the crack

depth and exact location could be identified in a more straightforward manner from the model updating. However, if the crack is close to the left or right node of the element, the influence range of the crack is likely to cross into the immediate adjacent element, as depicted in Figure 4.13(b) and (c). The implication on the inverse calculation (model updating) is that two cracks might be identified in the two adjacent elements, which would not be correct. More detailed examples will be given in the next section.

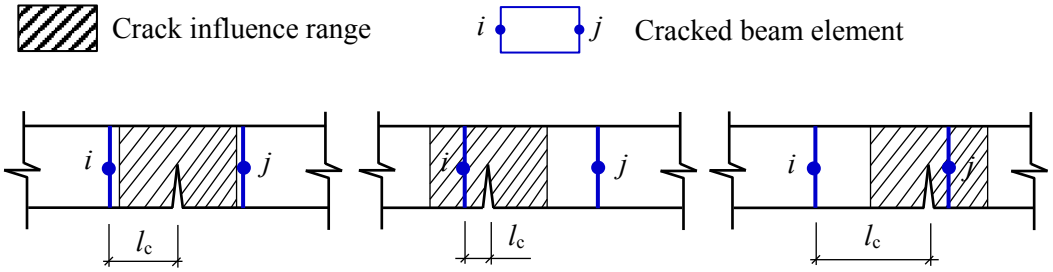

(a) Crack at element centre (b) Crack close to left node (c) Crack close to right node

Figure 4.13 Relationship between the crack influence range and the beam element

To tackle the above potential problem, an adaptive process is proposed herein. In this process, an adapted discretization will be involved if the first identification turns out to indicate two cracks which are too closely spaced within two adjacent elements. As a general guide, we propose to use a distance of $0.5h$ as a limiting criterion. In such a situation, the model will be re-meshed such that the influence range of the real crack can be mostly covered in one element, and the updating procedure is repeated on the adapted mesh.

Assuming that two closely spaced cracks satisfying the above distance threshold occur in the initial updating results, in element p-1 (crack depth ratio $\alpha_{p\text{-}1}$) and element p (crack depth ratio α_p). The real crack should lie between the two identified cracks, and the real crack location (L'_c) may be estimated using a simple interpolation method as:

$$L'_c = \frac{\alpha_{p-1} L_{c,p-1} + \alpha_p L_{c,p}}{\alpha_{p-1} + \alpha_p} \tag{4.14}$$

where $L_{c,p\text{-}1}$ and $L_{c,p}$ denote the locations of the two closely spaced cracks detected from the initial updating.

The adapted mesh will set the above estimated crack location to around the centre of the cracked element. The detailed process and the effectiveness of this adaptive approach will be illustrated in the examples in the Section 4.4.4.

4.4.3 Parameter updating algorithm

Genetic algorithm (GA) is also employed to perform the FE model updating for the cracked beam. As mentioned before in Chapter 3, various objective functions have been employed for model updating in the literature (e.g. Friswell, et al. [38]; Teughels, et al. [39]; Hao and Xia [40]). A general form of the objective function incorporating both eigenvalue and mode shape data can be defined as,

$$J = \frac{1}{N_{\mathrm{m}}} \sum_{i=1}^{N_{\mathrm{m}}} W_i \cdot \mathrm{abs}\left(\frac{\lambda_{\mathrm{m}i}^{\mathrm{d}}}{\lambda_{\mathrm{m}i}^{0}} - \frac{\lambda_{\mathrm{c}i}^{\mathrm{d}}}{\lambda_{\mathrm{c}i}^{0}} \right) + \frac{1}{N_{\mathrm{s}} N_{\mathrm{n}}} \sum_{i=1}^{N_{\mathrm{s}}} V_i \cdot \left(\sum_{j=1}^{N_{\mathrm{n}}} \mathrm{abs}\left(\varphi_{\mathrm{m}ji}^{\mathrm{d}} - \varphi_{\mathrm{c}ji}^{\mathrm{d}} \right) \right) \tag{4.15}$$

where, J is the objective function to be minimised, λ denotes the eigenvalue (= $(2\pi f)^2$), φ denotes the mode shape displacement, with the subscript 'm' indicating measured data and 'c' computed data, and the superscript 'd' indicating damaged (current) state and '0' the intact state. N_{f} is the number of eigenvalues to be included, N_s is the number of mode shapes to be included, N_{n} is the number of nodes in the mode shapes. W_i and V_i are the weights for the i^{th} eigenvalue and mode shape, respectively. It is noted that by using the eigenvalue ratio relative to the measured or computed intact state, the effect of any gross modelling errors brought by factors other than the crack can be reduced.

4.4.4 Application examples

The beams with three different boundary conditions presented in Section 4.3 are used as examples to demonstrate the FE model updating and damage identification process. Firstly, a single crack case is investigated and the crack is assumed to be at L_{c} = 350 mm from the left end of the beam. Two different crack depth ratios are used, with α being 0.3 and 0.5, respectively.

As mentioned in Section 4.3, the numerically simulated data are generated from the numerical experiments with 2D solid elements. Because no measurement errors are involved under this circumstance, for simplicity the weights W_i, V_j in the objective function Eq. (4.15) are set to be unity.

In the FE model, the beam is discretised into 10 elements, so there are totally 10 pairs of crack parameters to be updated when the cracked beam element model is used. It should be pointed out that for a cantilever beam the element closest to the free end would be entirely insensitive to the eigenvalue and mode shape data, therefore including the parameters of the free end element in the updating process could cause ill-conditioning and hence false updating result for this element. Such a problem could be resolved by resorting to additional measurement data which would have appropriate sensitivity to the free end element, such as ABC frequencies. As the present study focuses on the effectiveness of the crack model, we simply exclude the free end element in the updating parameters. So a total of 9 pairs or 18 crack parameters are considered in the cracked beam element model for cantilever beam and a total of 8 pairs or 16 crack parameters for free-free beam.

For a comparison, two sets of numerically simulated data are employed for the updating respectively, one includes the first 3 modes of information, and another includes the first 5 modes. For the search of the optimal solution, the GA function in Matlab is employed. The parametric settings for GA are given in Table 4.1.

Table 4.1 Parametric settings for GA

Parameter	Setting
Population size	5000
Fitness limit	-Infinite
Max generation	1500
Crossover fraction	0.7
Mutation rate	0.02

From monitoring the convergence progress during the searching process, it is found that a limit of maximum generation of 1500 is adequate to achieve satisfactory converging result.

(1) Updating results with the cracked beam element model

The updating results of crack locations using the cracked beam element model are summarised in Table 4.2-4.7. The updated crack depth ratios are shown in Figure 4.14 and 4.15. Note again that the exact updating results should be a crack in the 4th element with a crack depth ratio α = 0.3 in one case and α = 0.5 in the other case, and l_c = 50 mm.

Table 4.2 Updating results of free-free beam with α = 0.3

Element number	1	2	3	4	5	6	7	8	9	10
l_c/mm (3 modes)	-	-	-	46.1	-	-	-	-	-	-
l_c/mm (5 modes)	-	-	-	48.6	-	-	-	-	-	-

Note: the location values for elements other than the cracked ones are omitted from the table.

Table 4.3 Updating results of simply supported beam with α = 0.3

Element number	1	2	3	4	5	6	7	8	9	10
l_c/mm (3 modes)	-	-	-	49.5	-	-	-	-	-	-
l_c/mm (5 modes)	-	-	-	52.6	-	-	-	-	-	-

Table 4.4 Updating results of cantilever beam with α = 0.3

Element number	1	2	3	4	5	6	7	8	9	10
l_c/mm (3 modes)	-	-	-	60.2	-	-	-	-	-	-
l_c/mm (5 modes)	-	-	-	50.3	-	-	-	-	-	-

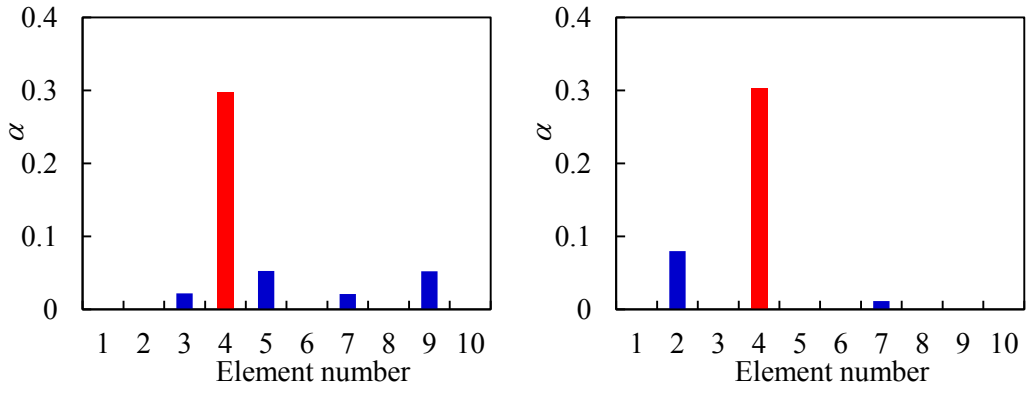

With 3 modes With 5 modes

(a) Free-free beam

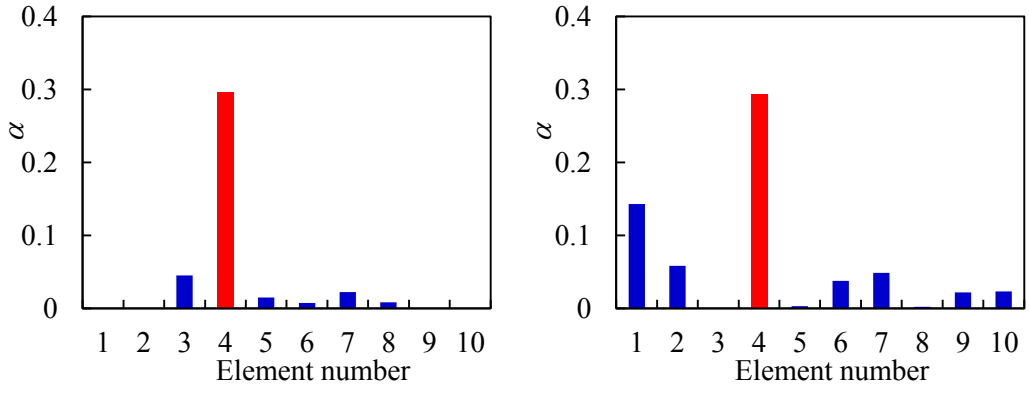

With 3 modes With 5 modes

(b) Simply supported beam

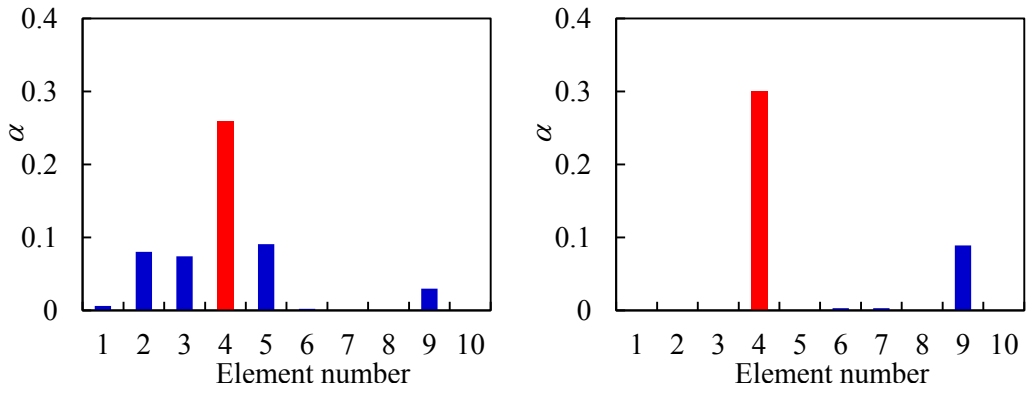

With 3 modes With 5 modes

(c) Cantilever beam

Figure 4.14 Updating results of beams with $\alpha = 0.3$

Table 4.5 Updating results of free-free beam with $\alpha = 0.5$

Element number	1	2	3	4	5	6	7	8	9	10
l_c/mm (3 modes)	-	-	-	48.1	-	-	-	-	-	-
l_c/mm (5 modes)	-	-	-	48.9	-	-	-	-	-	-

Table 4.6 Updating results of simply supported beam with $\alpha = 0.5$

Element number	1	2	3	4	5	6	7	8	9	10
l_c/mm (3 modes)	-	-	-	51.1	-	-	-	-	-	-
l_c/mm (5 modes)	-	-	-	50.6	-	-	-	-	-	-

Table 4.7 Updating results of cantilever beam with $\alpha = 0.5$

Element number	1	2	3	4	5	6	7	8	9	10
l_c/mm (3 modes)	-	-	-	43.7	-	-	-	-	-	-
l_c/mm (5 modes)	-	-	-	50.3	-	-	-	-	-	-

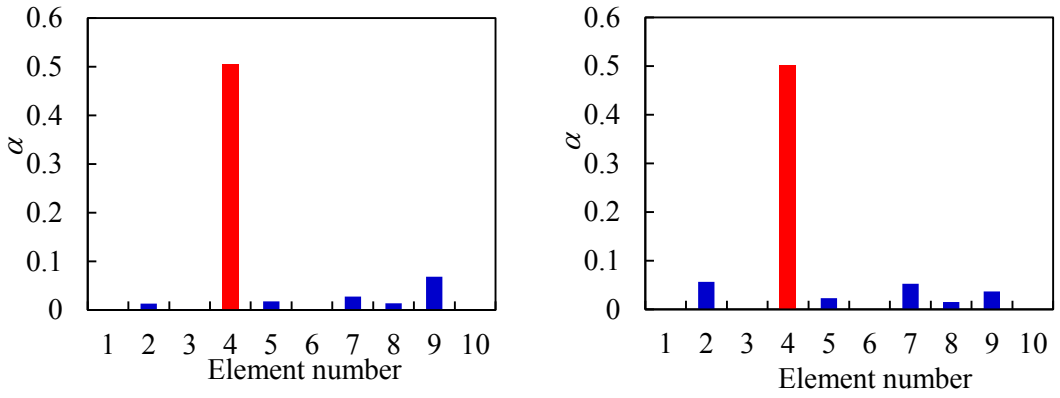

With 3 modes With 5 modes

(a) Free-free beam

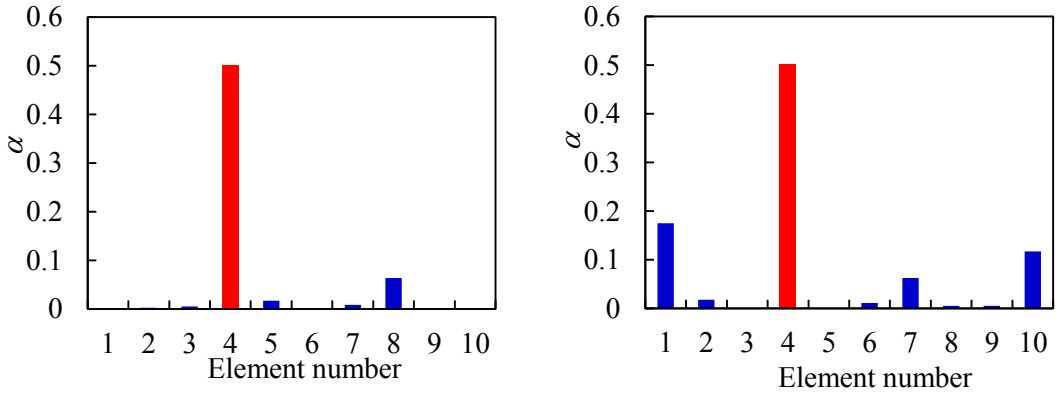

With 3 modes With 5 modes

(b) Simply supported beam

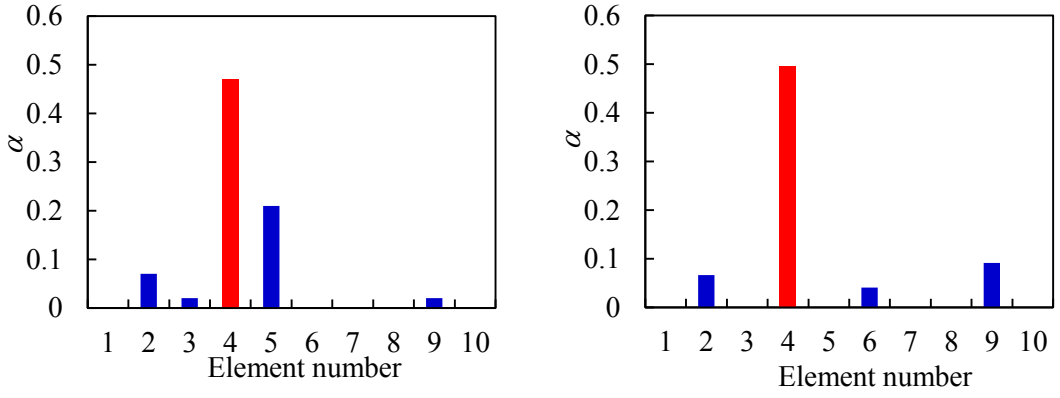

With 3 modes With 5 modes

(c) Cantilever beam

Figure 4.15 Updating results of cantilever beam with $\alpha = 0.5$

It can be seen that the updating results with both sets of the modal data can all find the correct cracked beam element. The updated α and l_c values are also reasonably accurate. The results with 5 modes of information are generally better than those with 3 modes. This is normally expected, but it should also be pointed out that the 3rd mode information has low sensitivity to the crack element in this particular case (as can be seen from Figure 4.6 and 4.7). So there are effectively only two modes of information in the case of using the first 3 modes.

(2) Updating results with the reduced stiffness model

The performance of the reduced stiffness model is also checked for benchmarking. Similar to the updating with cracked beam element model, each finite element is treated as a possible cracked element and the stiffness reduction ratio D_{ei} is used as updating parameter. The updating results of D_e for the cantilever beams are shown in Figure 4.16 and 4.17. It is noted that the last (10th) element at the free end is not involved in the updating (assumed intact).

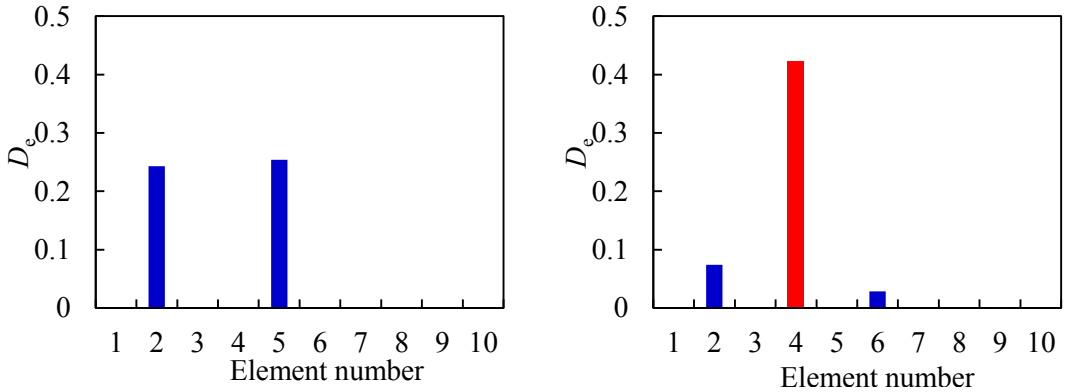

(a) With 3 modes (b) With 5 modes

Figure 4.16 Updating results of cantilever beam with $\alpha = 0.3$

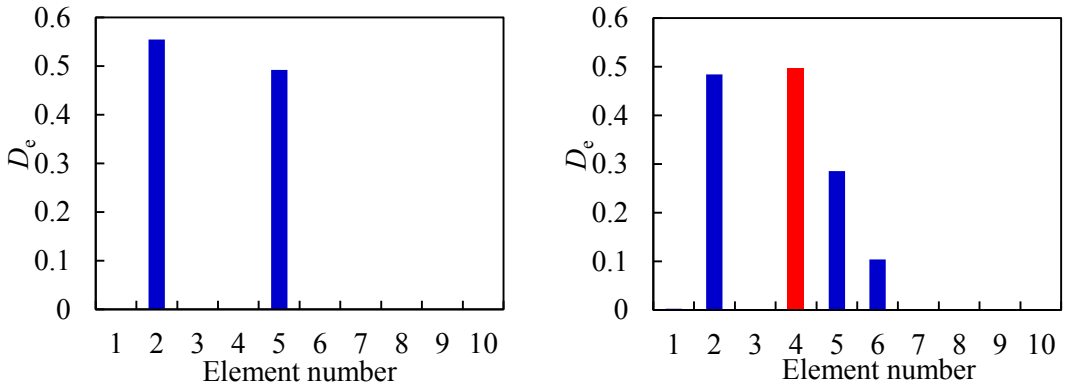

(a) With 3 modes (b) With 5 modes

Figure 4.17 Updating results of cantilever beam with $\alpha = 0.5$

It can be seen that the updating results are not correct for both crack scenarios when 3 modes of information are used. The actual crack (in the 4th element) is missed while there are two false cracks in the 2nd and 5th elements. When 5 modes of information are used, the results appear to be acceptable for beam with $\alpha = 0.3$, but not for beam with $\alpha = 0.5$, in which two major false cracks occur. The reason for the poor performance is attributable to the significant modelling error in the reduced stiffness model, as demonstrated in Section 4.3. Another thing to note is that it is difficult to interpret the depth and exact location of the identified crack from the updated D_e value with this model, as there is no explicit physical meaning of the parameter.

(3) Updating with a coarse mesh setting

The updating is also examined with a relatively coarse mesh setting. Five elements with l_e = 200 mm are used in the FE model. With the new mesh setting, the crack should be in the 2nd element with l_c = 150 mm. As the reduced stiffness method becomes even less physically meaningful with a coarse mesh, only the cracked beam element model is employed. The updating results of the cantilever beams are listed in Table 4.8 and the identified crack depth ratios for the α = 0.3 and 0.5 cases are shown in Figure 4.18 and 4.19, respectively.

Table 4.8 Updating results of cantilever beam with 5 elements

Crack depth ratio	$\alpha = 0.3$					$\alpha = 0.5$				
Element number	1	2	3	4	5	1	2	3	4	5
l_c/mm (3 modes)	-	146.6	-	-	-	-	150.6	-	-	-
l_c/mm (5 modes)	-	164.1	-	-	-	-	152.6	-	-	-

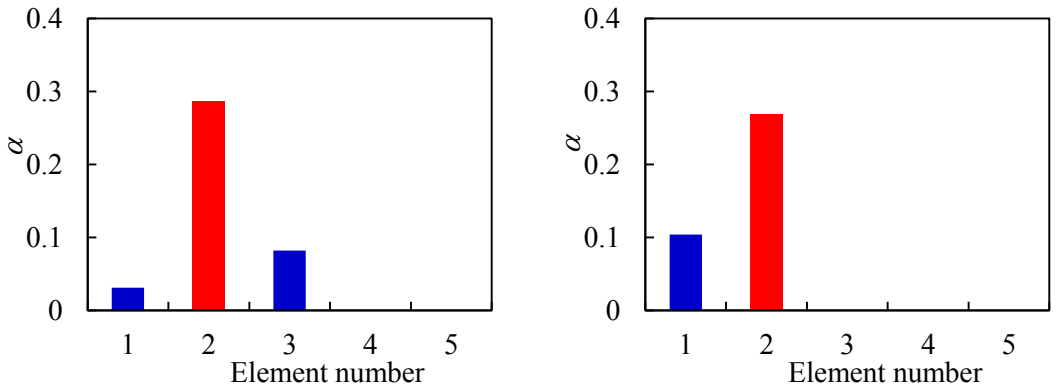

(a) With 3 modes (b) With 5 modes

Figure 4.18 Updating results of cantilever beam with $\alpha = 0.3$

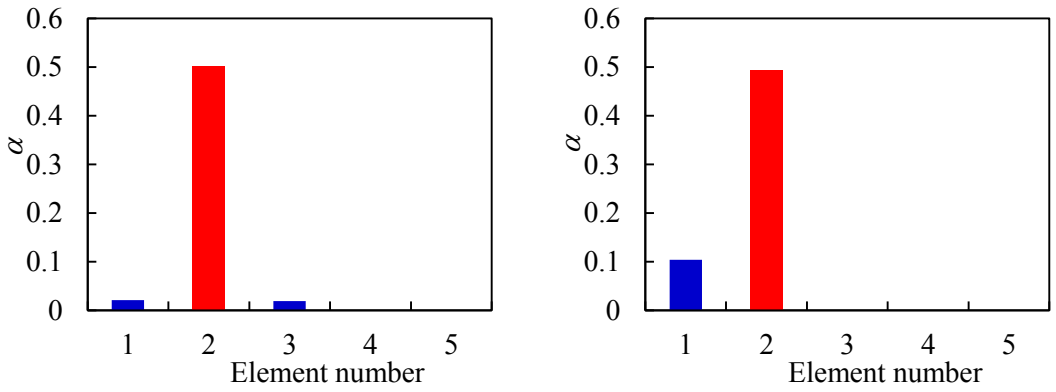

(a) With 3 modes (b) With 5 modes

Figure 4.19 Updating results of cantilever beam with $\alpha = 0.5$

It can be seen that good results can still be obtained even when only 5 elements are used in the FE model. It is particularly of interest to note that with the coarse mesh of just 5 elements, the explicit crack parameters can be identified quite accurately with

modal data from just the first three modes, and the accuracy from using the first three modes is almost the same as using the first five modes. Comparing to the equivalent stiffness method, where a coarse mesh would imply a loss of resolution and hence become less meaningful, the cracked beam model shows a further layer of advantage.

(4) Updating with adaptive discretisation

In the above examples, the crack is located at 350mm from the fixed end of the cantilever beam, and it is at the centre of the 4th beam element in the beam model. Now we consider some non-centred crack scenarios. Two cantilever beams with different crack locations are used in the calculation. Beam1 has a crack at 310mm from the fixed end while Beam2 has a crack at 390mm from the fixed end, as shown in Figure 4.20. All the other parameters are kept to be same as the ones used in Section 4.3. We still use 10 Timoshenko beam elements with l_e = 100 mm to update the beam model. Thus, the crack is located in the 4th beam element with l_c = 10 mm and l_c = 90 mm for the two beams, respectively, as depicted in Figure 4.20. It can be seen that in Beam1, the crack is very close to the left node of the beam element, while the opposite is true in Beam2. The crack depth ratio is set as α = 0.5 for the two beams.

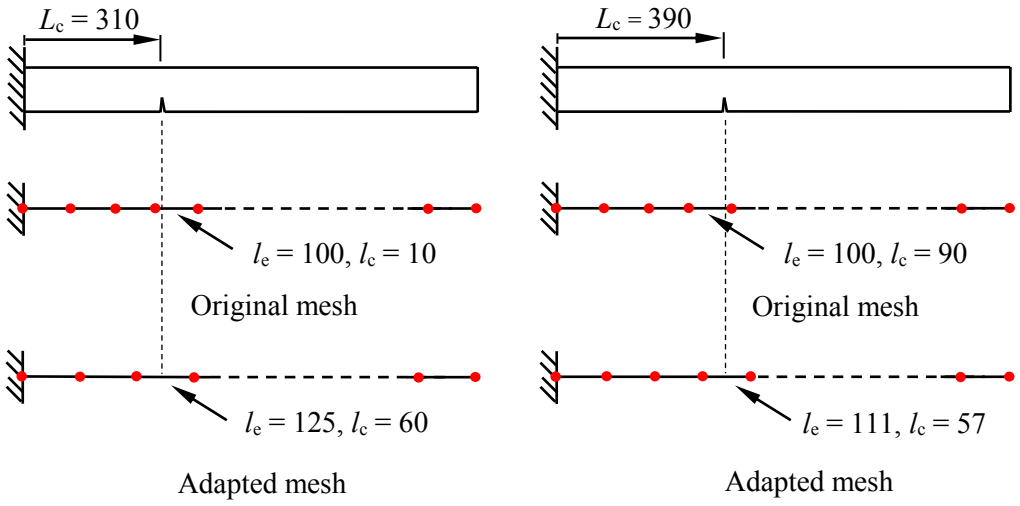

(a) Beam1 (b) Beam2

Figure 4.20 Examples with adaptive updating strategy (Unit: mm)

Model updating is then performed to identify the crack parameters. The results are presented in Figure 4.21, and Table 4.9. It can be seen that correct crack element number can be identified in all of the beams. However, the identified crack depth values are all lower than the actual value, especially for Beam1, in which the identified α value is around 15% lower than the actual value. This is apparently attributable to the fact that a 'false' crack is identified in the immediate next element to the actual crack. For Beam1 (l_c = 10 mm), a 'false' crack is identified in the left adjacent element, while for Beam2 (l_c = 90 mm), a 'false' crack is identified in the right adjacent element.

Table 4.9 Updating results of cantilever beams with non-centred crack

Element number	1	2	3	4	5	6	7	8	9	10
l_c/mm (Beam1)	-	-	-	9.5	-	-	-	-	-	-
l_c/mm (Beam2)	-	-	-	85.7	-	-	-	-	-	-

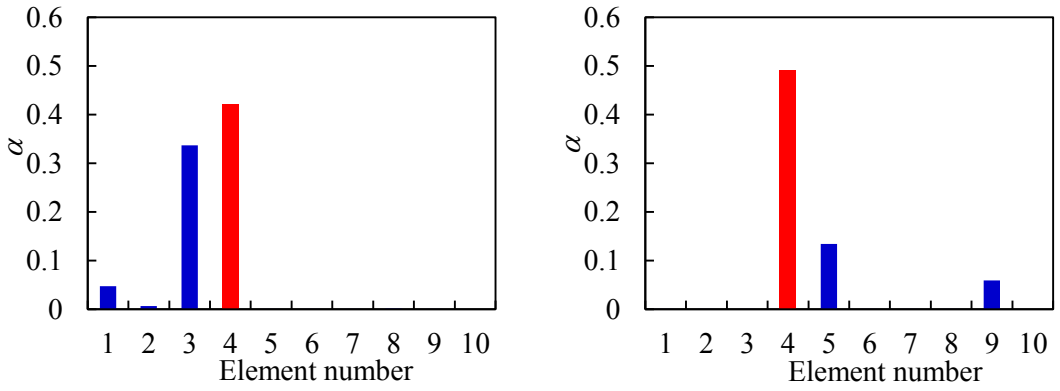

(a) Beam1 (b) Beam2

Figure 4.21 Updating results of beams with non-centred crack

As has been explained with Figure 4.13, the 'false' crack is the result of the influence range of the crack stretching into the adjacent element. This problem may be resolved readily using the adaptive approach as described in Section 4.4.2. With Eq. (4.14), the real crack location of the two beams can be estimated as L'_c = 305 and 395 mm for Beam1 and Beam2, respectively. The two beams are re-meshed to put the crack around the centre of the cracked beam element. Herein a uniform mesh is still

used in the re-meshed model while the number of elements is reduced to adjust the boundaries of the cracked element. It is found that when 8 elements are used in Beam 1, the estimated L'_c is quite close to the centre of the 3rd element (312.5 mm). As a result, the new mesh size is set as $l_e = 1000/8 = 125$ mm. The same method is applied on Beam 2, resulting in a new mesh size as $l_e = 1000/9 = 111$ mm.

Alternatively, the model may be re-meshed just in the neighbouring area of the crack but keep the remaining mesh unchanged, resulting in a non-uniform mesh setting. Either way should fit the purpose as long as the estimated crack location sits around the centre of the cracked element.

With the new mesh setting, the real crack should be in the 3rd element with $l_c = 60$ mm for Beam 1 and in the 4th element with $l_c = 57$ mm for Beam2. The FE models with the adapted mesh setting are updated and the results are presented in Table 4.10 and 4.11 and Figure 4.22. It can be seen that correct crack parameters can be obtained for all of the examples, which proves that the adaptive updating strategy is a success.

Table 4.10 Updating results with adapted mesh (Beam1)

Element number	1	2	3	4	5	6	7	8
l_c/mm	-	-	56.1	-	-	-	-	-

Table 4.11 Updating results with adapted mesh (Beam2)

Element number	1	2	3	4	5	6	7	8	9
l_c/mm	-	-	-	59.1	-	-	-	-	-

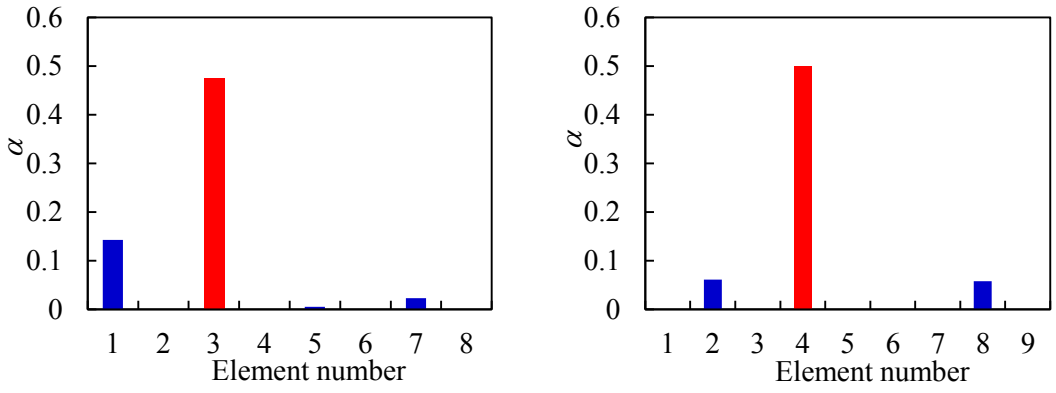

(a) Beam1 (b) Beam2

Figure 4.22 Updating results with adapted mesh

(5) Beam with multiple cracks

As has been stated in Section 4.4.1, there is no restriction on the number of cracks in the model updating with the cracked beam element model, so it can readily be used in the multiple cracks scenarios, barring any closely spaced adjacent cracks. As an example, the same cantilever beam but with 3 cracks, shown in Figure 4.23, is used to demonstrate the updating performance.

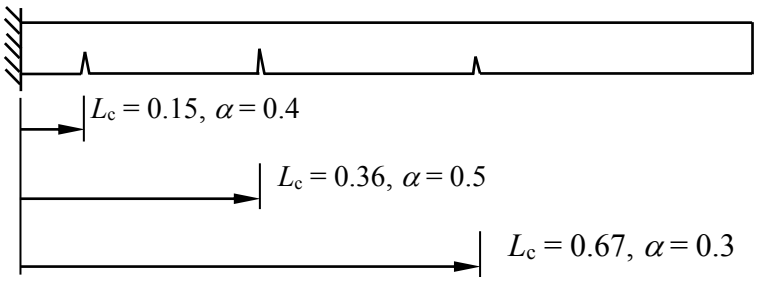

Figure 4.23 Beam with multiple cracks

Using 10 beam elements in the model, the actual cracks are located in elements 2, 4 and 7, and the crack parameters for the three cracks should be [α, l_c] = [0.4, 50], [0.5, 60], and [0.3, 70], respectively. The first 5 modes of information are used in the objective function and model updating results are presented in Table 4.12 and Figure 4.24. It can be seen that the three cracks can all be identified with good accuracy, showing the ability of the current model to identify multiple cracks.

Table 4.12 Updating results of beam with multiple cracks

Element number	1	**2**	3	**4**	5	6	7	8	9	10
l_c/mm	-	**55.2**	-	**59.7**	-	-	**64.0**	-	-	-

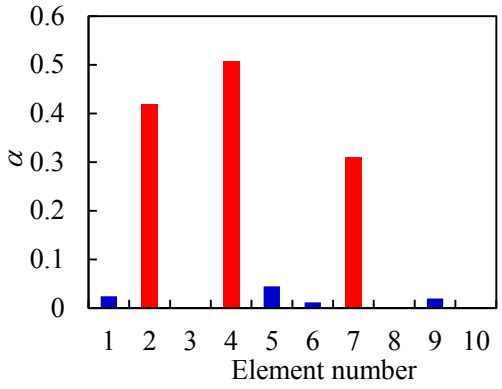

Figure 4.24 Updating results of beam with multiple cracks

4.5 Summary and conclusions

The crack identification in beam-like structures is a classic problem. Although there have been many studies on this subject, very few studies have achieved explicit representation of the crack parameters; and moreover, few have dealt with relatively thick beams typical in civil engineering structures. In this chapter, a comprehensive finite element model updating procedure has been developed for crack damage identification in thick beams. An individual crack is described using a cracked beam element model involving explicitly the relative crack location and the crack depth. The cracked beam element stiffness matrix is formulated taking into account the additional flexibility brought by the crack in accordance with the fracture mechanics principles. Shear deformation and coupling between the translational and longitudinal DOFs are all represented in the model. Both forward and FE model updating results have demonstrated superior performance of the cracked beam model as benchmarked against the reduced stiffness model. A few more specific conclusions may also be drawn:

(1) From the forward verifications, the cracked beam model can predict sufficiently accurately the natural frequencies and mode shapes of cracked thick beams up to 9 modes (6 modes were shown in the results), and in a consistent manner. On the other hand, the reduced stiffness model can only predict the modal data accurately for just the lowest couple of modes.

(2) In conjunction with a global searching technique (using GA herein), high quality model updating results can be obtained in both single crack and multiple cracks scenarios. In comparison, the reduced stiffness model has failed to identify the correct crack location in most of the scenarios.

(3) The issue with the crack influence range crossing into the adjacent beam element in the case where the location of the crack is too close to one end of the cracked element can be readily overcome by a simple adaptive procedure. This involves an adaptation of the initial discretization scheme so that the projected crack location from the first estimate is made at around the centre of a beam element in the adapted mesh. The procedure has been verified to result in satisfactory outcome.

(4) The cracked beam model has demonstrated superior performance in coping with limited amount of modal data, while a reduced number of beam elements are employed. This has been achieved without losing the preciseness of the crack identification in any significant way, thanks to the explicit representation of the crack information in the model.

5 Experimental investigation of crack identification in thick beams

5.1 Introduction

A model updating and damage identification approach using a cracked beam element model have been developed and verified with numerically simulated modal data in Chapter 4. While the theoretical concepts and principles underlying the development of the cracked beam element model may reasonably be examined against results generated from refined numerical simulations, physical experiments are still indispensable in order to test the behaviour of the theoretical model in a real measurement environment. Experimental studies serve also to further verify the accuracy of the crack beam element and its effectiveness in crack identification given the various constraints that exist in an experimental condition.

There have already been many experimental modal testing studies relating to the effects of cracks on the beam vibration properties and the development of crack models. Christides and Barr (1984) measured the lowest few natural frequencies of simply-supported intact and cracked steel beams to calibrate the stress decay rate assumed in the crack model. Chondros, et al. (1998) tested simply-supported intact and cracked aluminium beams to verify a crack model developed based on the stress distribution around the crack location; however only the fundamental natural frequency was measured and used in the verification. Swamidas, et al. (2004) conducted modal testing on a slender aluminium beam with a varying crack depth ratio from 0.1-0.5. The first four natural frequencies were obtained and used to verify the developed vibration theory for cracked Euler's beam. Ruotolo and Surace (1997) tested beams with multiple cracks. Three slender cantilever steel beams, each had two cracks, were tested and the first 4 natural frequencies and mode shapes were obtained. Crack identification was then conducted on the beams through model updating. Sinha, et al. (2002) conducted experimental modal testing and employed the test results to verify a cracked beam element, which was developed based on Euler-Bernoulli beam element with modified local flexural rigidity distribution in the vicinity of cracks.

It should be pointed out that most of the existing experiments have been conducted on rather slender beams. However, the relative effect of how a crack is modelled tends to diminish as the beam slenderness increases. According to a comparative study by Friswell and Penny (2002), several types of crack models, namely the simple reduced stiffness model, the discrete spring model, the model by Sinha, et al. (2002), and the model presented in Lee and Chung (2000) based on fracture mechanics, could predict the first 3-5 mode natural frequencies of cracked slender beams with similar accuracy. For a more stringent verification of a beam crack model it would be appropriate to employ sufficiently 'thick' beams, which are also more representative of beam members in civil engineering applications where a length to depth ratio is typically in the region of 10-15. Furthermore, some of the important effects of a crack, such as the local shear deformation and the coupling of different vibration modes, can only be observed properly from the vibration of thicker beams.

This chapter presents an experimental study on the effectiveness of the cracked beam element model for identification of cracks in relatively thick beams. To test the robustness of the theoretical model, thick beam specimens with a single crack or multiple cracks at randomly selected locations have been prepared. Modal tests have been carried out on these beams to extract the first few natural frequencies and mode shapes. The measured modal data are compared with the predicted results using the cracked beam element model. On the other hand, the measured modal data are also employed in an inverse crack identification procedure by means of finite element model updating, and the identified crack parameters (location and crack depth) are checked against the actual cracks in the beams. Furthermore, extended modal frequencies based on ABC frequencies have been extracted from the experiment as well. These frequencies, which help reduce the reliance on the mode shape data, can be incorporated in the modal data set for the finite element model updating. The incorporation of the measured ABC frequencies for the identification of the crack parameters proves to be effective.

5.2 Experimental programme

An experimental programme of modal testing has been conducted with a focus on the effect of cracks on thick beams, for which the cracked beam element model is expected to be particularly effective, and thereby verify the accuracy of the cracked beam element model. To cover different possible crack damage scenarios, different combinations of the cracks, including single-crack and multiple-crack scenarios and with different crack depths, were represented in the test beam specimens.

5.2.1 Test specimens

Five beam specimens were prepared for the tests. The beams were prepared in reduced scale and were made of aluminium. The choices of the material and the sizes have been made mainly for the sake of easy handling especially the creation of the cracks (by saw cuts), and they should not affect the comparative results. All beams had the same overall dimension of $L \times b \times h = 600 \times 50.8 \times 50.8$ mm, with L, b and h being the span length, and width and height of the solid cross-section, respectively. The length to sectional thickness (depth) ratio of the beams is thus about 12, which is representative of the category of thick beams.

The crack conditions of the test beams are shown in Figure 5.1, with labels of the beams as B0, B1-B4 in sequential order. Beam B0 was an intact beam as the reference. B1 and B2 both contained a single crack at the same location, but the cracks had different depths. B3 and B4 both had multiple (3 here) cracks of different depths; but B3 had more distinctly spaced cracks, whereas B4 had two of the cracks closely spaced to each other. Therefore, the specimens covered comprehensively the various aspects of cracked beams that may be of practical interest. All the cracks were created using saw cuts, and the width of each cut was approximately 1 mm. Detailed information of the cracks is shown in Table 5.1, in which α represents the crack to sectional depth ratio, and L_c is the distance between the crack location and the left end of the beam.

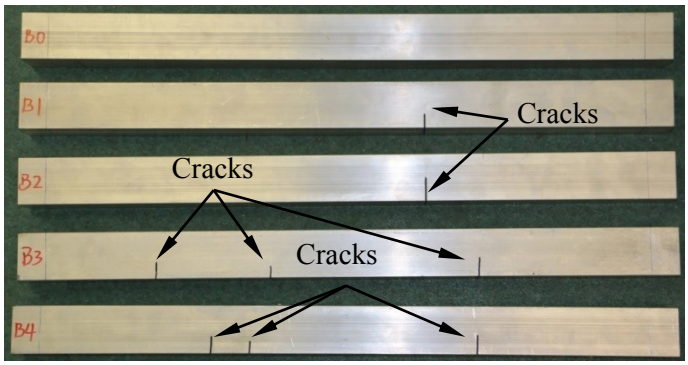

Figure 5.1 Beam specimens and configurations of cracks

Table 5.1 Crack information of the aluminium beam specimens

Beam label	Crack1		Crack2		Crack3	
	α	L_c/mm	α	L_c/mm	α	L_c/mm
B0	-	-	-	-	-	-
B1	0.3	375	-	-	-	-
B2	0.5	375	-	-	-	-
B3	0.35	125	0.25	230	0.4	420
B4	0.35	180	0.25	215	0.4	420

5.2.2 Modal testing setup

The tested beam was suspended with two strings at the two ends to create a free-free boundary condition, as shown in Figure 5.2. Hammer impact was used to apply excitation on the beam using the precision impact hammer (B&K type 8206-002) with an aluminium head. Trial tests indicated that with the aluminium head on the hammer a relatively flat impact force spectrum in the range of 0-10000 Hz could be achieved, and this well covered the frequencies of interest for the first several modes. The acceleration response of the beam was measured by the light-weight accelerometers (B&Kjær Delta Tron® 4508 type) as used in Section 3.3.

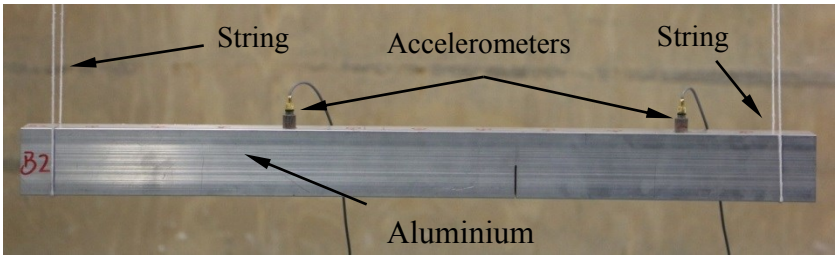

(a) Photo of test setup

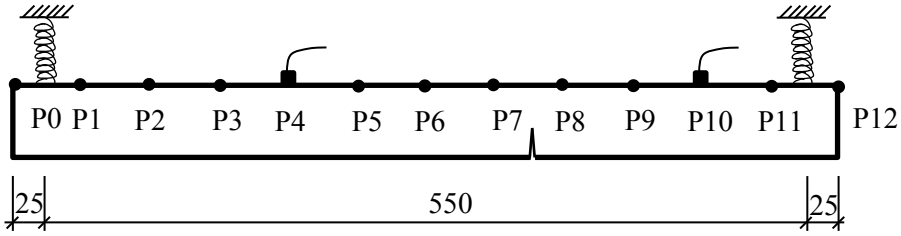

(b) Schematic view of the setup and measurement arrangement (Unit: mm)

Figure 5.2 Modal testing setup

The impact force and acceleration data were recorded with the data acquisition system as illustrated in Figure 3.3. The sampling rates for both the impact force and acceleration were set to be 25600 Hz. The record duration of the signals were set to be 16 s. It was found that the record time is just long enough to allow the vibrations die out, thus eliminating the leakage problem in the subsequent modal analysis.

Both the natural frequencies and mode shapes of the beams were measured from the modal testing. To extract the mode shapes, 11 uniformly distributed measurement locations were marked on the beam, as shown in Figure 5.2. During the tests, two accelerometers were attached at point P4 and P10 while impact was applied at each measurement location from P1 to P11 in a routine procedure.

The frequency response function (FRF) curves were calculated from the Fourier transform of the acceleration and impact force signals. As the actual excitation input by the hammer impact lasted only for a very short duration, on an order of less than 1ms, a force window was employed to eliminate the apparent noises in the remaining much longer recording period. 10 repeated tests were performed for each excitation

location and the FRF curves from the repeated tests were averaged to be used in the extraction of the modal frequencies and mode shapes.

5.2.3 Modal testing results

Representative FRF curve of beam B0 is presented in Figure 5.3. It shows very clear resonances as well as anti-resonances.

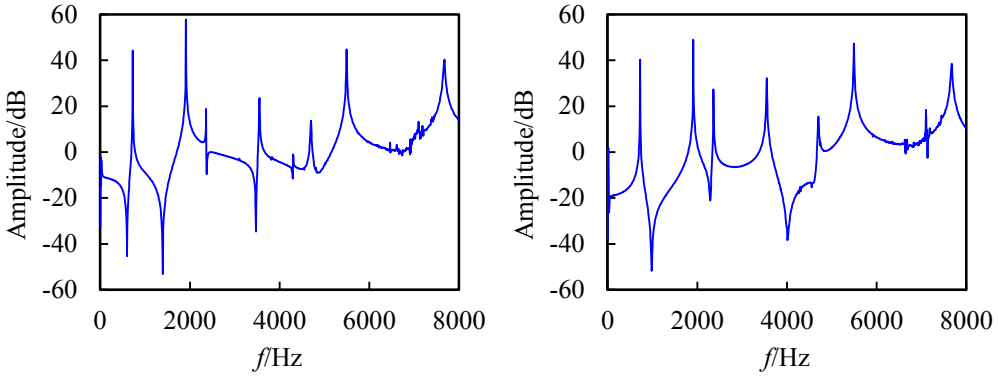

(a) Driving FRF at P4 (b) Transfer FRF between P4 and P10

Figure 5.3 Measured FRF curves

The natural frequencies and mode shapes of the beams can be extracted from the FRF curves easily using the standard peak-picking method. The lowest five modes of natural frequencies (f_N) are shown in Table 5.2. It can be seen that the frequency shifts brought by the cracks are generally in the range of 1%-15%, and can be as large as 20% for some specific modes and damage scenarios.

Table 5.2 Measured natural frequencies f_N (±% denotes relative change from B0)

Mode	B0	B1		B2		B3		B4	
	(Hz)	(Hz)	±%	(Hz)	±%	(Hz)	±%	(Hz)	±%
1	725.1	673.8	**7.1**	577.7	**20.3**	629.1	**13.2**	609.9	**15.9**
2	1912.6	1825.1	**4.6**	1702.3	**11.0**	1533.1	**19.8**	1481.7	**22.5**
3	3547.3	3532.9	**0.4**	3493.4	**1.5**	3022.8	**14.8**	3228.7	**9.0**
4	5493.9	5269.7	**4.1**	5142.4	**6.4**	5051.1	**8.1**	5273.6	**4.0**
5	7673.6	7560.6	**1.5**	7422.6	**3.3**	6894.3	**10.2**	7010.4	**8.6**

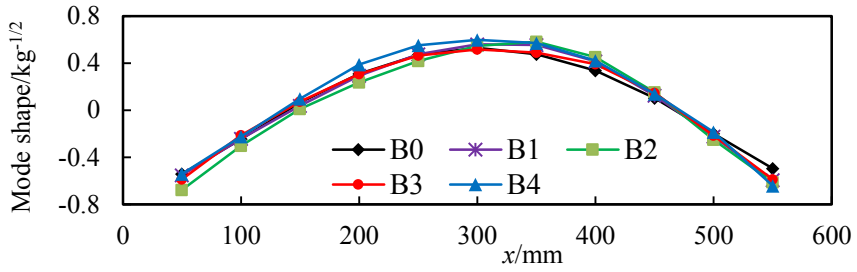

(a) 1st mode

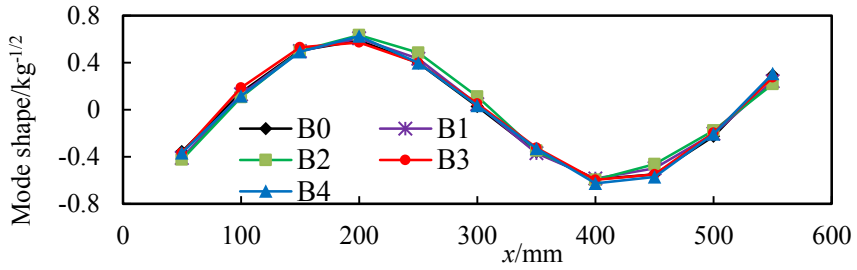

(b) 2nd mode

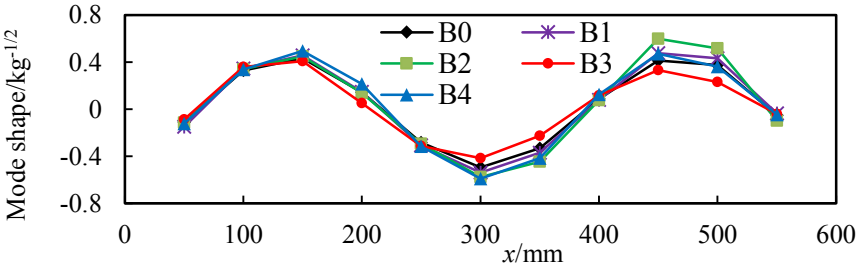

(c) 3rd mode

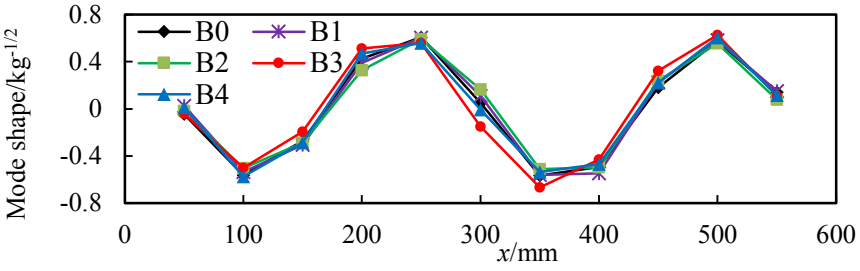

(d) 4th mode

Figure 5.4 Measured mass-normalized mode shapes from all 5 beam specimens

The mode shapes can be obtained from the amplitudes of the resonances in the FRF curves. The first four mass-normalized mode shapes for all specimens are presented in Figure 5.4. At this juncture it is worth noting that the arrangement of the relatively

coarse measurement grid was not aimed to obtain very smooth mode shape curves; instead it was aimed to restrict the number of mode shape data points to represent a practical measurement scenario. Nevertheless the accuracy of the mode shape data at the measured points is not affected by the mode shape resolution.

5.3 Verification of the prediction of modal properties by the cracked beam element model

The cracked beam element model outlined in Section 4.2 is verified against the measured modal testing results in this section. The intact and cracked beams are modelled with Timoshenko beam elements with high-accuracy cubic shape functions. 12 beam elements with uniform element length of 50 mm are used in the numerical models. This makes each element in the numerical model to have a length comparable to the actual beam depth, and this is regarded as appropriate considering that the crack influence range is generally about the order of the beam depth. For the same reason, further refinement of the mesh is deemed unnecessary with the use of the present cracked beam element model. Define the distance of the crack to the left end of the respective cracked element as l_c. With the above chosen numerical model setting, the crack will be in the 8th element for beam B1 and B2 (l_c = 25 mm), in the 3rd, 5th and 9th elements for beam B3 (l_c = 25, 30, and 20 mm), and in the 4th, 5th and 9th elements for beam B4 (l_c = 30, 15 and 20 mm).

By applying the crack parameters for each cracked beam specimen in the corresponding numerical model, the first five modes of natural frequencies and mode shapes of the beam specimens can be obtained.

For a comparison, the traditional reduced stiffness method is also employed to model the effect of the cracks and predict the modal properties with the Timoshenko beam model. This method assumes an equivalent reduced elemental stiffness to represent the effect of a crack, which effectively leads to a proportionally reduced element stiffness matrix as:

$$\mathbf{K}_{\mathrm{d}} = (1 - D)\mathbf{K}_0 \tag{5.1}$$

where, $\mathbf{K}_0$ and $\mathbf{K}_d$ are the stiffness matrix of the intact and damaged beam element, respectively.

As a matter of fact, there is no simple way to match up an actual crack with a certain element stiffness reduction, and understandably the equivalent stiffness reduction is also mesh (element) size dependent. For a fair and rigorous comparison, herein the stiffness reduction parameter D in the reduced stiffness model is determined in an optimised manner. For beams with a single crack, there is only one unknown D value for the element containing the crack in the whole model, whereas for the beams with multiple cracks, there are multiple unknown D values. The values of D are herein obtained by fitting the measured and predicted modal data of the cracked beams through a model updating procedure. For this purpose the first five natural frequencies are used to form the objective function J_1 for the optimization problem concerning D, as,

$$J_1 = \frac{1}{5}\sum_{i=1}^{5} \mathrm{abs}\left(\frac{f_{\mathrm{dNm}i}^2}{f_{\mathrm{0Nm}i}^2} - \frac{f_{\mathrm{dNc}i}^2}{f_{\mathrm{0Nc}i}^2} \right) \tag{5.2}$$

where, $f_{\mathrm{N}i}$ represents the i^{th} natural frequency; subscripts ‘c’ and ‘m’ stand for computed and the measured data, respectively; and subscripts ‘d’ and ‘0’ stand for the damaged and intact states of the beam, respectively.

Genetic algorithm (GA) is employed here as the optimization tool for the stiffness reduction parameter D. More details about the setting of GA will be given in Section 5.4. The D values found from this process may be considered as best approximation of the actual cracks in the context of equivalent stiffness reduction, and these values are subsequently employed in the reduced stiffness model to calculate the natural frequencies and mode shapes. A comparison with the experimental results for each mode individually will then bring out any inherent consistency issue with the method.

The verification is first carried out on the natural frequencies, and to simplify the comparison the frequency shift indicator defined in Eq. (4.12) is introduced, which is defined as the relative change of the i^{th} natural frequency of a cracked beam with respect to the intact state.

Thus for each cracked beam, the S_i values from the predicted natural frequencies using the cracked beam element model and the reduced stiffness model, respectively, are compared with S_i from the measured results, as shown in Figure 5.5. It shows that the predicted results using the cracked beam element model match very well the experimental results for all the modes in all the four cracked beams. The reduced stiffness model, on the other hand, achieves satisfactory prediction only for the beam with a single shallow crack (B1). For beams with a deep crack or multiple cracks, it cannot match for all the modes. This confirms the observation mentioned in Section 4.3, and it further indicates that the different stiffness reduction factors would be needed to represent the effects of the same crack on difference modes.

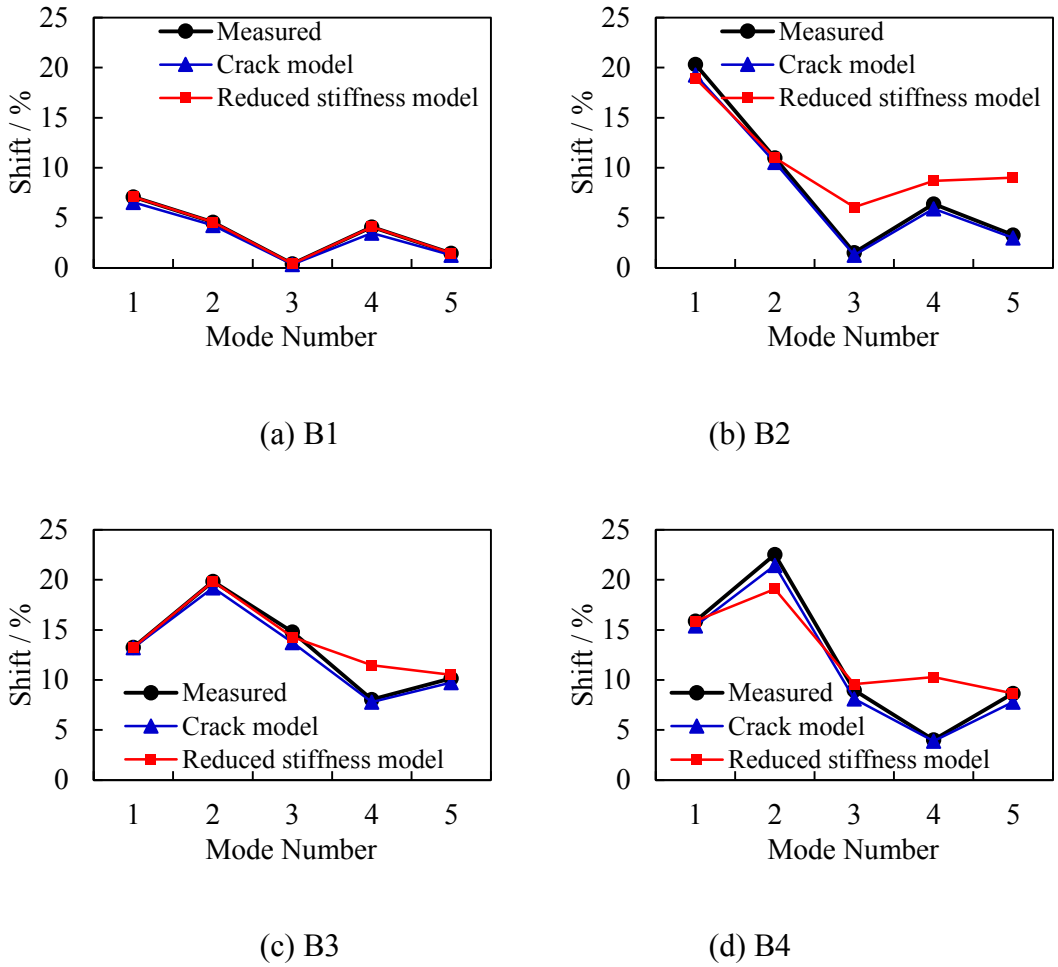

(a) B1 (b) B2

(c) B3 (d) B4

Figure 5.5 Comparison between frequency shifts

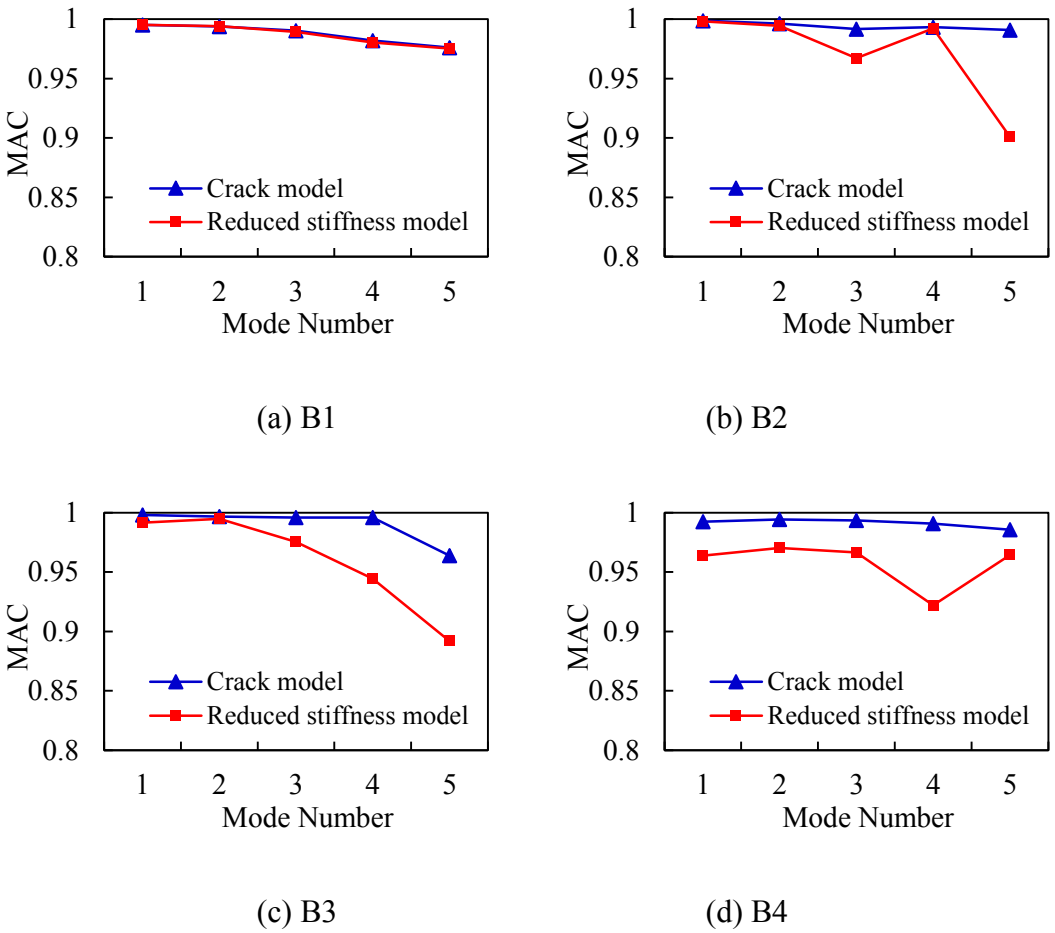

Figure 5.6 Comparison between MAC results

The Modal Assurance Criterion (MAC) values between the measured and predicted mode shapes of the cracked beams, which are defined in Eq. (4.13), are used to verify the accuracy of the two models regarding mode shape calculation.

Figure 5.6 shows the comparison between the MAC values from the two different models. It can be seen that the MAC values from the cracked beam element model are all greater than 0.964 and exceed 0.990 for the first 3 modes, indicating very good match between the measured and predicted mode shapes. However, the reduced stiffness model can only yield good MAC results for beam B1 with a single shallow crack. For the other beams, the MAC values are poor and this is particularly true for higher modes. In connection with the observations based on the natural frequencies in Figure 5.5, it can be seen the accuracy in the predicted mode shapes using the

reduced stiffness method tends to be poorer than the natural frequencies; the cracked beam element model, on the other hand, maintains consistent high accuracy for both.

5.4 Crack damage identification using the cracked beam element model

In this section the performance of the cracked beam element model when applied in crack damage identification is examined for the tested beam cases.

5.4.1 General consideration

The crack damage identification is carried out here using a finite element model updating procedure. For general applicability, each element in the FE model is considered as a potential cracked element and is modelled using the cracked beam element model with the crack depth ratio (α) and location (l_c) both unknown. Thus there is no limit on the number and locations of cracks to be identified in the beams. In the present situation, there are 12 elements in the beam model, so totally there are 24 unknown parameters. It is noted that the test beams under consideration had two free ends; as has been noted in Chapter 4, such the modal data (natural frequencies and mode shapes) would not be sensitive to the conditions in the elements at the beam ends. For simplicity and without losing generality, the two end elements in each beam are excluded from the updating operation and they are assumed to remain intact. This leaves 20 unknown parameters to be determined (updated).

The same objective function of the model updating in Section 4.4 is employed for the updating herein. It is formed with the eigenvalue and mode shapes of the first five modes,

$$J_2 = \frac{1}{N_N}\sum_{i=1}^{N_N} W_i \cdot \mathrm{abs}\left(\frac{f_{dNmi}^2}{f_{0Nmi}^2} - \frac{f_{dNci}^2}{f_{0Nci}^2}\right) + \frac{1}{N_S N_n}\sum_{i=1}^{N_S} V_i \cdot \left(\sum_{j=1}^{N_n} \mathrm{abs}\left(\varphi_{mji}^d - \varphi_{cji}^d\right)\right) \qquad (5.3)$$

where, J_2 is the objective function to be minimised, N_N (= 5) is the number of natural frequencies to be included and N_S (= 5) is the number of mode shapes to be included. N_n (= 11) is the number of nodes in the measured mode shapes. W_i and V_i are the

weights for the i^{th} eigenvalue and mode shape, respectively. The weights are generally chosen based on the presumed measurement accuracy of the respective type of the modal data and are assigned to be unity here for simplicity.

Genetic algorithm (GA) is employed to search the optimization solution for the objective function J_2. The GA function in Matlab is used in conjunction with the beam model to carry out the updatings. Basic parametric settings of the GA function are listed in Table 5.3.

Table 5.3 Parametric settings of GA

Parameter	Setting
Population size	5000
Fitness limit	-Infinite
Max generation	1500
Crossover fraction	0.7
Mutation rate	0.02

5.4.2 Model updating results with a standard mesh setting

Model updating is first carried out with the above-mentioned standard beam model setting with 12 beam elements. The results are shown in Figure 5.7 and Table 5.4.

Table 5.4 Updated crack locations (l_c) with standard mesh setting

Element number	1	2	3	4	5	6	7	8	9	10	11	12
B1	-	-	-	-	-	-	-	25.6	-	-	-	-
B2	-	-	-	-	-	-	-	24.9	-	-	-	-
B3	-	-	27.1	-	35.6	-	-	-	24.9	-	-	-
B4	-	-	-	32.2	17.4	-	-	-	23.7	-	-	-

Note: the location values for elements other than the cracked ones are omitted from the table.

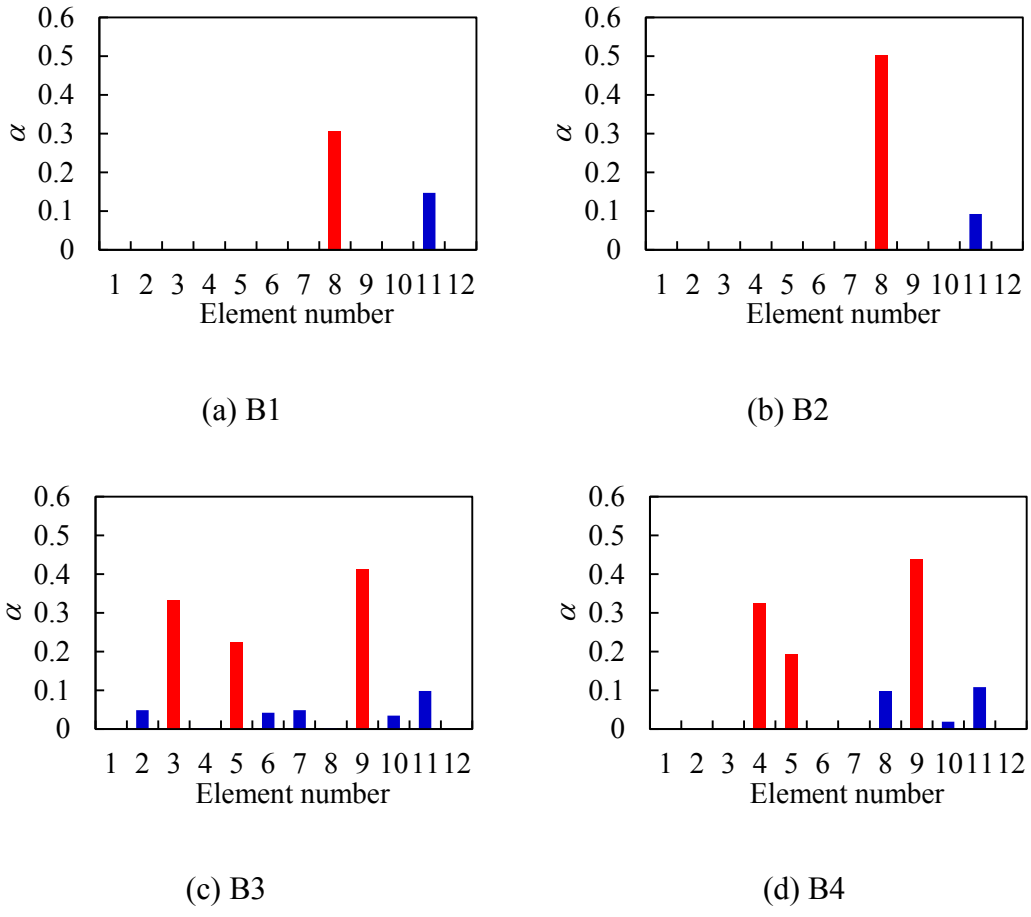

Figure 5.7 Updated crack depth ratios (α) with standard mesh setting

Comparing with the actual crack conditions shown in Figure 5.1 and summarised in Table 5.1, it can be seen that all the cracked elements have been identified correctly, with both the crack depth and crack location being determined at good accuracy. For the beams with a single crack (B1 and B2), the errors in the updated depth ratios (α) are smaller than 3%. For the beams with multiple cracks (B3 and B4), the errors in the updated depth ratios are generally smaller than 10%, except for the second crack in B4 which has an error of 23% and this is explicable by the fact that it is a relatively shallow crack. It should also be noted that a false crack is identified in the 11th element in all of the beams. As has been explained in Section 5.4.1, this is attributable to the low sensitivity of the modal data to changes in the elements close to the free end. The updated crack locations also have very high accuracy. By defining a crack location error as the normalised difference in the actual and updated crack positions within the element with respect to the element length, it can be seen

that the errors in the updated crack locations are generally lower than 10%. For the beams with multiple cracks, all the cracked elements are identified clearly. It can therefore be reasonably concluded that the crack damage identification with the cracked beam model is effective for the thick beams with practically any combinations of cracks.

5.4.3 Crack damage identification with less modal information and coarser mesh setting

In Section 5.4.2 the updating was conducted by employing the lowest 5 modes of modal data as input. However, for thick beams in a real life environment, measuring the first 5 modes, especially the mode shapes, to high accuracy could be difficult. At this juncture, it is worth noting the fact that the present cracked beam element model describes a crack in explicit terms, i.e., with the crack depth and location, therefore in principle it allows the use of a reduced number of elements for the beam without a gross loss of precision as would be the case when a reduced stiffness method is used.

Herein the performance of the updating with a reduced amount of modal information is checked. The lowest three modes of eigenvalues and mode shapes are considered, and the same objective function as shown in Eq. (5.3) is used. Because of the reduced amount of input information, to avoid ill-condition the updating parameter number is also reduced, taking advantage of the cracked element model as mentioned above. A coarser mesh setting with l_e equal to 100 mm is used in the beam model, making the total number of elements to be 6. After excluding the two elements at the free ends, there will be 8 parameters to be updated in the beam model.

The results for the crack damage identification using the coarser mesh setting are shown in Figure 5.8 and Table 5.5. Note that with the current mesh setting, for beams B1 and B2 the correct cracked element should be the 4th element with l_c = 75 mm; for beam B3 and B4 the cracked elements should be the 2nd, 3rd and 5th elements with l_c = 25, 30 and 20 mm and 80, 15, 20 mm, respectively. It can be seen that very accurate updating results can still be obtained. All the cracked elements are identified correctly, and errors in the updated crack depth ratios are less than 2% for the single-

crack beams and generally lower than 10% for the multiple-crack beams. The errors in updated crack locations are lower than 15% for all the beams.

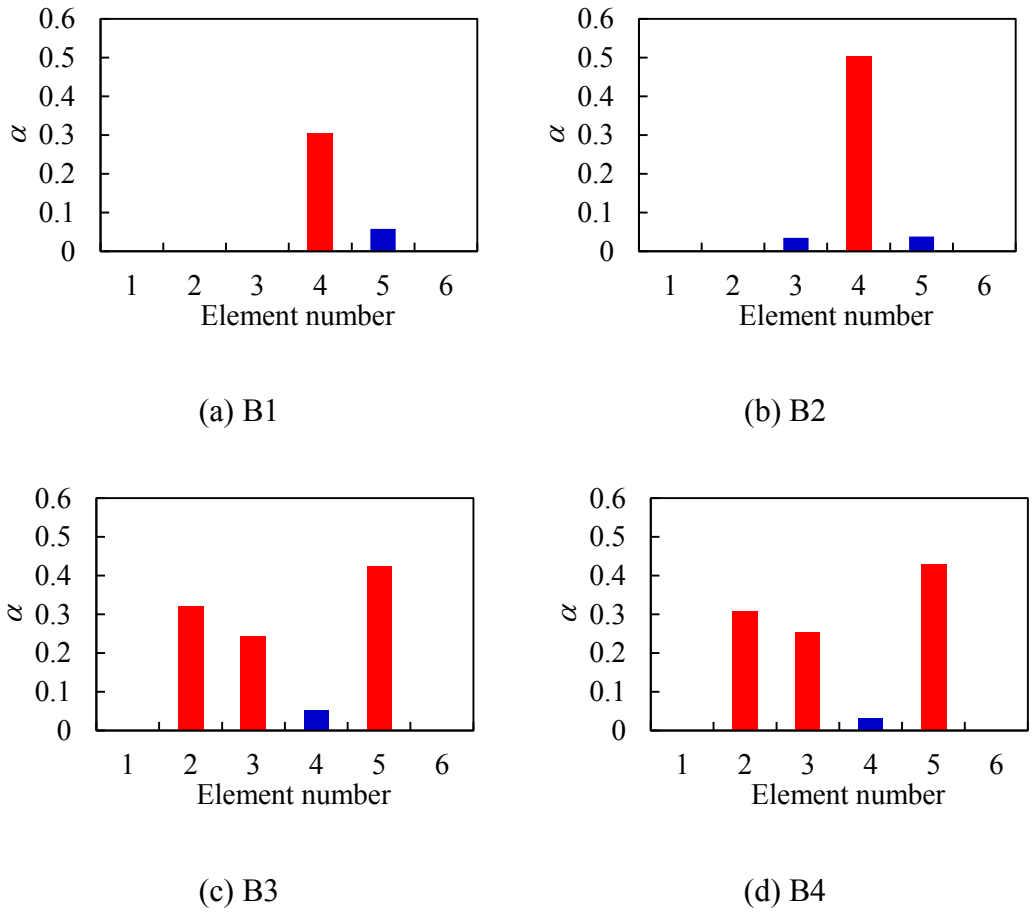

Figure 5.8 Updated crack depth ratios (α) with coarser mesh setting

Table 5.5 Updated crack locations (l_c) with coarser mesh setting

Element number	1	2	3	4	5	6
B1	-	-	-	74.3	-	-
B2	-	-	-	76.2	-	-
B3	-	23.3	28.1	-	31.1	-
B4	-	96.8	18.7	-	32.6	-

The above outcome with a reduced order of modal data being employed in conjunction with a coarse discretization is very favourable for practical applications,

and apparently this characteristic is unique with the current cracked element model because of the explicit description of the crack parameters.

It should be noted, however, that the present cracked beam element model assumes just one crack within an individual element length. With a coarse mesh setting and a larger element size, there will be increased likelihood that more than one crack may actually occur within an element length. One way to deal with such a scenario is to conduct several parallel updatings with different schemes of discretisation. By inspecting and comparing the results, one should be able to assess if multiple cracks might exist within a limited length of the beam.

5.5 Crack damage identification with ABC frequencies

The ABC frequencies, which have been extensively studied in Chapter 3, are employed in the damage identification of the cracked beams to examine its effectiveness with the cracked beam element model.

5.5.1 Obtaining ABC frequencies from the tested beams

To generate sufficient ABC frequencies, some supplementary tests were carried out on the beams described in Section 5.2. Driving excitations were applied on points P0, P2, P4, P8, P10, and P12 separately to facilitate the extraction of the one-pin ABC frequencies at these points. To generate the two-pin ABC frequency function curves at point (i, j), two accelerometers were attached at point i and j and excitations were carried out at the two points successively. Referring to Figure 5.2(b), the following two-pin configurations were tested: (i, j) = (P0, P12), (P0, P6), (P6, P12), (P2, P8) and (P4, P10).

The same signal processing strategy presented in Section 5.2.2 was used to obtain the FRF curves as well as ABC frequency function curves and the multi-DOF modal analysis method Rational Fraction Polynomial (RFP) method (Richardson and Formenti, 1982) is employed to smooth the measured FRF and ABC frequency function curves and extract the ABC frequencies. Representative FRF curve and ABC frequency function curves before and after applying RFP are shown in Figure

5.9. It can be seen that it is straightforward to find the ABC frequencies from the RFP-processed curves.

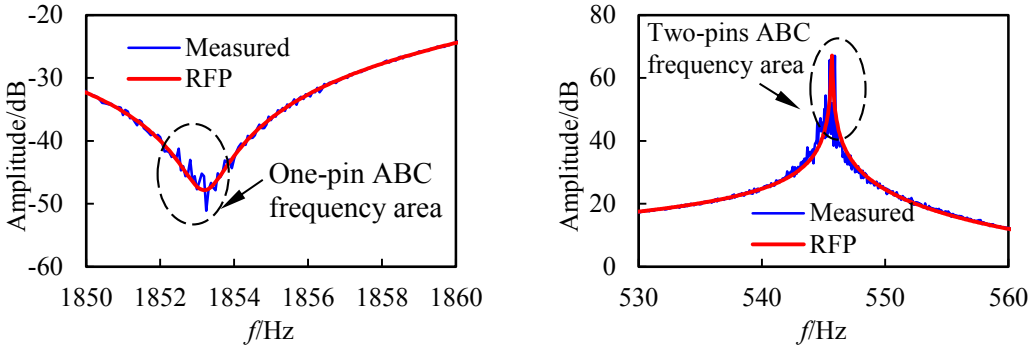

(a) FRF curve (close-in) (b) Two-pin ABC frequency function curve (close-in)

Figure 5.9 RFP technique for noisy antiresonances and two-pin ABC frequnecies

Table 5.6 One-pin ABC frequencies with 'pin' at P4 (f_A)

Mode	B0	B1		B2		B3		B4	
	(Hz)	(Hz)	±%	(Hz)	±%	(Hz)	±%	(Hz)	±%
1	594.2	565.8	**4.8**	508.8	**14.4**	517.6	**12.9**	476.7	**19.8**
2	1387.4	1284.8	**7.4**	1140.1	**17.8**	1139.7	**17.9**	1079.6	**22.2**
3	3466.7	3466.6	**0.0**	3440.4	**0.8**	3015.3	**13.0**	3125.4	**9.8**

Table 5.7 Two-pin ABC frequencies with 'pins' at P4 and P10 (f_A)

Mode	B0	B1		B2		B3		B4	
	(Hz)	(Hz)	±%	(Hz)	±%	(Hz)	±%	(Hz)	±%
1	562.3	533.6	**5.1**	479.1	**14.8**	489.3	**13.0**	452.4	**19.5**
2	1378.2	1277.4	**7.3**	1137.4	**17.5**	1130.8	**18.0**	1076.0	**21.9**
3	2652.8	2675.2	**-0.8**	2596.3	**2.1**	2570.5	**3.1**	2465.0	**7.1**

The lowest 3 modes of one-pin and two-pin ABC frequencies (denoted as f_A) from the above configurations were extracted from the FRF and ABC frequency function

curves. Selected results are presented in Table 5.6 and 5.7. It shows that the shifts of ABC frequencies brought by the cracks are around the similar range as that of natural frequencies.

5.5.2 FE model updating with ABC frequencies

The obtained one-pin and two-pin ABC frequencies are then used to perform model updating on the cracked beams. Two new objective functions with combined natural frequencies and one-pin ABC frequencies (J_3) or two-pin ABC frequencies (J_4) are used in the updatings, as:

$$J_3 = \frac{1}{N_{\mathrm{N}}} \sum_{i=1}^{N_{\mathrm{N}}} W_i \cdot \mathrm{abs}\left(\frac{f_{\mathrm{dNm}i}^2}{f_{0\mathrm{Nm}i}^2} - \frac{f_{\mathrm{dNc}i}^2}{f_{0\mathrm{Nc}i}^2} \right) + R_0 + R_2 + R_4 + R_8 + R_{10} + R_{12} \tag{5.4}$$

$$J_4 = \frac{1}{N_{\mathrm{N}}} \sum_{i=1}^{N_{\mathrm{N}}} W_i \cdot \mathrm{abs}\left(\frac{f_{\mathrm{dNm}i}^2}{f_{0\mathrm{Nm}i}^2} - \frac{f_{\mathrm{dNc}i}^2}{f_{0\mathrm{Nc}i}^2} \right) + R_{0,12} + R_{0,6} + R_{6,12} + R_{2,8} + R_{4,10} \tag{5.5}$$

In the equations, R (Rq. (5.6)) is a residual from the measured and computed one-pin or two-pin ABC frequencies. The subscript number of R is the 'pin' number. For example, R_2 is calculated from one-pin frequencies with 'pin' at point P2, and $R_{2,8}$ is calculated from two-pin ABC frequencies with 'pins' at points P2 and P8.

$$R = \frac{1}{N_{\mathrm{A}}} \sum_{i=1}^{N_{\mathrm{A}}} \mathrm{abs}\left(\frac{f_{\mathrm{dAm}i}^2}{f_{0\mathrm{Am}i}^2} - \frac{f_{\mathrm{dAc}i}^2}{f_{0\mathrm{Ac}i}^2} \right) \tag{5.6}$$

where, f_{A} stands for the one-pin or two-pin ABC frequencies. N_{A} is the modes of ABC frequencies used, which is set as 3 herein. Other symbols have the same meanings as in Eq. (5.3). It should be noticed that while measured ABC frequencies in Eq. (5.6) were obtained from the modal tests, their computed counterparts can be easily calculated by adding additional pins in the FE model.

The coarse mesh setting with l_{c} = 100 mm used in Section 5.4.3 is applied in the beam model. Figure 5.10 shows the results in terms of the crack depth in each element from the model updating with a combined natural and one-pin ABC frequencies (Eq. 11). It can be seen that very good updating results have been obtained with the inclusion of the ABC frequencies. All the cracked elements can be

identified with errors in crack depth ratios (α) less than 3% for single-crack beams and generally less than 10% for multiple-crack beams (except the shallow crack in beam B4 with an error of 20%). A check of the updated relative positions of the cracks within the individual elements as shown in Table 5.8 indicates that the crack positions have been identified with a similar level of accuracy as mentioned above.

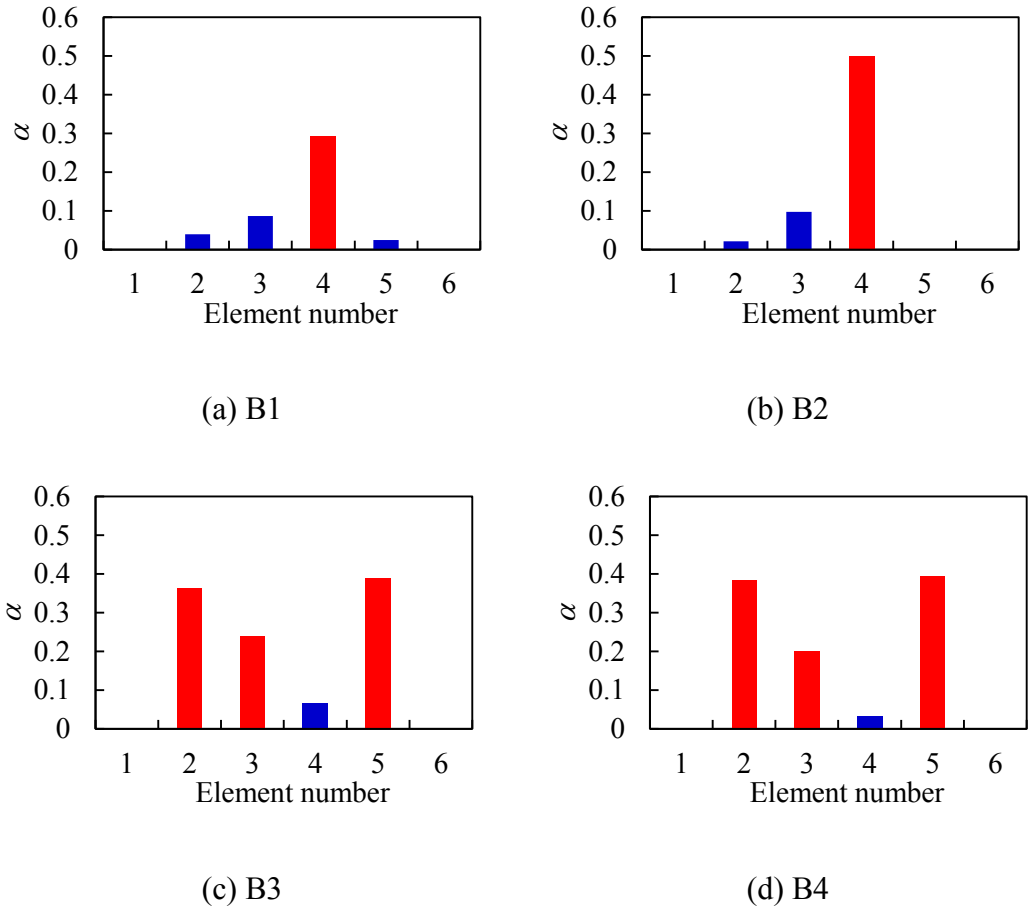

Figure 5.10 Updated crack depth ratios (α) with J_3

Table 5.8 Updated crack locations (l_c) with J_3

Element number	1	2	3	4	5	6
B1	-	-	-	76.9	-	-
B2	-	-	-	76.1	-	-
B3	-	27.9	23.1	-	21.7	-
B4	-	81.2	15.6	-	17.9	-

The crack depths from using a combination of the natural and two-pin ABC frequencies are shown in Figure 5.11 and Table 5.9. The results are also satisfactory. It should be noted that the test beams were quite stiff and this rendered the two-pin ABC frequencies to be in a high frequency range, and thus generally increased measurement error, particularly for in the two-pin ABC cases.

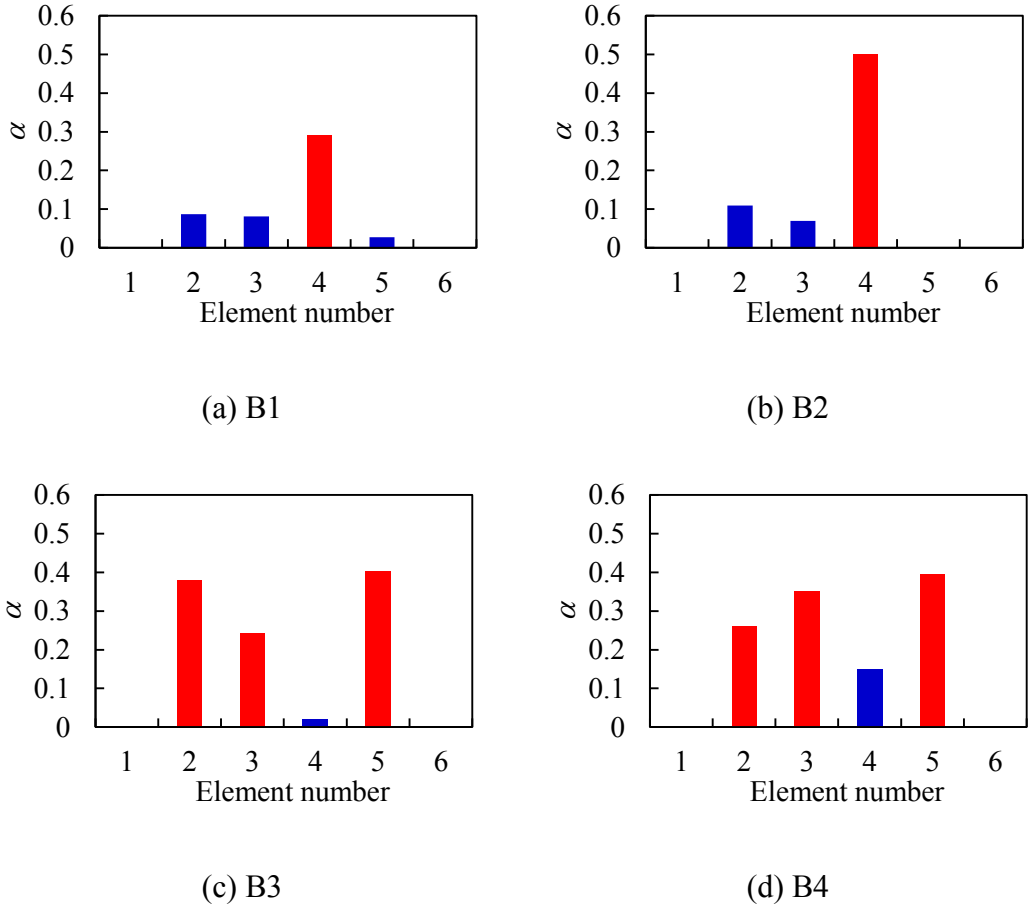

Figure 5.11 Updated crack depth ratios (α) with J_4

Table 5.9 Updated crack locations (l_c) with J_4

Element number	1	2	3	4	5	6
B1	-	-	-	74.7	-	-
B2	-	-	-	76.1	-	-
B3	-	27.4	42.7	-	23.1	-
B4	-	64.4	2.7	-	30.6	-

It is worth mentioning that the incorporation of the ABC frequencies provides a scope to expand dramatically the modal frequency data set, and this is deemed to be very beneficial for updating with the cracked beam element model because of the generally increased demand on the updating. With an appropriate sensitivity analysis (Tu and Lu, 2008), it is possible to choose the most sensitive configurations of pin locations to generate enough ABC frequencies for updatings with a large number of unknown parameters.

5.6 Summary and conclusions

An experimental study has been conducted to investigate the effectiveness of a cracked beam element model for the identification of crack damage in thick beams with measured modal data. Laboratory beam specimens with a length to thickness ratio around 10 were prepared with different crack scenarios, and modal testing was performed on these beams to extract the natural frequencies and mode shapes.

From the comparison between the measured modal data and those predicted using the cracked beam element model, it can be concluded that the cracked beam element model is sufficiently accurate in both single- and multiple-crack beam scenarios, and the accuracy is consistent across all modes being examined. In contrast, the conventional reduced stiffness model cannot achieve consistent accuracy in representing the crack effect on the natural frequencies and mode shapes for different modes.

The performance of the cracked beam element model in an inverse process to identify the crack parameters has been assessed with a finite element model updating procedure. Using the measured modal data from the tested beams, very good identification results have been achieved. In fact all cracked elements can be found correctly; and in most cases the crack depth and relative crack position within the cracked element can be determined with high accuracy. It has also been demonstrated that in cases where the available modal data may be limited (for

example to the lowest three modes), the cracked beam element model can still yield satisfactory crack identification with a coarse element discretization.

The cracked beam element model exhibits equally satisfactory results when the measured modal data is comprised of the natural frequencies along with the ABC frequencies which replace the mode shape data. In view of the fact that a variety of the ABC configurations exist, the incorporation of the ABC frequencies opens up an additional scope for the application of the cracked beam element model, especially in more complex situations where a large number of crack parameters may need to be identified.

6 Crack modelling and identification in box section beams

6.1 Introduction

Box section beams have been widely used in different types of engineering structures, from large-size box girders in bridge structures, medium-size beams and columns in buildings, to small-size vehicle frames. The main advantage of box section members is that sufficient bending and torsion stiffness can be achieved while the self-weight of the structure is greatly reduced. Box beams with small wall thickness belong to thin-walled members, and have been extensively studied since Vlasov (1961). In the service life of box beams, one critical issue is the development of cracks in the beam walls. One example is the development of fatigue crack of steel box beams under cyclic loading, especially at the welding locations (Nussbaumer, et al., 1999). Identification of the occurrence of cracks is thus an important topic for the monitoring and maintenance of box beam structures.

As has been stated in Chapter 1, vibration-based damage identification is one of the most effective approaches among various types of techniques for structural health monitoring and in the past, vibration-based damage identification has been applied on various types of structures, such as RC beams (Cerri and Vestroni, 2003; Unger et al., 2006), composite beams (Moaveni et al., 2008), and steel space structures like frame or truss (Hu, et al., 2001; Jones and Turcotte, 2002; Lu and Tu, 2004).

It is noted that most of the studies have dealt with solid section members, such as concrete beams, or solid steel members in space structures. Limited research has been devoted to crack damage identification of hollow section structures. Of the few relevant publications, two are summarized here. Liu, et al. (2003) studied the crack detection in hollow circular section beams. The crack detection method is based on the fact that a circumferential crack in a hollow section brings coupled vibration between longitudinal and bending vibrations, and thus an extra resonant peak appears in the frequency response function curve of the cracked beam. This method is capable of detecting the existence of cracks, but it is difficult to predict the severity (crack depth) and location parameters, especially when multiple cracks exist. Zheng and Fan (2003) analysed the vibration of cracked hollow section beams with circular

or square sections. The vibration functions were established by treating the cracked beams as an assembly of sub-segments linked up by rotational springs. The stiffness of the rotational springs was expressed with some local flexibility coefficients for the cracks, which were derived from fracture mechanics principles. It is noted that in the above study the stress intensity factors (SIFs) for cracks in plane sections were employed for the local flexibility calculation of hollow sections, and this treatment could bring in marked errors as cracks in hollow sections is a three-dimensional problem in nature and specific SIFs for this type of sectional configuration should be used.

This chapter is aimed for the crack identification of box section beams with a suitable cracked element description for this type of sections. First a cracked beam element model is developed for the cracked box section beams by extending the cracked beam element presented in Chapter 4 and 5. To calculate the local flexibility, the stress intensity factors (SIFs) for box section beams, which are not immediately available from the literature, are derived with an empirical approach combining FE simulation, parametric analysis and regression. The accuracy of the cracked beam element model for predicting the modal properties, particularly natural frequencies and mode shapes, of cracked box section beams is verified with numerically simulated examples. The cracked beam element is then incorporated in a model updating procedure for crack identification. Finally the cracked beam element model and the crack identification procedure are applied on experimental box beams with different configurations of cracks.

6.2 Cracked beam element model for box section beams

The cracked beam element model based on local flexibility and fracture mechanics as presented in Section 4.2 is extended to form the cracked beam element model for box section beams.

6.2.1 One-dimensional beam element for intact box section beams

Usually a cracked beam element model is formulated as an extension from the respective intact beam element model by incorporating the influence of cracks. For the box section beams, first a suitable one-dimensional beam element for the intact box beams is selected. The classic Euler-Bernoulli and Timoshenko beam elements are general choices for modelling beam-like structures. These beam elements can also be adopted for modelling box section beams. However, it is known that for relatively thin-walled box beams under loading, in-plane deformations such as warping, distortion and shear-lag effect cannot be ignored. The plane section assumption for classic beam elements does not strictly hold for box sections due to these effects. Consequently, marked modelling errors could arise when using classic beam models for box beams. To overcome this issue, some advanced one-dimensional beam elements have been developed in the past to account for the warping, distortion or shear-lag effects in thin-walled box beams. Some representative models have been summarized in Section 2.4.1.

The present study is mainly concerned about crack identification for box section beams. To simplify the formulation while retaining the essential effect of cracks, the classic Timoshenko beam element is selected for the modelling of intact box beams and forms the basis for the cracked beam element model. It can be readily replaced with some more advanced beam model as summarized above if needed. But as will be shown in Section 6.3 and 6.4, the Timoshenko-based cracked beam element model is sufficiently powerful for crack modelling and identification of box beams with either relatively thick or thin walls.

6.2.2 Crack model formulation

The additional flexibility for the cracked box section beam is established using the energy approach in conjunction with the fracture mechanics theory, as has been used in Section 4.2. For the sake of completeness, the relative theories and formulations are all presented here. Let the box section size be $B \times D$, as shown in Figure 6.1. The wall thicknesses for the horizontal and vertical walls are t_{sB} and t_{sD}, respectively. Assume that fracture of the beam is due to vertical bending and the crack starts from

the centre of bottom edge and propagates symmetrically towards the corners with a length of a_H ($\leq B/2$), which is defined as Stage 1 of the crack development. After the whole bottom wall is cracked, the crack goes up to the side walls with a depth of a_V ($\leq D$), defining as Stage 2.

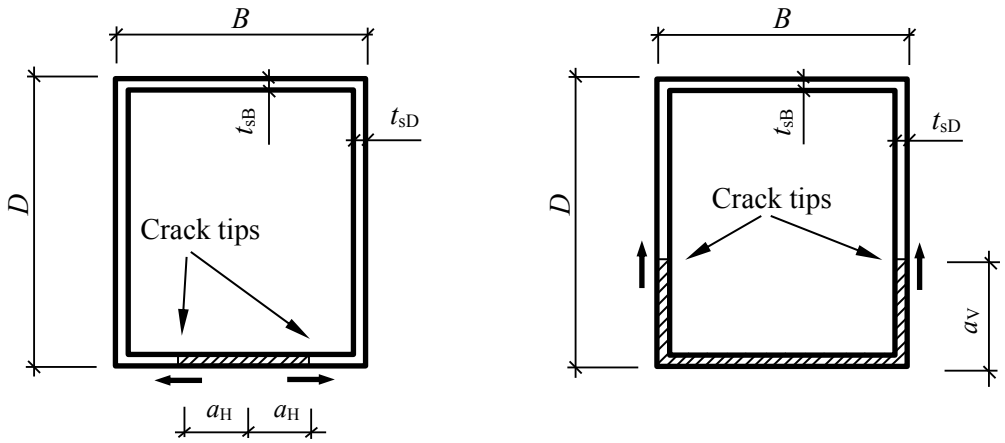

(a) Stage 1 (b) Stage 2

Figure 6.1 Crack development of box beam section

A cracked box beam element with 6 degrees of freedom (DOFs) in the x-y plane is developed to model the box beam with a cracked section shown in Figure 6.1. The DOFs consist of axial, transverse and rotational DOFs but without torsion, as shown in Figure 6.2. The element has a length of l_e and the crack is located at a distance of l_c from the left node. In Stage 1 of the crack propagation, the total crack length a can be calculated as $2a_H$, and in Stage 2 as $B+2a_V$. A crack length ratio is defined as the ratio of a_H to the width B, $\alpha_H = a_H/B$ ($\alpha_H \leq 0.5$). Similarly, a crack depth ratio for the crack in the vertical walls is defined as $\alpha_V = a_V/D$ ($\alpha_V \leq 1.0$). An overall crack depth ratio α is further defined as,

$$\alpha = \begin{cases} \alpha_H & \text{when crack is only in the bottom wall} \\ 0.5 + \alpha_V & \text{when crack propages into vertical walls} \end{cases} \tag{6.1}$$

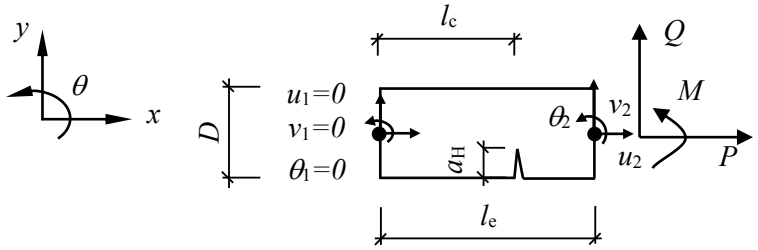

Figure 6.2 Loading state of a cracked beam element

The strain energy in the cracked beam element under a generalised load is equal to the strain energy of the intact beam element plus the additional strain energy brought by the crack, as shown in Eq. (6.2). The additional strain energy due to the presence of a crack can be evaluated by the fracture energy. Let the 3 DOFs at the left node be fixed, and the generalised load be axial load P (u_2), shear force Q (v_2) and bending moment M (θ_2).

$$U_{\mathrm{T}} = U_0 + U_{\mathrm{c}} \tag{6.2}$$

The additional strain energy brought by the crack U_{c} can be established according to the fracture mechanics theory as equal to the fracture energy:

$$U_{\mathrm{c}} = \int_{A_{\mathrm{c}}} G \mathrm{d}A \tag{6.3}$$

where, G is the energy release rate and A_{c} is the effective crack area. The relationships between the energy release rate G and the stress intensity factors (SIFs) can be expressed as (Tada et al., 2000),

$$G = \frac{1}{E'}\left(K_{\mathrm{I}}^2 + K_{\mathrm{II}}^2 + \frac{1}{1-\nu} K_{\mathrm{III}}^2 \right) \tag{6.4}$$

where K_{I}, K_{II} and K_{III} are the stress intensity factors for the open, sliding and tearing cracks, respectively; For plane stress, $E'=E$, and for plane strain, $E'=E/(1-\nu)$, where ν is the Poisson's ratio of the material.

For the cracked beam element considered in Figure 6.2, only the first SIF K_{I} needs to be considered for crack in Stage 1 whereas only the first two SIFs, K_{I} and K_{II}, exists for Stage 2. As the beam wall thickness is relatively thin, the crack problem is treated as plane stress.

The formulations of the first two types of SIFs can be expressed as (Liu, 1996; Tada et al., 2000):

$$K_{\mathrm{I1}} = \frac{P}{A_0}\sqrt{\pi a}F_{\mathrm{I1}}(a,...) \tag{6.5a}$$

$$K_{\mathrm{I2}} = \frac{MD}{2I}\sqrt{\pi a}F_{\mathrm{I2}}(a,...) \tag{6.5b}$$

$$K_{\mathrm{II}} = \frac{Q}{A_{\mathrm{e}}}\sqrt{\pi a}F_{\mathrm{II}}(a,...) \tag{6.5c}$$

where, K_{I1} and K_{I2} are the SIFs of mode I crack under axial loading and pure bending, respectively; K_{II} is the SIF of mode II under shear loading. A_0 is the sectional area of the box beam; I is the second moment of area of the box section; A_{e} is the effective shear area of the box beam section, which can be calculated as $A_{\mathrm{e}}=\kappa A_0$ and the shear coefficient κ for box beam is calculated with the equation recommended by Cowper (1966):

$$\kappa = \frac{10(1+\nu)(1+3m)^2}{(12+72m+150m^2+90m^3)+(11+66m+135m^2+90m^3)\nu+10n^2((3+\nu)m+3m^2)} \tag{6.6}$$

where, $m=(B-2t_{\mathrm{sD}})t_{\mathrm{sB}}/(Dt_{\mathrm{sD}})$, $n=(B-2t_{\mathrm{sD}})/D$.

There are three dimensionless terms F_{I1}, F_{I2} and F_{II} in Eq. (6.5), which are functions of geometrical parameters of the section and crack depth. Expressions for these terms will be presented in Section 6.2.3.

With Eq. (6.4) and (6.5), the strain energy release rate G for the current loading case can be written as:

For crack development in Stage 1,

$$G = \frac{1}{E}\left(\frac{P}{A_0}\sqrt{\pi a_{\mathrm{H}}}F_{\mathrm{I1}}^{\mathrm{H}} + \frac{D(M+Ql_e-Ql_c)}{2I}\sqrt{\pi a_{\mathrm{H}}}F_{\mathrm{I2}}^{\mathrm{H}}\right)^2 \tag{6.7a}$$

where $F_{\mathrm{I1}}{}^{\mathrm{H}}$ and $F_{\mathrm{I2}}{}^{\mathrm{H}}$ are terms related to cracks in Stage 1.

For crack development in Stage 2,

$$G=\frac{1}{E}\left[\left(\frac{P}{A_0}\sqrt{\pi a_{\mathrm{V}}}F_{\mathrm{I1}}^{\mathrm{V}}+\frac{D\left(M+Ql_e-Ql_c\right)}{2I}\sqrt{\pi a_{\mathrm{V}}}F_{\mathrm{I2}}^{\mathrm{V}}\right)^2+\left(\frac{Q}{A_{\mathrm{e}}}\sqrt{\pi a_{\mathrm{V}}}F_{\mathrm{II}}^{\mathrm{V}}\right)^2\right] \tag{6.7b}$$

where $F_{\mathrm{I1}}{}^{\mathrm{V}}$, $F_{\mathrm{I2}}{}^{\mathrm{V}}$ and $F_{\mathrm{II}}{}^{\mathrm{V}}$ are terms related to cracks in Stage 2.

The strain energy of an intact Timoshenko beam element U_0 can be calculated as:

$$U_0=\frac{1}{2}\int_0^{l_{\mathrm{e}}}\left[\frac{\left(M+Ql_{\mathrm{e}}-Qx\right)^2}{EI}+\frac{Q^2}{GA_{\mathrm{e}}}+\frac{P^2}{EA_0}\right]\mathrm{d}x \tag{6.8}$$

With the total strain energy of the cracked beam, the flexibility can then be obtained by invoking Castigliano's theorem as:

$$c_{ij}=\frac{\partial U_{\mathrm{T}}}{\partial F_i\partial F_j}=\frac{\partial U_0}{\partial F_i\partial F_j}+\frac{\partial U_{\mathrm{c}}}{\partial F_i\partial F_j} \tag{6.9a}$$

$$\text{or}\qquad c_{ij}=c_{ij,0}+c_{ij,\mathrm{c}} \tag{6.9b}$$

where, c_{ij} is the total local flexibility and F_i is the force applied on the i^{th} DOF of the beam node. $c_{ij,0}$ is the flexibility of the intact beam element, and $c_{ij,\mathrm{c}}$ is the additional flexibility due to the presence of the crack.

With Eq. (6.7), (6.8) and (6.9), the additional flexibility for the cracked beam element can be calculated as:

For crack only in Stage 1:

$$c_{ij,\mathrm{c}}=\frac{2\partial^2}{\partial F_i\partial F_j}\int_0^{a_{\mathrm{H}}}\frac{t_{\mathrm{sB}}}{E}\left[\left(\frac{P}{A_0}\sqrt{\pi a}F_{\mathrm{I1}}^{\mathrm{H}}+\frac{D\left(M+Ql_e-Ql_c\right)}{2I}\sqrt{\pi a}F_{\mathrm{I2}}^{\mathrm{H}}\right)^2\right]\mathrm{d}a \tag{6.10a}$$

For crack goes into Stage 2:

$$\begin{aligned}c_{ij,c}=&\frac{2\partial^2}{\partial F_i\partial F_j}\int_0^{0.5B}\frac{t_{\mathrm{sB}}}{E}\left[\left(\frac{P}{A_0}\sqrt{\pi a}F_{\mathrm{I1}}^{\mathrm{H}}+\frac{D\left(M+Ql_e-Ql_c\right)}{2I}\sqrt{\pi a}F_{\mathrm{I2}}^{\mathrm{H}}\right)^2\right]\mathrm{d}a\\&+\frac{2\partial^2}{\partial F_i\partial F_j}\int_0^{a_{\mathrm{V}}}\frac{t_{\mathrm{sD}}}{E}\left[\left(\frac{P}{A_0}\sqrt{\pi a}F_{\mathrm{I1}}^{\mathrm{V}}+\frac{D\left(M+Ql_e-Ql_c\right)}{2I}\sqrt{\pi a}F_{\mathrm{I2}}^{\mathrm{V}}\right)^2+\left(\frac{Q}{A_{\mathrm{e}}}\sqrt{\pi a}F_{\mathrm{II}}^{\mathrm{V}}\right)^2\right]\mathrm{d}a\end{aligned} \tag{6.10b}$$

where, i, j = 1, 2, 3, and F_1=P, F_2=Q, F_3=M.

It can be seen that there are 2 parameters representing explicitly the crack information in c_{ij}, namely crack depth a and crack location l_{c}.

The complete 6×6 stiffness matrix for the element can be obtained by inverting the flexibility matrix and satisfying the force equilibrium in the elements, as follows:

$$\mathbf{K}_c = \mathbf{T} * \mathbf{C}^{-1} * \mathbf{T}^T \tag{6.11}$$

where **C** is the 3×3 flexibility matrix with c_{ij} as its elements. **T** is the transformation matrix,

$$T = \begin{bmatrix} -1 & 0 & 0 \\ 0 & -1 & 0 \\ 0 & -l_e & -1 \\ 1 & 0 & 0 \\ 0 & 1 & 0 \\ 0 & 0 & 1 \end{bmatrix} \tag{6.12}$$

6.2.3 Stress intensity factors (SIFs) for cracked square box beams

To calculate the additional flexibility in Eq. (6.10), the SIFs for box section beams are required. The SIFs are defined to represent the strength of the stress fields surrounding the crack-tip and are determined by the boundaries of the cracked body and loads imposed (Tada et al., 2000). As have been summarized in Section 2.4.2, there have been some models for calculating of SIFs of box section beams. But most of those models mainly focus on the first type (open) crack. Among various types of methods, the FE modelling approach is an effective and straightforward way for the estimation of SIFs. With proper model setting, highly accurate SIFs can be extracted from FE analysis (Carpinteri et al., 2006; Dunn et al., 1997; Wang et al., 2005).

To obtain a full list of SIFs for both open and sliding cracks in both development stages of a cracked box section beam, FE modelling approach is adopted in this study to establish the SIF formulations. The values of SIFs are calculated from FE modelling for cracked box sections with varying geometrical parameters. With parametric analysis, the main parameters that may influence the SIFs are determined. Subsequently, a regression analysis is applied to establish empirical formulas for the SIFs.

Commercial FE package ABAQUS is used to generate the SIF values for crack box beams. As a special type of box section, herein a square box beam with uniform wall thickness is used as an example. Other types of sections, such as rectangular box section or sections with non-uniform wall thickness, can be applied with the same procedure. The box beam is simulated with 4-node shell element with reduced integration (S4R). To precisely model the crack behaviour, a series of ring meshes are applied around the crack tip, as shown in Figure 6.3.

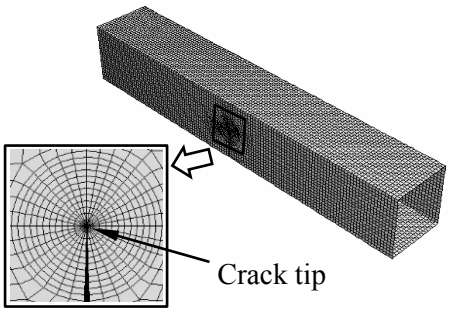

Figure 6.3 FE model of the cracked box beam

In order to deal with the singularity of stress and strain fields at the crack tip, the 'degenerate element control' command in ABAQUS is used at the crack tip. To output the stress intensity factors of the structure, the 'Contour integral evaluation' command, which could calculate the J-integral in fracture mechanics, is used in the FE model. Once the cracks are defined, both the mode I and mode II SIFs can be directly output by the software.

The dimensionless terms as defined in Eq. (6.5) are studied with parametric analysis. Parameters that may influence the SIFs include crack length (a_H or a_V), wall thickness to sectional width ratio (t_s/B), and sectional width (B). The following parameter ranges are considered based on engineering application experiences: B= 20-200 mm; t_s/B= 0.02-0.1; a_H= 0-B/2; a_V= t_s-B/2.

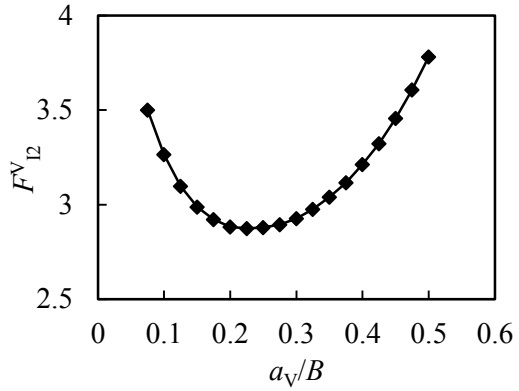

(a) F^{V}_{I2} versus a_V/B

(t_s/B = 0.05, B = 100 mm)

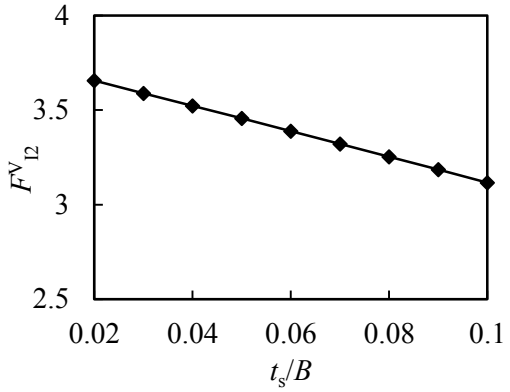

(b) F^{V}_{I2} versus t_s/B

(a_V/B = 0.45, B = 100 mm)

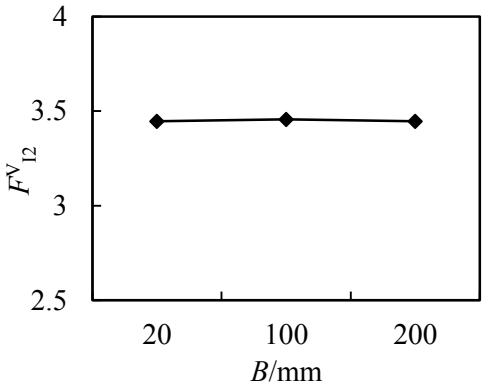

(c) F^{V}_{I2} versus B (t_s/B = 0.05, a_V/B = 0.45)

Figure 6.4 Parametric study results for F^{V}_{I2}

The parametrical analysis results for dimensionless term F^{V}_{I2} in Stage 2 are shown in Figure 6.4. It can be seen that F^{V}_{I2} is quite sensitive to a_V/B and t_s/B, whereas is almost constant under different B values. Consequently, F^{V}_{I2} can be expressed as:

$$F^{V}_{I2} = F^{V}_{I2}\left(a_V/B, t_s/B\right) \tag{6.13}$$

A regression analysis is then carried out to obtain the expression for Eq. (6.13). The parametric study results show that a linear function can be used to describe the F^{V}_{I2} versus t_s/B relationship while a quartic function is suitable for the F^{V}_{I2} versus a_V/B relationship,

$$F_{I2}^{V} = m\left(a_V/B\right)\cdot\left(t_s/B\right) + n\left(a_V/B\right) \tag{6.14}$$

where,

$$m\left(a_V/B\right) = -12.151 + 57.042\left(a_V/B\right) - 215.499\left(a_V/B\right)^2 + 376.957\left(a_V/B\right)^3 - 267.067\left(a_V/B\right)^4$$

$$n\left(a_V/B\right) = 5.269 - 24.092\left(a_V/B\right) + 100.185\left(a_V/B\right)^2 - 182.504\left(a_V/B\right)^3 + 138.946\left(a_V/B\right)^4$$

Comparisons of K^{V}_{I2} of Stage 2 from FE modelling and Eq. (6.14) predictions are shown in Figure 6.5. It can be seen that the results match quite well with each other, with errors smaller than 1%.

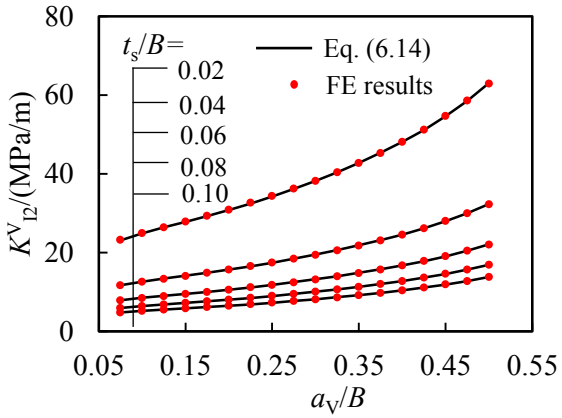

Figure 6.5 Comparison of K^{V}_{I2} from FE modelling and Eq. (6.14)

Other SIF terms can be obtained with the same approach and the complete results of SIF equations are listed in the Appendix A. With the SIF equations, the flexibility matrix for the cracked beam element as presented in Eq. (6.10) can be calculated.

6.3 Application of the cracked beam element in vibration analysis and crack damage identification

The established cracked beam element model in Section 6.2 is first verified with numerically simulated examples. Both forward prediction for modal data and inverse crack damage identification via model updating are carried out with the cracked beam element model.

6.3.1 Vibration analysis with the cracked beam element

The performance of the cracked beam element for box section beam in the prediction of the beam vibration properties, particularly the natural frequencies and mode shapes, is verified with numerical examples. Square box beams with uniform wall thickness are used as examples in the verification.

A square box beam with dimension as $B \times t_s \times L = 100 \times 10 \times 2000$ mm, as shown in Figure 6.6, is simulated. It has a t_s/B ratio of 0.1. The basic material properties are set as: $E = 201$ GPa, $\rho = 7850$ kg/m^3, $\nu = 0.3$. The boundary condition of the beam is set to be cantilever. The crack is set at $L_c = 600$ mm from the fixed end of the beam and assumed to have the form as shown in Figure 6.1(b). Two crack depth ratios, $\alpha = 0.8$ and 1.0 (i.e., α_V = 0.3 and 0.5), are used in the calculations. The FE model established with shell elements in Section 6.2.3 is used to generate numerically simulated modal data for the intact and cracked beams. Only transverse bending modes in the simulation results are selected and applied in the following calculation.

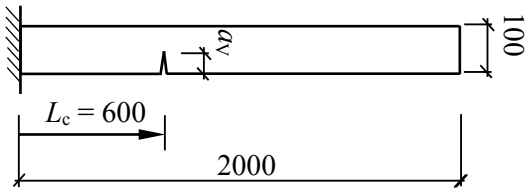

Figure 6.6 Numerically simulated beam (Unit: mm)

In the beam element models, 5 Timoshenko beam elements, including 4 intact and 1 cracked, are used. Timoshenko stiffness and mass matrices with high-accuracy cubic shape functions are used for the intact elements, while the cracked beam element model described in Section 6.2 is used for the cracked element. The cracked element is the 2nd element and the distance of the crack to the left end of the cracked element is $l_c = 200$ mm. The natural frequencies and mode shapes for the transverse modes are predicted with the beam element model (to be referred to as 'predicted') and the results are compared with the refined FE model as discussed below.

Table 6.1 summarises the comparison between the numerically simulated and the predicted lowest four natural frequencies. The relative differences between the

simulated and predicted frequencies are included as ε in percent. Results show that the beam element models predict the first couple modes of frequencies very accurately for both the intact and cracked beams. The 3rd and 4th modes have larger but still reasonable errors in the predicted results (1.5-4.8%).

Table 6.1 Cantilever box beams with t_s/B = 0.1 (Unit: Hz)

Mode	Intact			Cracked (α_V = 0.3)			Cracked (α_V = 0.5)		
	Simulated	Predicted	ε/%	Simulated	Predicted	ε/%	Simulated	Predicted	ε/%
1	25.9	26.0	**0.4**	23.8	24.1	**1.2**	21.1	21.4	**1.2**
2	157.5	158.3	**0.5**	154.0	155.4	**0.9**	149.8	151.6	**1.2**
3	421.3	427.7	**1.5**	388.7	402.8	**3.6**	356.6	373.7	**4.8**
4	776.6	809.0	**4.2**	767.2	802.7	**4.6**	763.0	799.2	**4.7**

The indicator defined as the relative shift of the natural frequency brought by the crack, S_i, is used to further benchmark the effectiveness of the cracked beam element model, as shown in Eq. (4.12).

Figure 6.7 shows the comparison between numerically simulated and predicted frequency shifts of the beams. It can be seen that good match can be achieved for all the four modes.

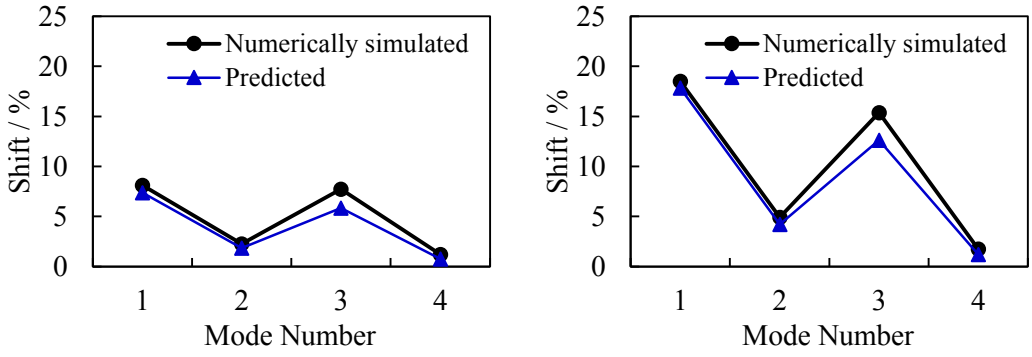

(a) α = 0.8 (b) α = 1.0

Figure 6.7 Comparisons between numerically simulated and predicted frequency shifts (t_s/B= 0.1)

The accuracy of the cracked beam element model for prediction of mode shapes is tested with the Modal Assurance Criterion (MAC), as defined in Eq. (4.13).

Table 6.2 MAC results between numerically simulated and predicted mode shapes

Mode	$t_s/B = 0.1$			$t_s/B = 0.02$		
	Intact	$\alpha_V = 0.3$	$\alpha_V = 0.5$	Intact	$\alpha_V = 0.3$	$\alpha_V = 0.5$
1	1.000	1.000	1.000	1.000	1.000	1.000
2	1.000	1.000	1.000	1.000	1.000	1.000
3	1.000	1.000	0.998	1.000	0.999	0.998
4	1.000	0.999	0.998	0.999	0.999	0.997

The MAC results for the first 4 mode shapes are compared and listed in Table 6.2. It can be seen that the MAC values with the crack model are all greater than 0.998, indicating very good match between the numerically simulated and predicted mode shapes.

6.3.2 Crack damage identification using the cracked beam element model

The cracked beam element model is then used for crack identification in the numerically simulated beams. The crack identification is carried out via a finite element model updating procedure. The beam element model established in Section 6.3.1 is adopted for updating. For generality each element in the beam model is considered as a potential cracked element and is modelled using the cracked beam element with both crack depth ratio (α) and location (l_c) unknown. Therefore there is no limit on the number and location of cracks to be identified in the beams. In the present model there are 5 beam elements in the model, thus 10 unknown crack parameters need be updated. It is noted that the beam element close to the free end of the cantilever beam will be insensitive concerning the modal data. To avoid ill-conditioning at the beam end, the end element is excluded from the updating and assumed to be intact, leaving 8 parameters to be determined from the updating.

A similar objective function to Eq. (5.3) is employed for the updating. It incorporates the lowest four modes of eigenvalue and mode shape data, as shown below,

$$J = \frac{1}{N_{\mathrm{m}}} \sum_{i=1}^{N_{\mathrm{m}}} W_i \cdot \mathrm{abs}\left(\frac{\lambda_{\mathrm{m}i}^{\mathrm{d}}}{\lambda_{\mathrm{m}i}^{0}} - \frac{\lambda_{\mathrm{c}i}^{\mathrm{d}}}{\lambda_{\mathrm{c}i}^{0}} \right) + \frac{1}{N_{\mathrm{s}} N_{\mathrm{n}}} \sum_{i=1}^{N_{\mathrm{s}}} V_i \cdot \left(\sum_{j=1}^{N_{\mathrm{n}}} \mathrm{abs}\left(\varphi_{\mathrm{m}ji}^{\mathrm{d}} - \varphi_{\mathrm{c}ji}^{\mathrm{d}} \right) \right) \tag{6.15}$$

where, J is the objective function to be minimised, λ denotes the eigenvalue (= $(2\pi f)^2$), φ denotes the mode shape displacement, with the subscript 'm' indicating numerically simulated data and 'c' computed data, and the superscript 'd' indicating damaged (current) state and '0' the intact state. N_{f} (= 4) is the number of eigenvalues to be included, N_{s} (= 4) is the number of mode shapes to be included, N_{n} (= 5) is the number of nodes in the mode shapes. W_i and V_i are the weights for the i^{th} eigenvalue and mode shape, respectively. As the modelling errors in the modal data tend to increase with mode number, lower weights should be assigned to higher modes. In the updatings here the weights W_i and V_i are set to be inversely proportional to the mode order, i.e. equal to $1/i$, with i= 1, 2, 3 and 4.

Genetic algorithm (GA) is employed to search for the optimal solution in the model updating. Herein the GA function in Matlab is employed and the basic parametric settings for the GA are listed in Table 6.3.

Table 6.3 Parametric settings for GA

Parameter	Setting
Population size	3000
Fitness limit	-Infinite
Max generation	1500
Crossover fraction	0.7
Mutation rate	0.02

The updating results of the four cracked beams are given in Table 6.4 and Figure 6.8. It can be seen that the correct cracked element can be identified for all of the four beams. The updated crack parameters have good accuracy. Errors in the crack depth ratios (α) are in the range of 0.3%-2.7% and errors in the crack locations (l_{c}) are

around 5%. The results suggest that the cracked beam element model is effective in the crack damage identification of box section beam.

Table 6.4 Updated crack locations (l_c) of the beams (Unit: mm)

Element number	t_s/B= 0.1					t_s/B= 0.02				
	1	2	3	4	5	1	2	3	4	5
With α = 0.8	-	207	-	-	-	-	209	-	-	-
With α = 1.0	-	209	-	-	-	-	207	-	-	-

Note: the location values for elements other than the cracked ones are omitted from the table.

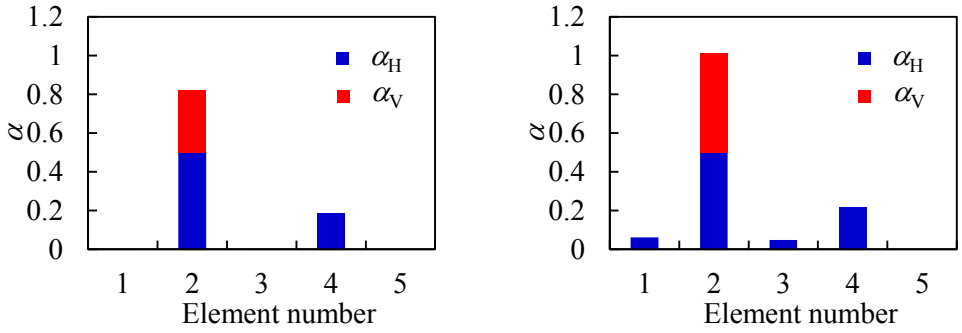

(a) α = 0.8 (b) α = 1.0

Figure 6.8 Updated crack depth ratios (α) of box beams (t_s/B = 0.1)

6.3.3 Performance of the cracked beam element model on thin-walled box section beams

The numerical simulated beam presented in Section 6.3.1 and 6.3.2 has a t_s/B ratio as 0.1, which can be categorized as a thick-walled beam. Results show that the cracked beam element model performances well for both vibration property predictions and crack damage identification of the thick-walled box section beams. In structural engineering, there exists a vast amount of thin-walled box section beams. It has been summarized in Section 6.2.1 that the modelling of thin-walled box section beams with one-dimensional beam element is more challenging due to the presence of in-plane deformations. The same issue exists in the crack modelling of thin-walled box section beams. Some more advanced one-dimensional beam elements as summarized in Section 6.2.1 can be employed to formulate the cracked beam element model for

thin-walled box section beams. However, as the Timoshenko beam element is still one of the most widely used beam model and easy to formulate, in the present study the Timoshenko-based cracked beam element model as developed in Section 6.2 is employed. The performance of the cracked beam element for modal data prediction and crack identification is verified again numerically simulated thin-walled box beam in this section.

The same square box beam as shown in Figure 6.6 is used in the verification. But now a much thinner wall thickness (t_s = 2 mm) is applied on the beam. So the dimension of the beam will be $B \times t_s \times L = 100 \times 2 \times 2000$ mm and the t_s/B ratio is 0.02. All the other parameters, including material properties, boundary condition and crack parameters, are left to be the same as the thick-walled beam.

The same beam models with 4 intact and 1 cracked Timoshenko beam elements are used to predict the natural frequencies and mode shapes of the thin-walled box beams. The comparison between numerically simulated and predicted lowest four natural frequencies is shown in Table 6.5.

Table 6.5 Cantilever box beams with t_s/B = 0.02 (Unit: Hz)

Mode	Intact			Cracked (α_V = 0.3)			Cracked (α_V = 0.5)		
	Simulated	Predicted	ε/%	Simulated	Predicted	ε/%	Simulated	Predicted	ε/%
1	28.2	28.1	**0.0**	25.5	25.5	**0.0**	22.5	22.6	**0.0**
2	168.7	170.4	**1.0**	164.3	166.4	**1.3**	159.9	162.4	**1.6**
3	422.8	457.7	**8.2**	390.8	424.8	**8.7**	362.6	394.1	**8.7**
4	642.9	860.6	**33.9**	641.6	853.2	**33.0**	641.1	849.6	**32.5**

It can be seen that the cracked beam element model is able to predict the first couple modes of natural frequencies with similar accuracy to those from the thick-walled beams. But for the 3rd and 4th modes, the errors in the predicted results are considerably large (8.2% - 33.9%). The reason for the poor prediction of higher mode frequencies is due to the strong presence of warping, distortion and shear-lag effects in the thin-walled section, as explained in Section 6.2.1.

The relative shifts of the natural frequencies brought by the crack as defined in Eq. (4.12) are presented in Figure 6.9. It can be seen that the numerically simulated and predicted results have good match for all the modes. It indicates that by calculating the relative shift of frequency, the modelling errors brought by non-classic beam effects can be greatly eliminated and the cracked beam element model is capable of predicting the frequency shifts accurately up to the first four modes.

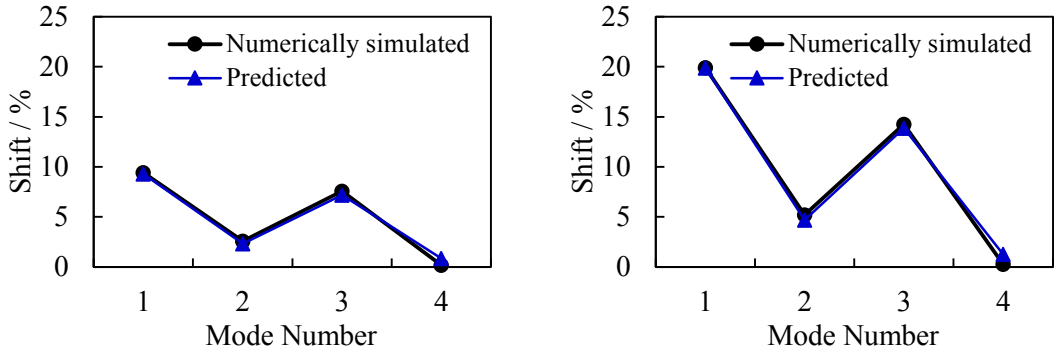

(a) $\alpha = 0.8$ (b) $\alpha = 1.0$

Figure 6.9 Comparisons between numerically simulated and predicted frequency shifts ($t_s/B = 0.02$)

MAC results of the first 4 mode shapes have been shown in Table 6.2. It can be seen that the MAC values are all greater than 0.997. It shows that the cracked beam element model is able to predict the mode shapes with high accuracy even though strong non-classic beam effects are presented.

The crack damage identification procedure presented in Section 6.3.2 is subsequently applied on the cracked thin-walled box beams. Model updating results are presented in Figure 6.10 and Table 6.4. It can be seen that the correct cracked element can be identified for both beams. The updated crack depth ratios and locations have similar levels of accuracy to those from the thick-walled beams. It clearly shows that the Timoshenko-based cracked beam element model performances well for crack damage identification of both thick-walled and thin-walled box beams.

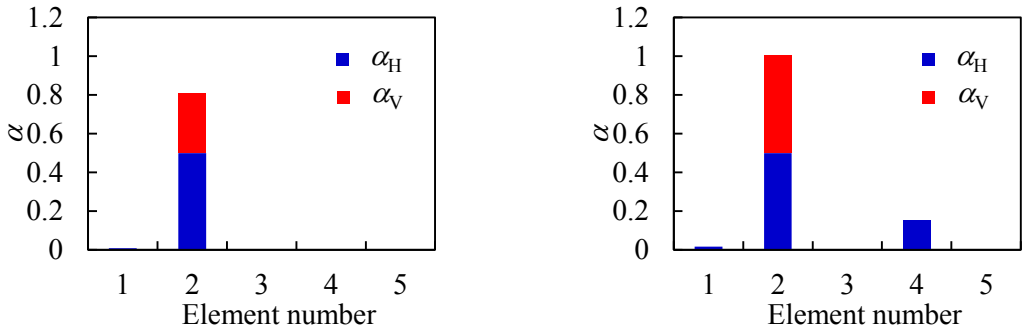

(a) $\alpha = 0.8$ (b) $\alpha = 1.0$

Figure 6.10 Updated crack depth ratios (α) of box beams ($t_s/B = 0.02$)

6.4 *Experimental verification with the cracked beam element model*

An experimental programme of modal testing with square box section beams has been conducted to further verify the cracked beam element model for this type of beams. Both single-crack and multiple-crack beams were prepared for the tests to cover different possible crack damage scenarios in box beams.

6.4.1 Test specimens

Five square steel box section beams with dimension as $B \times t_s \times L = 100 \times 5 \times 1200$ mm were prepared in the modal testing programme, as shown in Figure 6.11.

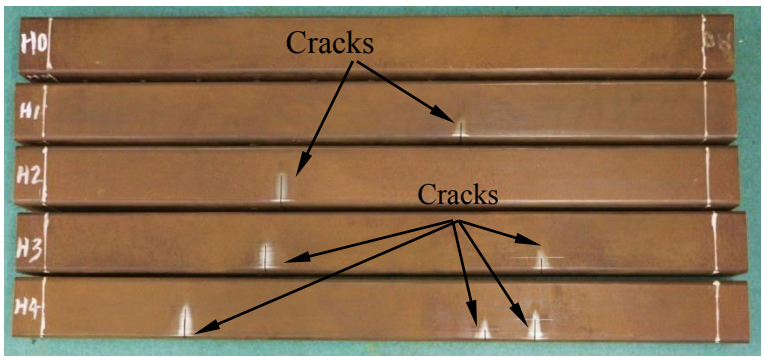

Figure 6.11 Box beam specimens

The beams are labelled as H0, H1-H4 in sequential order, with beam H0 being an intact beam as the reference. Beams H1-H4 are cracked beams, and the cracks all propagate into the vertical walls (i.e., having the form shown in Figure 6.1(b)). The arrangements of the cracks were made to represent different cracked beam scenarios, including having both single and multiple cracks. Beams H1 and H2 contained a single crack at the same relative location but different crack depth ratios. Beams H3 and H4 have 2 and 3 cracks, respectively. In beam H3, the two cracks are remotely spaced whereas in beam H4, two of the cracks are closely spaced. The cracks were created with saw cuts and the width of the cut is around 1mm. Detailed information of the cracks is presented in Table 6.6.

Table 6.6 Crack depth and location information

Beam label	Crack1		Crack2		Crack3	
	L_c/mm	α (α_V)	L_c/mm	α (α_V)	L_c/mm	α (α_V)
H0	-	-	-	-	-	-
H1	750	0.79 (0.29)	-	-	-	-
H2	450	1.01 (0.51)	-	-	-	-
H3	420	0.94 (0.44)	870	0.74 (0.24)	-	-
H4	290	0.99 (0.49)	780	0.68 (0.18)	860	0.84 (0.34)

6.4.2 Modal testing setup

Free-free boundary conditions were created for the tested beam with two strings, as shown in Figure 6.12. The test procedure and instrumentation were similar to what was described in Section 5.2. The same impact hammer and light-weight accelerometers were used to excite the beam and record the response. After some trial tests, it was found that the sampling rates and record duration settings used in Section 5.2 were reasonable settings for the current tests. So the parameters were kept to be the same.

Both the natural frequencies and mode shapes of the beams were measured during the modal testing. To extract the mode shapes, 11 uniformly distributed measurement locations were marked on the beam, as shown in Figure 6.12(b). An accelerometer

was attached at location P4 while another one was attached to the bottom side of the beam at the same span location. The reason for such arrangement was primarily to enable the identification of global bending modes and a detailed explanation will be given in Section 6.4.3. During the tests, impact was applied at each measurement location from P1 to P11 in a routine procedure.

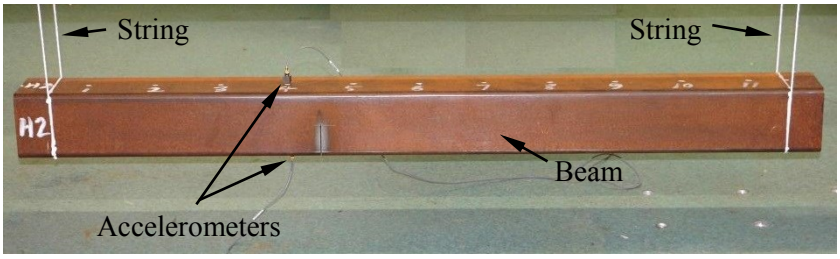

(a) Photo of the setup

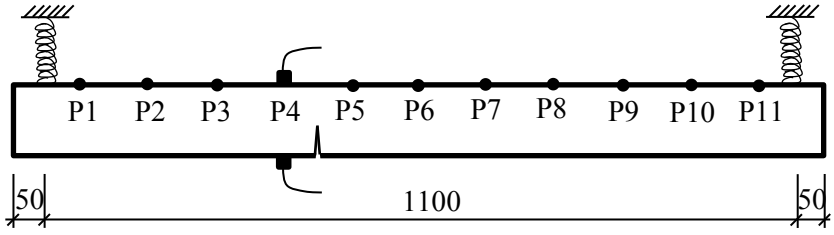

(b) Schematic view of the setup (Unit: mm)

Figure 6.12 Modal testing setup

Frequency response function (FRF) curves were calculated with the Fourier transform of the impact force and acceleration signals. To reduce the additive noises in the FRF curves, general signal processing techniques such as windowing and averaging were applied. A force window was employed to eliminate the noises in the force signal, and 10 repetitive tests were performed for each excitation location and the obtained FRF curves were averaged to get the final FRF curve.

6.4.3 Modal testing results

A representative measured FRF curve from the intact beam H0 is shown in Figure 6.13. It can be noticed that the curve is of good quality and has clear resonances. With the standard peak-picking method, the natural frequencies and mode shapes of the beam can be extracted from the FRF curve.

It should be noted that there are some 11 resonances in the frequency range of 1000-2000 Hz, but not all these resonances belong to transverse bending modes. To identify from the modal testing results the transverse bending modes, which are the modes used for crack identification with the cracked beam element model, the mode shapes need to be employed to distinguish these modes from the local modes.

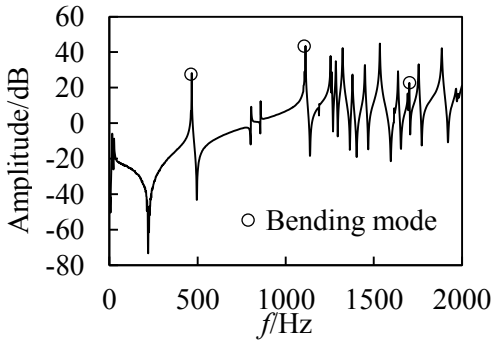

Figure 6.13 Driving FRF curve at point P4 of beam H0

It has been mentioned in Section 6.4.2 that two accelerometers were attached at both sides of the tested beam, so two sets of mode shapes were obtained for the beams. For a global transverse bending mode, the mode shapes extracted from the top and bottom accelerometers should match each other consistently. To assist in a more precise identification, the Timoshenko beam element model is used to provide an approximate prediction of the transverse bending mode shapes and calculate the MAC values between the predicted and measured modes. The measured modes which give high MAC values can be identified as real bending modes (With MAC values at least higher than 0.95).

It is found that basically there are three types of modes in the FRF curves, and the corresponding measured mode shape displacements are shown in Figure 6.14, where x is the beam span location. The curves shown in Figure 6.14(a) are not correlated to any bending mode and can be easily discarded. The curves in Figure 6.14(b) show good match with each other. After comparing with the predicted modes, it is confirmed that this is the 2nd bending mode for the beam. The two curves in Figure 6.14(c) also show good correlation with the predicted mode shape (1st mode). However, it is noted that the mode shapes from the two accelerometers have opposite bending directions. In other words, it is not a global bending mode, but a mode with

local vibration of box walls. This kind of local vibration modes has been observed and discussed in Hung et al. (1995) and should as well be discarded.

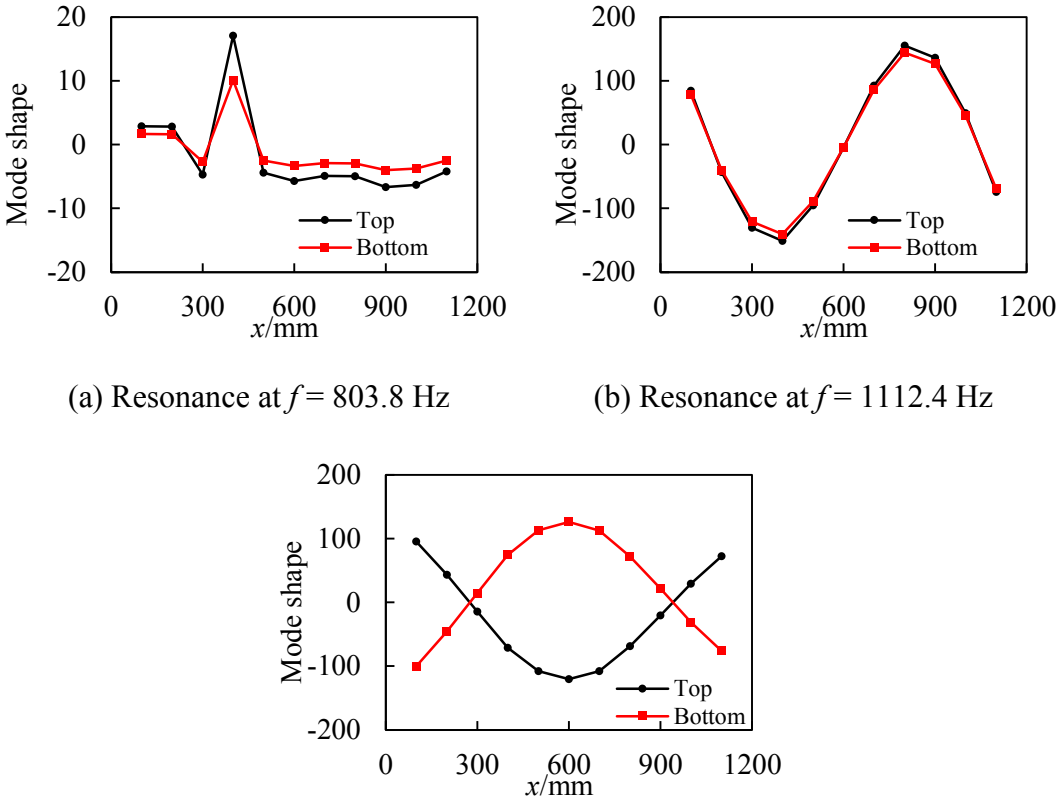

(a) Resonance at f = 803.8 Hz

(b) Resonance at f = 1112.4 Hz

(c) Resonance at f = 1284.8 Hz

Figure 6.14 Comparisons of measured mode shapes from top and bottom accelerometers

With the above strategy, the lowest 3 bending modes of the tested box beams can be picked from the FRF resonances, as shown in Figure 6.13. The extracted natural frequencies and mass-normalized 1st mode shapes for all the five beams are shown in Table 6.7-6.8 and Figure 6.15.

Table 6.7 Measured and predicted natural frequencies of beams H0, H1 and H2 (Unit: Hz)

Mode	H0			H1			H2		
	Measured	Predicted	ε/%	Measured	Predicted	ε/%	Measured	Predicted	ε/%
1	466.9	466.9	**0.0**	385.4	390.6	**1.3**	305.6	306.3	**0.2**
2	1112.4	1176.7	**5.8**	1010.6	1075.7	**6.4**	954.4	1000.8	**4.9**
3	1701.6	2107.6	**23.9**	1679.5	2106.5	**25.4**	1666.3	2096.8	**25.8**

Table 6.8 Measured and predicted natural frequencies of beams H3 and H4 (Unit: Hz)

Mode	H3			H4		
	Measured	Predicted	ε/%	Measured	Predicted	ε/%
1	334.0	329.8	**-1.3**	339.0	334.6	**-1.3**
2	817.6	844.9	**3.3**	677.6	706.0	**4.2**
3	1585.7	1763.1	**11.2**	1341.4	1508.4	**12.4**

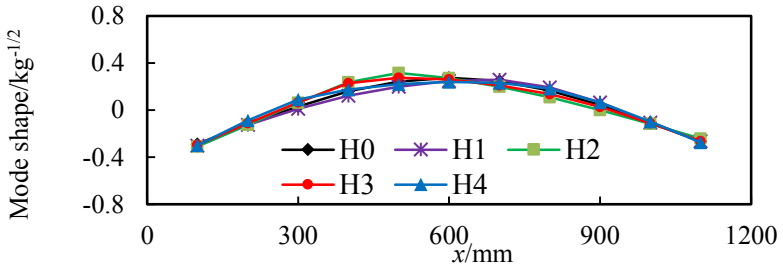

(a) 1st mode

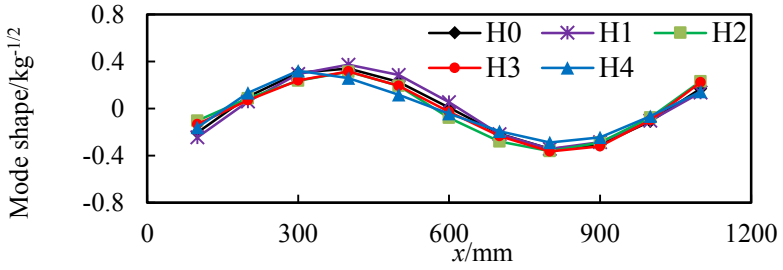

(b) 2nd mode

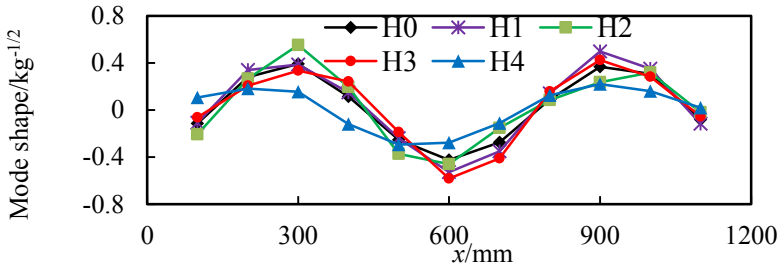

(c) 3rd mode

Figure 6.15 Measured mode shapes for the first three bending mode from all 5 beam specimens

6.4.4 Verification of the prediction of modal properties by the cracked beam element

Beam models with the cracked beam element are used to predict the natural frequencies and mode shapes of the tested beams. The beam models include 6 beam elements with uniform length as 200 mm. As the elastic modulus of the steel beams are not available, the first natural frequency of the intact beam H0 is first used to do a preliminary updating and the resulted elastic modulus is 208 GPa.

Comparison of measured and predicted natural frequencies are shown in Table 6.7 and 6.8. It can be seen that similar to the observation in Section 6.3.1, the beam models are able to predict the frequencies of lower modes with good accuracy but the errors in the 3rd mode frequency are considerably large. The errors are due to the presence of non-classic beam effects, as explained in Section 6.3.

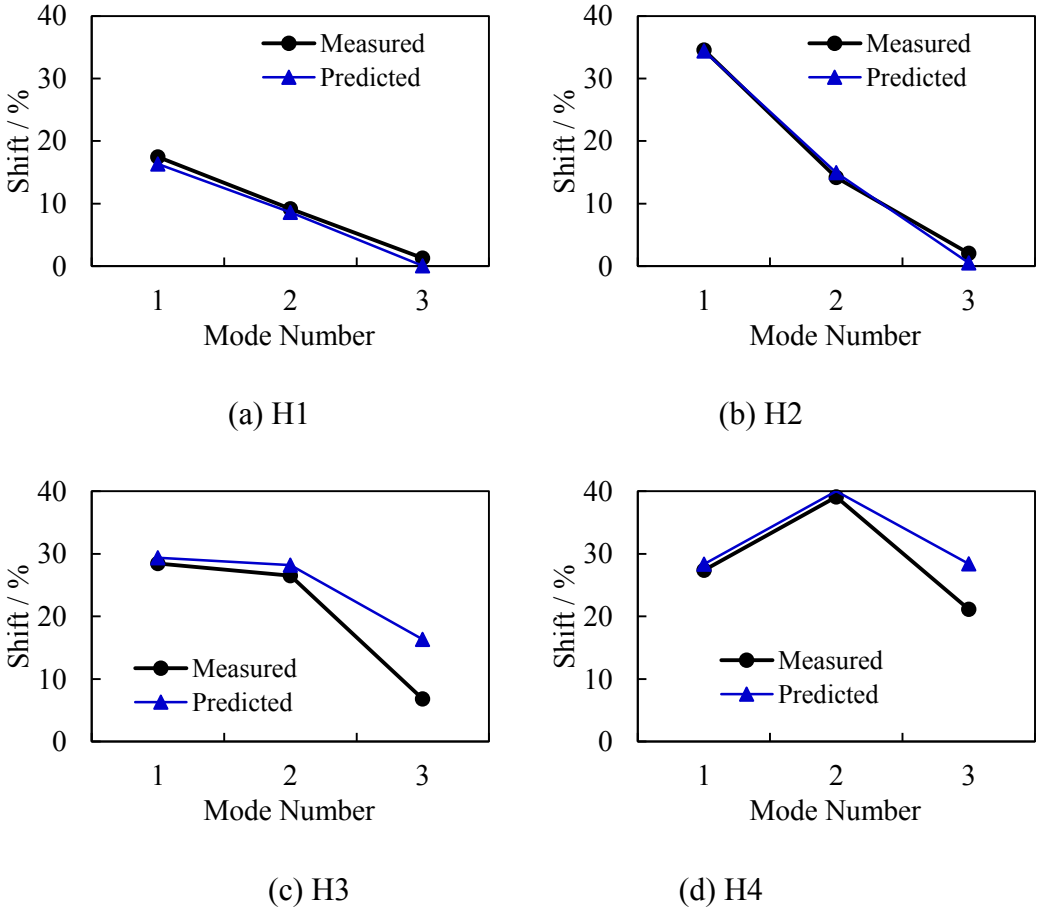

Figure 6.16 Comparisons between measured and predicted frequency shifts

However, the predicted frequency shifts of the first three modes of beams with a single crack (beam H1 and H2) match very well with the measured results, as shown in Figure 6.16. For the beams with multiple cracks, the frequency shifts of the first couple of modes also match well. For the 3rd mode, the errors are higher than those of single crack beams. One explanation is that the presence of a crack alters the effect of shear lag on the beam behaviour and with multiple cracks the deviation from a standard Timoshenko beam is amplified. This phenomenon further indicates the limitation of using a Timoshenko beam element on modelling the vibration of box beams, particularly for higher modes and in the presence of multiple cracks.

MAC results between the measured and predicted mode shapes are shown in Table 6.9. The MAC values are close to 1 for the first two modes of all beams. For beams with multiple cracks, the MAC values are slightly lower but still exceed 0.950.

Table 6.9 MAC results between measured and predicted mode shapes

Mode	H0	H1	H2	H3	H4
1	1.000	0.998	0.998	0.999	0.999
2	0.999	0.997	0.998	0.997	0.998
3	0.996	0.996	0.973	0.951	0.963

6.4.5 Model updating and crack damage identification

The model updating strategy presented in Section 6.3.2 is applied on the tested beams to identify the cracks. The beam models contain 6 equal-length beam elements but the two free end elements are excluded from the updating to avoid ill-conditioning. So totally there are 8 updating parameters. The actual crack parameters for the beams are listed here for the later comparison with the (inverse) updating results. For beam H1, the crack is in the 4th element with [α, l_c]= [0.79, 150]; for beam H2, the crack is in the 3rd element with [α, l_c]= [1.01, 50]; for beam H3, the cracks are in the 3rd and 5th elements, with [α, l_c]= [0.94, 20] and [0.74, 70], respectively; for beam H4, the cracks are in the 2nd, 4th and 5th elements with [α, l_c]= [0.99, 90], [0.68, 180] and [0.84, 60], respectively. The measured first 3 modes of

natural frequencies and mode shapes are used to form the objective function with Eq. (6.17) and GA is employed to search for the optimistic solution.

Table 6.10 Model updating results of crack locations l_c (Unit: mm)

Element number	1	2	3	4	5	6
H1	-	-	-	150 (150)	-	-
H2	-	-	63 (50)	-	-	-
H3	-	-	50 (20)	-	46 (70)	-
H4	-	89 (90)	-	170 (180)	77 (60)	-

Note: the values in the parentheses are actual crack locations.

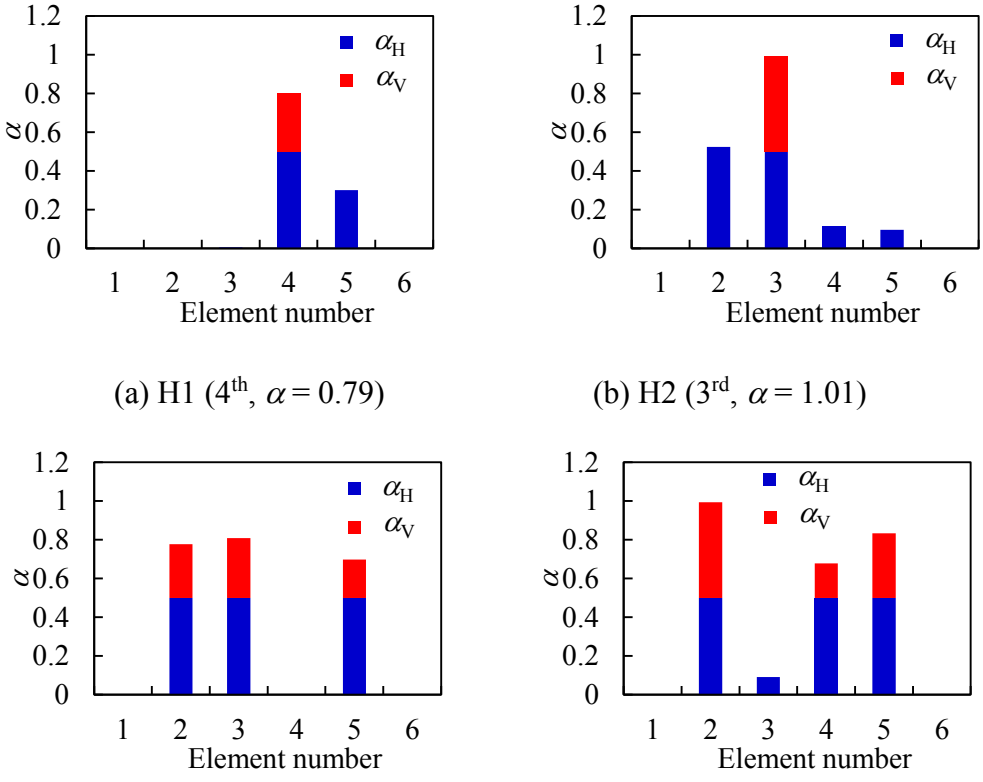

(a) H1 (4^{th}, $\alpha = 0.79$) (b) H2 (3^{rd}, $\alpha = 1.01$)

(c) H3 (3^{rd} and 5^{th}, $\alpha = 0.94$ and 0.74) (d) H4 (2^{nd}, 4^{th} and 5^{th}, $\alpha = 0.99$, 0.68 and 0.84)

Figure 6.17 Model updating results of crack depth ratios α

The updated results are presented in Table 6.10 and Figure 6.17. It can be seen that the correct crack element number can be identified for both the single-crack and

multiple-crack beams. Compared with the actual crack conditions shown in Figure 6.11 and summarized above, it is found that the updated crack depth ratios and locations have very good accuracy. The crack depth ratios (α) generally have errors lower than 6% except the one in the 3rd element of beam H3 (with error as 13%). Errors in the crack locations (l_c) are all smaller than 15%. It is noted that a marked false crack is identified in the 5th element in beam H2 and in the 2nd element in beam H2 and H3. As explained earlier, this is partly attributed to the low sensitivity of elements close to the beam end to the modal information, and partly due to measurement errors in modal testing results and modelling errors in the beam element model. Overall, the crack identification with the cracked beam element may be regarded as successful for both the single-crack and multiple-crack beams.

6.5 Summary and conclusions

A cracked beam element model has been developed for the crack damage identification of box section beams. The model is formulated taking into account the additional flexibility brought by the crack, using Timoshenko beam as the base element. The additional flexibility is established in accordance with the fracture mechanics theory. Shear deformation and coupling between transverse and longitudinal DOFs are also represented in the model. To calculate the additional flexibility matrix, the stress intensity factors for cracked box section beams have been derived from an empirical approach combining FE simulation, parametric analysis and regression.

The cracked beam element model has been verified against numerically simulated modal data. Results show that the model is capable of predicting the natural frequencies of the lowest modes with high accuracy but larger errors incur for higher modes, especially for thin-walled beams. However, the modelling errors can be largely eliminated when the relative shift of the frequency is calculated. The mode shapes can also be predicted with good accuracy. The cracked beam element model was then employed in a crack identification process via finite element model

updating. Results show that the cracks can be identified with high accuracy for both the thick-wall and thin-wall beams.

The cracked beam element model was subsequently verified against experimentally measured modal data from five square box section beams. Different crack scenarios with both single-crack and multiple-crack were created in the tested beams. Modal test was carried out on the box beams to extract the natural frequencies and mode shapes. The first three bending modes were extracted from the measurements. Comparison between the measured and predicted natural frequency shifts as well as mode shapes showed good accuracy for both the single-crack and multiple-crack beams. Crack identification results have also shown that correct cracks can be identified for both single-crack and multiple-crack beams. The updated crack depth and relative crack position within the cracked element generally have achieved good accuracy.

The outcome from this study paves a way for the extension of the cracked beam element model to other types of cross-sections for the crack damage identification purposes.

7 Conclusions and recommendations for further research

7.1 Conclusions

This thesis is devoted to studying some of the important issues related to the vibration-based damage identification. Two major topics are of main interest in the thesis. The first one is to enhance the modal dataset by using the 'artificial boundary condition' (ABC) frequencies. The second one is to develop a robust crack damage identification approach for thick beams, and to benefit from the use of ABC frequencies in such identification. Special conclusions have been provided in the separate chapters and herein some of the main conclusions are summarized.

7.1.1 ABC frequencies and their applications in model updating

(1) Experimental modal tests are carried out on laboratory-scale structures to extract ABC frequencies from a real measurement environment. Different groups of structures are employed in the tests, including flexible steel beams with fixed end boundary conditions, thick and stiff aluminium beams with free-free boundary conditions, and an RC beam with simply supported boundary conditions.

(2) Experimental results show that one-pin and two-pin ABC frequencies of the first few modes can be obtained with good quality from relatively simple modal testing setups with a careful implementation of modal testing and data analysis procedures, including applying the Rational Fraction Polynomial (RFP) method. For some more sophisticated structures, as the stiff aluminium beams and the RC beam with realistic boundary conditions, it is still possible to extract the first few modes of ABC frequencies with acceptable quality.

(3) After examining a few major error sources in ABC measurement, it is found that the ABC frequencies can be measured with similar accuracy as natural frequencies for the relative simple test setups while the ABC frequencies from the relative thick and stiff aluminium beams and the RC beam also have reasonable accuracy, although not as good as the natural frequencies.

(4) Model updating results show that incorporating ABC frequencies in the data set significantly improves the parameter identification results, and both single- and multi-damage scenarios in the experimental steel beams can be identified correctly. In comparison, the results using combined natural frequencies and limited mode shapes exhibit less satisfactory results due to higher measurement errors in the mode shapes. For the stiff aluminium beams, ABC frequencies also perform quite well for model updating and crack identification of both the single- and multi-cracked beams.

7.1.2 Crack identification in thick beams with a cracked beam element

A crack identification procedure with a cracked beam element model for thick beams is first established.

(1) A cracked beam element model is established for the crack modelling of thick beams. The cracked beam element model is formulated by taking into account the additional flexibility brought by the crack in accordance with the fracture mechanics principles. Compared with other commonly used crack models, the current cracked beam element model have superior performance in two important aspects, 1) the model is capable of providing a consistent and accurate representation of the effect of a crack on the vibration properties of a cracked beam for practically all modes of interest; 2) the model takes into account specific features concerning the vibration of thick beams, including shear deformation and coupling between the flexural and longitudinal modes. The crack parameters, namely the crack depth and the relative crack location, can be explicitly involved in the stiffness matrix of the cracked element.

(2) The cracked beam element model is capable of predicting sufficiently accurate natural frequencies and mode shapes of cracked thick beams up to 9 modes and in consistent manner. On the other hand, the widely used reduced stiffness model can only predict the modal data accurately for just the lowest couple of modes.

(3) A crack damage identification procedure incorporating the cracked beam element model is developed for thick beams via model updating. The procedure has no limitation on the number, severity and locations of cracks in the cracked beam. To

overcome the issue with the crack influence range crossing into the adjacent beam element in the case where the location of the crack is too close to one end of the cracked element, an adaptive procedure is employed in discretization of the beam model.

(4) The crack identification procedure is verified with numerically simulated modal data and results show that correct crack elements can be identified and the updated crack parameters have high accuracy. On the other hand, model updating with the reduced stiffness method cannot always result in correct crack information.

(5) The crack identification procedure is subsequently verified against modal testing results from an experimental study. Five aluminium thick beams with different crack scenarios are tested in the laboratory environment to extract the first few modes of natural frequencies and mode shapes. Forward verification and inverse crack damage identification with the cracked beam element model both show the crack model is of high accuracy.

(6) From the verifications with the numerically simulated and measured modal data, it is noted that there is another merit for the cracked beam element model. As the crack parameters are explicitly presented in the cracked beam element model, the model updating results are generally independent of the element size in the FE model. So a reduced number of beam elements can be used in the FE model to reduce the number of updating parameters when a limited amount of modal data is available. This will not lose the preciseness of the identified crack information in any significant way. On the other hand, the updated damage parameters with the reduced stiffness model are highly depended on the element size of the FE model.

The procedure is then adapted for the application on a specific cross-section type, i.e., the box section.

(1) The cracked beam element model is extended for the modelling of cracked box section beams. The model uses Timoshenko beam as the base element and the additional flexibility needs to be re-formulated. To calculate the additional flexibility matrix, the stress intensity factors for cracked box section beams have been derived from an empirical approach combining FE simulation, parametric analysis and regression.

(2) The cracked beam element model is first verified against numerically simulated modal data. Forward verification shows that the crack model is capable of predicting the natural frequency and mode shapes with generally good accuracy. For thin-walled box section beams, the predicted natural frequencies of higher modes have considerably large errors due to the presence of non-classic effects. Bu the modelling errors can be largely eliminated when the relative shift of the frequency is calculated. Crack identification with the cracked beam element model show that the cracks can be identified with high accuracy for both the thick-wall and thin-wall beams.

(3) Subsequently, experimental modal data from five square box section beams used to verify the cracked beam element model. The tested beams have different crack configurations, including both single-crack and multiple-crack scenarios. Both forward verification and inverse crack identification with the cracked beam element model give satisfactory results.

7.2 Recommendations for further research

In the present study, ABC frequencies have been successfully extracted from modal testing of laboratory structures. The possibility of measuring high quality ABC frequencies from real-life structures should be examined in the next stage of work. In real-life structures, many factors, such as more complex boundary conditions and uncontrollable ambient noises, will make it more challenging to obtain good FRF curves. As the extraction of ABC frequencies require the FRF curves to be of good quality in their entirety rather than only around the resonances, it can be anticipated that other challenging issues will arise and need to be addressed to get reliable ABC frequencies.

The possibility of utilizing ABC frequencies for model updating with some special requirements should also be studied. One example is that there are always some local areas in the FE model that are of low sensitivity to the conventional modal data and ill-conditioning might happen to the related model parameters in model updating. By carefully choosing the artificial pins, it is possible to generate some ABC frequencies

that have high sensitivity to those parameters. With these ABC frequencies added to the updating, it is possible to tackle the ill-conditioning of the related parameters.

On the crack modelling and identification, it is possible to extend the current approach on some other types of structural sections, such as I-section or circular hollow section beam- columns. It should also be noted that in the present study, the cracks considered are all assumed to be vertical in the beam sections. In real-life structures, it is possible that the developed cracks have relative angles to the beam sections due to setting of the welding directions or initial imperfection of the material. Including the angle of a crack into the crack damage identification procedure can be a future topic.

It is noted that crack modelling and identification of RC structures are more challenging than those of steel structures due to the complicated nature of crack development in RC structures. To the author's knowledge, the reduced stiffness model is still the most widely used damage model in model updating and damage identification of RC beam structures. In civil engineering, RC beams with the section thickness to length ratios around 10-15 are quite common and can be categorized as thick beams. As discussed in the Chapter 1 and 4, the reduced stiffness model is of great limitation for the crack modelling and identification of thick beams. The establishment of some more sophisticated crack model for the crack identification of RC beam structures should be another aim for the next stage of study.

References

Ashory, M. R. (1999). "High quality modal testing methods. " *PhD thesis*, University of London, UK.

Aydin, K. (2013). "Influence of crack and slenderness ratio on the eigenfrequencies of Euler-Bernoulli and Timoshenko beams." *Mechanics of Advanced Materials and Structures*, 20(5), 339-352.

Baghiee, N., Esfahani, M. R., and Moslem, K. (2009). "Studies on damage and FRP strengthening of reinforced concrete beams by vibration monitoring." *Engineering Structures*, 31(4), 875-893.

Bamnios, Y., Douka, E., and Trochidis, A. (2002). "Crack identification in beam structures using mechanical impedance." *Journal of Sound and Vibration*, 256(2), 287-297.

Bažant, Z. P. (1990). "Justification and improvement of Kienzler and Herrmann's estimate of stress intensity factors of cracked beam." *Engineering Fracture Mechanics*, 36(3), 523-525.

Brighenti, R., and Carpinteri, A. (2013). "Surface cracks in fatigued structural components: A review." *Fatigue & Fracture of Engineering Materials & Structures*, 36(12), 1209-1222.

Carneiro, S. H. S., and Inman, D. J. (2002). "Continuous model for the transverse vibration of cracked Timoshenko beams." *Journal of Vibration and Acoustics*-Transactions of the ASME, 124(2), 310-320.

Carrera, E., Giunta, G., and Petrolo, M. (2011). *Beam structures: Classical and advanced theories*, John Wiley & Sons.

Carrera, E., and Varello, A. (2012). "Dynamic response of thin-walled structures by variable kinematic one-dimensional models." *Journal of Sound and Vibration*, 331(24), 5268-5282.

Casas, J. R., and Aparicio, A. C. (1994). "Structural damage identification from dynamic-test data." *Journal of Structural Engineering*-ASCE, 120(8), 2437-2450.

Cerri, M. N., and Vestroni, F. (2003). "Use of frequency change for damage identification in reinforced concrete beams." *Journal of Vibration and Control*, 9(3-4), 475-491.

Chondros, T. G., Dimarogonas, A. D., and Yao, J. (1998). "A continuous cracked beam vibration theory." *Journal of Sound and Vibration*, 215(1), 17-34.

Christides, S., and Barr, A. D. S. (1984). "One-dimensional theory of cracked Bernoulli-Euler beams." *International Journal of Mechanical Sciences*, 26(11-1), 639-648.

Cowper, G. (1966). "The shear coefficient in Timoshenko's beam theory." *Journal of Applied Mechanics*, 33(2), 335-340.

D'Ambrogio, W., and Fregolent, A. (2004). "Dynamic model updating using virtual antiresonances." *Shock and Vibration*, 11(3-4), 351-363.

D'Ambrogio, W., and Fregolent, A. (2003). "Results obtained by minimising natural frequency and antiresonance errors of a beam model." *Mechanical Systems and Signal Processing*, 17(1), 29-37.

D'Ambrogio, W., and Fregolent, A. (2000). "The use of antiresonances for robust model updating." *Journal of Sound and Vibration*, 236(2), 227-243.

Darpe, A. K., Gupta, K., and Chawla, A. (2004). "Coupled bending, longitudinal and torsional vibrations of a cracked rotor." *Journal of Sound and Vibration*, 269(1-2), 33-60.

Dharmaraju, N., and Sinha, J. K. (2005). "Some comments on use of antiresonance for crack identification in beams." *Journal of Sound and Vibration*, 286(3), 669-671.

Dilena, M., and Morassi, A. (2010). "Reconstruction method for damage detection in beams based on natural frequency and antiresonant frequency measurements." *Journal of Engineering Mechanics*-ASCE, 136(3), 329-344.

Dilena, M., and Morassi, A. (2009). "Structural health monitoring of rods based on natural frequency and antiresonant frequency measurements." *Structural Health Monitoring*-an International Journal, 8(2), 149-173.

Dilena, M., and Morassi, A. (2004). "The use of antiresonances for crack detection in beams." *Journal of Sound and Vibration*, 276(1-2), 195-214.

Dimarogonas, A. D. (1996). "Vibration of cracked structures: A state of the art review." *Engineering Fracture Mechanics*, 55(5), 831-857.

Dimarogonas, A. D., and Papadopoulos, C. A. (1983). "Vibration of cracked shafts in bending." *Journal of Sound and Vibration*, 91(4), 583-593.

Doebling, S. W., Farrar, C. R., Prime, M. B., and Shevitz, D. W. (1996). "Damage identification and health monitoring of structural and mechanical systems from changes in their vibration characteristics: A literature review." Los Alamos National Lab., NM, United States.

Dotti, F. E., Cortinez, V. H., and Reguera, F. (2013). "Mode I stress intensity factor for cracked thin-walled composite beams." *Theoretical and Applied Fracture Mechanics*, 67-68, 38-45.

Douka, E., Bamnios, G., and Trochidis, A. (2004). "A method for determining the location and depth of cracks in double-cracked beams." *Applied Acoustics*, 65(10), 997-1008.

Dunn, M. L., Suwito, W., and Hunter, B. (1997). "Stress intensity factors for cracked I-beams." *Engineering Fracture Mechanics*, 57(6), 609-615.

Ewins, D. J. (1984). *Modal testing: Theory and practice*, Research studies press, Letchworth, UK.

Farrar, C. R., and Doebling, S. W. "An overview of modal-based damage identification methods." *Proc., Proceedings of DAMAS Conference*, Citeseer, 269-278.

Friswell, M., and Mottershead, J. E. (1995). *Finite element model updating in structural dynamics*, Springer Science & Business Media.

Friswell, M. I., and Penny, J. E. T. (2002). "Crack modeling for structural health monitoring." *Structural Health Monitoring*-an International Journal, 1(2), 139-148.

Gao, H., and Herrmann, G. (1992). "On estimates of stress intensity factors for cracked beams and pipes." *Engineering Fracture Mechanics*, 41(5), 695-706.

Ghafoori, E., and Motavalli, M. (2011). "Analytical calculation of stress intensity factor of cracked steel I-beams with experimental analysis and 3D digital image correlation measurements." *Engineering Fracture Mechanics*, 78(18), 3226-3242.

Giannoccaro, N. I., Messina, A., Nobile, R., and Panella, F. W. (2006). "Fatigue damage evaluation of notched specimens through resonance and anti-resonance data." *Engineering Failure Analysis*, 13(3), 340-352.

Gordis, J. H. (1999). "Artificial boundary conditions for model updating and damage detection." *Mechanical Systems and Signal Processing*, 13(3), 437-448.

Gordis, J. H. (1996). "Omitted coordinate systems and artificial constraints in spatially incomplete identification." *Modal Analysis*-the International Journal of Analytical and Experimental Modal Analysis, 11(1-2), 83-95.

Gordis, J. H., and Papagiannakis, K. (2011). "Optimal selection of artificial boundary conditions for model update and damage detection." *Mechanical Systems and Signal Processing*, 25(5), 1451-1468.

Hanson, D., Waters, T. P., Thompson, D. J., Randall, R. B., and Ford, R. A. J. (2007). "The role of anti-resonance frequencies from operational modal analysis in finite element model updating." *Mechanical Systems and Signal Processing*, 21(1), 74-97.

He, J. M., and Fu, Z. F. (2001). *Modal analysis*, Butterworth-Heinemann, Oxford, UK.

Hu, N., Wang, X., Fukunaga, H., Yao, Z. H., Zhang, H. X., and Wu, Z. S. (2001). "Damage assessment of structures using modal test data." *International Journal of Solids and Structures*, 38(18), 3111-3126.

Jones, K., and Turcotte, J. (2002). "Finite element model updating using antiresonant frequencies." *Journal of Sound and Vibration*, 252(4), 717-727.

Kienzler, R., and Herrmann, G. (1986). "An elementary theory of defective beams." *Acta Mechanica*, 62(1-4), 37-46.

Kikidis, M. L., and Papadopoulos, C. A. (1992). "Slenderness ratio effect on cracked beam." *Journal of Sound and Vibration*, 155(1), 1-11.

Kim, Y. Y., and Kim, J. H. (1999). "Thin-walled closed box beam element for static and dynamic analysis." *International Journal for Numerical Methods in Engineering*, 45(4), 473-490.

Kyprianou, A., Mottershead, J. E., and Ouyang, H. (2005). "Structural modification. Part 2: Assignment of natural frequencies and antiresonances by an added beam." *Journal of Sound and Vibration*, 284(1-2), 267-281.

Lee, Y. S., and Chung, M. J. (2000). "A study on crack detection using eigenfrequency test data." *Computers & Structures*, 77(3), 327-342.

Lele, S. P., and Maiti, S. K. (2002). "Modelling of transverse vibration of short beams for crack detection and measurement of crack extension." *Journal of Sound and Vibration*, 257(3), 559-583.

Li, S. M., Shelley, S., and Brown, D. (1995). "Perturbed boundary condition testing concepts. " in: *Procedings of the 13th International Modal Analysis Confernce*, Society of Experimental Mechanics, Inc., Nashville, Tennessee, United States, 902-907.

Liebowitz, H., Vanderveldt, H., and Harris, D. (1967). "Carrying capacity of notched columns." *International Journal of Solids and Structures*, 3(4), 489-500.

Liew, K. M., Hung, K. C., and Lim, M. K. (1995). "Vibration of stress-free hollow cylinders of arbitrary cross section." *Journal of Applied Mechanics*-Transactions of the ASME, 62(3), 718-724.

Liu, D., Gurgenci, H., and Veidt, M. (2003). "Crack detection in hollow section structures through coupled response measurements." *Journal of Sound and Vibration*, 261(1), 17-29.

Lu, Y., Mao, L., and Tu, Z. G. (2008). "Practical considerations in FE model updating with artificial boundary condition frequencies. " in: *Porceedings of the 10th International Symposium on Structural Engineering for Yong Experts*, Beijing, China, 2008, pp. 72-79.

Lu, Y., and Tu, Z. G. (2008). "Artificial boundary condition approach for structural identification: A laboratory perspective." *Proceedings of the 26th International Modal Analysis Conference,* Society of Experimental Mechanics, Inc., Orlando, Florida, United States.

Lu, Y., and Tu, Z. G. (2004). "A two-level neural network approach for dynamic FE model updating including damping." *Journal of Sound and Vibration*, 275(3-5), 931-952.

Luo, Q., Li, Q., and Tang, J. (2002). "Shear lag in box girder bridges." *Journal of Bridge Engineering*-ASCE, 7(5), 308-313.

Mao, L., and Lu, Y. (2011). "Extraction of artificial boundary frequencies for damage identification." *Journal of Physics: Conference Series*, 305(1), 10.1088/1742-6596/305/1/012051

Marwala, T. (2010). *Finite-element-model updating using computational intelligence techniques: applications to structural dynamics*, Srpinger Science & Bussiness Media, Berlin, Germany.

Mehrjoo, M., Khaji, N., and Ghafory-Ashtiany, M. (2014). "New Timoshenko-cracked beam element and crack detection in beam-like structures using genetic algorithm." *Inverse Problems in Science and Engineering*, 22(3), 359-382.

Meruane, V. (2013). "Model updating using antiresonant frequencies identified from transmissibility functions." *Journal of Sound and Vibration*, 332(4), 807-820.

Meruane, V., and Heylen, W. (2011). "Structural damage assessment with antiresonances versus mode shapes using parallel genetic algorithms." *Structural Control & Health Monitoring*, 18(8), 825-839.

Moaveni, B., He, X., Conte, J. P., and De Callafon, R. A. (2008). "Damage identification of a composite beam using finite element model updating." *Computer-Aided Civil and Infrastructure Engineering*, 23(5), 339-359.

Morassi, A., and Rocchetto, L. (2003). "A damage analysis of steel-concrete composite beams via dynamic methods: Part I. Experimental results." *Journal of Vibration and Control*, 9(5), 507-527.

Mottershead, J. E. (1998). "On the zeros of structural frequency response functions and their sensitivities." *Mechanical Systems and Signal Processing*, 12(5), 591-597.

Mottershead, J. E., and Friswell, M. I. (1993). "Model updating in structural dynamics - a survey." *Journal of Sound and Vibration*, 167(2), 347-375.

Mottershead, J. E., Link, M., and Friswell, M. I. (2011). "The sensitivity method in finite element model updating: A tutorial." *Mechanical Systems and Signal Processing*, 25(7), 2275-2296.

Mthembu, L., Marwala, T., Friswell, M. I., and Adhikari, S. (2009). "Bayesian evidence for finite element model updating." in: *Proceedings of the 27h International Modal Analysis Conference*, Orlando, FL, United States.

Nahvi, H., and Jabbari, M. (2005). "Crack detection in beams using experimental modal data and finite element model." *International Journal of Mechanical Sciences*, 47(10), 1477-1497.

Nam, D. H., Choi, S., Park, S., and Stubbs, N. (2005). "Improved parameter identification using additional spectral information." *International Journal of Solids and Structures*, 42(18-19), 4971-4987.

Ndambi, J. M., Vantomme, J., and Harri, K. (2002). "Damage assessment in reinforced concrete beams using eigenfrequencies and mode shape derivatives." *Engineering Structures*, 24(4), 501-515.

Nussbaumer, A. C., Fisher, J. W., and Dexter, R. J. (1999). "Behavior of long fatigue cracks in cellular box beam." *Journal of Structural Engineering*-ASCE, 125(11), 1232-1238.

Okamura, H., Watanabe, K., and Takano, T. (1973). "Applications of the compliance concept in fracture mechanics." *ASTM special technical publication*(536), 423-438.

Ostachowicz, W. M., and Krawczuk, M. (1991). "Analysis of the effect of cracks on the natural frequencies of a cantilever beam." *Journal of Sound and Vibration*, 150(2), 191-201.

Pandey, A. K., Biswas, M., and Samman, M. M. (1991). "Damage detection from changes in curvature mode shapes." *Journal of Sound and Vibration*, 145(2), 321-332.

Papadopoulos, C. A., and Dimarogonas, A. D. (1987). "Coupled longitudinal and bending vibrations of a rotating shaft with an open crack." *Journal of Sound and Vibration*, 117(1), 81-93.

Papadopoulos, C. A., and Dimarogonas, A. D. (1987). "Coupling of bending and torsional vibration of a cracked timoshenko shaft." *Ingenieur Archiv*, 57(4), 257-266.

Peeters, B., Abdel Wahab, M., De Roeck, G., De Visscher, J., De Wilde, W., Ndambi, M., and Vantomme, J. "Evaluation of structural damage by dynamic system identification." in: *Proceedings of the International Seminar on Modal Analysis*, Katholieke Universiteit Leuven, Belgium, 1349-1362.

Perera, R., and Torres, R. (2006). "Structural damage detection via modal data with genetic algorithms." *Journal of Structural Engineering*-ASCE, 132(9), 1491-1501.

Qian, G. L., Gu, S. N., and Jiang, J. S. (1990). "The dynamic behavior and crack detection of a beam with a crack." *Journal of Sound and Vibration*, 138(2), 233-243.

Qiao, P. Z., Lu, K., Lestari, W., and Wang, J. L. (2007). "Curvature mode shape-based damage detection in composite laminated plates." *Composite Structures*, 80(3), 409-428.

Rade, D. A., and Lallement, G. (1998). "A strategy for the enrichment of experimental data as applied to an inverse eigensensitivity-based fe model updating method." *Mechanical Systems and Signal Processing*, 12(2), 293-307.

Ratcliffe, C. P. (1997). "Damage detection using a modified laplacian operator on mode shape data." *Journal of Sound and Vibration*, 204(3), 505-517.

Razak, H. A., and Fayyadh, M. M. (2013). "Sensitivity of natural frequencies to composite effects in reinforced concrete elements." *Mechanics of Advanced Materials and Structures*, 20(6), 441-453.

Reissner, E. (1946). "Analysis of shear lag in box beams by the principle of minimum potential energy." *Quarterly of Applied Mathematics*, 5(3), 268-278.

Ricci, P., and Viola, E. (2006). "Stress intensity factors for cracked T-sections and dynamic behaviour of T-beams." *Engineering Fracture Mechanics*, 73(1), 91-111.

Richardson, M. H., and Formenti, D. L. "Parameter estimation from frequency response measurements using rational fraction polynomials." in: *Proceedings of the 1st international modal analysis conference*, Union College Schenectady, NY, United States, 167-186.

Ruotolo, R., and Surace, C. (1997). "Damage assessment of multiple cracked beams: Numerical results and experimental validation." *Journal of Sound and Vibration*, 206(4), 567-588.

Rytter, A. (1993). "Vibration based inspection of civil engineering structures." *PhD thesis*, Aalborg University, Denmark.

Shen, M. H. H., and Pierre, C. (1994). "Free-vibrations of beams with a single-edge crack." *Journal of Sound and Vibration*, 170(2), 237-259.

Shen, M. H. H., and Pierre, C. (1990). "Natural-modes of Bernoulli-Euler beams with symmetric cracks." *Journal of Sound and Vibration*, 138(1), 115-134.

Shi, Z. Y., and Law, S. S. (1998). "Structural damage localization from modal strain energy change." *Journal of Sound and Vibration*, 218(5), 825-844.

Shi, Z. Y., Law, S. S., and Zhang, L. M. (2000). "Optimum sensor placement for structural damage detection." *Journal of Engineering Mechanics*-ASCE, 126(11), 1173-1179.

Sinha, J. K., Friswell, M. I., and Edwards, S. (2002). "Simplified models for the location of cracks in beam structures using measured vibration data." *Journal of Sound and Vibration*, 251(1), 13-38.

Sohn, H., Farrar, C. R., Hemez, F. M., Shunk, D. D., Stinemates, D. W., Nadler, B. R., and Czarnecki, J. J. (2004). "A review of structural health monitoring literature: 1996-2001." Los Alamos National Laboratory Los Alamos, NM, United States.

Swamidas, A. S. J., Yang, X., and Seshadri, R. (2004). "Identification of cracking in beam structures using Timoshenko and Euler formulations." *Journal of Engineering Mechanics*-ASCE, 130(11), 1297-1308.

Tada, H., Paris, P. C., and Irwin, G. R. (2000). "The stress analysis of cracks handbook." The american society of mechanical engineers, New York, United States.

Toribio, J., Alvarez, N., Gonzalez, B., and Matos, J. C. (2009). "A critical review of stress intensity factor solutions for surface cracks in round bars subjected to tension loading." *Engineering Failure Analysis*, 16(3), 794-809.

Tsang, S. W. F., and Chu, L. Y. L. (2011). "An experimental study of the tension stiffening effect on the structural stiffness of reinforced concrete cantilevered balcony structures using resonant frequency measurement approach." *Construction and Building Materials*, 25(5), 2690-2699.

Tu, Z. G., and Lu, Y. (2008). "FE model updating using artificial boundary conditions with genetic algorithms." *Computers & Structures*, 86(7-8), 714-727.

Unger, J. F., Teughels, A., and De Roeck, G. (2006). "System identification and damage detection of a prestressed concrete beam." *Journal of Structural Engineering*-ASCE, 132(11), 1691-1698.

Viola, E., Nobile, L., and Federici, L. (2002). "Formulation of cracked beam element for structural analysis." *Journal of Engineering Mechanics*-ASCE, 128(2), 220-230.

Vlasov, V. Z. (1961). "Thin-walled elastic beams. " Israel Program for Scientific Translations, Jerusalem, Israel.

Wahl, F., Schmidt, G., and Forrai, L. (1999). "On the significance of antiresonance frequencies in experimental structural analysis." *Journal of Sound and Vibration*, 219(3), 379-394.

Wroblewski, A. C., Pesch, A. H., and Sawicki, J. T. (2014). "Structural change quantification in rotor systems based on measured resonance and antiresonance frequencies." *Journal of Engineering for Gas Turbines and Power*-Transactions of the ASME, 136(2), DOI: 10.1115/GT2013-95930.

Xie, Y. J., and Wang, X. H. (2004). "Application of G*-integral on cracked structural beams." *Journal of Constructional Steel Research*, 60(9), 1271-1290.

Xie, Y. J., Wang, X. H., and Lin, Y. C. (2004). "Stress intensity factors for cracked rectangular cross-section thin-walled tubes." *Engineering Fracture Mechanics*, 71(11), 1501-1513.

Xie, Y. J., Xu, H., and Li, P. N. (1998). "Crack mouth widening energy-release rate and its application." *Theoretical and Applied Fracture Mechanics*, 29(3), 195-203.

Zerbst, U., Heinimann, M., Donne, C. D., and Steglich, D. (2009). "Fracture and damage mechanics modelling of thin-walled structures - an overview." *Engineering Fracture Mechanics*, 76(1), 5-43.

Zhang, S. H., and Lyons, L. P. R. (1984). "A thin-walled box beam finite-element for curved bridge analysis." *Computers & Structures*, 18(6), 1035-1046.

Zhang, Y. H., and Lin, L. X. (2014). "Shear lag analysis of thin-walled box girders adopting additional deflection as generalized displacement." *Journal of Engineering Mechanics*-ASCE, 140(4).

Zheng, D. Y., and Fan, S. C. (2003). "Vibration and stability of cracked hollow-sectional beams." *Journal of Sound and Vibration*, 267(4), 933-954.

Zheng, D. Y., and Kessissoglou, N. J. (2004). "Free vibration analysis of a cracked beam by finite element method." *Journal of Sound and Vibration*, 273(3), 457-475.

Zhou, S. J. (2010). "Finite beam element considering shear-lag effect in box girder." *Journal of Engineering Mechanics*-ASCE, 136(9), 1115-1122.

Zonta, D., and Bernal, D. (2006). "Strain-based approaches to damage localization in civil structures." in: *Proceedings of the 24th International Modal Analysis Conference*, St. Louis, MO, United States.

Appendix A: Stress intensity factors (SIFs) for box section beams

The stress intensity factors (SIF) for box beams can be expressed as:

For cracks at stage 1:

$$K_{\mathrm{I1}}^{\mathrm{H}} = \frac{N}{A_0}\sqrt{\pi a_{\mathrm{H}}}\,F_{\mathrm{I1}}^{\mathrm{H}}\left(a_{\mathrm{H}}/B, t_{\mathrm{s}}/B\right)$$

$$\text{where, } F_{\mathrm{I1}}^{\mathrm{H}}\left(a_{\mathrm{H}}/B, t_{\mathrm{s}}/B\right) = m\left(a_{\mathrm{H}}/B\right)\cdot\left(t_s/B\right) + n\left(a_{\mathrm{H}}/B\right)$$

$$m\left(a_{\mathrm{H}}/B\right) = -0.975 - 1.341\left(a_{\mathrm{H}}/B\right) + 17.283\left(a_{\mathrm{H}}/B\right)^2 - 83.681\left(a_{\mathrm{H}}/B\right)^3 + 111.982\left(a_{\mathrm{H}}/B\right)^4$$

$$n\left(a_{\mathrm{H}}/B\right) = 1.011 - 0.092\left(a_{\mathrm{H}}/B\right) + 0.572\left(a_{\mathrm{H}}/B\right)^2 + 5.989\left(a_{\mathrm{H}}/B\right)^3 - 9.190\left(a_{\mathrm{H}}/B\right)^4$$

$$K_{\mathrm{I2}}^{\mathrm{H}} = \frac{MB}{2I}\sqrt{\pi a_{\mathrm{H}}}\,F_{\mathrm{I2}}^{\mathrm{H}}\left(a_{\mathrm{H}}/B, t_{\mathrm{s}}/B\right)$$

$$\text{where, } F_{\mathrm{I2}}^{\mathrm{H}}\left(a_{\mathrm{H}}/B, t_{\mathrm{s}}/B\right) = m\left(a_{\mathrm{H}}/B\right)\cdot\left(t_s/B\right) + n\left(a_{\mathrm{H}}/B\right)$$

$$m\left(a_{\mathrm{H}}/B\right) = -1.885 - 3.596\left(a_{\mathrm{H}}/B\right) + 31.962\left(a_{\mathrm{H}}/B\right)^2 - 131.227\left(a_{\mathrm{H}}/B\right)^3 + 156.844\left(a_{\mathrm{H}}/B\right)^4$$

$$n\left(a_{\mathrm{H}}/B\right) = 1.0013 - 0.0078\left(a_{\mathrm{H}}/B\right) - 0.0936\left(a_{\mathrm{H}}/B\right)^2 + 7.8811\left(a_{\mathrm{H}}/B\right)^3 - 10.9710\left(a_{\mathrm{H}}/B\right)^4$$

For cracks at stage 2:

$$K_{\mathrm{I1}}^{\mathrm{V}} = \frac{N}{A_0}\sqrt{\pi a_{\mathrm{V}}}\,F_{\mathrm{I1}}^{\mathrm{V}}\left(a_{\mathrm{V}}/B, t_{\mathrm{s}}/B\right)$$

$$\text{where, } F_{\mathrm{I1}}^{\mathrm{V}}\left(a_{\mathrm{V}}/B, t_{\mathrm{s}}/B\right) = m\left(a_{\mathrm{V}}/B\right)\cdot\left(t_s/B\right) + n\left(a_{\mathrm{V}}/B\right)$$

$$m\left(a_{\mathrm{V}}/B\right) = -7.407 + 36.068\left(a_{\mathrm{V}}/B\right) - 137.172\left(a_{\mathrm{V}}/B\right)^2 + 241.490\left(a_{\mathrm{V}}/B\right)^3 - 162.964\left(a_{\mathrm{V}}/B\right)^4$$

$$n\left(a_{\mathrm{V}}/B\right)=5.346-23.645\left(a_{\mathrm{V}}/B\right)+105.557\left(a_{\mathrm{V}}/B\right)^{2}-192.984\left(a_{\mathrm{V}}/B\right)^{3}+152.806\left(a_{\mathrm{V}}/B\right)^{4}$$

$$K_{\mathrm{I2}}^{\mathrm{V}}=\frac{MB}{2I}\sqrt{\pi a_{\mathrm{V}}}F_{\mathrm{I2}}^{\mathrm{V}}\left(a_{\mathrm{V}}/B,t_{\mathrm{s}}/B\right)$$

$$\text{where, } F_{\mathrm{I2}}^{\mathrm{V}}\left(a_{\mathrm{V}}/B,t_{\mathrm{s}}/B\right)=m\left(a_{\mathrm{V}}/B\right)\cdot\left(t_{\mathrm{s}}/B\right)+n\left(a_{\mathrm{V}}/B\right)$$

$$m\left(a_{\mathrm{V}}/B\right)=-12.151+57.042\left(a_{\mathrm{V}}/B\right)-215.499\left(a_{\mathrm{V}}/B\right)^{2}+376.957\left(a_{\mathrm{V}}/B\right)^{3}-267.067\left(a_{\mathrm{V}}/B\right)^{4}$$

$$n\left(a_{\mathrm{V}}/B\right)=5.269-24.092\left(a_{\mathrm{V}}/B\right)+100.185\left(a_{\mathrm{V}}/B\right)^{2}-182.504\left(a_{\mathrm{V}}/B\right)^{3}+138.946\left(a_{\mathrm{V}}/B\right)^{4}$$

$$K_{\mathrm{II}}^{\mathrm{V}}=\frac{P}{A_{\mathrm{e}}}\sqrt{\pi a_{\mathrm{V}}}F_{\mathrm{II}}^{\mathrm{V}}\left(a_{\mathrm{V}}/B,t_{\mathrm{s}}/B\right)$$

$$\text{where, } F_{\mathrm{II}}^{\mathrm{V}}\left(a_{\mathrm{V}}/B,t_{\mathrm{s}}/B\right)=m\left(a_{\mathrm{V}}/B\right)\cdot\left(t_{\mathrm{s}}/B\right)^{2}++n\left(a_{\mathrm{V}}/B\right)\cdot\left(t_{\mathrm{s}}/B\right)+p\left(a_{\mathrm{V}}/B\right)$$

$$m\left(a_{\mathrm{V}}/B\right)=-42.923-748.211\left(a_{\mathrm{V}}/B\right)+6810.320\left(a_{\mathrm{V}}/B\right)^{2}-17903.959\left(a_{\mathrm{V}}/B\right)^{3}+15145.796\left(a_{\mathrm{V}}/B\right)^{4}$$

$$n\left(a_{\mathrm{V}}/B\right)=-16.369+359.143\left(a_{\mathrm{V}}/B\right)-2115.288\left(a_{\mathrm{V}}/B\right)^{2}+4824.795\left(a_{\mathrm{V}}/B\right)^{3}-3810.311\left(a_{\mathrm{V}}/B\right)^{4}$$

$$p\left(a_{\mathrm{V}}/B\right)=2.514-14.370\left(a_{\mathrm{V}}/B\right)+82.745\left(a_{\mathrm{V}}/B\right)^{2}-177.632\left(a_{\mathrm{V}}/B\right)^{3}+136.118\left(a_{\mathrm{V}}/B\right)^{4}$$

Appendix B: List of publications

Hou, C. C., Lu, Y. (2016). "Identification of cracks in thick beams with a cracked beam element model." *Journal of Sound and Vibration*. (Submitted)

Hou, C. C., Lu, Y. (2016). "Experimental study of crack identification in thick beams with a cracked beam element model." *Journal of Engineering Mechanics*-ASCE. (Submitted)

Hou, C. C., Lu, Y. (2016). "Identification of cracks in box section beam-column members with a cracked beam element model." *International Journal of Solids and Structures*. (Submitted)

Hou, C. C., Mao, L., and Lu, Y. (2016). "Experimental study of generating artificial boundary condition frequencies and application in dynamic model updating." *Journal of Structural Engineering-ASCE* (Submitted)

Hou, C. C., Lu, Y. (2016). "Identification of cracks in beams- recent development and laboratory verification." *6th European Conference on Structural Control*, 11-13 July, Sheffield, England.

Hou, C. C., Lu, Y. (2015). "On the measurement errors of extracting ABC frequencies for damage identification." *16th European Bridge Conference*, 23-25 June, Edinburgh, UK.

Lu, Y., **Hou, C. C.**, and Mao, L. (2014). "Dynamic measurement for extended frequencies from model and full-size structural components." *9th International Conference on Structural Dynamics*, 30 June- 2 July, Porto, Portugal.

Lu, Y., Mao, L., **Hou, C. C.**, and Zhu. H. H. (2013). "Structural identification with extended modal frequency data and application involving discontinuities." *the 6th International Conference on Structural Health Monitoring of Intelligent Infrastructure*, 9-11 September, Hong Kong, China.